University
of Southampton

Geometries and mechanics of veins and dykes

by Richard R Jackson

Doctor of Philosophy

September 1992

UNIVERSITY OF SOUTHAMPTON

ABSTRACT

FACULTY OF SCIENCE

GEOLOGY

Doctor of Philosophy

GEOMETRIES AND MECHANICS OF VEINS AND DYKES

by Richard Robert Jackson

The mechanics of vein and dyke formation is investigated from field observations of natural fracture systems and by using techniques from rock fracture mechanics. Veins from the Culm Basin near Millook Haven, south-west England, are used to develop and test hypotheses that natural crack geometry can be used to infer paleostress conditions and propagation histories from the time of their initiation.

It is suggested that veins initially propagate as essentially mode I (extension) fractures. Local crack-induced stresses generated through mechanical interaction, or by subsequent loading effects on pre-existing cracks may involve mixed-mode deformations, which can produce minor cracks and structures that accommodate shear displacements. Sigmoidal vein profiles and vein fillings are modelled as outgrowths of mechanical crack interaction, under fixed boundary conditions, and in the absence of high finite shear strains. Maps of overlapping veins with a wide range of geometries, sizes and spacing values are explained in terms of selective mechanical interaction and the stress shielding effect of longer fractures upon shorter fractures. Straight, strongly overlapping veins imply the controlling influence of a relatively high remote crack-parallel compressive stress.

En echelon vein arrays are re-examined in terms of the kinematics of transtension-transpression. Determination of displacements across vein arrays and from fibres and wall-rock markers, indicate that there is a spectrum of vein geometries which can be directly related to wall-rock displacements. The role of tectonic stress and fluid pressure in the generation of an effective tensile stress for initial vein growth is investigated using examples of en echelon vein arrays. The results indicate that vein initiation and growth may be tectonically driven (deformation induced) and is not entirely dependent on high internal fluid pressures.

The frequency and spatial distribution of vein thickness and spacing in sedimentary rocks is analysed and the mechanical role of layer thickness on fracture development examined. Negative exponential and power-law (fractal) distributions are the most appropriate models to explain the range of vein thickness and spacing values. Departures from the power-law model are not simply sampling artifacts, but instead represent real differences in maximum vein thickness and spacing values, which can be attributed to the effects of fracture propagation through layered rocks.

Observations of Tertiary mafic dykes from around Easdale, north-west Scotland, indicate that many variably oriented dykes share common sub-horizontal opening directions. The stress control of dyke intrusion is examined, with analysis of the stress ratio for individual dykes indicating local transtensional loading conditions. Examination of the structure of the chilled margins, flow lineations and the textural zonation of the dykes, suggest that magma solidified on the dyke walls as it continued to flow in the dyke interior. Measurements of dyke thickness variation and estimates of Reynolds numbers yield values well within the regime for laminar flow.

ACKNOWLEDGEMENTS

I wish to thank Dave Sanderson for supervising my research and for his guidance during the preparation of this thesis. Discussions with Jim Andrews in the field in North Cornwall and elsewhere, were of great benefit to me.

Many people have contributed to my research. In particular I would like to thank Read Mapeo for discussions during fieldwork around Bude and along the coast of North Cornwall. Also David Peacock for many interesting discussions and for his help with the final thesis collation. I also acknowledge illuminating discussions and correspondence with Terry Engelder and David Pollard, who also provided me with helpful comments and suggestions on an early draft of Chapter 5. I would like to thank Barry Marsh for all of the photographic processing, and for the production of the thesis plates at very short notice.

This research was supported by a studentship from the Natural Environmental Research Council.

CONTENTS

Chapter 4 Vein thickness and spacing in layered rocks

Chapter 5 Transtensional modelling of en echelon vein arrays

Chapter 6 Dyke intrusion and paleostress analysis

1 INTRODUCTION

Modern mechanical concepts of the formation of natural fracture systems (joints, veins, dykes and faults) began with the application of the Coulomb criterion (Anderson 1951) and the recognition of the role of pore fluid pressure in brittle fracture (Hubbert & Rubey 1959, Secor 1965). Since these advances, the ability to infer paleostress conditions from the geometry of natural fractures has greatly benefited from more recent contributions made by fracture mechanics, experimental deformation and numerical modelling. Experimental studies have shown that the fracturing of rock under compression is the product of a series of processes which involve the nucleation, growth, interaction and fusion of multiple microcracks (Griffith 1920, Tapponier & Brace 1976, Paterson 1978, Kranz 1983). In the early stage of the fracturing process these microcracks are tensile (mode I) and parallel to the maximum compressive stress. Using the results from some of these studies, a variety of methods have been developed which can be used to relate joint, vein and dyke orientations to near-field and remote stress (Engelder & Geiser 1980, Segall & Pollard 1987, Aydin & DeGraff 1987), fracture dilation and dyke intrusion to driving stress magnitude (Delaney *et al.* 1986), and crack kinking and curvature to remote differential stress (Olson & Pollard 1989, Crulkshank *et al.* 1991). Theoretical analyses of crack interaction problems in the geological literature include those by Du & Aydin (1991), Olson & Pollard (1991), and Wu & Pollard (1992).

In this thesis, the geometry and mechanics of vein and dyke formation is investigated using a combination of field observations of veins and dykes, and by applying principles of fracture mechanics. Many veins and dykes are analogous to mode I elastic cracks since their walls have simply opened to accommodate infilling material; although field observation and theory suggest that inelastic deformation is an important addition. This idealisation of veins and dykes as mode I cracks is shown to be reasonable for their initiation and propagation, but many veins and dykes utilise pre-existing cracks under various loading conditions which may involve a component of mixed-mode deformation. The idealisation also provides a guide for data collection and for the extrapolation of theoretical studies to interpretation of the field data. Examination of field relations and measurements of vein sets from around Millook Haven, SW England are used to test hypotheses that natural fracture patterns can be used to infer paleostress orientations and fracture propagation histories. Field observations of Tertiary mafic dykes from around Easdale, NW Scotland are used to investigate hypotheses about intrusion mechanisms and to analyse the stress control of dyke intrusion.

The thesis is divided into six chapters that each stand as independent studies. Each chapter is closely related to one another, as they all deal with the description and the analysis of the geometries and mechanics of various natural fracture problems:

Chapter 2 deals with vein formation in the Culm Basin, south-west England. The geometries and kinematics of vein sets developed in the Crackington Formation, mainly around Millook Haven are described. This chapter serves to introduce the field examples used, and also discusses the relations between vein formation and fold development.

Chapter 3 deals with the structural interpretation of veins in the context of rock fracture mechanics. This study focuses on how fracture mechanics can be applied to the interpretation of certain vein patterns and on geometric parameters which can be measured at outcrops; and how they relate to mechanical aspects of vein initiation and growth.

Chapter 4 is an investigation of vein thickness and spacing in layered sedimentary rocks. Distribution models are evaluated, the mechanical control of layer thickness on vein development is examined, and the extension and strain accommodated by the veining analysed.

Chapter 5 deals with the interpretation of en echelon vein arrays. The geometry of en echelon veins is re-examined in the context of transtensional-transpressional deformation and quasi-static models postulated by Pollard and co-authors (Pollard *et al.* 1982, Delaney *et al.* 1986). The role of tectonic stress and internal fluid pressure on the growth of en echelon veins and the development of conjugate en echelon veins is also investigated.

Chapter 6 provides an analysis of mafic dyke intrusion, using mapped examples of Tertiary dykes from around Easdale, north-west Scotland. This study combines field observations and theoretical models which are relevant to understanding the opening of dykes. This leads to the development of a simple mechanical model.

Chapter 7 summarises the results and conclusions from each study.

2

Vein formation in the Culm Basin, south-west England

2.1 INTRODUCTION

This chapter is concerned with the geometries and kinematics of some natural vein systems in Upper Carboniferous rocks of the Culm Basin in south-west England (Fig.2.1a). The objective of this study is to describe the geometry and orientation of some of these vein sets, and relate some of them to aspects of the structural development of the basin. Much of the terminology used in the description of veins is illustrated here. Observations on different vein configurations, profile geometries and their mineral infills are reviewed. Some of the concepts used in fracture mechanics analysis, which have implications for inferring vein propagation histories, are also introduced. These aspects are developed in later chapters.

Veins and solution-transfer structures, which are common deformation features of low-grade terranes, are well developed in the Culm Basin. The vein systems in the basin provide an opportunity to examine a variety of vein geometries in various structural settings, and observe their relationships to folding, faulting, cleavage and shear zone development. The veins described are from areas of upright folding around Hartland Quay [SS223248] and from an upright to recumbent fold transition sequence between Wanson Mouth [SS195012] and Millook Haven [SS184003](Fig.2.1b). References are made to other localities, although the main emphasis is on the area around Millook Haven.

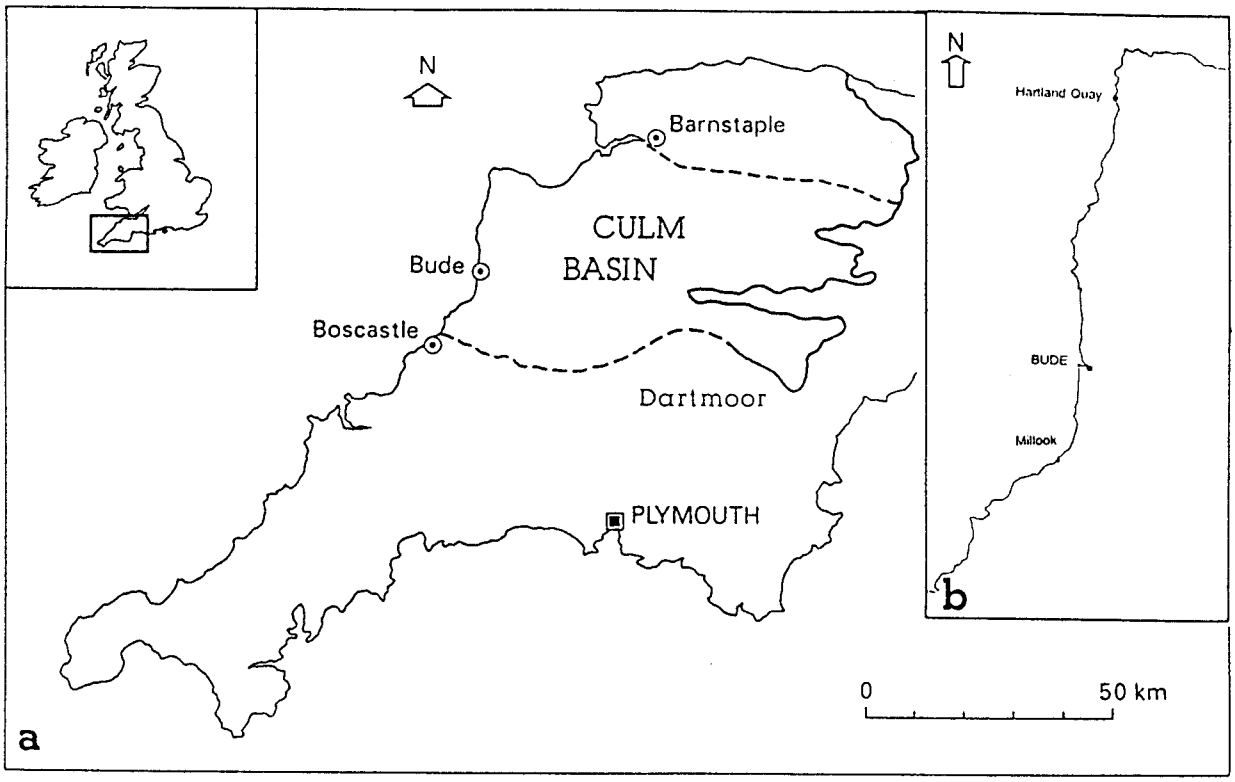

Figure 2.1. [a] Map showing the position of the Cuim Basin, and [b] the iocation of the study areas referred to in the text.

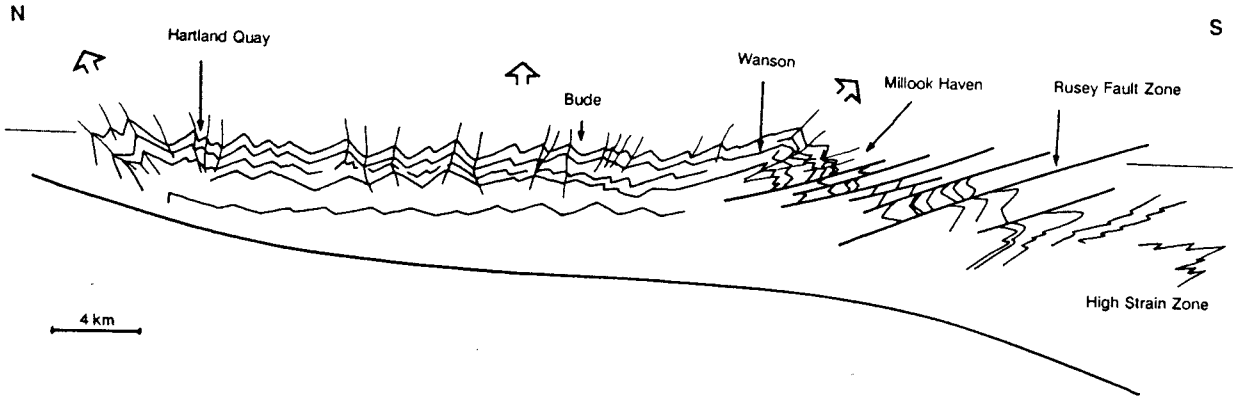

Figure 2.1. [c] Schematic structural cross section of the Culm Basin from Hartland to Rusey, illustrating the fanning of fold facing directions and the transition from upright to recumbent folding near the southern basin margin.

2.2 REGIONAL STRUCTURAL SETTING

The Culm Basin records a period of progressive, high-level Variscan deformation which produced a complex fold geometry with a broad fanning of facing directions (Fig.2.1c). Deformation within the basin has generally been described in terms of the development of chevron folds (Ramsay 1974) with horizontal shortening of 35-60% (Sanderson 1979) (Table 2.1) during N-S directed compression (*eg.* Whalley & Lloyd 1986). The rocks involved are of Upper Carboniferous age and comprise interbedded sandstone and shale sequences (Crackington, Bude & Bideford Formations)(Edmonds *et al.* 1979, Freshney *et al.* 1972)(Table 2.2). Regional metamorphic grade is in the upper diagenetic-anchizone range (Primmer 1985, Cornford *et al.* 1987) and generally increases both southwards and northwards; corresponding with a general change in fold attitude and increased spaced-cleavage development and vein formation.

Most of the folds have E-W trending axes which are virtually horizontal (Edmonds *et al.* 1979, Freshney *et al.* 1972). The folds are approximately cylindrical (chevron variety) with conical terminations. These folds also include a range of geometries through flat-topped box-folds with tightly folded cores to more concentric geometries. These features suggest some may be detachment (Jamison 1987) or lift-off folds (Mitra & Namson 1989) which have developed above local decollement horizons. On a broad scale, fold axial planes are steeply inclined or subvertical between Bude and Widemouth, and farther north near Hartland Quay they are steeply inclined to the south. The folds become south facing with shallow north dipping or horizontal axial planes between Wanson and Miliook Haven. These transitions of fold attitude and facing across the basin were described by Zwart (1964) and Dearman (1969), with the general southerly decrease of interlimb angle and overturning of fold axial planes discussed by Sanderson (1974, 1979) who modelled the rotation in terms of south-directed simple shear. The effects of this overthrust shear in terms of modifications to individual pre-existing, upright chevron folds was noted by Zwart (1964) and Dearman (1967), and later re-examined by Lloyd & Whalley (1986) and Whalley & Lloyd (1991).

	HARTLAND QUAY	DUCKPOOL	WIDEMOUTH-WANSON	WANSON-FOXHOLE POINT	MILLOOK-CRACKINGTON
AXIAL PLANE	Inclined S	Subvertical	Subvertical	Subvertical or inclined N	Recumbent or shallowly inclined N
INTERLIMB ANGLE	50-60°	45-90°	45-60°	25-55°	25-45°
SHORTENING*	45%	≈30%	30-50%	≈45%	≈50%
FLATTENING*	-	-	20-30%	30-40%	30-50%
CLEAVAGE	Weak/moderate	Weak	Weak	Moderate	Moderate
FOLD ENVELOPE	Flat	Flat	Flat	Flat, inclined N	Inverted
OTHER STRUCTURES	Early contractional faults, duplexes	Early contractional faults	Wedge-faults, duplexes	Early contractional structures	E-W extensional faults

Table 2.1. Summary of the general structural features of the Culm Basin, and the structural changes associated with the main fold transition [* shortening estimated from fold 2θ angles after Sanderson (1974, 1979)].

UPPER CARBONIFEROUS (SILESIAN)						
NAMURIAN					WESTPHALIAN	Age
R_2			G_1		G_2	Goniatite Zones
a	b	c	a	b		
BIDEFORD FORMATION						North Devon
CRACKINGTON FORMATION					BUDE FORMATION	North Cornwall Coast

Table 2.2. Stratigraphic setting of the Crackington and Bude Formations as they occur in the coastal section of north Cornwall, based on Freshney et al. (1979).

Cleavage is only subordinately developed in the Bude Formation (Lower Westphalian), occurring as a slaty cleavage in the mud rocks, and occasionally as a weak spaced-cleavage in sandstones near fold hinges. Within the Crackington Formation (Namurian-Westphalian) cleavage is more penetrative and varies according to local structural position and lithology. Although these cleavages are approximately axial planar, several cleavage generations occur at some locations (Dearman 1967, Beach 1977).

Faults are common throughout the basin and show similar relations with vein and fold development. They can be divided into three overlapping categories: [1] early structures associated with episodes of layer-parallel shortening prior to folding (Mapeo & Andrews 1991, Jackson & Mapeo 1992) and faults accompanying fold initiation and amplification (Whalley & Lloyd 1986, Mapeo & Andrews 1991, Tanner 1989, 1992); [2] faults which modify folds or accommodate shortening during folding (Ramsay 1974, Lloyd & Whalley 1986, Whalley & Lloyd 1991); and [3] faults which cut through all previous structures (Freshney *et al.* 1972).

2.3 GENERAL FEATURES OF VEIN SETS

2.3.1 Vein distribution

The vein sets are confined mainly to sandstone units within an interbedded sequence of sandstones and shales, and they are generally oriented at high angles to bedding. Vein distribution is also affected by other factors apart from the host rock properties. These include sedimentary and bedform features such as ripple and prod marks, and load casts at bed interfaces (Fig.2.2a). A range of vein outcrop configurations can be observed at localities around Millook Haven, and elsewhere within the Crackington Formation. Figure 2.2 shows a selection of typical vein configurations for Millook Haven which are described in their accompanying captions, and in the following sections.

Figure 2.2

[a] Veins confined to troughs of a rippled sandstone bed, showing that bedform geometry can have a mechanical effect on vein initiation and growth (Millook Haven: inverted fold limb).

[b] Outcrop configuration for veins in normal limbs, Millook Haven. This vein set is characterised by numerous closely spaced and overlapping veins, and en echelon veins with a range of vein-array angles.

[c] Conjugate en echelon and strongly overlapping vein sets in normal limbs at Millook Haven.

[d] Criss-cross outcrop pattern of veins in inverted fold limbs, showing examples of veln offsets.

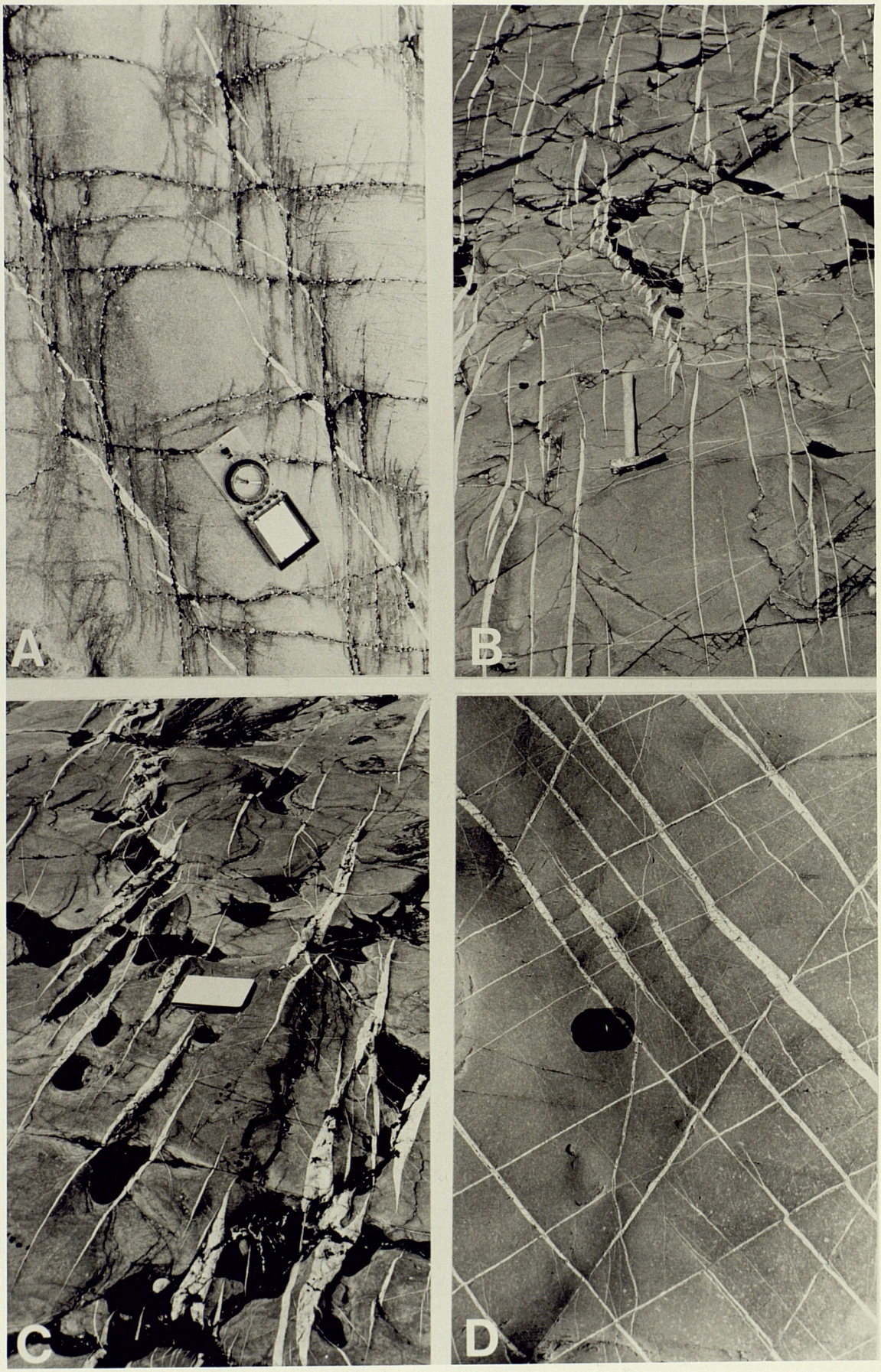
A
B
C
D

2.3.2 Morphology

At Millook Haven, there are a number of recognisable geometric forms for the veins: [a] single, overlapping or closely spaced; [b] en echelon [c] branched and forked; [d] kinked and curved and [e] pull-aparts and veins which link to produce small scale faults.

Overlapping

At localities in the Crackington Formation, few isolated veins have been observed: single veins are more commonly found as coplanar or overlapping arrays. Figures 2.2b and 2.2c show characteristic vein outcrop configurations, commonly seen on bedding planes within normal fold limbs at Millook Haven. These vein patterns consist of numerous coplanar and overlapping veins with a wide range of spacing values and geometries. Some of these veins occur in en echelon or conjugate en echelon arrays (Fig.2.2c). Figure 2.2d shows a vein pattern that is common for the inverted fold limbs at Millook. This criss-cross geometry is made up of several overprinting vein sets, where earlier primary vein geometries have been modified, or have been subsequently loaded and cross-cut by later phases of veining. In Fig.2.2d cross-cutting and offset relations are clearly visible.

A vein can be described as being effectively *isolated* when it is separated from neighbouring veins by a distance $\geq$ the vein half-length. This means that the region $\leq$ vein half-length defines a critical radius, within which significant mechanical crack interactions are expected (Chapter 3, Lawn & Wilshaw 1975). The development of these types of vein configurations are examined in Chapter 3.

En echelon

Veins often form arrays characterised by left and/or right stepping, overlapping cracks (Fig.2.3). En echelon arrays usually contain veins of constant orientation and overlap, although some may contain smaller, subarrays with different senses of step. The volume of rock between overlapping veins, which maintains wall-rock continuity between veins in arrays, are termed *bridges* (Farmin 1944, Nicholson & Pollard 1985) (Fig.2.3). These show a variety of morphologies often with differing aspect ratios, curvature, and fracturing (Fig.2.3). Their morphology is dependent on array geometry and propagation history, since bridges generally have to bend and rotate or fracture (Figs.2.2b and 2.2d) to accommodate vein dilation.

Figure 2.3

[a] An example of part of a planar vein showing a rotated and fractured bridge with lateral extension fractures.

[b] Example of a vein array showing distinctive wedge-shaped terminations and incipient-fracture of the rock bridges.

[c] Example of a vein array with relatively planar bridges which have been subject to negligable amounts of rotation during vein dilation. Several veins display forked terminations.

[d] Example of a vein array with rock bridges cut by secondary fractures. Some of the vein tips show branched or forked terminations. Individual veins represent a wide range in the amounts of dilation.

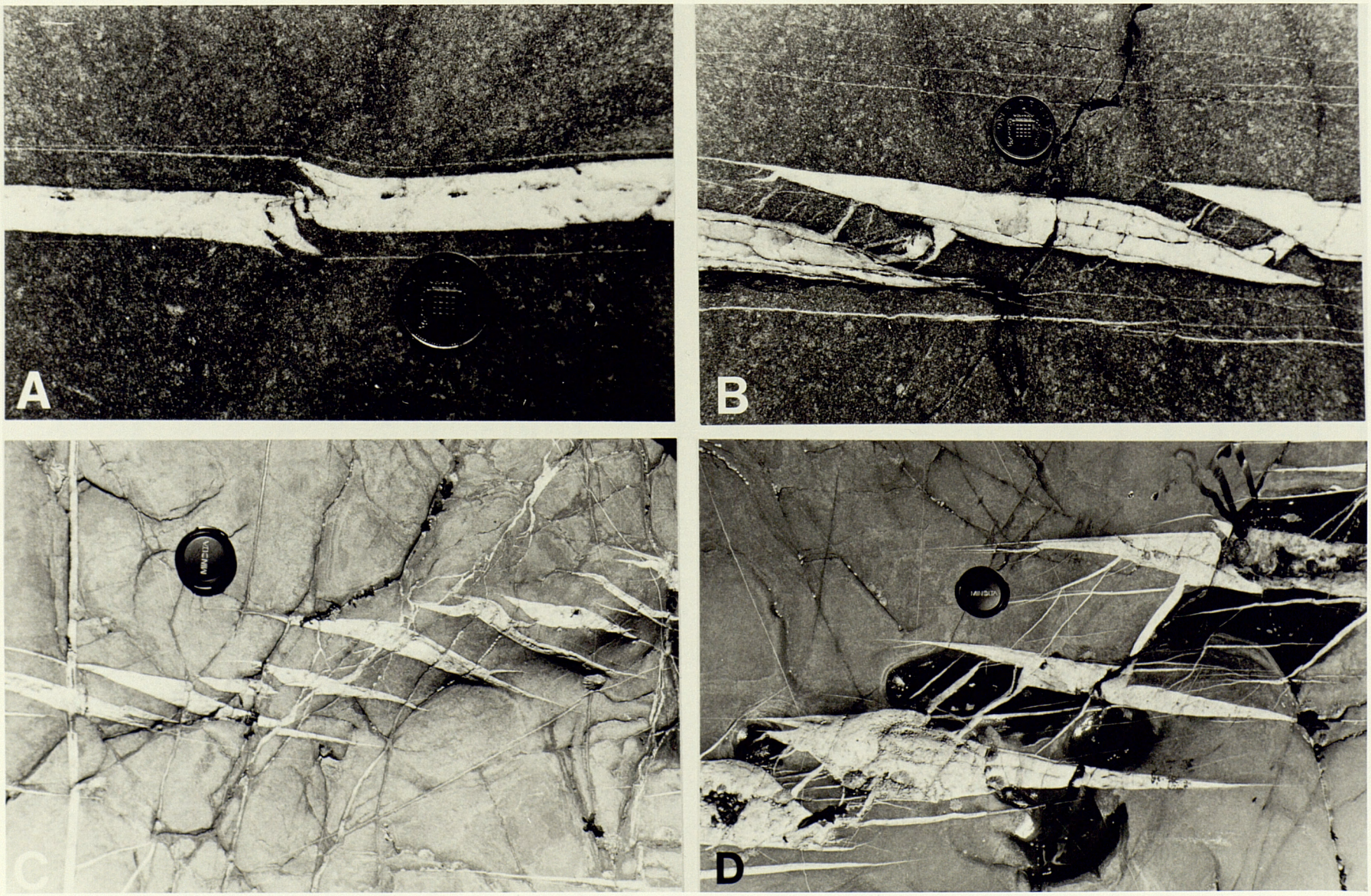
A
B
C
D

Branched and forked

Angular symmetric or asymmetric forks and branches are commonly found near vein terminations. Figures 2.2c and 2d show several examples of crack forking for veins in en echelon arrays. In the fracture mechanics literature several models have been postulated to explain crack bifurcation: [a] instability of the crack tip stress intensity with consequent secondary fracture initiation or [b] dynamic crack growth under conditions of increased energy release rate, *G* (Lawn & Wilshaw 1975, Ingraffea 1987). This indicates that some of the vein termination structures can either represent mechanical interaction during initial growth, *ie*. they are mixed-mode fractures; or alternatively, where vein fill is discontinuous in structure or texture, they may be the product of subsequent loading along a pre-existing parent vein. Dynamic growth could be dismissed for most veins, since quasi-static or subcritical crack growth is more realistic under geological conditions.

Curved and kinked

Curved and kinked cracks are minor structures which form near the terminations of a larger parent vein, and whose trend is abruptly different from that of the parent vein. This group of structures includes: [a] splay and tail-cracks, [b] horsetails and [c] pinnates. They are generally associated with the subsequent modification and loading of pre-existing cracks. Observational and theoretical studies (Cottrell & Rice 1980, Olson & Pollard 1989, Pollard & Segall 1987) indicate that mode I crack growth on a pre-existing, planar crack will change propagation direction (*ie*. kink) if the host crack is subjected to sufficiently intense mixed mode I-II loading. This kink direction is the direction which maximises K_I and reduces K_{II} (mode I, II stress-intensity factors respectively) at the tip of each new crack increment. This suggests that the veins will propagate away from the host vein at an angle which maximises the local tensile stress acting across the incipient propagation path. So these structures which form near, and propagate away from vein terminations (and margins) can be used to indicate the sense of slip accommodated by the host crack and also the maximum compression direction traced out at the time of initiation. Type examples of these types of structures, and their mechanism of formation are illustrated and analysed in Chapter 3.

Figure 2.4

[a] An example of part of a compound vein pull-apart from Saltstone Strand [1865 0055], which has developed into a small scale fault. Offsets along the fault can clearly be observed from the vein fibres and from the displacement of ripple-marks on the bedding surface (marked in chalk). Slip along this array has been transmitted through a series of bends by the formation of rhomb-shaped vein pull-aparts. The amount of vein opening is approximately equal to the slip transmitted through each bend. Splay or tail-cracks and en echelon veins are present at both terminations of this fault.

[b] Close-up view of part of the southern termination of the structure, where details of the pull-apart and fibre geometry can be observed.

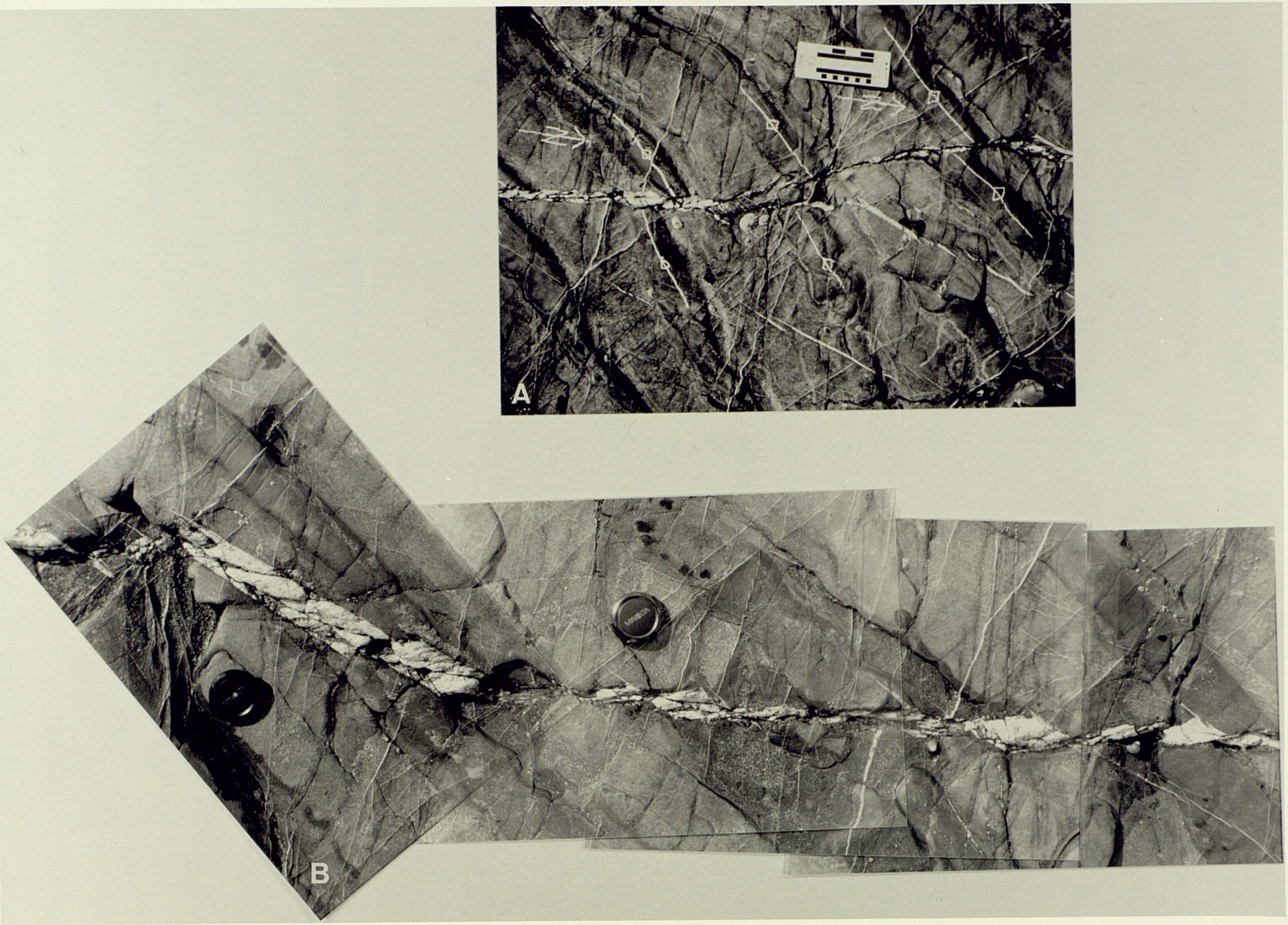
A
B

Pull-aparts and small scale faults

Secondary fracturing often occurs in the rock bridges, or in steps and bends of some en echelon arrays. Where fractures bridge, and link the steps in echelon crack arrays, either through mechanical interaction or by subsequent loading, rhomb-shaped cavities commonly form. These structures are termed vein pull-aparts. If extension fractures link the segments further, then slip along the array can be accommodated by opening of the rhomb (pull-apart) with the opening approximately equal to the slip transmitted through the step or bend. Eventually these structures may fuse to form small scale compound fault zones.

Figure 2.4 shows an example of this type of structure on a bedding surface in the Crackington Formation, near Saltstone Strand. Figure 2.4a shows a detail of the central part of the fault, with rhomb-shaped vein pull-aparts and a secondary splay structure. The opening and shear displacements are clearly indicated by the offsets of the sedimentary ripple marks. Figure 2.4b shows a closer view of the southern termination, where details of the pull-apart and fibre geometry can be observed.

2.4 VEIN TEXTURES

2.4.1 General overview

The veins described here are from outcrops around Millook Haven and Hartland Quay. They are infilled with quartz and carbonate (ankerite or siderite). Both minerals are intergrown, although quartz is more abundant than carbonate. Minor amounts of chlorite have been reported for some veins from the Hartland Quay area (Beach 1977, Kerrich *et al.* 1978); this was not observed for the samples investigated here.

A variety of vein fibre morphologies and growth habits which occur together, have developed contemporaneously. Representative examples of these from Millook Haven have been examined in

Figure 2.5

[a] Polished slab of part of a vein array, showing the composite infill geometry (horizontal field of view 60mm).

[b] Thin-section (XPL) of part of a vein array showing bridge and infill geometry. This example illustrates the asymmetric and composite structure of the infill. There is an early crack-seal rind, adjacent to one side of the vein separated from domains of equant and columnar grains. Grain nucleation along the partition is initially random. These features suggest initial crack-seal fibre growth, followed by successive increments of antitaxial growth. The bridge between the veins is unbroken, parallel sided and curved with the fibres and columnar morphologies radially arranged. Note the large patches of carbonate druze (horizontal field of view 60mm).

[c] General view of composite vein structure showing the fibrous and irregular druze domains separated by a partition surface. In detail the partition surface is irregular and comprises layers of included wall-rock and fine grained silicates. The fibrous zone comprises of intergrown quartz and carbonate with their long axes length slow and inclined at high angles to the vein margins.

[d] Columnar and interpenetrant growth habits.

[e] Serrated and sutured grain boundaries indicating that local dissolution and some modification of the primary growth textures has occurred.

[f] Carbonate inclusions forming nearly euhedral rhombs within a groundmass of finer grained carbonate.

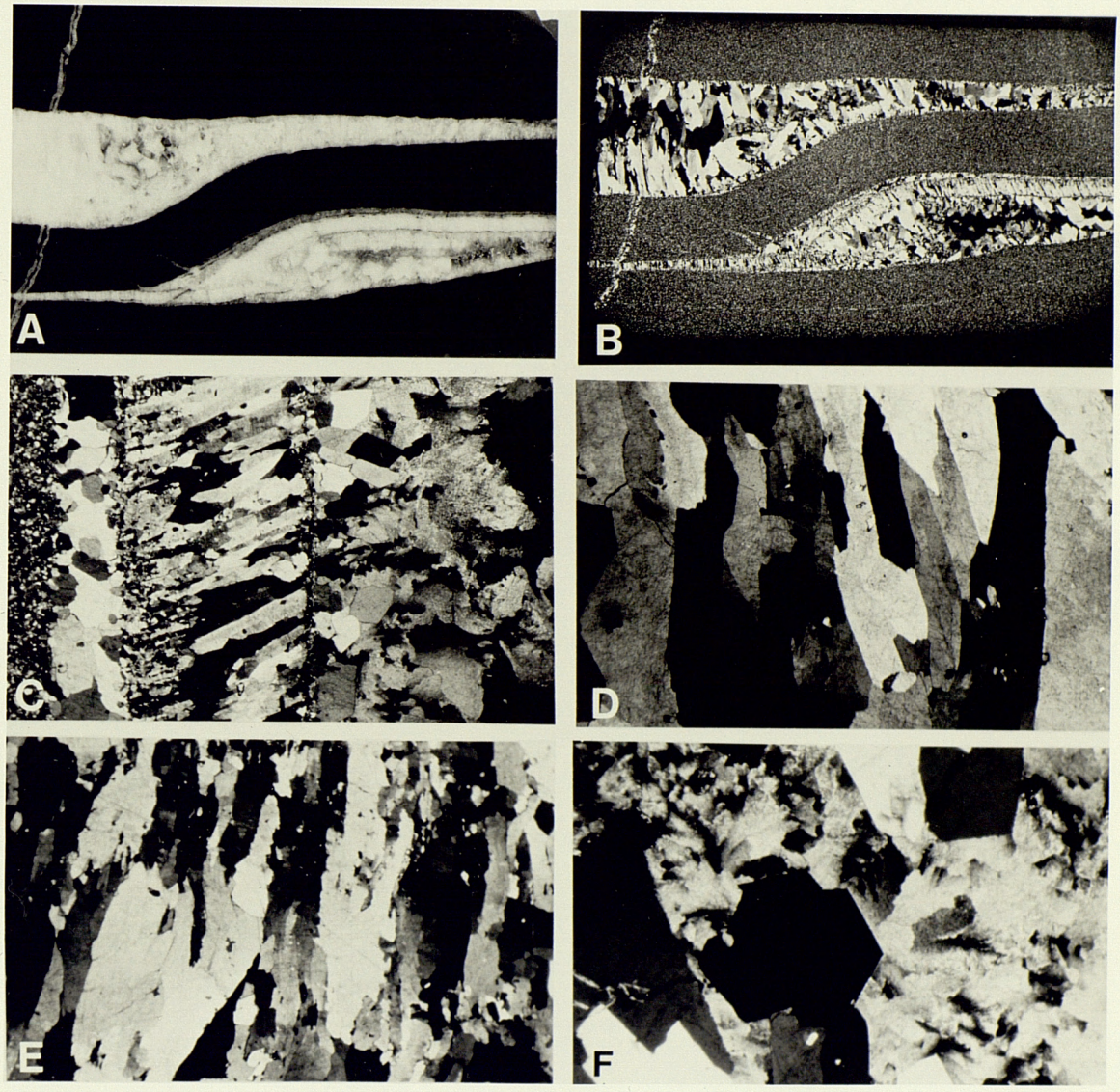
A
B
C
D
E
F

thin-section and polished slabs. For individual veins there are often complex variations of internal composition and texture. Several microstructural domains can be defined. Many of the veins are characterised by axially distributed fibrous domains separated from a domain containing textures typical of druzy infill. However, the most significant aspect of structure, especially for veins in echelon arrays, are their composite growth histories involving both antitaxial and composite crack-seal processes (Durney & Ramsay 1973, Ramsay 1980, Cox 1987) and growth in a free-fluid.

2.4.2 Microstructures

Most veins are fibrous in thin section with many infills comprising of both fibrous morphologies and more equant habits. Figure 2.5a shows a polished slab of part of en echelon array from Millook Haven. In thin-section (Fig.2.5b) this example is seen to have a composite infill history. The growth textures are asymmetric, and crack-seal and druze-infill habits occur together.

Figure 2.5c shows a profile through part of the vein, illustrating the change of growth habit towards the vein centre. At the crack margins subequant grains are present which display no crystallographic preferred orientation (Fig.2.4c). This suggests a general lack of growth off the crack walls. Where an adjacent fibrous zone is present, it is narrow, and for most of the examples examined, it is in the range < 1-10mm wide. This zone contains fibrous intergrowths of quartz and carbonate with their long axes length slow and inclined at high angles (65-90°) to the vein margins (Fig.2.4d). Some examples are slightly curved or sigmoidal. This zone then passes into a domain of coarse equant and irregular shaped grains separated by a subplanar partition surface (Fig.2.4c)(Cox & Etheridge 1983, Cox 1987). These surfaces consist of thin layers of opaque, fine grained material and included wall-rock fragments. Many samples contain several different partition surfaces.

The domain of coarse and irregular grains contains growth habits of the type attributed by Beach (1977) to the infill of fluid-filled cavities. At crack margins or adjacent to partition surfaces no crystallographic preferred orientation of grains was observed. Grain shape, size and orientation are variable, with subhedral and wedge shaped grains, and grains with columnar and fibrous habits developed. Grain boundaries for the columnar forms are unilateral and interpenetrant (Fig.2.5d). The

number of grains generally decreases away from the domain boundaries, although patches of fine grained quartz intergrown with carbonate occur. Some of these carbonate inclusions form nearly euhedral rhombs (Fig.2.5f) in a groundmass of fine grained carbonate. Because of the extreme birefringence of the carbonate, little of the textural features of this infill type were visible. However, where visible some of the samples contained narrow twins with low intensities. Figure 2.5e indicates that some local dissolution has occurred, as many grains have serrated and sutured edges; non-equilibrium substructures are also often developed (*eg.* mosaic texture).

2.4.3 Interpretation of microstructures

The examples discussed here demonstrate that vein growth and dilation usually involves several different crack-seal processes and growth mechanisms, which leads to the formation of varied textures within individual veins and echelon arrays. As a result, veins often have composite growth histories, which involve more than one stage of opening and sealing. At Millook Haven the veins exhibit syntaxial and stretched-grain crack-seal habits; antitaxial microstructures; columnar grains which develop fibrous morphologies; and subhedral-irregular habits more typical of druze infill (Beach 1977). For the composite veins in arrays, growth generally involves initial formation of coplanar crack-seal veins followed by antitaxial growth. This can involve detachment and subsequent overgrowth of the initial fibrous zone (both internally and adjacent to the wall-rock) followed by druze infill (*cf.* Nicholson 1991). The formation of the irregular and subhedral infill may be a reflection of the vein growth kinetics. Inclusion band separations described for crack-seal veins, typically have increment lengths of 0.01-0.1mm (Ramsay 1980, Cox 1987). So if fibre growth surfaces fail to maintain equilibrium with crack propagation and dilation, fibrous morphologies cease to develop and euhedral habits are favoured.

The examples of veins examined from Millook Haven suggest that the primary vein growth textures are overprinted or modified to varying degrees by dissolution-precipitation processes. These effects are only locally important and generally indicate low strains. Some of these deformation features probably formed during stages of vein growth, while others may be attributed to modification during regional deformation and fold development.

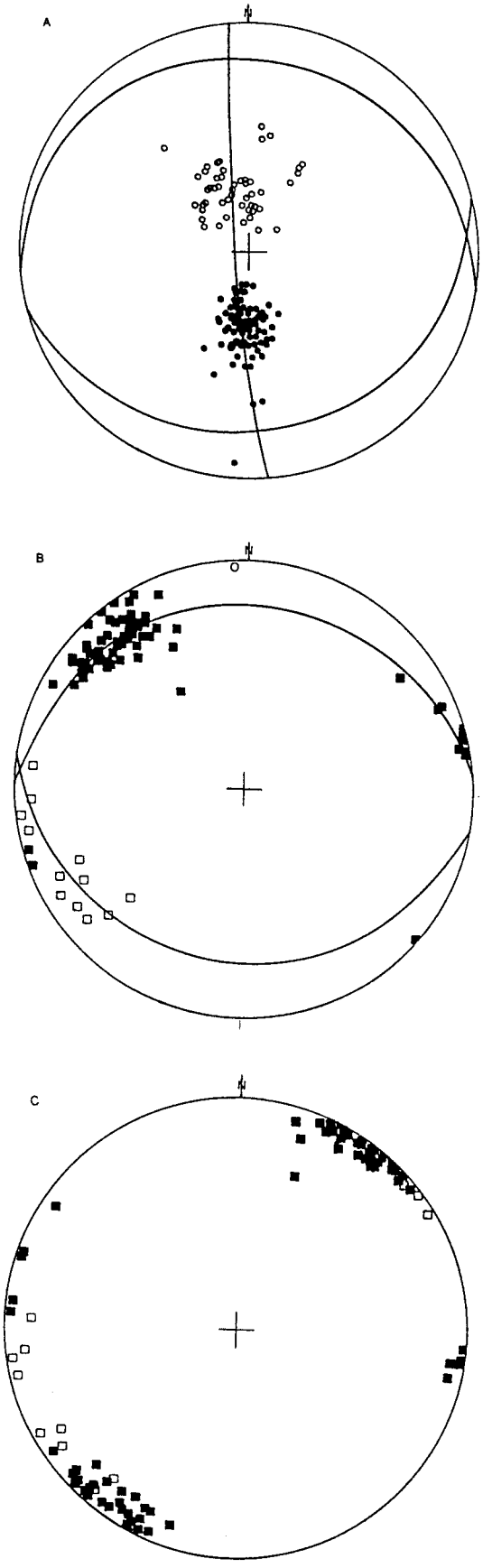

Figure 2.6. Orientation data for Millook Haven: [a] Poles to bedding for normal (o) and inverted limbs (●)(n = 215) [b] Poles to veins for normal limbs (empty squares) and inverted limbs (solid squares)(n = 88) [c] Poles to veins after rotation about the fold axis to horizontal.

2.5 MILLOOK HAVEN

Previous work by Mackintosh (1967) and Beach (1977) indicated that some veins at this locality can be related to early phases of deformation which pre-date folding. However, no detailed analysis of their kinematics was given. In the sections following, the early regional vein set and its subsequent modification during folding is described. Other vein sets do occur, which have formed through a variety of processes, *eg.* hinge stretching and limb accommodation, and fibre-sheets produced during flexural-slip. These vein sets are not discussed here.

Structure

At Millook Haven the folds are recumbent and south-facing with virtually horizontal (0-10°) E-W axes (Fig.2.6a). These folds are asymmetric with unequal length limbs. The north dipping inverted limbs are longer, and in some cases up to 20% thinner relative to the shorter, normal limbs. Fold interlimb angles are in the range 25-60° (mean ≈ 45°), indicating that some folds probably accommodated subsequent shortening increments after lock-up through flattening. This has mainly occurred through the formation of limb and hinge accommodation structures, and cleavage. Sanderson (1974) described the variation of shortening strain in these folds, suggesting that flattening (pure shear) after lock-up represents 20-30% of shortening. Faults trending E-W, sub-parallel to strike are present which cut through both normal and inverted limbs and hinges. These faults cut bedding at angles of 20-70° and are inclined more steeply in normal limbs than in inverted limbs, where many examples eventually pass into bed-parallel detachments. These faults are clearly extensional, as they relate to lengthening of fold limbs. Some of these structures were attributed by Ramsay (1974) to accommodation during chevron fold-development (see Ramsay 1974, fig. 26b). However, this fault geometry is common throughout the coastal section, particularly between Wanson Mouth and Tintagel (Freshney *et al.* 1972).

Normal fold limbs

At Millook Haven in the normal fold limbs the dominant vein set mainly comprises of planar, constantly oriented veins (V_1 of Mackintosh 1967) with a mean azimuth of 130° (Fig.2.7a). The outcrop patterns for this vein set (Fig.2.2b) indicates that many of the veins are strongly overlapping. This

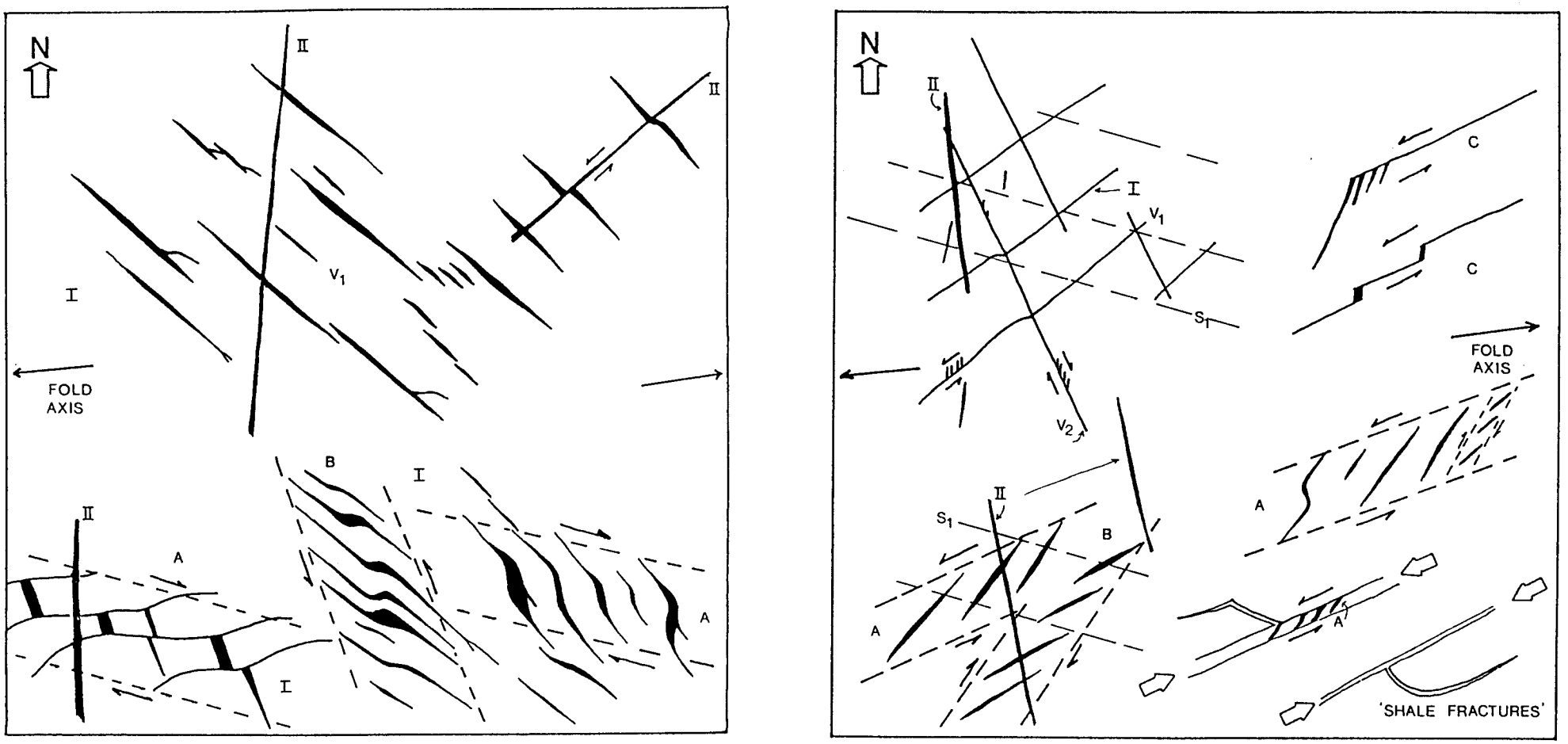

Figure 2.7. Map view summary of vein sets exposed on bedding-plane surfaces at Millook Haven (not to scale) for: [a] Normal limbs (conjugate sets of en echelon veins are A and B; regionally distributed and overlapping veins (V_1) with forked and branching terminations), and [b] vein sets exposed on bedding-plane surfaces for inverted limbs (conjugate vein sets are A and B; branching terminations (S); pinnate veins (P); and irregular shale-filled cracks). S1 is the local trend of the spaced solution cleavage.

configuration is rather unusuai since the veins are relatively planar, and show few features diagnostic of mutual crack interaction, which would be expected for closely spaced, overlapping veins. Some of the larger, planar and composite veins have forked terminations. Measurements of fibre orientations for this vein set (Fig.2.8a) indicate that they are generally at high angles (70-90°) to vein margins, although some are more oblique, *ie.* <70° (sinistral). The sinistral component suggests this vein set either opened subparallel to the remote principal stress, σ_1, or, alternatively was subsequently loaded at a high angle.

Many of these veins occur as en echelon arrays, some of which merge vertically or horizontally into single, planar veins. These en echelon veins sometimes form conjugate sets (Beach 1975) with mean array trends of about 095° and 165° (*A* and *B* respectively, Fig.2.7a). The vein arrays show a continuous variation of geometry with straight and sigmoidal profiles, a range of bridge morphologies, and variable amounts of dilation within individual arrays and between adjacent sets (Fig.2.3). In some arrays the veins are strongly curved or kinked, suggesting there has been significant mechanical interaction within the arrays. Some of these veins reach large dimensions and so represent significant amounts of dilation and extension. The effects of solution transfer are often very apparent since many veins are truncated against solution-seams (Chapter 5). There are later vein sets present with near N-S orientations which cut through or offset all these vein sets and the spaced cleavage.

Inverted fold limbs

In the inverted fold-limbs the vein geometries are more complex than the normal limbs. There are two dominant vein sets (Fig.2.7b) (V_1 & V_2), which often intersect to form a crisscross network on bedding-plane surfaces (Fig.2.2d). The mean azimuths for these sets are: V_1 050° and V_2 160°. They do not generally occur as discrete, planar veins as on the normal limbs. However, some veins of the 050° set are identifiable as discrete veins, where many examples have thin forks or branches that often extend for several metres. Measurements of vein fibres (Fig.2.8b) indicate opening directions for V_1 were at high angles to the vein margins, or slightly oblique (dextral). V_2 fabrics are also at high angles, or slightly oblique (sinistral). The intersections and offset structures for these veins indicate that both dextral and sinistral offsets are produced for V_1 and V_2. Pinnate veins and pressure-solution zones

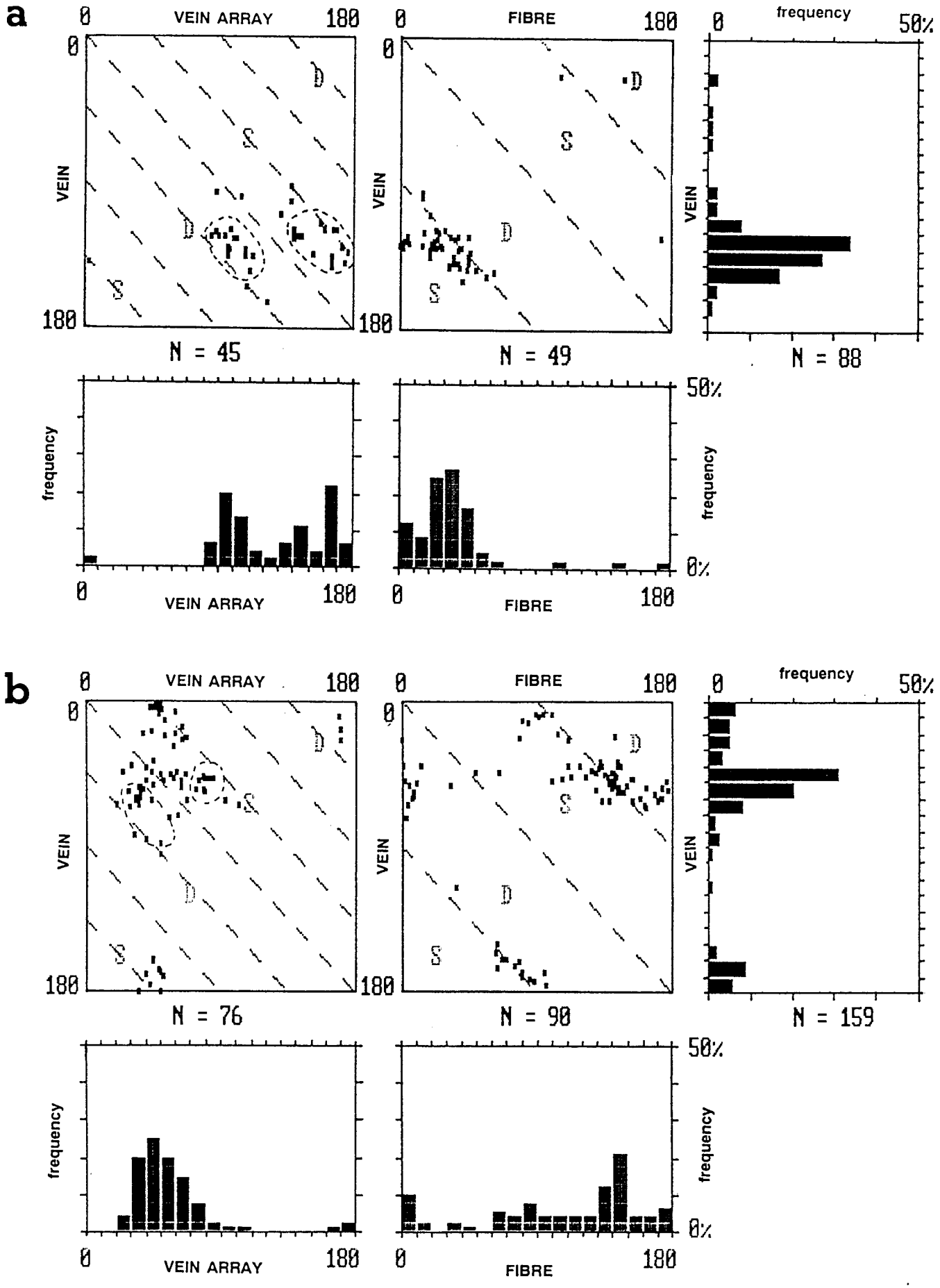

Figure 2.8. Orientation data for veins (azimuths) from Millook Haven for [a] normal limbs and [b] inverted limbs. D and S represent dextral and sinistral senses of displacement. The hatched fields outline conjugate en echelon vein sets.

(Fig.2.7b) which are common to many examples, indicate slip subparallel to the vein margins. These features suggest that both sets were sheared and modified during a subsequent loading of V_1 and V_2 in an approximate N-S direction (Chapter 3). Beach (1977) incorrectly interpreted these vein sets as contemporaneous conjugate sets of shear fractures (wrench type).

Although V_1 and V_2 were subsequently loaded synchronously, they did not initiate as conjugate shear fractures. This relationship is only an apparent one, because as is later demonstrated, V_1 veins are folded around the fold-axes, so they pre-date the folds. The V_2 set is not seen in normal limbs, so it is likely to be syn-fold, indicating that the principal compressive stress, σ_1 orientation determined for the pre-fold set V_1 was maintained during folding. For the V_2 set to be initiated in the same stress system as V_1 veins, the fold-limb would have had to rotate through the vertical and into the extensional field of the shear couple. V_1 veins are common to both fold-limbs and are folded about the subhorizontal fold axes. On the normal fold limbs this set trends NW-SE, while on the inverted limbs it is in a general NE-SW direction. Direct evidence of this is present at Foxhole Point where individual veins can be traced on bedding surfaces across and around fold-hinges. Compared to the normal fold limbs, these limbs contain vein sets which display evidence of having being subsequently loaded and modified. The spaced cleavage in the inverted limbs is also more penetrative than in the normal fold limbs.

Pre-fold vein initiation and syn-fold modification

The pre-fold hypothesis for the veins at Millook can be tested by rotating the veins with bedding, about the mean fold axis to the horizontal. The orientations of veins for normal and inverted limbs can then be compared. Vein orientations measured in the bed profile are thought to have undergone negligible modification during folding. Figure 2.6b shows the orientation of the V_1 and V_2 veins in their present attitude and Fig.2.6c after the correction procedure has been applied. There is a good correlation for vein orientations between fold limbs. For these veins, after restoration, the orientation within bedding prior to folding is NW-SE (320°). This orientation is markedly oblique (*ie.* they did not originate in a stress field symmetrical to the folds) when compared to the general E-W trend of the fold-axes (086°) and for folds throughout the Culm Basin.

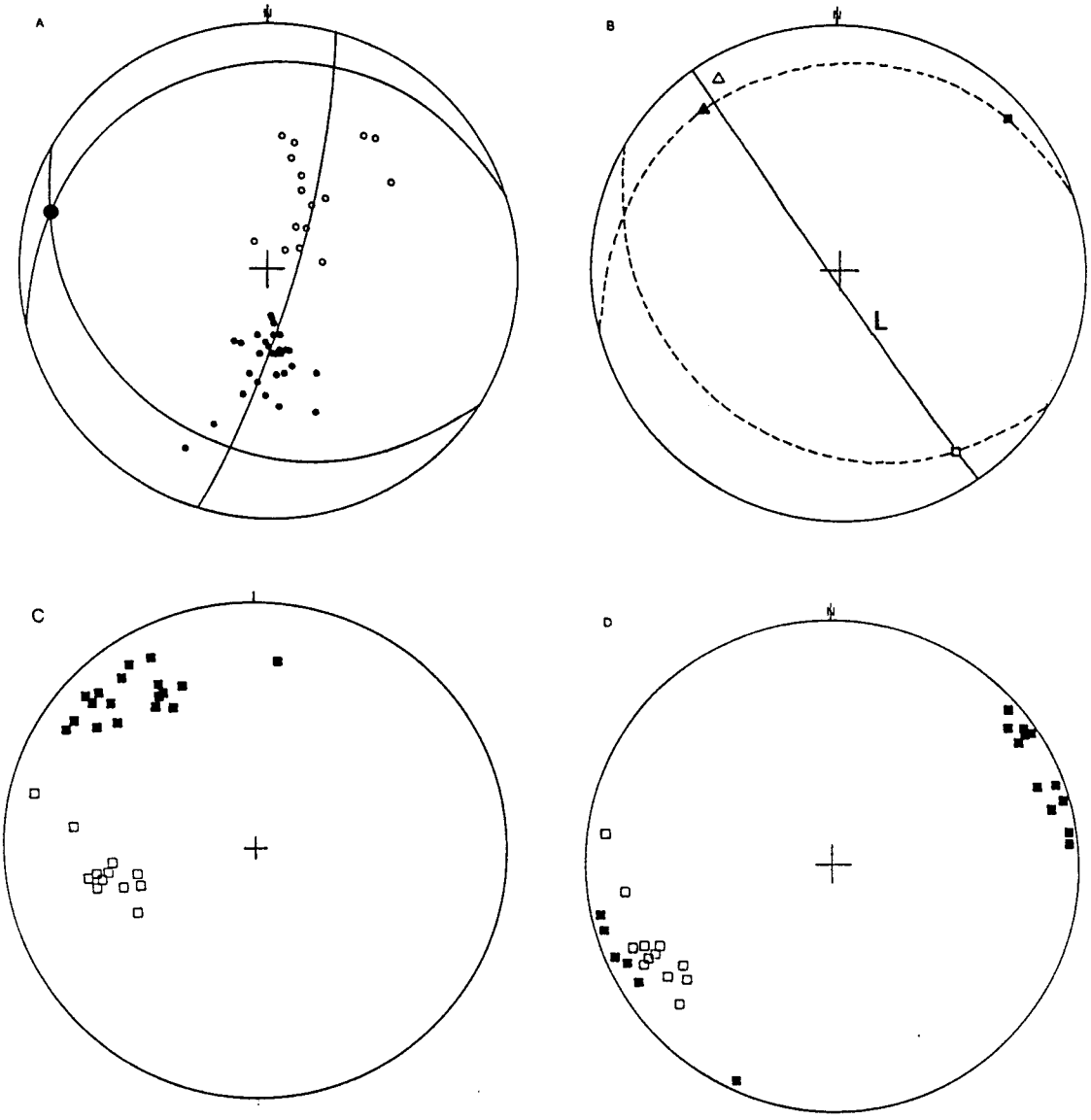

Figure 2.9. Orientation data for Foxhole Point: [a] Poles to bedding for normal (o) and inverted (●) fold limbs [b] Bedding-vein intersection lineation for vein sets on normal limbs (□) and inverted fold limbs (■) in their present position. The veins have been corrected for tectonic rotation by rotating them with bedding about the fold axis, to the horizontal (veins in normal (△) fold-limbs and inverted (▲) fold-limbs). Note that they are oblique to the fold axis orientation. The line (L) through the stereogram shows the mean azimuth of the vein sets, after unfolding about the fold-axis. [c] Poles to veins for the normal (o) and inverted (●) fold-limbs. (d) Poles to veins for both limbs, after rotation within bedding, about the fold axis to the horizontal.

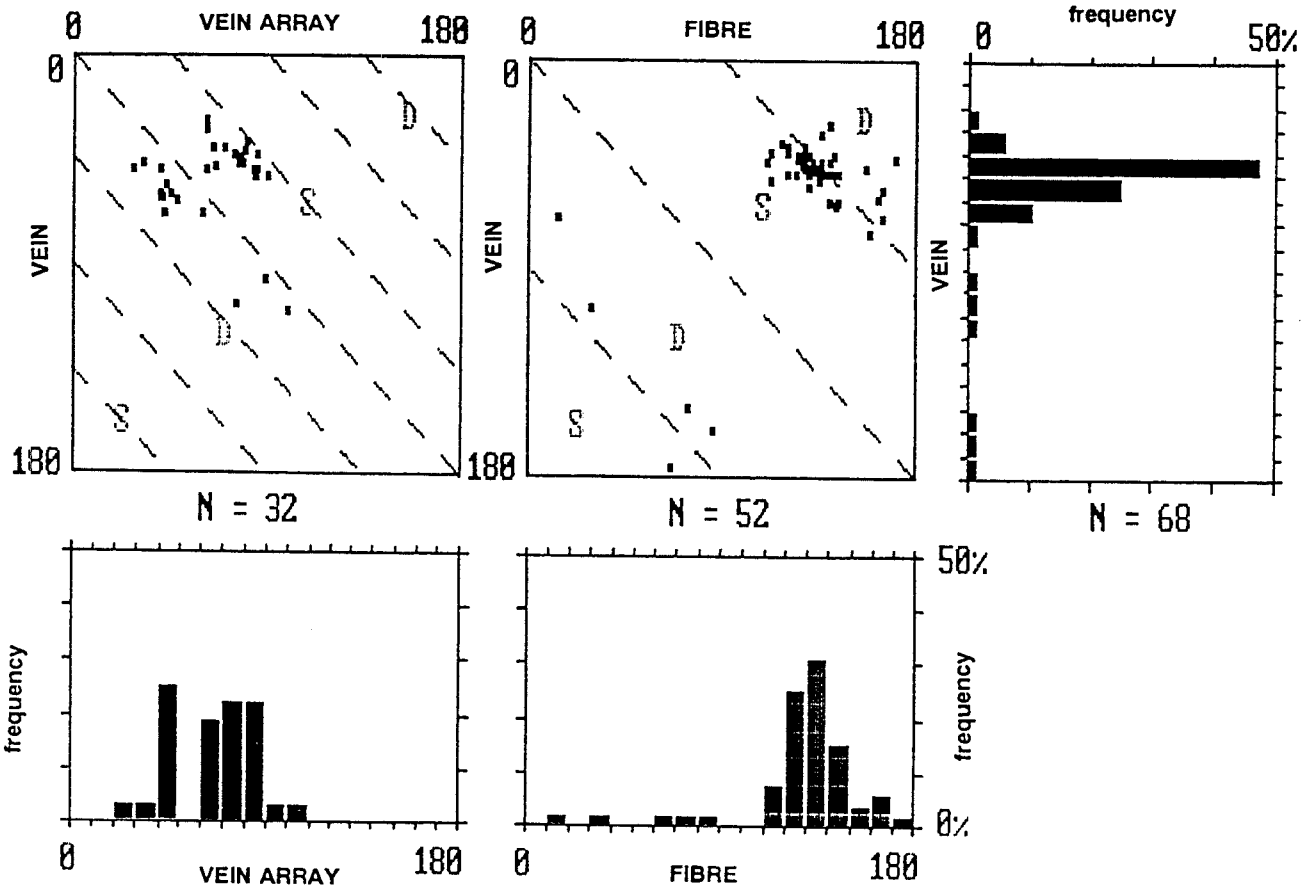

Figure 2.10. Orientation data for veins (azimuths) from Foxhole Point for inverted fold limbs. D and S represent dextral and sinistral senses of displacement.

2.6 OTHER LOCATIONS

2.6.1 Wanson Mouth-Foxhole Point

To the north, between Widemouth [199026] and Wanson Mouth [198013], the folds are upright or slightly overturned to the south with axial planes dipping about 80° N. Farther south, between Wanson Mouth and Saltstone Strand [1917 0086] the folds are asymmetric and overturned or with axial planes shallowly inclined northwards (10-45°). Between Saltstone Strand and Foxhole Point fold limbs are generally inverted and north dipping. At Saltstone Strand the fold axial planes are shallowly inclined to the north. A variety of vein geometries occur, and many are consistent with those described for Millook Haven. Folds exposed in the cliffs above Saltstone show a continuous range of minor asymmetries with axial surface dips of 0-45° N (*cf.* Freshney *et al.* 1966, fig.3) which are consistent with folds lying on the normal limb of an antiform (Freshney *et al.* 1972). A number of small-scale fault zones which trend N-S and post-date the folds, are exposed in the foreshore.

At Foxhole Point [186007] the folds are recumbent, with longer inverted, downward-facing limbs. At this locality the fold axes trend WNW-SSE, with a mean attitude of 8/286° (Fig.2.9a). Some of these fold axes are curved. The geometries of veins exposed on inverted limbs are shown in Fig.2.10; the normal fold limbs were not exposed in plan view at this locality so their geometries cannot be compared. Figure 2.12b shows the intersection-lineation for a vein which was traced around a single fold at Foxhole Point which has then been restored to the horizontal. This example provides convincing evidence for the pre-fold hypothesis for V_1 veins at this locality and for Millook Haven. Three-dimensional measurements of vein orientations and their restoration to the horizontal are shown in Fig.2.9d.

2.6.2 Hartland Quay

Structure

Folding of the Upper Carboniferous rocks between Hartland Point [230277] and Hartland Quay [223248] show significant variations in fold geometry and internal deformation. The folds are generally

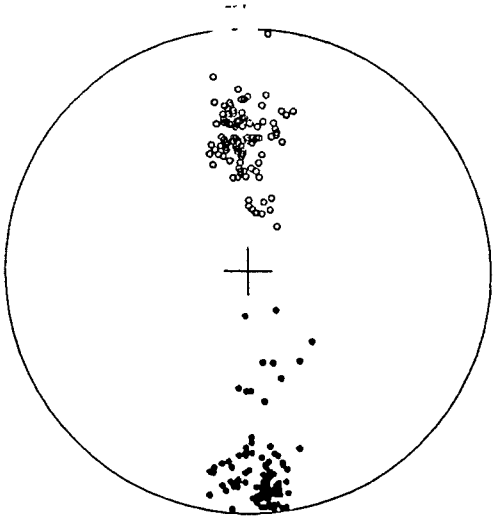

[a]

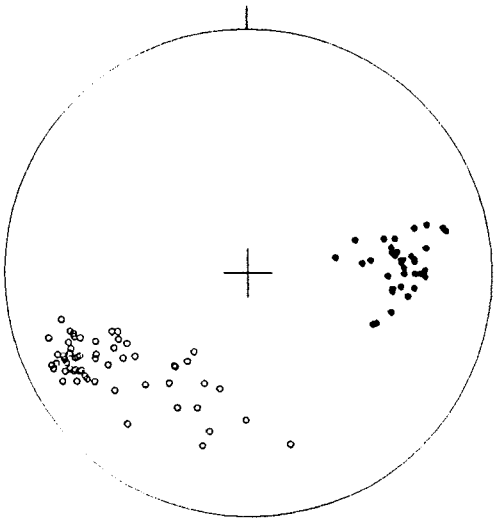

[b]

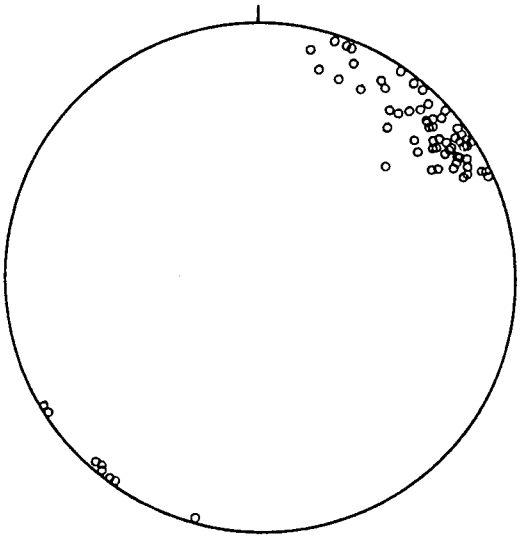

[c]

Fig.2.11. [a] Poles to bedding (n = 217) [b] Poles to veins and [c] veins corrected for tectonic rotation (n = 99).

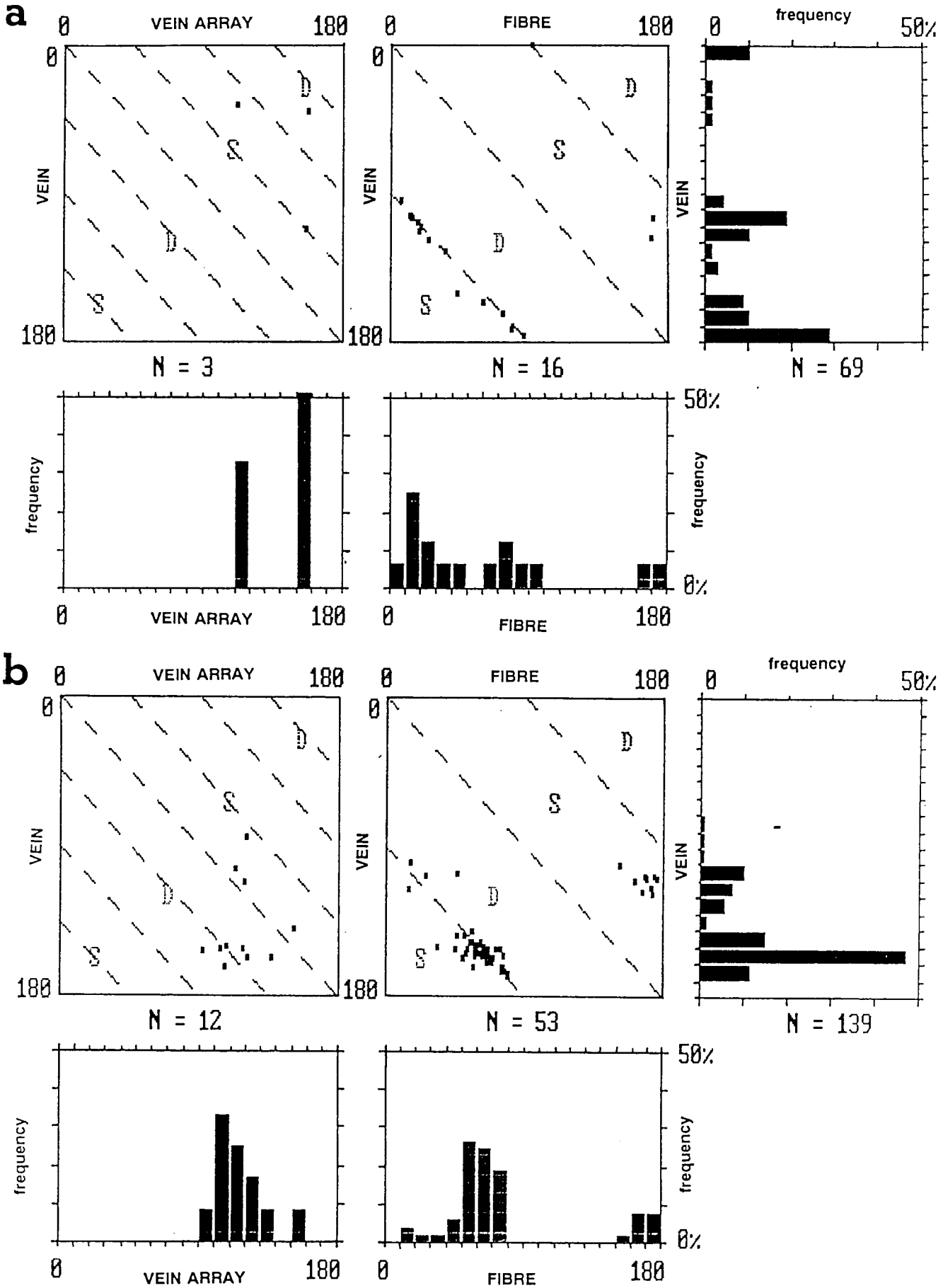

Figure 2.12. Orientation data for veins (azimuths) from Hartland Quay for [a] north dipping limbs and [b] south dipping limbs. D and S represent dextral and sinistral senses of displacement.

cylindrical with conical terminations and parallel or chevron profiles. Interlimb angles vary from 90-45° although they are more commonly 50-60° with a mean of 56° for the Warren Beach section [2225 2478] (Fig.2.11a). Here the folds are mostly asymmetric with limbs of unequal length. The north-younging limbs are shorter with dips in the range 70-90°; locally they are inverted. Some examples of overturned folds occur, as at the end of the slipway at Hartland Quay and at Speke's Mill [2262 2378]. Limb-thrusts, saddle-reefs and other geometric accommodation features (Ramsay 1974) are common. Axial plane surfaces are curvilinear and in cliff profiles they steepen upwards. The axial planes are inclined 45-90° southwards, mainly in the range 60-80° (Warren Beach mean dip 73/171°). Fold axes are virtually horizontal (mean cylindrical best-fit 2/086°).

Cleavage is subordinately developed and varies from a divergent-fanning slaty cleavage in the mud rocks to a convergent spaced cleavage in sandstones, near fold hinge zones. Laminated sheets of slickenfibres on many bedding planes indicate interbed slip approximately orthogonal to fold axes (*cf.* Tanner 1989). In detail the slickenfibre lineation patterns are more complex than this, several generations are present and systematic changes of orientation occur across folds. Some indicate slip oblique to the mean fold axis. Small scale duplex and imbricate thrust structures are commonly found. They show a wide range of orientations as a result of varying amounts of folding and flattening. The morphological features of some of these structures were summarised by Tanner (1989, 1992), who attributed their formation to flexural-slip during chevron-fold development. These structures although kinematically related to fold development, and remaining mechanically active until steeply dipping (≈60°), are perhaps more likely to have formed prior to fold amplification when initial limb dips were low (<5°) and in orientations which were favourable for layer-parallel shortening (Jackson & Mapeo 1992). Small subvertical NW- and NE-trending wrench faults with lateral displacements varying from a few millimetres to several metres are also present. Movements on these faults show several phases of vertical and horizontal slip.

Multiple phases of extension vein formation are also apparent (Hancock 1972, Beach 1977). The veins often occur as irregularly spaced, cluster zones (0.1m to 1.0m wide) which contain strongly overlapping veins. On bedding planes the veins may extend for tens of metres, usually greater than

the available outcrop. In plan view the veins have tapering profiles, often with forks and branches. The veins are mainly confined to single beds and terminate at bed margins, where some examples are locally displaced by bedding slip surfaces.

North limbs

During the study, 3D orientations of veins were taken wherever possible (Fig.2.11b). As many veins are exposed as lineations on steeply dipping or overturned beds, some measurements were recorded as pitches. Figure 2.12a shows data for north dipping limbs at Hartland Quay. There is one dominant set present, with a mean trend of 175° and an average attitude of 60/265°. The vein fibre plots indicate that the majority of these veins open at high angles to their margins (Fig.2.12a). En echelon vein arrays are also associated with this vein set; they are of the low angle and low overlap variety (Chapter 5).

South limbs

In the south dipping limbs the dominant vein set has a mean trend of 155°, and a mean attitude of 65/065° (Fig.2.11b). Figure 2.12b indicates that most examples from this set have normal opening displacements. On many of these veins subsequent loading effects are evident in the form of pinnate veins. They indicate mainly dextral slip. A set of low angle en echelon arrays are also associated with this vein set.

Pre-fold initiation test

Figure 2.11b shows poles to veins for the vein sets in north and south dipping limbs at Hartland Quay. Figure 2.16b shows their attitude after restoration to the horizontal: their coincidence supports the assertion that the veins have been folded around the fold axes, so these veins probably initiated prior to folding.

Prior to folding the veins had an orientation of NW-SE (320°)(*cf.* 326° of Beach 1977). This is asymmetric to the fold axes and oblique to the strain history implied by the fold geometry. This vein geometry which is very similar to the V_1 vein sets described from Millook Haven and Foxhole Point,

dextral transpression. In this present study of veins from Hartland Quay there is insufficient data to confirm if the folding was transpressional. However, the data described here supports the pre-fold vein hypothesis.

2.7 REGIONAL IMPLICATIONS

2.7.1 Pre-fold vein initiation

From the study of vein sets at Millook Haven, Hartland Quay and other locations, evidence has been accumulated that fractures initiated and grew prior to fold development. However their geometries were subsequently modified, as the fractures continued to grow, or they were loaded during fold initiation and amplification: in some cases new vein sets were generated. Some veins were probably initiated during episodes of layer-parallel shortening prior to buckling.

Many vein configurations for normal fold limbs at Millook, which typically comprise of strongly overlapping and closely spaced veins, lack many features considered to be diagnostic of mechanical crack interaction (Chapter 3). This type of geometry suggests that there was a high compressive remote stress parallel to the veins as they were apparently inhibited from changing their propagation paths (Chapter 3). Restoration of some of the veins to the horizontal indicates a pre-fold orientation of NW-SE (320°) prior to folding. As these veins are considered to be essentially compression-parallel fractures, this implies that the regional principal stress, σ_1 was subhorizontal within bedding in a NW-SE direction, *ie.* the veins indicate the minimum principal stress, σ_3 was subhorizontal in a NE-SW direction. From study of the kinematics of vein sets at Millook Haven and Foxhole Point, this NW-SE σ_1 orientation persisted during folding. This can also be inferred from the syn-fold V_2 set present in the inverted fold limbs at Millook which cut through, offset and displace many examples of V_1 veins. In the inverted fold limbs at Millook the V_1 and V_2 veins and their associated arrays are cross-cut or displaced across a penetrative spaced pressure-solution cleavage.

2.7.2 The fold transition sequence

The main upright to recumbent fold transition sequence between Widemouth Bay and Millook Haven has been described by Sanderson (1979). It shows a general southwards decrease of fold interlimb angle, and a corresponding increase in heterogenous pressure-solution, cleavage development, and vein formation. Sanderson (1979) modelled the changes in fold style in terms of a southerly directed simple shear modification to initially upright chevron folds. In detail the deformation is more complex, and there are several features, summarised below which suggest that this treatment should be re-evaluated:

[1] The differences in strain history between normal and inverted fold limbs.

[2] The obliquity of strain with respect to the fold axes. Vein geometries and kinematics for inverted limbs indicate higher and more non-coaxial strains than the right way-up normal limbs.

[3] The asymmetry of the folds in the inverted sequences with their longer, thinned inverted limbs suggests some sectional area change has occurred.

[4] Fold facing variations across the basin suggest north and south directed overthrust shear has occurred.

2.7.3 Transpression during fold development

In the previous sections it has been argued that the maximum regional stress σ_1, prior to fold development was NW-SE and that this was maintained during folding. This stress orientation is oblique to the E-W fold-axes and suggests that observed structural relations in the Culm Basin are not simply the result of N-S directed compression. This obliquity is consistent with dextral E-W transpression prior to and during fold development. Modelling the Culm Basin in these terms leads to horizontal shortening, accommodated by folding and thrusting, with a transcurrent shear parallel to the basin margins. Partitioning of the deformation would be expected and there would be complex

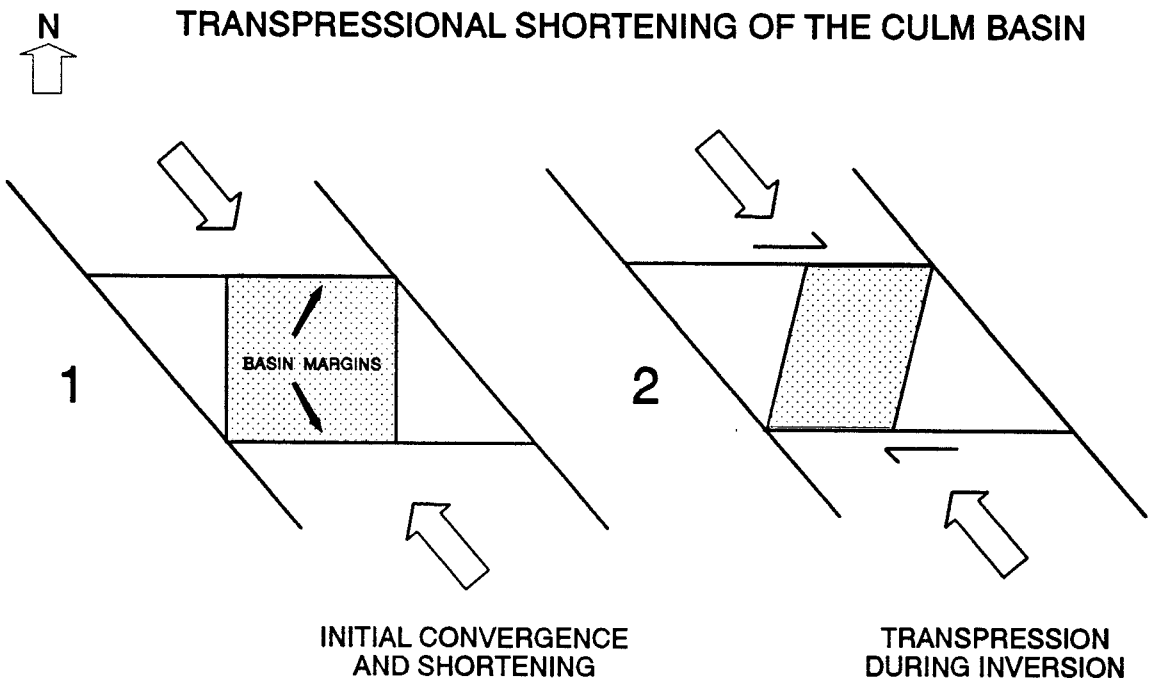

Figure 2.13. Schematic diagram to illustrate how transpression could be generated by oblique convergence and closure of the Culm Basin: [1] Initial convergence and shortening [2] transpression accompanied by folding and thrusting (north and south directed overthrust shear) during inversion of the basin.

strain patterns near the basin margins. In some cases leading to the reactivation of basin bounding faults as high-angle thrusts. Such features are geometrically consistent with the observed deformation and the overall structure of the Culm Basin, *eg.* the fold facing fan may represent extrusion of the basin fill.

Figure 2.13 shows how transpression might be generated in the Culm Basin by oblique convergence at the southern margin of the basin, *ie.* an approximate 320° convergence of an E-W striking basin. South of the Rusey Fault Zone and towards the Tintagel High Strain zone the regional Variscan transport direction is consistently towards the NNW, so transpression within the basin may be generated by the interaction between the regional shortening and the basin margins (if one assumes that the Rusey Fault Zone represents an original basin boundary). The transpression would then be a relatively local phenomena mainly restricted to the basin margins. However, the presence of these vein sets and their consistent fold relations throughout the Culm Basin suggests that early and syn-fold transpression occurred basin wide; although its effects are more pronounced adjacent to the basin margins. Recent reviews of the structural style of central SW England, which have been in terms of foreland basin or fore-deep development (Shackleton *et al.* 1982, Seago & Chapman 1988, Hartley & Warr 1990) followed by structural inversion (Selwood 1990) are compatible with the transpressional deformation and inversion envisaged for the Culm Basin. Additionally the suite of pre- and syn-fold contractional and extensional structures described by Mapeo & Andrews (1991) for the Bude Formation, indicate that the stress system required for their formation is comparable to that which has been determined for these early vein sets.

2.8 DISCUSSION

2.8.1 Vein formation and fold development

In the Wanson Mouth-Millook Haven section the application of rotational deformation models of fold development, such as those described by Sanderson (1979,1982) and Ridley & Casey (1989) allows observations of vein geometry and opening history to be compared with fold kinematics. Figure 2.14

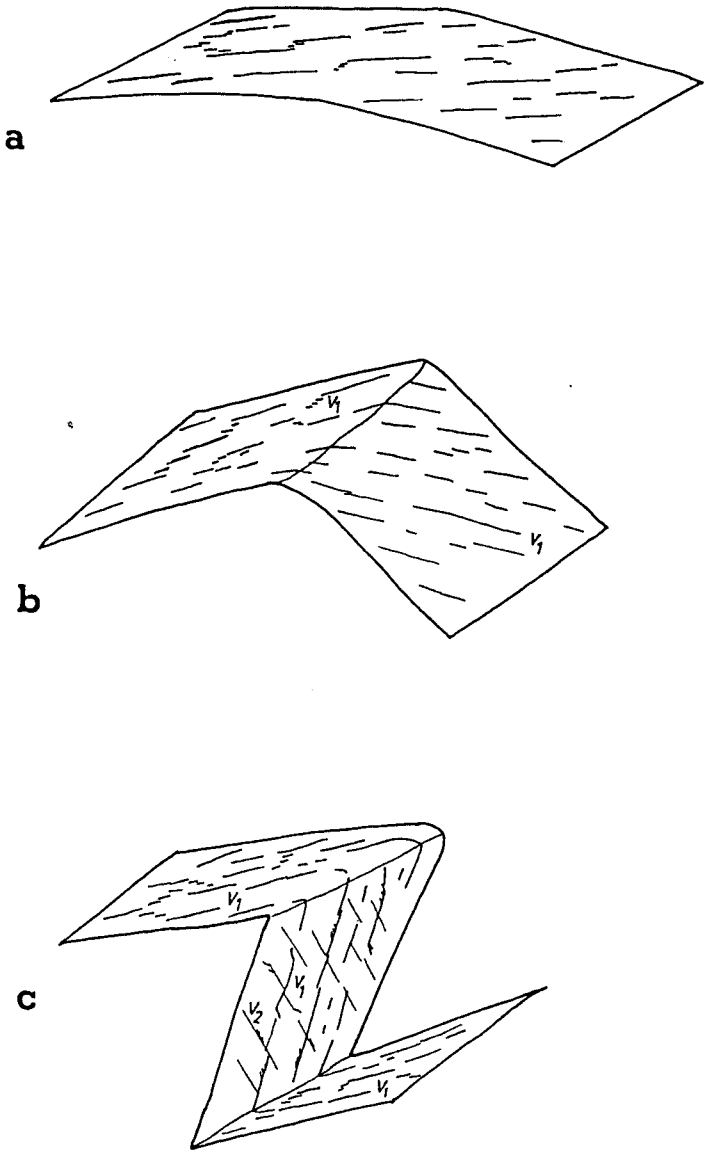

Figure 2.14. Schematic diagrams showing the kinematic development of veins and folding at Millook Haven:

[a] Initiation stage: initial vein growth and propagation during episodes of layer-parallel shortening, prior to significant amounts of buckling.

[b] Buckling stage: continued vein growth and modification during fold amplification, as the fold limbs begin to rotate relative to the remote stress.

[c] Rotation stage: continued vein formation and modification through interaction and loading effects. Development of fold asymmetry as the inverted fold limbs grow in length at the expense of normal limbs as layering rolls through hinges.

shows schematically how some of the veins can be related to fold development at Millook Haven. Some of the veins are expected to be initiated early, or in the layer-parallel shortening stage prior to folding (Fig.2.14a). They continue to dilate after the onset of buckling as further strain amplifies and tightens initially low-amplitude structures (Fig.2.14b). Continuing imposed strain and hinge migration before the folds are significantly tight leads to the asymmetry observed at Millook, with further shear leading to rotation and overturning of fold-limbs. During this phase, the inverted fold-limbs would have rotated through the vertical and into the extensional field of the overthrust shear couple so pre-existing vein sets are modified if they continue to dilate. Many of these veins would then be obliquely loaded and opened as they no longer lie in a principal stress plane. New syn-fold vein sets may be initiated, so complex vein intersection and cross-cutting relations will result (Fig.2.14c). Normal fold-limbs will be expected to have a more simple deformation history as they have undergone less rotation and stress reorientation relative to the inverted limbs.

Observations of vein geometry and kinematics from the Wanson-Millook section agree qualitatively with this model, although it does not fully explain the deformation history for the folds. The transpressive nature of deformation at Millook combined with the large components of flattening strain and layer extension require further explanation. There is a clear association between vein formation and solution-cleavage during fold development at Millook. The variation of bed thicknesses between normal and inverted limbs indicates there are sectional area or volume changes from limb to limb. This could be accommodated by bed-parallel extension and bed-normal contraction. For the inverted limbs layer-parallel extension during folding largely occurred through vein dilation and flattening by pressure-solution. In contrast the normal limbs have a more simple deformation histories. This type of folding may best be described as transpressional. A model to explain the vein geometries and opening histories in relation to fold development at Millook Haven, is envisaged as comprising the following, partially overlapping stages:

[1] Initiation of compression-parallel fractures (veins) during episodes of layer-parallel shortening.

[2] Fold amplification with hinge migration along layering as early symmetric buckles develop more asymmetric shapes. Vein dilation continues.

[3] Continued folding with vein modification and formation as limbs rotate relative to remote stress.

[4] Overturned limbs grow in length, at the expense of normal limbs as layering rolls through hinges. Flattening and layer extension in inverted limbs accompanied by vein dilation, as they are thinned.

2.9 CONCLUSIONS

[1] There are a wide range of vein geometries present which have formed during essentially a single phase of deformation. The vein geometry produced is partly dependent on initial vein orientation with respect to remote stress.

[2] Vein distribution is effected by other parameters apart from the host-rock properties. These may include local irregularities in the bedform geometry such as load casts and ripple marks.

[3] Vein infill textures are extremely variable, many examples indicate composite growth histories that involve several growth mechanisms during different stages of their development.

[4] The veins initiated prior to fold development: they are essentially compression-parallel structures.

[5] The principal stresses were oblique to the fold-axes because prior to folding the maximum principal stress, σ_1 was directed NW-SE. This was maintained during main fold amplification.

[6] During folding, early vein sets were modified due to oblique loading and opening effects as fold limbs were rotated relative to the remote stresses. New vein sets were initiated during fold development.

[7] Complex cross-cutting and vein intersection relations were generated in the inverted fold limbs. Normal limbs have a simpler deformation history as they were subject to less stress re-orientation, by maintaining a relatively constant attitude in fold development. These phases of vein development can then in turn be related to a rotational deformation model.

[8] Structural relations between vein development and folding in the Culm Basin are consistent with an overall pre- and syn-fold E-W dextral transpression. This transpression may be generated by oblique convergence, and the interaction between regional Variscan thrust transport (NNW) and an E-W trending basin margin. The folding at Millook Haven is best described as transpressional.

3

Geometry and mechanics of veins: constraints from profiie and displacement analysis

3.1 INTRODUCTION

Veins are produced by the filling of cracks in rock by invading mineralising fluids. To accommodate infilling material the crack must open. This opening and sealing mainly occurs as a series of intermittent or cyclic cracking events (Ramsay 1980), with individual crack-seal increments typically 0.01-0.1mm wide (Ramsay 1980, Cox 1987). These episodes may be recorded and tracked by textures and microstructures such as fibres (Durney & Ramsay 1973, Ural *et al.* 1991), wall-rock inclusions (Cox & Etheridge 1983) and fluid-inclusion trails (Cox 1987).

This chapter focuses on the geometrical and mechanical aspects of vein formation. From analysis of the profile and displacement characteristics of veins, important information about the kinematics of vein initiation and growth can be gained. By idealising veins as elastic cracks in rock, vein opening can be analysed in terms of wall-rock displacements and understood in terms of the principles of fracture mechanics. By applying theoretical concepts from fracture mechanics (Lawn & Wilshaw 1975, Pollard & Segall 1987) and by comparison with some numerical experiments (Olson & Pollard 1989,1991), the influence of mutual crack interaction and of remote stress on vein propagation path and shape can be determined. This allows inferences to be made about the causative stresses and propagation histories implied by certain vein geometries. Apparent contradictions between field

observations and some theoretical and experimental models are also illustrated and discussed. Specific studies carried out here include:

[1] Analysis of the outcrop patterns of vein sets and the variation of aspect ratio between isolated and overlapping veins. This was done to see if field measurements and observations agree with theoretical and experimental hypotheses about vein growth boundary conditions (*eg.* constant remote differential stress) and mechanical crack interaction.

[2] Examination of the effects of crack interaction on vein initiation and growth, and to recognise features which are diagnostic of this mechanism.

[3] Study of vein opening displacements for various different geometries, by the analysis of vein thickness distribution using displacement-distance (d-x) methods. This was done in order to test elastic crack models, and to compare with similar studies for fault behaviour.

[4] See if inferences about the sequence of vein growth and the mechanisms of formation of en echelon and overlapping veins can be made through field observation and measurement.

3.2. VEINS AS ELASTIC CRACKS

Veins can be idealised as cracks in a homogeneous isotropic solid that deforms elastically to accommodate opening and infill. Following the conventions of fracture mechanics (Lawn & Wilshaw 1975) there are 3 modes of crack loading: mode I (opening), mode II (sliding) and mode III (tearing) (Fig.3.1). Cracks that have only opening displacement acting in x_1 are called mode I; mode II cracks have relative shear displacements in x_2 perpendicular to the crack periphery and mode III cracks have relative shear displacements in x_3 parallel to the crack periphery (Fig.3.1). These three modes constitute possible variations in the loading field which may occur in combination to produce a mixed-mode deformation. Mixed-mode deformation involves components of relative displacement across

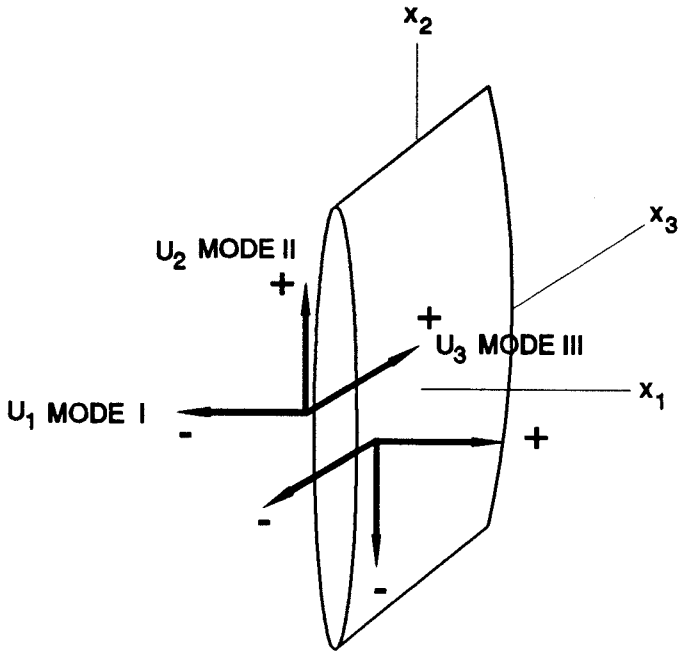

Figure 3.1. The relative displacements of crack peripheries related to the deformation mode. The displacement components are u_i. Opening displacements are mode I, sliding displacements perpendicular to the crack periphery are mode II, and sliding displacements parallel to the periphery are mode III. The ± signs are used to distinguish displacements between each crack wall at $x_1 = 0^+$ and at $x_1 = 0^-$.

a crack in 2 or 3 coordinate directions. The displacements associated with each crack mode, are given by Pollard & Segall (1987, eq. 8.34) as

$$u_1 = \pm(\Delta\sigma_I)\frac{(1-\nu)}{\mu}(a^2 - x_2^2)^{1/2} + (\Delta\sigma_{II})\frac{(1-2\nu)x^2}{2\mu} \tag{3.1}$$

$$u_2 = \pm(\Delta\sigma_{II})\frac{(1-\nu)}{\mu}(a^2 - x_2^2)^{1/2} + (-\Delta\sigma_I)\frac{(1-2\nu)x^2}{2\mu} \tag{3.2}$$

$$u_3 = \pm\left(\frac{\Delta\sigma_{III}}{1-\nu}\right)\frac{(1-\nu)}{\mu}(a^2 - x_2^2)^{1/2} \tag{3.3}$$

where u_1, u_2 and u_3 are the mode I, II and III displacement components at adjacent points across the crack, $\pm$ refer to the direction of movement of the spatial coordinates (x_1, x_2, x_3) and a is crack half-length. The material is linear elastic with Poisson's ratio ν and shear modulus μ. The first variables, $\Delta\sigma_I$, $\Delta\sigma_{II}$, and $\Delta\sigma_{III}$ are the components of driving stress for each mode. Each crack mode is also associated with a distinct distribution of stress at the crack tip (Fig.3.2a), approximated by

$$\sigma_{ij} \approx \frac{\left(K_I f_{ij}^{I}(\theta) + K_{II} f_{ij}^{II}(\theta) + K_{III} f_{ij}^{III}(\theta)\right)}{(2\pi r)^{1/2}}, \quad R < r < a \tag{3.4}$$

where σ_{ij} are the remote stress components, (r,θ) are polar coordinates, and $f_{ij}(\theta)$ is a function of the angle θ which is dependent on the mode of loading. K_I, K_{II} and K_{III} are the mode I, II, and III stress intensity factors (Lawn & Wilshaw 1975) and $R < r < a$ is the crack tip process zone (K-dominant region) (Kanninen & Popelar 1985). The stress intensity factors are measures of the magnitude of the stress concentration at the crack tip, whose values are dependent on factors such as the loading conditions, and the shape and length of the crack. The stress components all decay as $(a/r)^2$ from the crack centre. The stress singularity predicted at the crack tip from equation (3.4) is not achieved

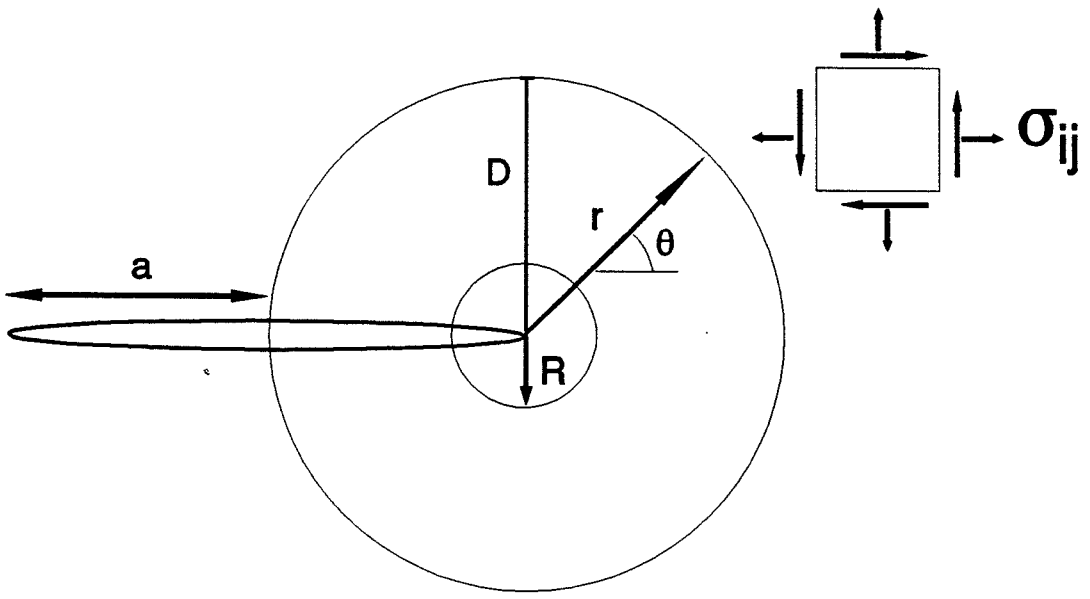

[a]

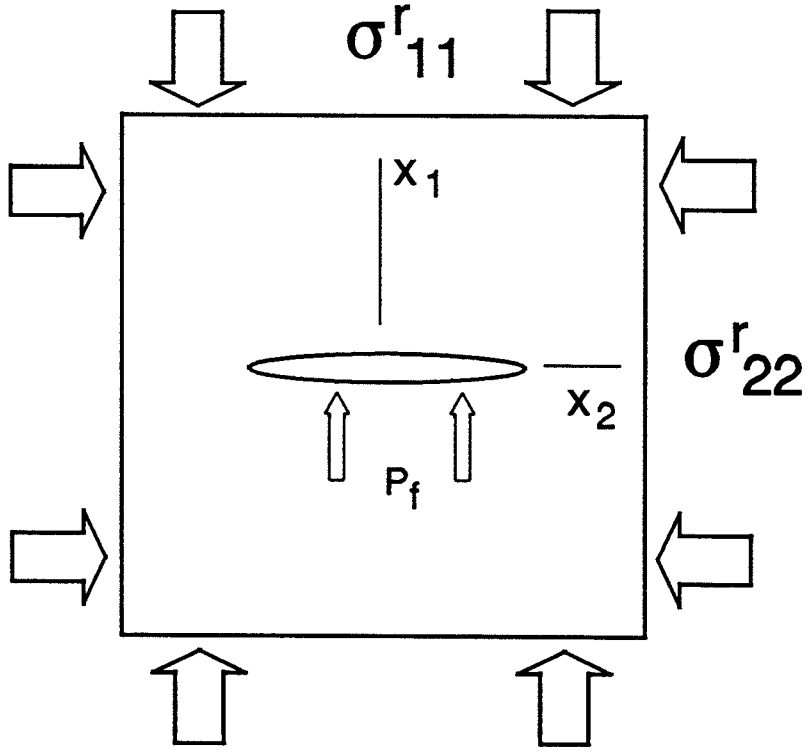

[b]

Figure 3.2. [a] Idealisation of a mode I crack of length 2a. The remote stress components are σ_{ij} and polar coordinates centred at the crack tip are r and θ. The region R <r <D is the inelastic or K-dominant region. [b] Idealisation of a vein as a mode I crack in an elastic solid. P_f is an internal fluid, and the horizontal remote principal stresses are σ^r_{11} (least compressive) and σ^r_{22} (most compressive).

because inelastic deformation and subcritical crack growth prevents the tip from being perfectly sharp where r <R. This is because no real material can accommodate infinite stress without permanent deformation near the crack tip. Inelastic deformation and chemical dependent fracture are reviewed by Anderson & Grew (1977) and Atkinson & Meredith (1987).

For an isolated crack in an elastic body, the mode I stress intensity factor, K_I has the expression

$$K_I = Y(\sigma^r_{11} - P_f)\sqrt{\pi a} \qquad (3.5)$$

where Y is a numerical modification factor to account for crack geometry (Atkinson 1987), σ^r_{11} are the remote stress components, a is half-crack length and P_f is an internal fluid pressure (Fig.3.2b). The quantity $(\sigma^r_{11} - P_f)$ is called the driving stress (Pollard & Segall 1987). Opening or closing displacement in mode I is driven solely by the difference between σ^r_{11} (remote normal stress) and σ^c_{11} (crack normal stress). A mode I crack will propagate dynamically when K_I exceeds the fracture toughness of the material, K_{IC} ($K_I > K_{IC}$). Although stress corrosion at the crack tip may enable subcritical growth at a lower stress intensity. Fluid pressure and remote stress contribute to both crack dilation and the resultant stress intensity factor.

The energy release rate, or crack extension force, G which is a measure of the energy available for an increment of crack propagation, is related to the stress intensity factors by the equation

$$G = K^2(1 - \nu^2)/E \qquad (3.6)$$

(Lawn & Wilshaw 1975, Segall 1984) where ν is Poissons's ratio and E is Young's modulus. Under these conditions a criterion requiring the energy release rate to reach a critical value for catastrophic fracture to initiate, is given by

$$G = G_C \qquad (3.7)$$

which is equivalent to the relationship $K_I > K_{IC}$ used for the stress intensity factor, K. The crack extension force is dependent on internal fluid pressure and remote stress. This results in an expression for *G* in terms of driving-stress and host-rock stiffness as

$$G = (1 - \nu^2)(\sigma^r_{11} - P_f)^2 \sqrt{\pi a}/E \qquad (3.8)$$

which suggests that *G* should increase linearly with crack length 2*a*, if subject to constant loading conditions.

For a vein to propagate, combining equations (3.6), (3.7) and (3.8) means that the loading conditions can be expressed by

$$(\sigma^r_{11} - P_f) \geq \left(\frac{2G_C\mu}{\pi a\,(1 - \nu)} \right)^{1/2} \qquad (3.9)$$

This provides a very general term, since G_C can include energy which is dissipated through non-linear elastic behaviour, *eg.* subcritical crack growth (Atkinson 1984, Atkinson & Meredith 1987).

3.3 CRACK PROPAGATION

A mode I crack will propagate dynamically when K_I exceeds K_{IC}. As long as the loading remains pure mode I, the crack will follow a straight path, but for mixed-mode loading the propagation direction may change. If the crack is subject to mixed-mode (I-II) loading this can result in a rotation of the most tensile principal stress so that it is no longer normal to the crack tip (Cottrell & Rice 1980, Segall & Pollard 1987). In subsequent propagation increments the crack tip may reorient itself so that mode I loading is restored. If these loading conditions are gradual or continuous, the crack will have a smoothly curving path, minimising the stress intensity factor, K_{II} ($K_{II} = 0$)(Cottrell & Rice 1980, Sumi *et*

al. 1985, Schultz 1988). A sudden change in K_I/K_{II} induced by changes in the loading directions at the crack front would produce a kink in the fracture trace if propagation resumed.

Examples of vein propagation and termination structures

Selected examples from a wide range of kinked and curved vein and solution-transfer structures, present in the terminal regions of veins from the Millook Haven area, are illustrated in Fig.3.3 and discussed in their accompanying captions. These structures have a wide range of geometries, reflecting different conditions during vein formation or modification effects through subsequent loading. The simplest structures present include straight and curvilinear kinks or splay cracks which grew away from the terminations of many veins. Figure 3.3a shows a vein tip with the trace of a splay crack projecting about 0.30m into the host-rock at an acute angle of 25°.

Theoretical analyses of the effects of different stress states on the shape and propagation paths of pre-existing mode I fractures (Cottrell & Rice 1980, Sumi *et al.* 1985, Melin 1987) indicate that new crack growth by mode I failure at a crack tip crack will initiate with a kink if the parent crack is subject to sufficiently intense mixed-mode (I-II) loading. This kink-angle, α, is a function of the stress state active during the initiation of the new crack increment and the magnitude of the ratio K_I/K_{II} (Cottrell & Rice 1980). The direction of crack kinking is the direction that maximises K_I and reduces K_{II} to 0 for each new increment of propagation. This direction is partly determined by the orientation of the crack with respect to the remote stress components. If the remote shear stress is dextral, the kink-angle α is negative, and vice versa. Figure 3.4a illustrates the relationship between the remote shear sense (σ_{xy}) and the direction of crack kinking. Cottrell & Rice (1980) and Cruikshank *et al.* (1991) show that the mode I stress intensity factor, K_I at the tip of a new crack growth increment on a pre-existing fracture can be approximated by

$$K_I = 1/4[3\cos(\alpha/2) + \cos(3\alpha/2)]k_I \qquad (3.10)$$

$$-3/4[\sin(\alpha/2) + \sin(3\alpha/2)]k_{II}$$

Figure 3.3

Examples of vein propagation and termination structures from Millook Haven

[a] Kinked tail-crack at the termination of a host vein. The kink angle is ≈25° and the vein infill indicates normal opening. Fracture mechanics theory states that when a mode I crack is subject to mixed-mode I-II loading, the result is a rotation of the local tensile stress so that it is no longer normal to the crack tip. Cottrell & Rice 1980 have shown that when this occurs the crack tip reorients itself so pure mode I propagation is maintained. So this example may trace out temporal variations of mixed-mode loading.

[b] Angular asymmetric branches and forks developed in the terminal region of a vein. Mineral fibres are at high angles to the vein margins. The infill of the branch fractures is continuous in texture and mineralogy with the parent vein, suggesting that the structure is primary, *ie.* does not represent subsequent loading of a pre-existing crack. These types of structures may be characteristic of cracks propagating under conditions of varying energy release rate, *G*.

[c] A multiple horsetail array consisting of secondary sub-parallel veins, branching at angles of 25-65° from the parent vein. The sense of slip along the parent vein is sinistral. This group of structures form in response to shearing along pre-existing cracks.

[d] Pinnate veins developed along the margin of a host vein. The infill fabric of the pinnates are oriented at high angles to the margins, and oblique to the fabric within the host vein. Sense of displacement is sinistral. There is also evidence for shear displacement parallel to the vein margin, indicated by granulation structures and local pressure-solution effects.

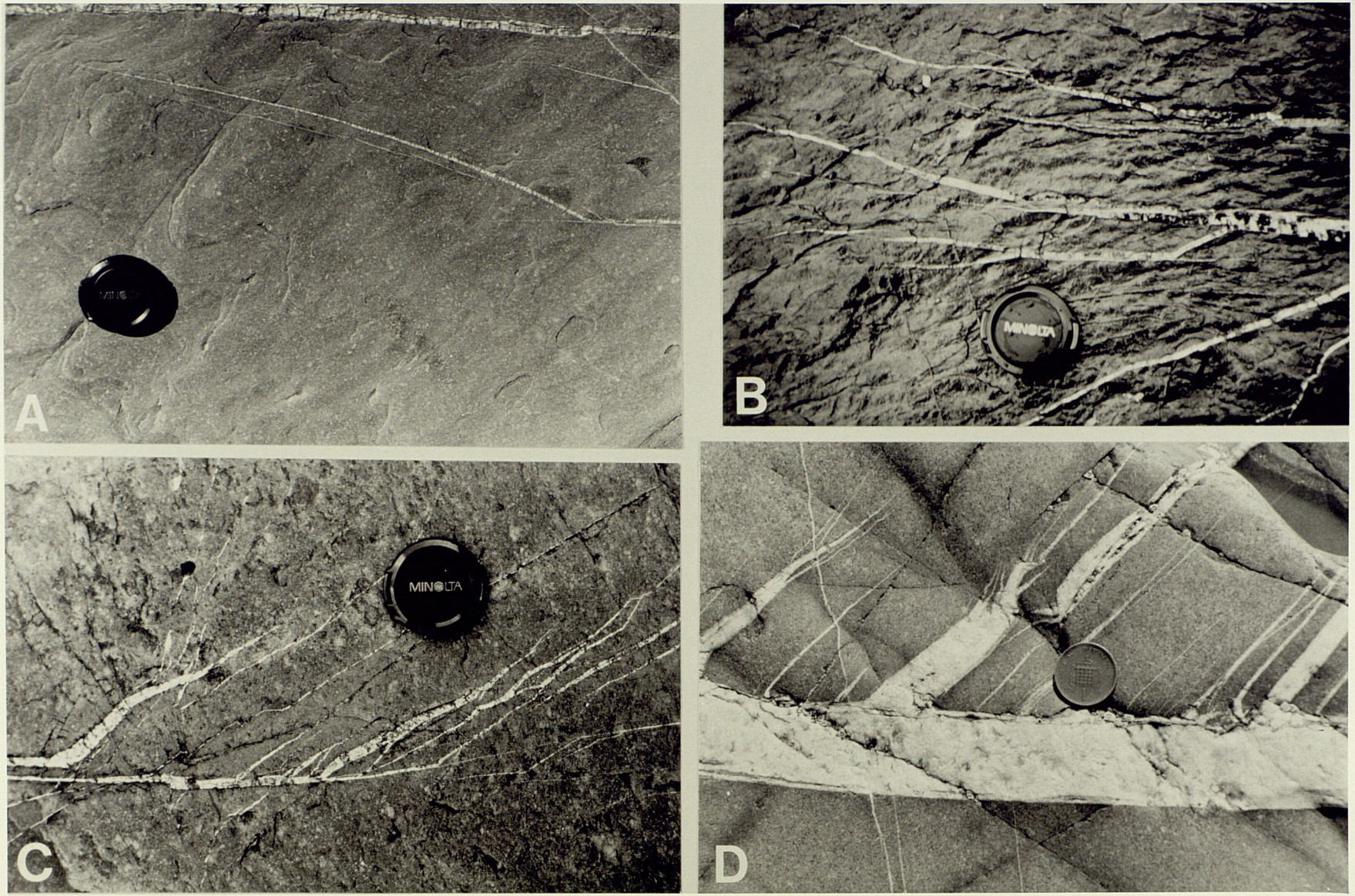
A
B
MINOLTA
C
MINOLTA
D

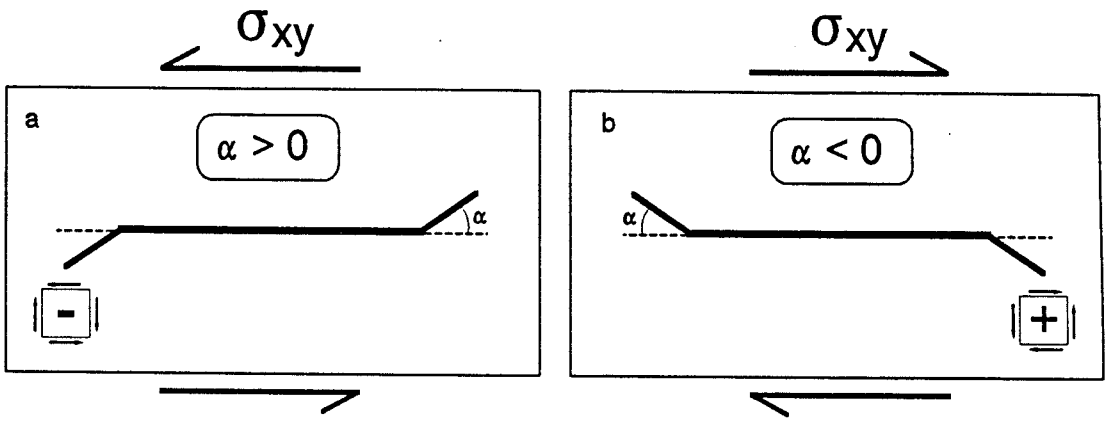

[a]

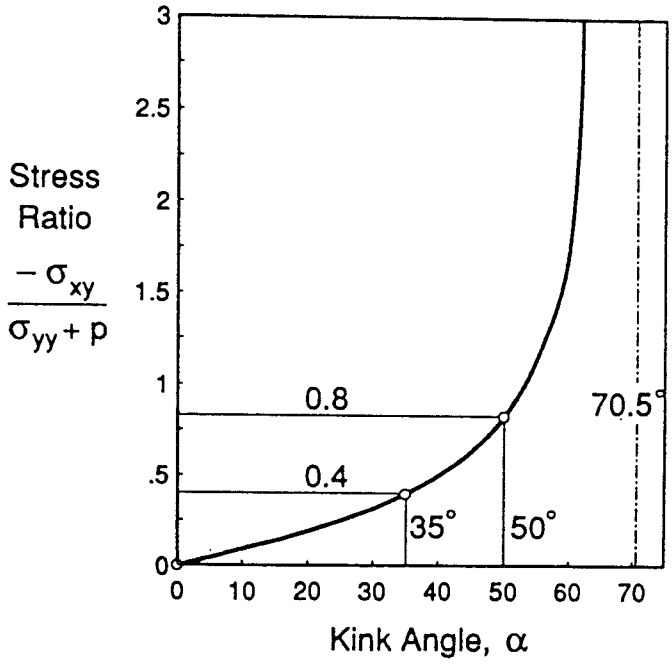

[b]

Figure 3.4. [a] Relationship of the sense of splay, or tail crack formation at the end of a pre-existing crack to the remote shear stress. [b] Relations between the ratio of far-field stresses and the kink angle (α) in degrees at the end of a mode I crack (from Cruikshank et al. 1991, fig.7). The kink angle is related to the ratio of in-plane mode II shear stress (σ_{xy}) and driving stress.

where k_I and k_{II} are the stress intensity factors for the parent crack. The orientation of the increment of crack growth can be found by solving the expression

$$K_{II} = 1/4[\sin(\alpha/2) + \sin(3\alpha/2)]k_I + 1/4[\cos(\alpha/2) + 3\cos(3\alpha/2)]k_{II} \quad (3.11)$$

where $K_{II} = 0$,

$$\frac{-k_{II}}{k_I} = \frac{\sin(\alpha/2) + \sin(3\alpha/2)}{\cos(\alpha/2) + 3\cos(3\alpha/2)} \quad (3.12)$$

for the kink-angle, α. Solutions to equation (3.12) for positive values of k_{II}/k_I, are given by Cruikshank *et al.* (1991). These results can be expressed in terms of the stress ratio, and they are represented graphically in Fig.3.4b. According to Cruikshank et al. (1991, equ.3a-c) we can express the crack kink-angle in degrees, in terms of small values of mode II loading by

$$\alpha \approx -2\frac{k_{II}}{k_I} = \frac{-2\sigma_{xy}}{\sigma_{yy} + P_f} \quad (3.13)$$

where σ_{yy} and σ_{xy} are the remote normal stress and shear stress components respectively. Re-examining some of the examples of vein structures (opening cracks) from Millook Haven (Fig.3.3) means that many termination structures could be interpreted as simple kinks or tail cracks. For Figure 3.3a the kink-angle, α = -25° so according to Fig.3.4b the stress ratio for this kink was

$$\frac{\sigma_{xy}}{\sigma_{yy} + P_f} = 0.2 \quad (3.14)$$

A second example shown in Fig.3.5 (and enclosure in pocket), is a map of a small scale compound

Figure 3.5. Map of vein splay structures associated with a small compound fault zone, Saltstone Strand, North Cornwall (1865 0055)(Chapter 2). A series of extension fractures have linked to form a compound pull-apart. Slip along the zone has been transmitted through a series of steps and bends by the formation of rhomb shaped vein pull-aparts. The amount of vein opening is approximately equal to the slip transmitted through each bend. Strain accommodation within the array has been localised in transtensional and transpressional bends. Tail-cracks and en echelon veins are present at both terminations of this fault.

COMPOUND VEIN PULL-APART

SALTSTONE STRAND
NORTH CORNWALL

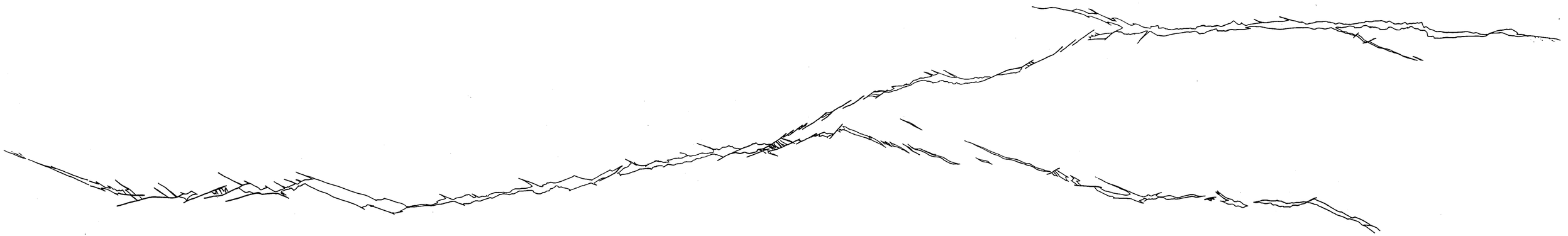

10cm

N

fault zone with secondary vein structures near its terminations. The fault is described in its accompanying caption, with details of its tectonic setting given in Chapter 2. The splays near the fault terminations are about 1m long and they are orientated in a dextral (counterclockwise) sense at angles of about 25°. The stress ratio for these kink structures was -0.2 (Fig.3.4b).

These examples of vein termination structures from the Millook Haven area illustrate part of the range of vein geometries present, which have variable orientations and different ages. These examples probably only reflect stress states which existed over a few square metres, so any inferences about the regional stress states using this method must be made with care. The changes in orientation of kinked extensions to mode I cracks are sensitive to all components of the stress field. Examples of idealised tail cracks, for various far-field loading conditions, described by Cruikshank *et al.* (1991) suggest that the crack-parallel stress has an important role in influencing the initial crack path stability, and consequently on the shape of a new increment of crack growth on a pre-existing fracture. Where the remote crack-parallel stress is compressive the propagation path of a tail crack will converge towards the parent crack; with less path convergence resulting if this compression is reduced or becomes zero. Additionally, many deformation experiments involving brittle materials have indicated that a planar crack subjected to shear loading will tend to develop a kink or splay crack at one or both of its ends instead of propagating in-plane (Brace & Bombolakis 1963, Nemat-Nasser & Horii 1982). From these observations a simple rule that can be defined is that a splay crack or kinked extension will tend to turn towards, or grow parallel to the direction of maximum compression.

Other groups of fractures found near vein terminations include branches (Fig.3.3b) and horsetails (Fig.3.3c). The singularity in stress predicted for a crack tip, indicates that any secondary stresses or structures induced by loading on a parent vein, should initiate there and propagate away from its termination. This hypothesis is supported by the many observations of vein and solution-transfer structures concentrated near vein terminations. Curved and kinked tail cracks are also described for fault terminations (Rispoli 1981, Cruikshank *et al.* (1991), dyke traces (Pollard & Muller 1976) and for oceanic ridges (Pollard & Aydin 1984).

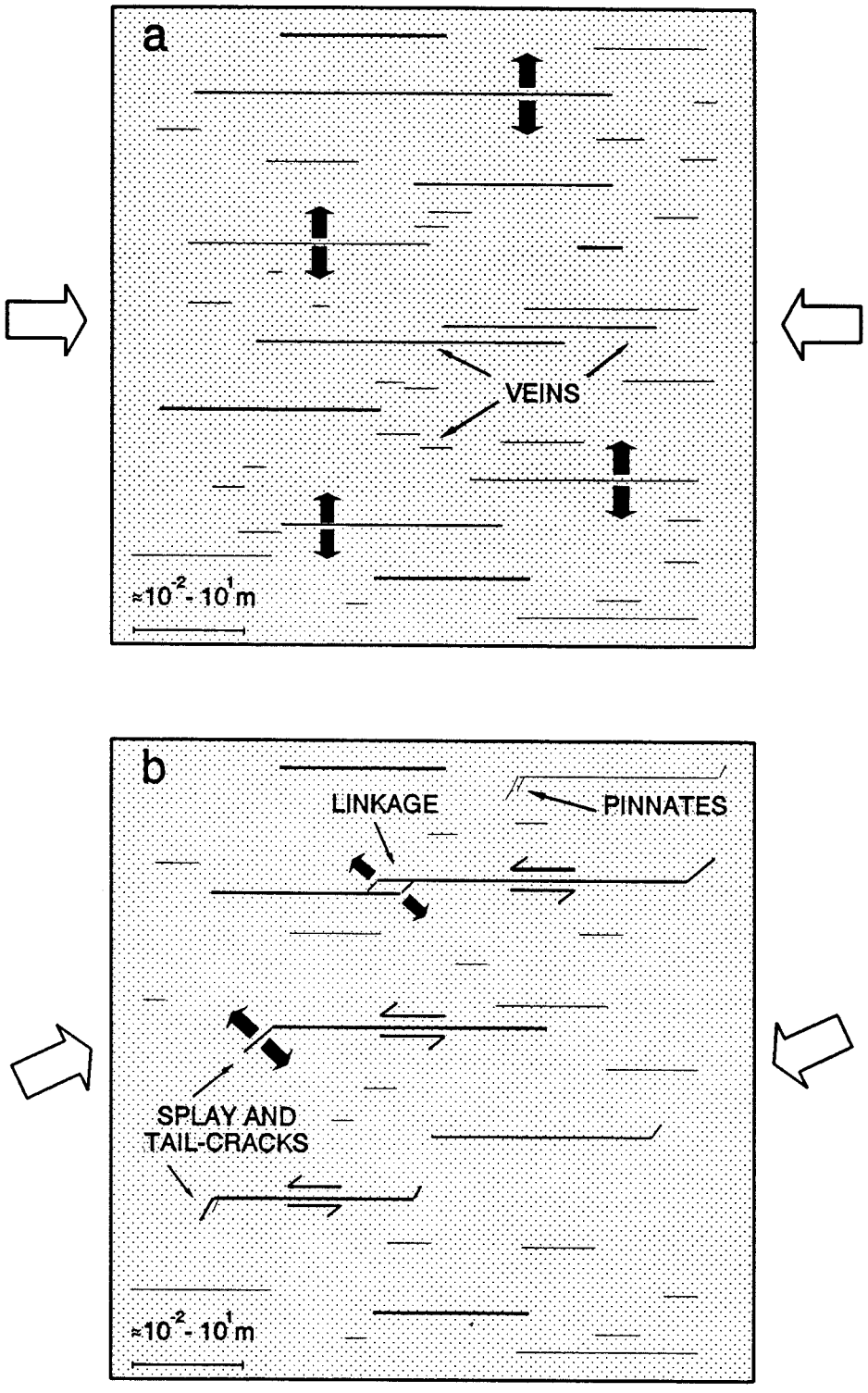

Figure 3.6. [a] Initial opening of a set of unevenly spaced and overlapping veins. The large heavy arrows are the inferred directions of remote maximum horizontal compressive stress (σ^r_{22}). [b] The veins are loaded and sheared during a subsequent deformation episode. Kinked extensions and splay cracks develop near one, or both ends of some veins, and some veins may become linked. Pinnate veins also develop along some vein margins, where slip is accommodated along part of the vein length, rather than occurring simultaneously along the entire vein length and then propagating to each end. The effects of mechanical interaction may also contribute to this mechanism of vein loading and modification.

Veins projecting from the sides rather than at terminations of veins often have similar orientations and geometries to structures that form near crack tips due to subsequent loading (Pollard & Segall 1987, Cruikshank *et al.* 1991). These structures which are commonly called pinnates, are thought to be produced by local stress concentration and/or by irregularities along a vein margin affecting the distribution of slip induced by loading. Figure 3.3d shows pinnate veins developed along the margin of a parent vein, where the sense of displacement is sinistral.

General conclusions for conditions of vein formation at Millook Haven: I

Following substantial initial mode I growth, some of the veins were modified through subsequent loading effects, inducing significant components of mixed-mode deformation. It is suggested that shear displacements induced by loading along some veins, propagated towards their terminations and caused fracturing along the veins and at their ends. Figure 3.6 illustrates a possible sequence of formation for some of the splay and tail cracks, and pinnate veins observed at Millook Haven. Mechanical interaction between some of the veins was probably also significant.

3.4 CRACK INTERACTION

The observed geometries of many veins, joints and dikes indicate the widespread occurrence of crack interaction. Since the dilation of a single crack creates a non-uniform stress state this has an important effect on the growth of neighbouring cracks; especially where crack separation is small compared to the crack dimensions. The dilation of an isolated crack produces only a mode I stress intensity factor. For closely spaced cracks mechanical interaction changes this and induces an additional mode II stress intensity factor which may produce crack twisting and a change in the propagation path. Various effects attributable to crack interaction can be seen in natural examples of veins from North Cornwall.

Effects of mechanical interaction on overall geometry of a vein set

Figure 3.7a is a map of vein traces on a bedding surface ($12m^2$) in Crackington Formation sandstone at Millook Haven, North Cornwall. Two main characteristics are important at this locality: [1] multiple

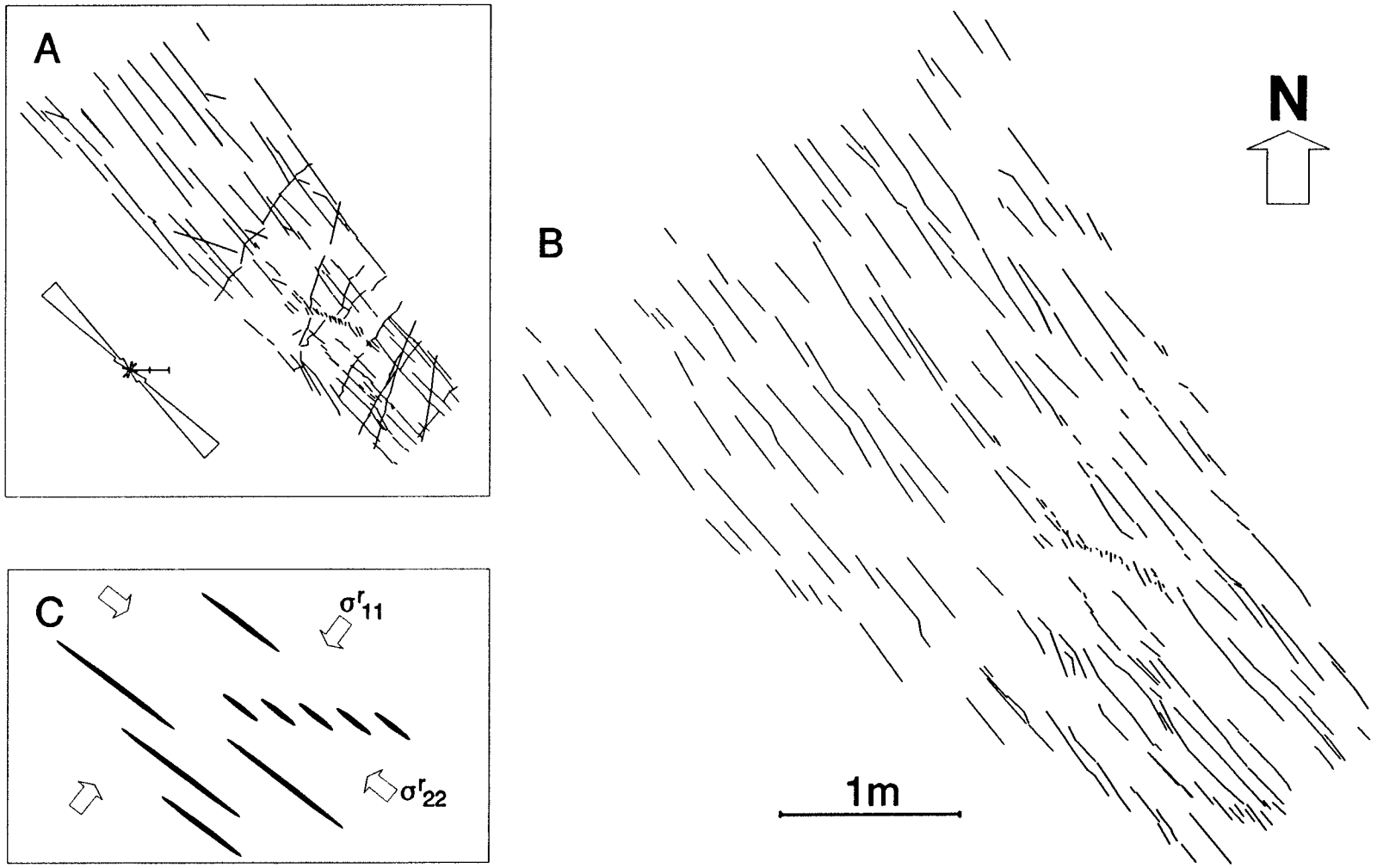

Figure 3.7. Map of vein traces from a normal fold limb on a bedding surface in Crackington Formation sandstone at Millook Haven, North Cornwall. [a] Overall vein outcrop configuration. [b] This shows the first vein set (NW-SE) which is characterised by sets of numerous closely spaced subparallel veins, and en echelon vein arrays with a wide range of spacing values and vein-array angles. Some of these form conjugate en echelon arrays. [c] This illustrates, diagrammatically the inferred initial remote stress configuration responsible for initiation and growth of the first vein set.

closely spaced subparallel veins that range in length from a few millimetres to several metres, and [2] contemporaneous en echelon veins that are an order of magnitude smaller in length with low ratios of length to width (aspect). The mapped traces represent the maximum vein dimensions since they are confined to a single sandstone bed (0.37m thickness). This outcrop configuration is very interesting since it is not immediately apparent that the veins were interacting, as they mainly have straight propagation paths and large overlaps in relation to their separation. One main vein set is present at the location (Fig.3.7b). The geometric differences between this vein set and the combined sets (Fig.3.7a) suggests they did not form synchronously, and that they each reflect very different remote stress configurations. The first vein set (Fig.3.7b) trends NW-SE and is comprised of closely spaced subparallel veins of variable length with distinctive overlaps (20% to 100%), and in places, en echelon geometries. These en echelon arrays are characterised by a wide range of vein-array angles (Chapter 5, Jackson & Sanderson 1991) and crack separations. The second vein set is apparently more simple, comprising of widely spaced coplanar veins that do not form obvious arrays.

Figure 3.7c shows schematically, the initial remote stress configuration the first vein set may have experienced. Although initial vein growth is expected to be mainly perpendicular to the effective tensile stress ($S_h = \sigma'_{11}$), subsequent growth would be controlled by the local stress field induced by the fractures themselves. There is little indication of the more obvious effects of elastic crack interaction, such as vein curvature or modification of propagation paths. This suggests other factors may play a significant role, and that a further controlling influence on vein growth may have been a strong remote compressive crack-parallel stress ($S_H = \sigma'_{22}$). This would be required to maintain the high crack path stability present for vein sets at this particular locality. This explanation is offered by Cottrell & Rice (1980) in their theoretical treatment of curved and kinked cracks, where they showed that high compression parallel to cracks will tend to inhibit veering of crack propagation paths, even in the presence of a local shear stress normal to a crack tip. Further evidence for this is provided by Olson & Pollard (1988,1989) who employed a displacement discontinuity method (Crouch & Starfield 1983) to study idealised crack behaviour under various loading conditions. Their numerical experiments which involved constant remote stress orientation, at constant K_I, illustrated the effects the stress ratio and crack tip interaction have on the path stability of overlapping cracks.

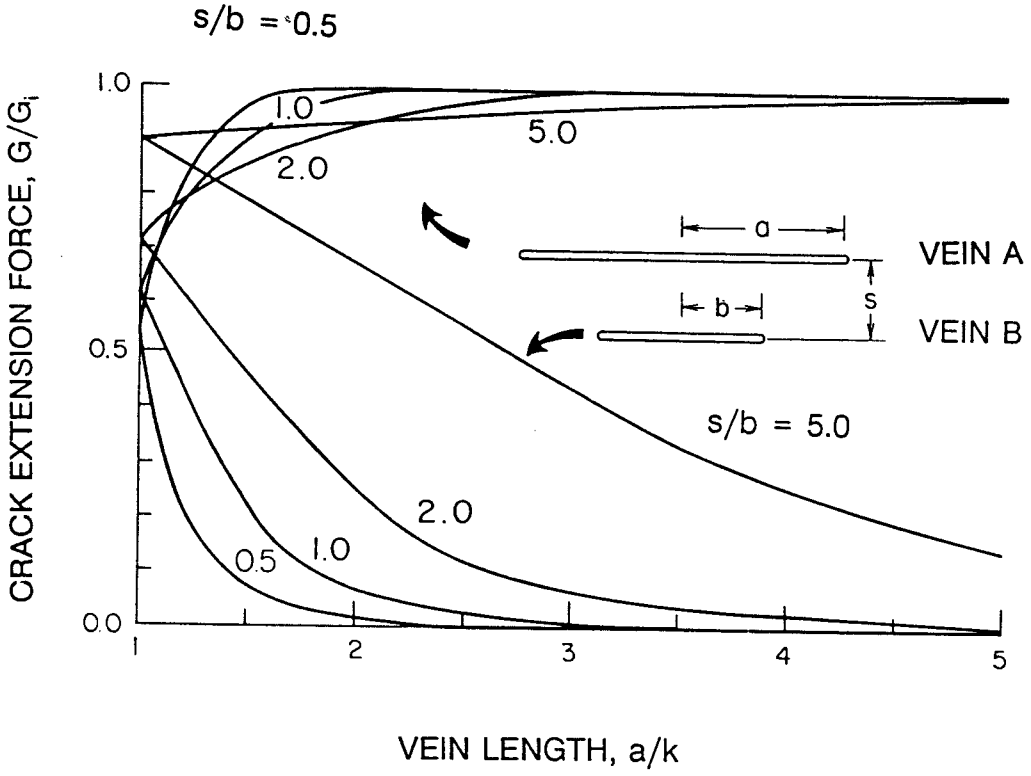

Figure 3.8. Relative crack extension force, G, against vein length ratio for two parallel veins of lengths a and b with orthogonal spacing s. The upper four curves correspond to vein A and the lower four to vein B (adapted from Segall & Pollard 1983, fig.11).

The quasi-static growth of a simple parallel array of extension fractures was investigated by Segali & Pollard (1983), who showed that the crack extension force, G, is dependent on driving stress, crack length and the magnitude of mechanical interaction between overlapping cracks. Crack extension force varies for individual cracks within an array, increasing linearly as a function of crack length for a constant applied stress (Lawn & Wilshaw 1975). As a general rule this means that the propagation of the longest cracks is favoured. Figure 3.8 illustrates this effect for two parallel cracks of half-length a and b, separated by perpendicular distance $2s$. The crack extension forces G are normalised by the extension forces for two isolated cracks of equivalent length and applied stress, G_i. This value G/G_i is shown as a function of a/b for four different values of s/b (Fig.3.8). The graph indicates that two closely spaced cracks of equal length will have a lower crack extension force than two widely separated cracks of identical length. As the crack length ratio (a/b) increases, the normalised extension force, G/G_i, for the longest crack increases toward unity, whereas the crack extension force for the shorter crack drops to zero. Taking $a/b > 2$ the longer crack will remain unaffected by the stress perturbation generated by the shorter crack; irrespective of the crack spacing. For the shorter crack G/G_i decreases with closer crack spacing and higher a/b. The effect would be to inhibit growth of the shorter crack as the longer crack grows.

This treatment of crack interaction for simple overlapping crack arrays provides a plausible mechanical explanation for the observed vein patterns and the distribution of vein length and spacing for outcrops around Millook Haven (Fig.3.7). Applying the analysis to the trace map, illustrates that as the first vein set evolved and the veins grew in length, the propagation of more and more of the veins was suppressed as favoured (longer) veins interacted with increasingly distant neighbours, *ie* the longest veins tended to restrict the growth of the shorter veins as they were located within the region of stress perturbation. This selective growth due to mechanical interaction has produced strongly overlapping veins, and en echelon and conjugate en echelon arrays containing veins of low aspect ratio. Additional factors which influence the vein patterns observed at Millook Haven include layer thickness. Since the veins are mainly confined to single beds within a layered sequence of contrasting elastic

Figure 3.9. Two subparallel veins which have propagated towards one another, following a convergent propagation path. In this example the resultant propagation path was a probably a response to the heterogeneity of the local stress field due to mechanical interaction. Note that linkage is only acheived by the fracture of the rock bridge between the overlapping veins.

properties, their longest and shortest dimensions are effectively constrained. Time dependent behaviour such as stress relaxation (or strain hardening and softening) are also likely to be significant when it is considered that vein growth occurs over a geological timescale.

Overlap of two propagating veins

Figure 3.9 shows an example of two parallel, overlapping veins from Millook Haven with propagation paths that have veered toward one another. The mineral fibres in the vein pairs and in their kinked tips are at high angles to the vein margins indicating normal opening. The interaction of the two cracks caused the vein tips to veer towards the neighbouring vein surfaces, although the vein tips do not actually reach the neighbouring vein margins, suggesting that there may have been a large component of compression parallel to these veins. This type of geometry is characteristic of elastic interaction, where vein tip kinking or curvature reflects the local crack-induced stress fields (Cottrell & Rice 1980, Olson & Pollard 1989). The veering of these vein pairs and the near tip-to-plane linkages indicate a decrease of crack path stability (Cottrell & Rice 1980, Sumi *et al.* 1985). The K_{II} factor which must have been induced by mechanical crack interaction, caused the vein tips to deviate from their original linear propagation path to a kinked one. This particular example also suggests that if a remote crack-parallel compression existed, it must have been reduced once initial vein overlap had occurred.

The enhancing and inhibiting effects of mechanical interaction on the propagation of closely spaced cracks was investigated by Pollard *et al.* (1982) for en echelon fractures, and by Aydin & Schultz (1990) for strike-slip faults. These analyses illustrate that the crack extension force for underlapped cracks is essentially the same as that for an isolated crack (Fig.3.10a), but it increases sharply as the crack tips propagate towards each other. This is because each crack enhances propagation of its neighbour by inducing a local tensile stress in the tip region of the neighbouring crack. When the tips overlap, this induced stress becomes compressive, resulting in a sharp reduction of the crack extension force, so that crack growth will tend to terminate. These perturbations in the local stress field also induce shear displacements on neighbouring cracks, which effects their propagation paths.

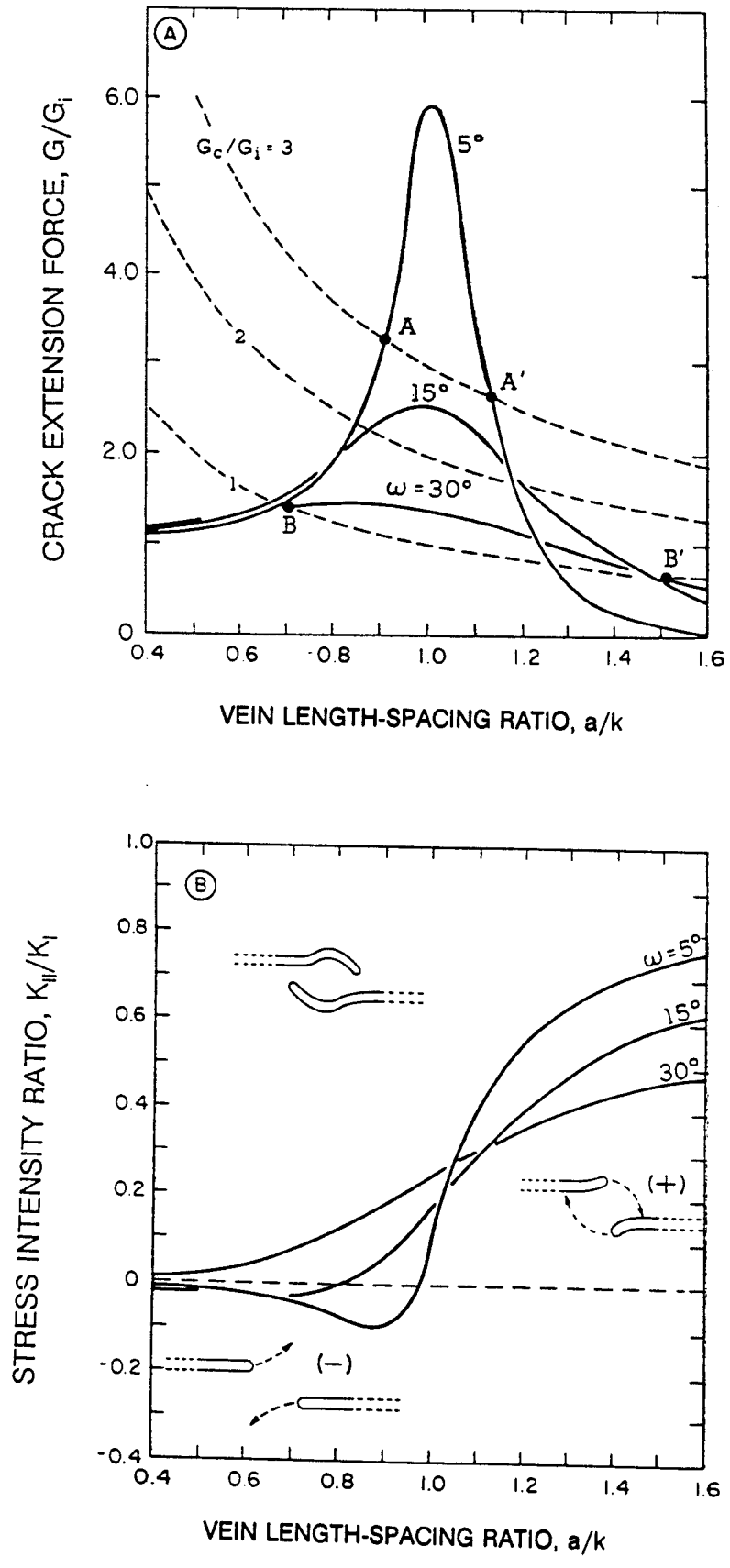

Figure 3.10. [a] Crack extension force G normalised by that for an equivalent isolated crack, G_i, plotted against the crack length to spacing ratio. [b] Ratio of K_{II}/K_I shown against the crack length to spacing ratio (from Pollard et al. 1982, fig.12).

To estimate propagation paths for en echelon and overlapping cracks Pollard *et al.* (1982) used a propagation path factor K_{II}/K_I. Using this factor, the qualitative form of a crack propagation path can be deduced from the sign and relative magnitude of the ratio. Figure 3.10b shows the K_{II}/K_I ratio plotted against various values of the crack length to spacing ratio (a/k), indicating the strong dependence of the propagation path factor on crack spacing. The graph indicates that for small values of b/c, crack interaction effects are minimal. For larger values and smaller array-angles the ratio becomes negative. Positive values of k_{II} are associated with cracks that offset to the right and negative values of k_{II} with cracks that offset to the left (Fig.3.10b). For larger values of K_{II}/K_I the angle that the crack propagation path makes with the parent crack plane increases. This idealisation of crack propagation paths and the role of the stress intensity ratio indicates that approaching propagating cracks initially diverge or turn away from each other. After the crack tips overlap and they are nearly opposite, the crack propagation path factor indicates strong path convergence with increasing overlap. This mechanism provides one possible explanation for the behaviour of many overlapping veins, dykes and faults, since crack linkage is nearly always from tip-to-plane rather than tip-to-tip.

In the analysis of mechanical interaction by Aydin & Schultz (1990), the propagation energy, G, at the inner tips of two overlapping cracks is normalised by that for an isolated crack for different spacings (Fig.3.11). Where $G/G_i = 1$ there is no interaction between the cracks. Ratios of $G/G_i \neq 1$ reflect crack interaction either enhancing (>1) or suppressing (<1) the propagation of two en echelon cracks. Figure 3.11 shows the curves of crack propagation energy for four geometric cases of overlap and spacing. Applying this analysis to closely spaced, overlapping veins ($s/k = 0.01, 0.1$) indicates that the propagation energy increases as two crack tips approach each other. Beyond zero overlap ($a/k = 1$) the propagation energy decreases sharply. For widely spaced veins $s/k > 1$ there is little change.

En echelon veins

As previously outlined, the variation of the crack extension force, G, with crack overlap has an important effect on vein propagation paths. For en echelon arrays, as vein separation decreases and

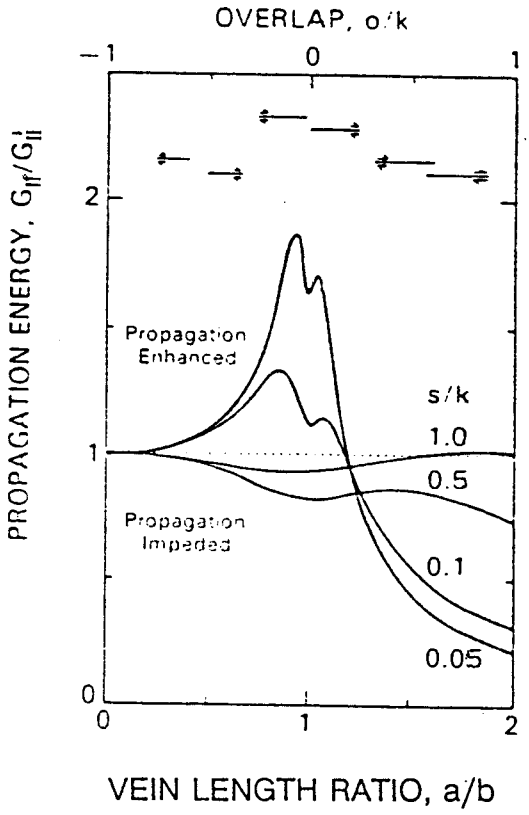

Figure. 3.11. Relative crack extension force, G, for overlapping cracks. (Aydin & Schultz 1990)

overlap occurs the crack extension force, *G* drops below the value for an equivalent isolated crack. This parameter effects the rate of crack extension, so vein propagation may terminate at some stable overlap position (unless driving-stress increases) to produce an en echelon array. The magnitude of this mechanical interaction is strongly influenced by crack separation, with elastic interaction most significant in vein arrays with low crack separations and array angles. This type of geometry brings the crack tip stress concentrations closest together. The treatment of crack interaction for en echelon vein arrays, in terms of the role of the crack extension force, is appropriate for arrays with array-angles <30° (Fig.3.10a). For angles of >30° the crack extension force approaches that for an isolated crack. Examples of various en echelon vein geometries and a discussion of their formation are presented in Chapter 5.

General conclusions for conditions of vein formation at Millook Haven: II

After substantial initial mode I growth, many veins became close enough together to induce significant crack interaction. For the closely spaced and strongly overlapping fractures, the stress perturbation and shielding effect of longer veins on shorter veins rationalises the observed distributions of vein size and spacing. For some veins, their outcrop patterns and the stability of their inferred propagation paths implies the presence of a high remote compressive stress parallel to the veins at the time of formation.

Effect of mechanical interaction on size distribution in a vein set

Figure 3.12a shows the frequency distribution of length to width (aspect) ratio for veins in the Crackington Formation from localities between Foxhole Point and Millook Haven. These measurements are from the pre- and syn-foid vein sets which are oriented NW-SE and NE-SW (Chapter 2, Jackson 1991, Beach 1977). The data shown in Fig.3.12a consists of measurements of: [1] single veins of regional extent which are often closely spaced or slightly overlapping, and [2] veins that occur in en echelon and conjugate en echelon arrays. The veins in en echelon arrays are often parallel to the regional veins, occurring near their terminations, and in the areas between individual regional veins. The en echelon veins generally do not have sigmoidal profiles, and they show no

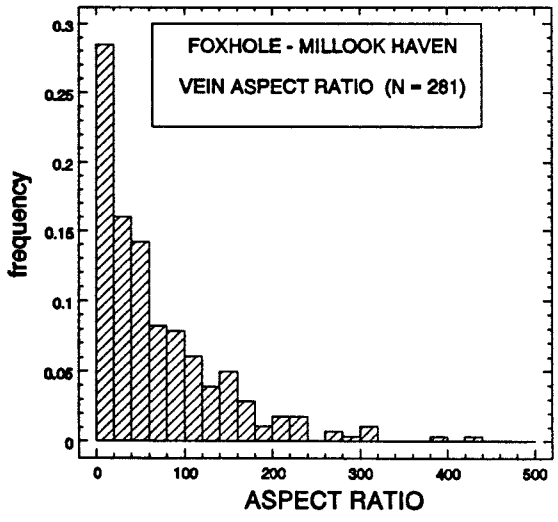

[a]

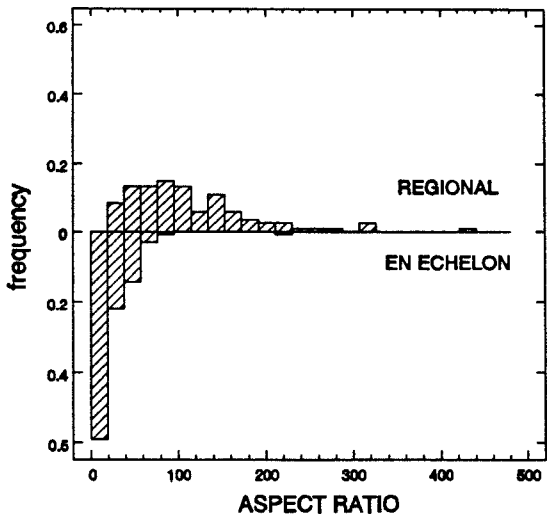

[b]

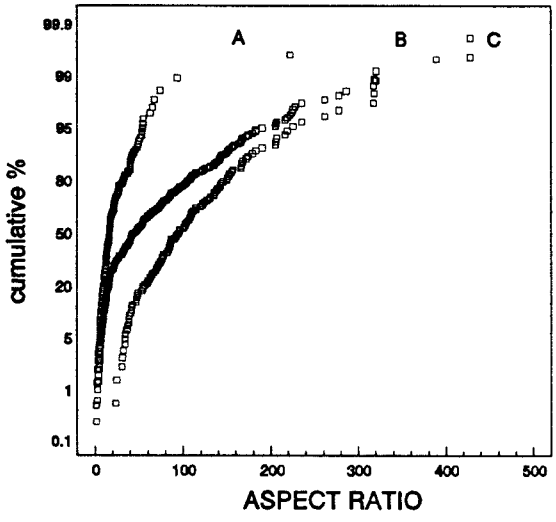

[c]

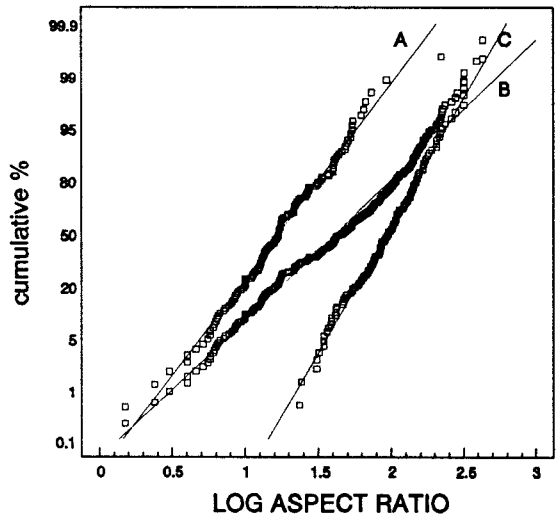

[d]

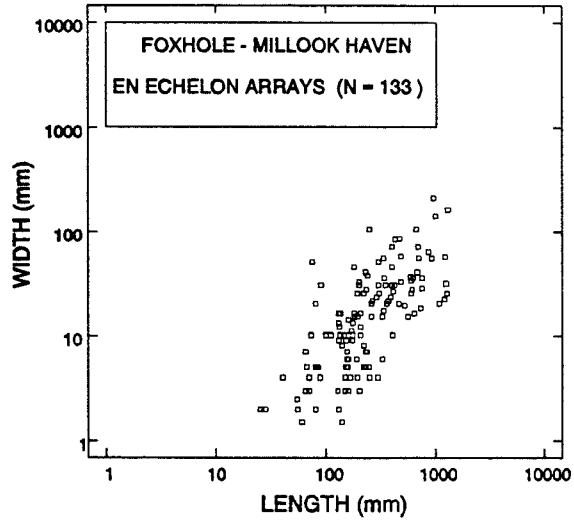

[e]

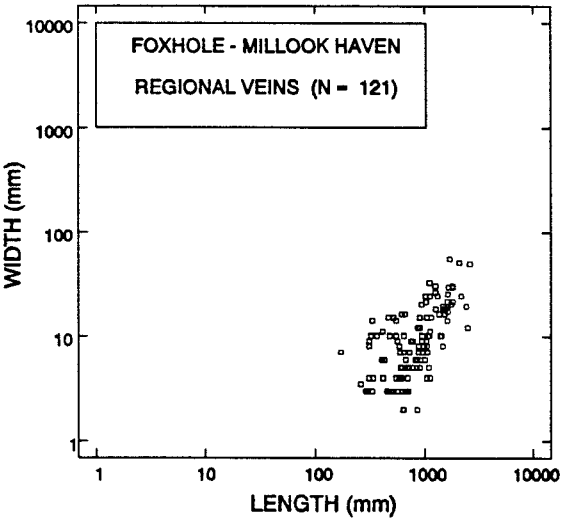

[f]

Figure 3.12. Plots of the range and distribution of vein length to width (aspect) ratio.

evidence for deformation that invoived large shear strains. The vein aspect ratio for the whoie dataset ranges between 1.5 and 427.5, with 43% of the data in the range 1.5-20.

Figure 3.12b shows the frequency distribution of aspect ratio for the two groups of vein geometry. Although there is some overlap between the groups, it is obvious that the veins in en echelon arrays are characterised by lower aspect ratios relative to veins that do not have en echelon configurations. An arithmetic (normal) probability plot of aspect ratio (Fig.3.12c) for the en echelon (A), regional (B) and the total number of veins (C), indicates that vein aspect ratio is not normally distributed. Figure 3.10d displays the log-transformed values of aspect ratio on an arithmetic probability graph, indicating that vein aspect ratio has a lognormal distribution. Log-log plots of length against width for veins in en echelon arrays and the regional veins (Figs.3.12e and 3.12f) suggest that vein width is proportional to length for both the en echelon and the regional veins. Figure 3.12e indicates that the en echelon veins are nearly one order of magnitude shorter in length than the regional veins (Fig.3.12f). The distribution and range of vein length and aspect ratio can be understood mechanically, by considering the elastic interaction which occurs between closely spaced veins. As explained previously, this geometry favours elastic interaction with the result that propagation of the longest veins tends to be favoured. This effect results in a vein population characterised by many shorter veins with low aspect ratios and relatively few long veins with high aspect ratios.

Effects of multiple crack interaction on vein shape

The effect of mechanical interaction on propagating veins can result in pronounced changes of crack profile geometry. For example the deformation fields and the internal fluid pressure within an array of closely spaced or en echelon cracks would work against the dilation of adjacent crack tips. Numerical experiments of the influence of elastic interaction on crack shape are described by Delaney & Pollard (1981). Their results indicate that the sides of closely spaced elastic cracks warp, their opposite sides straighten and adjacent crack tips become tapered (Fig.3.13). These model results may be compared with the shapes of closely spaced veins. Figures 3.14a and 14b shows two typical examples of closely spaced veins which have blunt and wedge-shaped tips. The abrupt thinning and convex inward curvature of adjacent vein walls for these examples are considered to

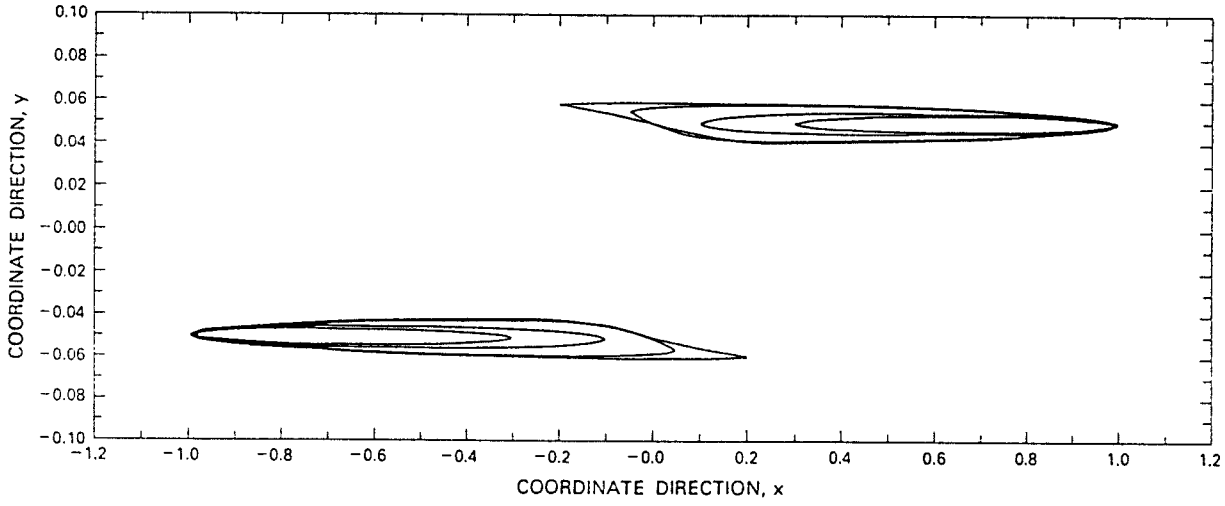

Figure 3.13. Shapes of dilated pairs of collinear and offset cracks subject to uniform internal pressure, from a continuum-mechanical experiment described by Delaney & Pollard (1981).

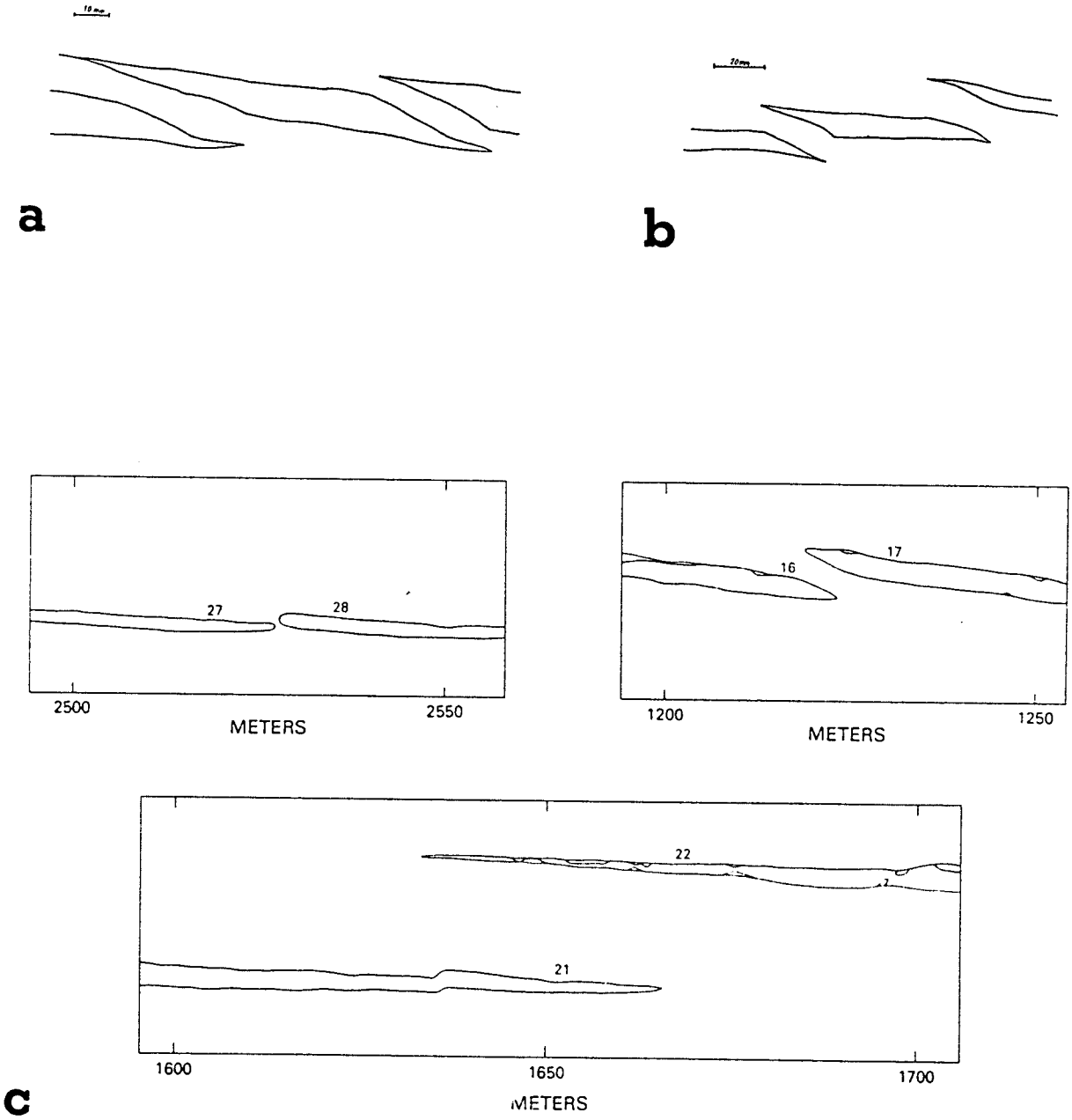

Figure 3.14. [a,b] Line diagrams of blunt and wedge-shaped vein tips from Millook Haven. [c] Typical forms of dyke segment ends with different offset and separation (Delaney & Pollard 1981, fig.10b).

be the result of mechanical crack interaction. Similar observations can be made for some dykes. Fig.3.14 shows some forms of dyke segment terminations with different offset and separation values. These particular examples are from the north-east Ship Rock dyke segment (Delaney & Pollard 1981). They display wedge-shaped and blunt tips: features typical of multiple crack interaction. To more fully analyse the effect on vein shape, vein displacement analysis is introduced in the next section.

3.5 ANALYSIS OF VEIN DILATION AND DISPLACEMENTS

3.5.1 Dilation and displacement

For many veins there is a visible record of the displacement that has occurred during dilation, which may be tracked by fibres and wall-rock markers. Using fibres, a variety of methods have been developed (Elliot 1972, Wickham 1973, Durney & Ramsay 1973, Ellis 1986) to determine host-rock incremental and finite strain values. These methods assume vein-fibre growth is syntectonic and displacement controlled. Despite the many viable interpretations made using these methods of strain analysis, the basis of some of their assumptions are disputed (Cox 1987, Urai *et al.* 1991). Since veins almost always represent multiple cracking events, it is necessary to determine the vein opening history, and establish independently if fibres track vein opening displacements.

The length $2a$ and distribution of thickness along veins are quantities that can be measured (Fig.3.15a). Since the dilational shape should be preserved by the mineral infill these quantities can be related to the crack displacement field, if veins are idealised as pure mode I elastic cracks. In this study vein thickness is assumed to be equal to the sum of the dilational displacements.

Crack dilation is defined by Pollard & Segall (1987, eq. 8.35) as

$$\Delta u = u_1(0^+,x_2) - u_1(0^-,x_2) \qquad (3.17)$$

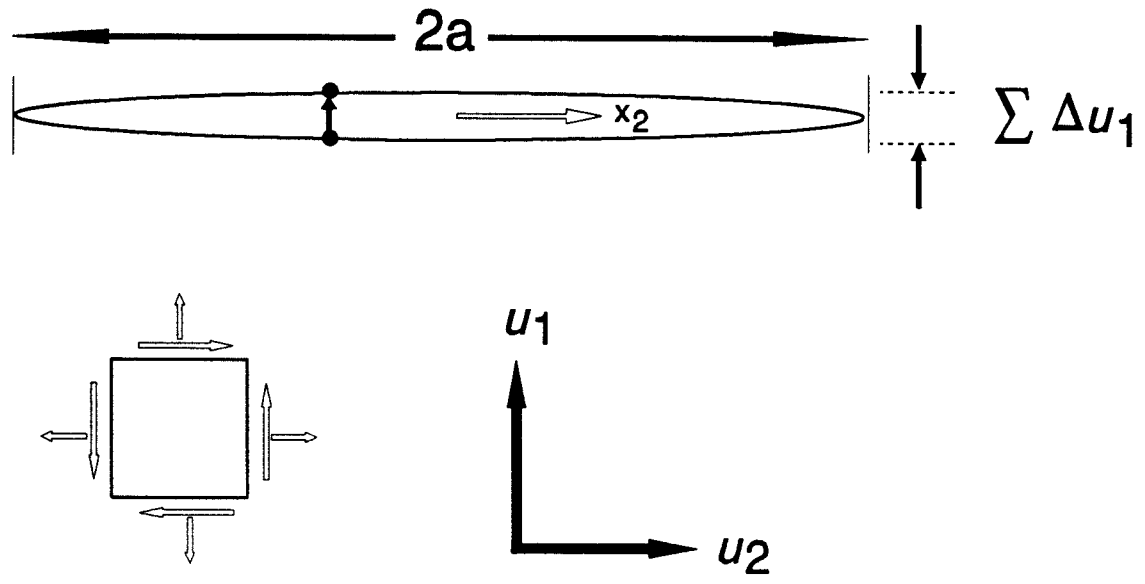

[a]

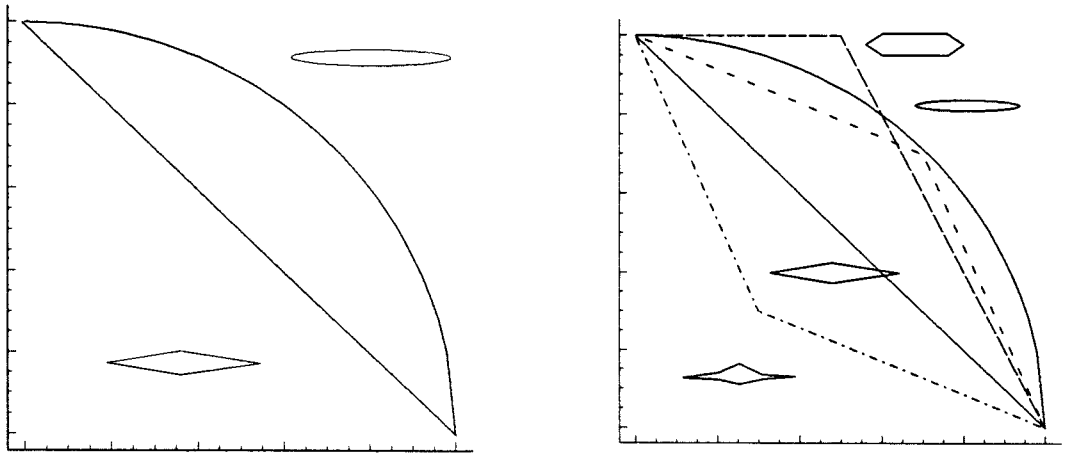

[b] [c]

Figure 3.15. [a] Idealisation of a vein as a pure mode I crack, with conventions for measurement of displacement (u_1, u_2), cumulative vein opening displacements, $\Sigma \underline{u}_1$, and the stress components. [b] Normalised graph of displacement for an elastic crack with elliptical and linear conical distributions. Insets show idealised crack profiles with thier corresponding displacement distribution. [c] Normalised graph of displacement illustrating the types of displacement distribution profiles. Insets show idealised vein shapes and their corresponding profile.

where 0^+ and 0^- refer to the movement of the upper and lower crack walls. For an elliptical mode I crack the distribution of displacement is given by

$$\Delta\, u_1(x_2) = \left(\frac{2(1 - \nu)}{\mu}\right)\Delta\sigma_1(a^2 - x_2^2)^{1/2} \qquad (3.18)$$

By idealising a vein as a mode I crack, the opening displacement (u_1) represented by dilation can be expressed by

$$\Delta u_1 = (\sigma_{11}^r - P_f)\left(\frac{2(1 - \nu)}{\mu}\right)(a^2 - x_2^2)^{1/2} \qquad (3.19)$$

Since rock does not fulfil the theoretical requirements of being homogeneous and elastic, significant deviations would be expected for graphs of vein opening displacement.

To analyse vein dilation in terms of the wall-rock displacements a modified displacement-distance method described by Williams & Chapman (1983) is used. Distance (x) is measured along the vein periphery with displacement (d) equal to vein thickness. For a single, isolated vein the simplest way of expressing the displacement is to consider a crack of half-length a given by

$$d = S(a^2 - x^2)^{1/2} \qquad (3.20)$$

where S is a constant representing the host-rock elastic properties and driving stress and x is the distance from the crack centre. Normalising the displacement by the crack length gives

$$D = S(1 - (x/a)^2)^{1/2}$$

For an ideal elastic crack the opening displacement has an elliptical form with a maximum at the

crack centre, tapering of to zero at the tips. Figure 3.15b shows a graph of normalised displacement for an elliptical crack, also shown superimposed is a linear (conical) profile. Figure 3.15b shows a selection of idealised d-x profile types for cracks with displacement distributions that deviate from the ideal elastic crack profile. The insets show approximate vein shapes that will produce these profile types. These vein profile types are illustrated and discussed in section 3.7.

3.6 OBSERVATIONS FOR SELECTED VEIN GEOMETRIES

3.6.1 Isolated veins

At Millook Haven the vein densities and overlaps are generally very high, so the effects of multiple crack interaction mean that isolated veins can rarely be identified. To examine the displacement characteristics of individual, isolated veins an alternative study area was selected. Measurements were made of veins in Lower Jurassic rocks in an area of relatively simple structure near Kilve [ST148844-60] in North Somerset. The veins are infilled with calcite and contained within homogeneous limestones from an interbedded limestone-shale sequence. The examples analysed range in length from <0.50-250mm and have a wide range of orientations. The veins are intermediate in size between microcracks and mesoscopic veins, and are probably associated with the more extensive E-W vein sets and veining accompanying the development of the regional extensional faults (Peacock 1991, Peacock & Sanderson 1991).

Analysis of vein thickness-distance (D-x)(Fig.3.16) indicates that individual veins correspond reasonably well to a conical profile, although the bulk of the data plot between this profile and the elliptical profile expected for elastic cracks (Fig.3.15b). Comparable observations for this type of dispersion of displacement have been made for the distribution of slip for single faults (Muroaka & Kamata 1983, Walsh & Watterson 1988), fault arrays (Peacock & Sanderson 1991) and veins (Peacock 1991). This data set has many analogies with the cumulative slip distribution on a fault, where a single planar fault accumulates displacement with the amount of slip proportional to fault length (Walsh & Watterson 1988). As the d-x profiles of isolated veins may reflect the number of

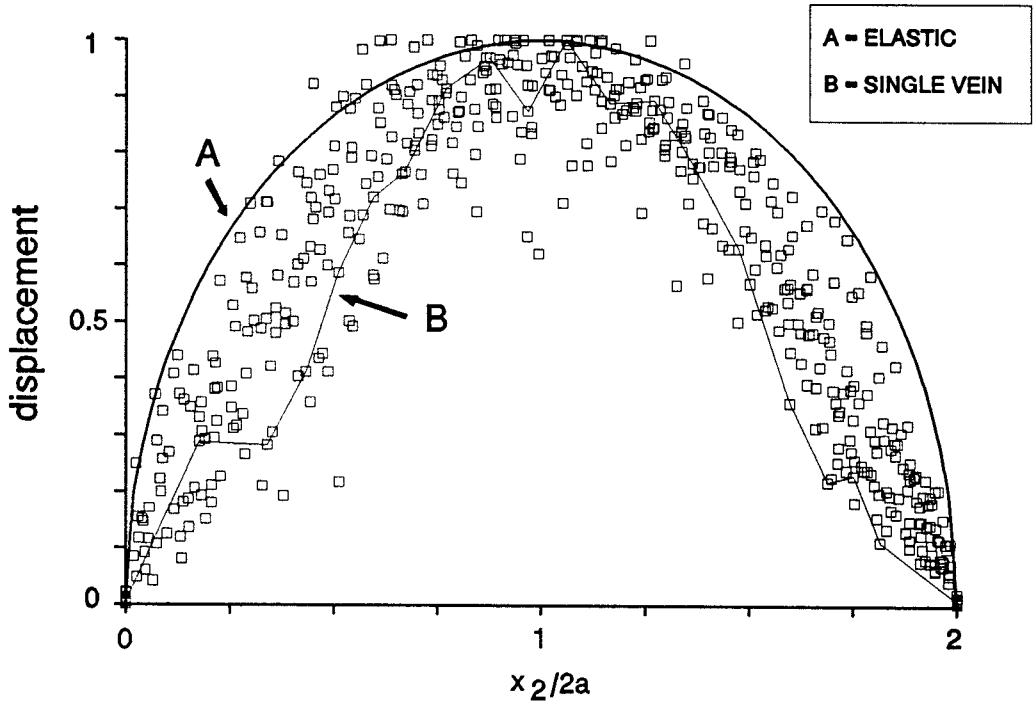

Figure 3.16. Normalised graph of thickness plotted against distance along veins for 15 isolated veins in Lower Jurassic rocks from Kilve, North Somerset.

increments of crack propagation during dilation, and the lateral variation of growth between the vein tip and its centre, a cumulative growth model is probably more justified. An additional explanation for the variations, is that the stress singularity predicted for a crack tip, is not achieved. As displacement at the vein tips is unlikely to diminish entirely to zero, some inelastic and permanent deformation must be accommodated there.

3.6.2 Overlapping and en echelon veins

An example of the effects on the propagation of two overlapping veins was shown in Fig.3.9. A d-x graph for this example (Fig.3.17a) indicates that vein thickness distribution is characterised by asymmetric profiles that depart from ideal elastic crack profiles. For increasing crack overlap these profiles will tend to develop a flat central portion with flanks marking steep displacement gradients. Figures 3.17b and 17c show two further examples of d-x analysis for veins in echelon arrays. They are also characterised by asymmetric displacement profiles.

The effects of increasing overlap on the displacement profiles of veins can be demonstrated graphically from a d-x analysis of the elastic crack shapes produced in a series of numerical experiments by Delaney & Pollard (1981)(Fig.3.13). Figure 3.18 shows the sequence of d-x graphs for each crack. It is very apparent that with increasing overlap, the departures from the ideal elastic crack profile become more pronounced, as d-x profiles become progressively more asymmetric and conical in shape. These effects can be attributed to mechanical interaction of the two fractures, where the stress concentrations of each crack tip and its internal fluid pressure are working against the dilation of its neighbour. Individual veins in en echelon arrays can be visualised as separate cracks that are mechanically interacting with their neighbours. Within en echelon arrays, individual veins usually display a range of shapes and hence displacement characteristics. These features are largely dependent on the array configuration, the array-angle, and the position of the vein within the array. Dilation across en echelon arrays often remains fairly constant with approximate conical profiles and displacement minima. The d-x profiles are dependent on the amount of bridge rotation, bridge shape and thickness as bridges have to bend and/or rotate or fracture to accommodate the displacement produced by vein dilation.

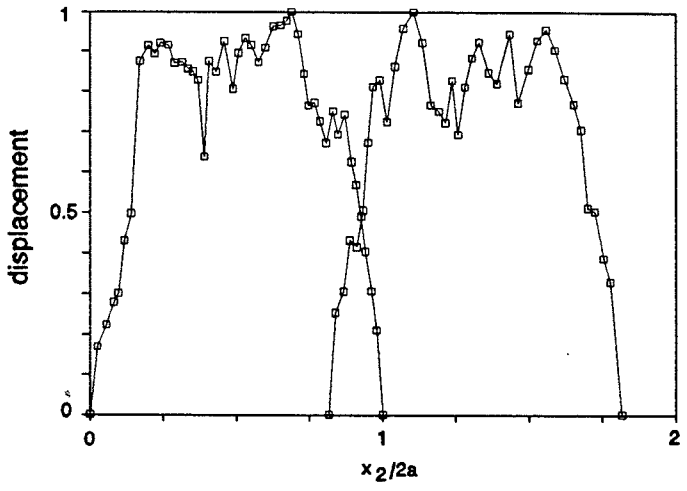

[a]

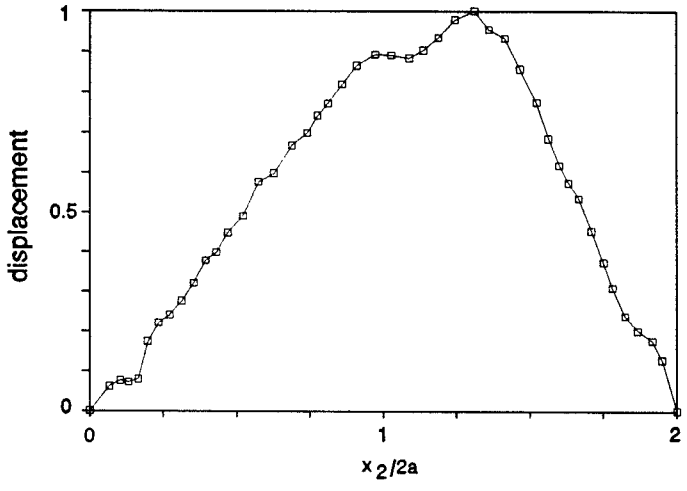

[b]

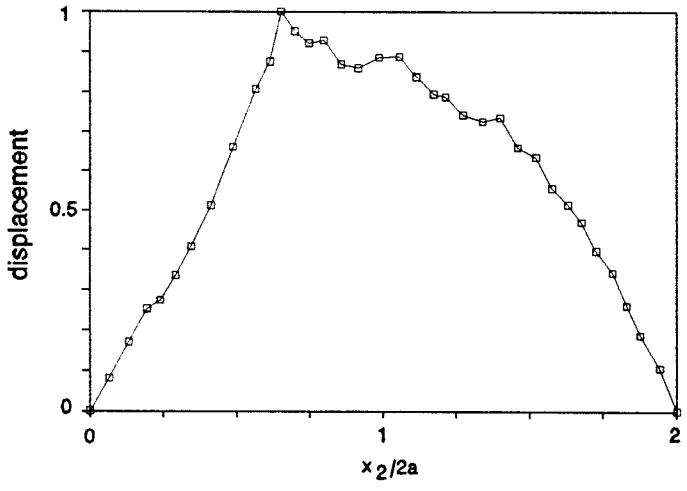

[c]

Figure 3.17. D-x analysis plots of: [a] the example shown as Fig.3.9 [b & c] examples shown as Figs.3.14a and 3.14b.

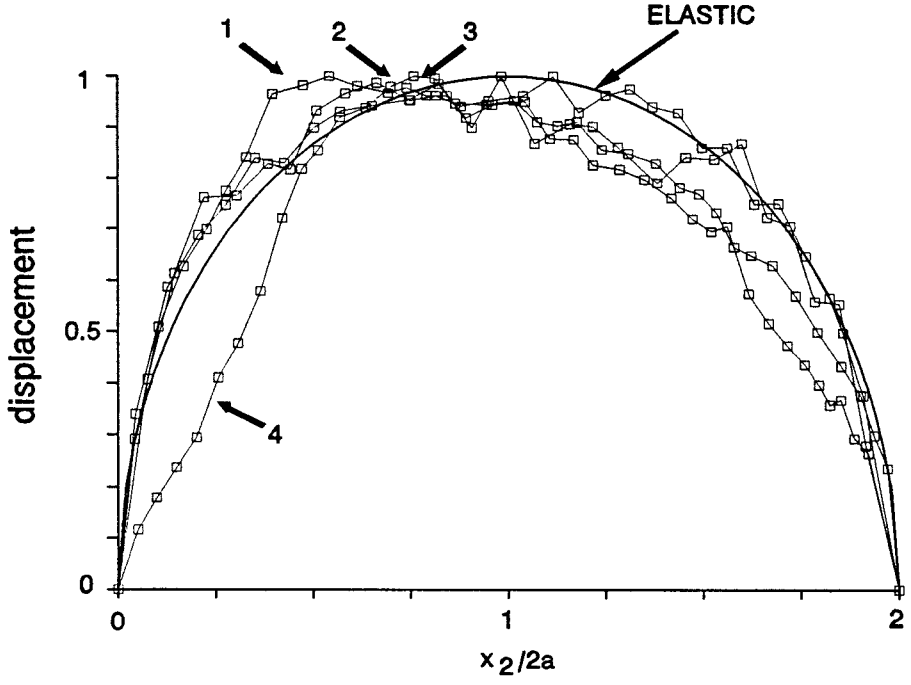

Figure 3.18. D-x analysis of the sequence of elastic cracks produced during a continuum-mechanical experiment described by Delaney & Pollard (1981)(Fig.3.13).

3.6.3 Single, composite veins

Veins are commonly composed of discrete segments that have coalesced during growth. Nicholson & Pollard 1985 have described how some veins have developed through the propagation, interaction and linkage of individual en echelon vein segments. For some veins, remnant structures and irregularities preserved in the vein margins allow recognition of stages in their development (Chapter 5). These features are usually marked by displacement (width) minima on graphs of displacement-distance. So veins of this type generally have complex d-x characteristics which reflect their propagation history.

3.6.4 Comparisons with the dilational form of dykes

Dykes are an interesting case of crack dilation as they generally represent one phase of magma injection and hence a single opening event. Descriptions of the contact displacements for dyke intrusion are given for the Ship Rock Dyke, New Mexico by Delaney & Pollard (1981). The north-eastern dyke and its individual en echelon segments were idealised as mode I cracks, so the distribution of dyke dilation can be described by equation (3.16). The elliptical form of this equation describes the dyke shape reasonably well (Fig.3.19). Departures from this simple elliptical profile were attributed by Delaney & Pollard (1981) to host-rock brecciation and erosion during dyke growth. Based on the analysis of vein profiles and their displacements, it is instructive to re-examine Delaney & Pollard's data for the Ship Rock dyke segments. Two main types of deviation from the elliptical, elastic crack profile can be recognised:

[1] Steep displacement gradients that occur at the dyke tips, while the central part of the displacement graph has a flat portion (Fig.3.19b). This observation is consistent with the view that these departures from the simple elliptical form are due to elastic interaction of adjacent dyke segments (Fig.3.11). Typical forms for the distal ends of some dykes (Fig.3.14b) show blunt and asymmetric wedge-shaped tips: characteristics usually diagnostic of multiple crack interaction.

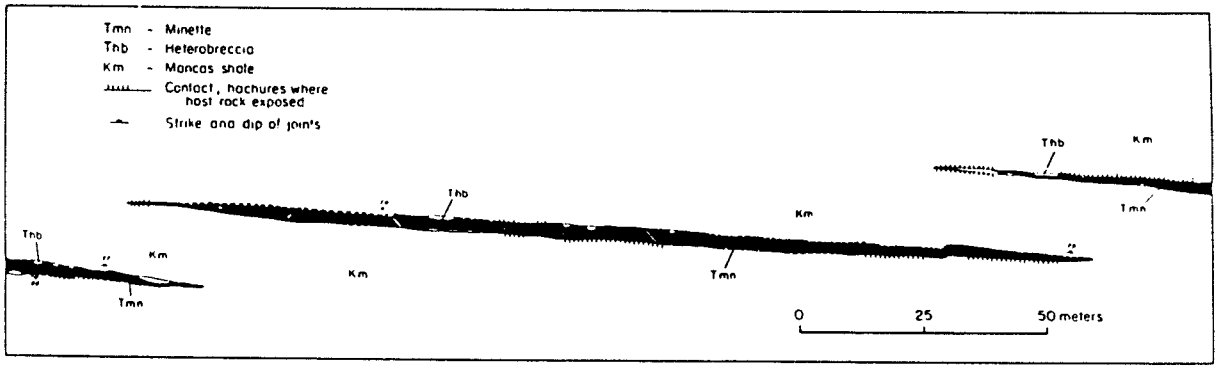

[a]

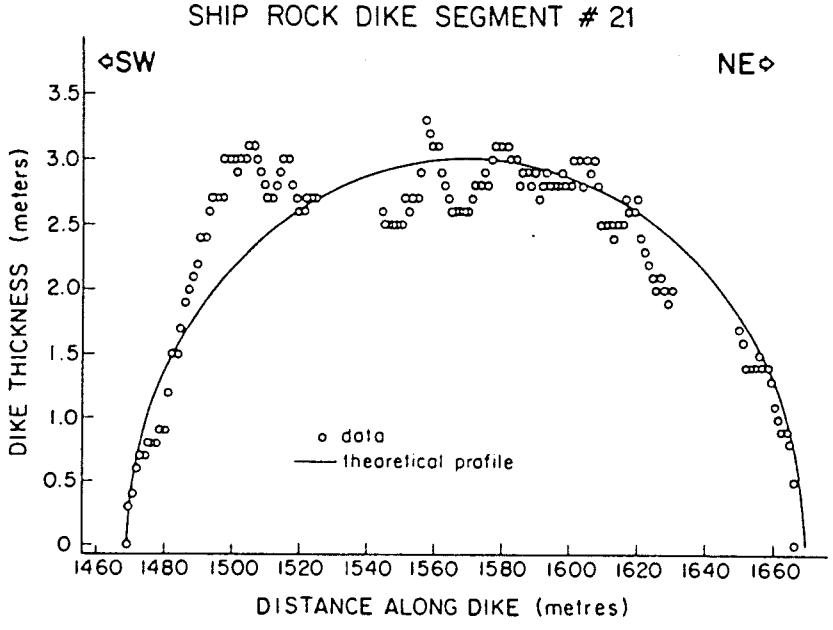

[b]

Figure 3.19. [a] Map of several dyke segments from near Ship Rock, New Mexico (Pollard & Segall 1987, fig.8.20). This dyke was the subject of a study by Delaney & Pollard (1981). [b] Normalised graph of dyke thickness plotted against distance along the dyke for one of the Ship Rock dyke segments (Pollard & Segall 1987).

[2] Minor variations in the graph profile with local displacement minima suggest that fusion of earlier echelon dyke segments has occurred. Support for this can be seen in the small steps and irregularities at the dyke margins (Fig.3.19a).

A second example of a thickness-distance for a dyke is provided by Pollard & Muller (1976) for the Walsen Dyke, Colorado. The graph which is reproduced in Fig.3.19c is also marked by departures from the elastic profile. These departures include a prominent displacement minima that may mark a point of linkage (*ie.* the coalescence and fusion of two dyke segments): this is shown as an addition to the original plot of Pollard & Muller (1976).

3.6.5 Discussion of results

The elliptical displacement profile for a single isolated elastic crack is similar to the slip distribution produced in a single earthquake (Aki & Richards 1980, Scholz 1990). These models may be compared with faults which record cumulative slip episodes (Muroaka & Kamata 1983, Walsh & Watterson 1987). In general these profiles indicate maximum slip near the fault centre with displacement tapering off to zero at the edges. As slip accumulates the crack increases its length, so accumulated displacement during repeated propagation tends to produce a conical d-x graph profile. Cumulative slip models such as the arithmetic growth model of Walsh & Watterson (1987), suggest that faults accumulate displacement according to the elliptical elastic crack model, with each slip increment being proportional to fault length. This profile approximates to the linear (conical) profile. Therefore, if veins or faults initiate at a point or as en echelon arrays, growth with progressive displacement will tend to produce a cone shaped profile, as heterogeneities like steps or bends are smoothed out. Slip or displacement minima on d-x graphs may therefore indicate areas of strain accommodation and/or points of crack linkage.

3.7 VEIN PROFILE GEOMETRIES AND PROPAGATION HISTORIES

From field observations of different vein profile geometries and the analysis of their d-x characteristics, important information about the kinematics of vein initiation and growth, as well as temporal and spatial changes in loading conditions can be gained. Stages in crack growth and termination which can be identified from the type examples previously described are shown diagrammatically in Fig.3.20 and summarised below:

[1] Initially a rock may comprise of approximately isolated cracks (Fig.3.20a). These may form through local stress concentration caused by randomly oriented and distributed heterogeneities. Those flaws which are favourably oriented for growth will propagate preferentially, *ie.* aligned with their longest dimension parallel to the remote maximum compressive stress.

[2] Stress concentration at the crack tips causes the fracture to propagate as long as sufficient fluid pressure and driving stress is maintained (Fig.3.20b).

[3] With continued crack growth some of the veins in the rock volume may start to overlap and interact with neighbouring veins (Fig.3.20c). This selective mechanical interaction can produce en echelon and conjugate en echelon vein arrays.

[4] For individual veins or coplanar and overlapping veins, as the stress fields at adjacent crack tips become perturbed, mixed-mode loading will be induced, which may lead to local deviation of vein propagation paths. For veins with small separations, connecting fractures, non-continuous with the principal crack tip may cut rock bridges into adjacent crack sides to link with the adjacent crack segment (Fig.3.20d).

[5] Where adjacent vein segments have fused this can lead to a significant increase in crack dilation. These remnant points of crack linkage may be marked by lateral extension fractures and stepped or irregular vein margins. These features usually show up on d-x graph profiles as displacement minima as they are often points of reduced vein thickness.

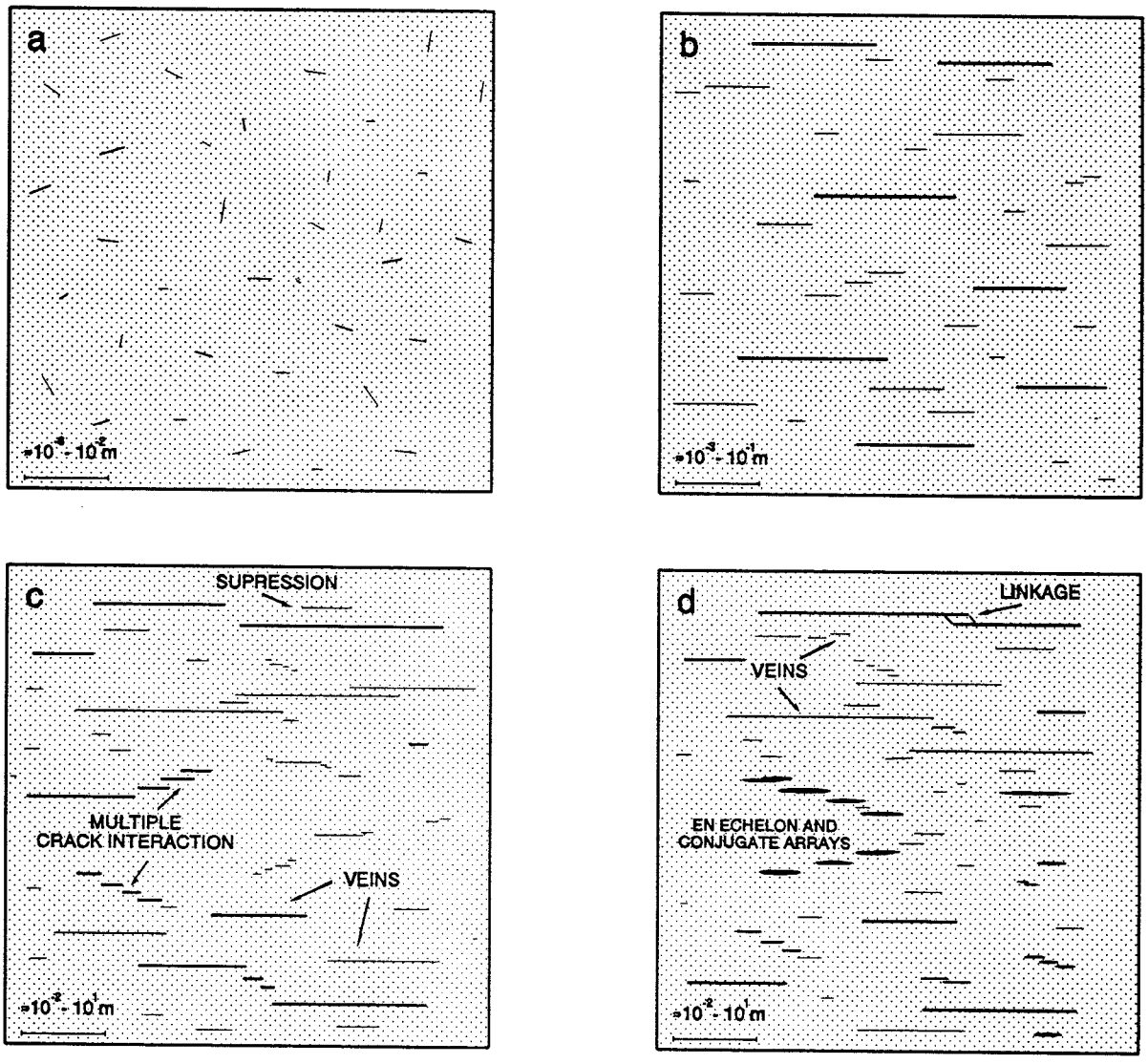

Figure 3.20. Propagation and growth sequence model for the formation of sets of closely spaced subparallel veins, en echelon vein arrays and conjugate en echelon vein sets. This model is based on field observations of vein geometries described in previous sections, and from the results of some numerical experiments described by Olson & Pollard (1991).

[a] Rock mass containing many randomly distributed flaws and grain-scale cracks that can act as stress-concentrators during compressive deformation.

[b] Accumulation of applied strain and stress cycles result in the formation of cracks with different lengths. These are aligned perpendicular to the least compressive principal stress.

[c] Formation of a vein set with 'older' veins increasing in length through crack coalescence and fusion, with the initiation of new veins. This results in an increase of total vein length and a gradual decrease of average vein spacing. Interaction amongst existing cracks leads to further vein growth through selective mechanical interaction, with a strong tendency to the formation of en echelon arrays.

[d] The final geometry of the vein set with the formation of overlapping, en echelon and conjugate vein sets. The en echelon veins have a wide range of vein-array angles, and overlap and spacing values.

3.8 DISCUSSION AND SUMMARY

3.8.1 Propagation paths

Vein geometry is partly determined by the path traced out by the crack tip during propagation and the state of stress in the host-rock. Where the loading conditions are non-uniform we would expect curved and/or kinked veins if the loading conditions are smooth and continuous. If the least compressive stress changes orientation along the vein propagation path, a shear stress is resolved, and hence part of the vein may experience mixed-mode I-III loading and a change in the near tip stress. In some cases the crack may break down into multiple segments, which have en echelon patterns in cross-section (Chapter 5, Pollard *et al.* 1982, Nicholson & Pollard 1985, Nicholson & Ejfior 1987).

The high overlaps for some vein sets observed in the Crackington Formation, suggest that a strong remote compressive crack-parallel stress was present. This would have been required to be present at the time of vein growth to maintain the high crack path stability, and inhibit curvature of vein propagation paths and linkage due to the local fracture-induced stresses. From this we can deduce that the vein propagation paths were strongly dependent on the remote differential stress parallel to the vein arrays.

3.8.2 Vein initiation and growth

The various geometries and stages of vein development observed from analysis of profile geometry and the d-x analysis of thickness distribution for veins and vein arrays, illustrate the relationship between vein shape and their propagation history. The formation of many of the vein geometries can be explained in terms of the effects of selective mechanical crack interaction and stress shielding.

For the natural examples described here the wide range of vein-array angles (see Section 5.1) and separation values for many en echelon veins, together with contemporaneous subparallel and overlapping veins, supports a mechanism of selective interaction and growth from initially random

distributed flaws. This type of growth mechanism for veins is not surprising since microcrack growth, coalescence and crack fusion is well known from experimental rock deformation (*eg.* Dey & Wang 1981, Costin 1987). These microstructures generally initiate from local stress concentrations, resulting from mismatching of elastic properties along grain boundaries (Tapponier & Brace 1976) or from natural flaws (Kranz 1983, Engelder & Lacazette 1990) or voids in rock. These microcracks then propagate parallel to the greatest principal compressive stress (Peng & Johnson 1972, Nemat-Nasser & Horii 1982, Kranz 1983). The various stages of deformation observed from rock deformation experiments suggest that veins and joints should result from pre-existing cracks and that they initially propagate as mode I cracks. Recently, numerical experimental modelling of the initiation and growth of veins and joints through the interaction of randomly distributed flaws (Olson & Pollard 1991, Wu & Pollard 1992) has provided useful insights into the analysis of natural fracture patterns.

3.9 CONCLUSIONS

Detailed observations and measurements of vein profiles and their terminations yields important information about processes of vein formation. Examination of the displacements across veins and vein arrays provides useful observational links between theoretical and experimental investigations of vein initiation and growth. From these results we can verify hypotheses about the stress states and the host-rock response implied by some vein traces. General conclusions which emerge from this study are summarised:

[1] Veins initially propagate as essentially mode I cracks. The geometry of their propagation path (*eg.* branches, splays and tail cracks) can be used to infer paleostress trajectories and to monitor changes in loading conditions.

[2] Vein initiation and growth kinematics can be described in terms of selective mechanical interaction. This can lead to the formation of en echelon and conjugate en echelon vein sets which have a wide range of vein-array angles and separation values.

[3] Variation of vein aspect ratio can be understood mechanically by considering the elastic interaction which occurs between closely spaced veins. Since the crack extension force increases linearly with vein length, and there is nearly an order of magnitude of variation of vein aspect ratio, this assumption implies a similar range of $(\sigma'_{11} - P_f)$ values.

[4] Displacement distance (d-x) plots for isolated veins (mode I fractures) display approximate conical displacement profiles. The scatter in the data is consistent with similar observations made for fault slip (mode II, III), suggesting that single event elastic crack models do not adequately describe vein shape and that cumulative slip models of the type discussed by Walsh & Watterson (1987) and Peacock & Sanderson (1991) for faults may be more appropriate.

[5] Different stages of vein initiation and growth during the interaction, coalescence and fusion of cracks can be identified from vein d-x profiles. Where the crack overlap is low the graphs are characterised by data plotting above the conical profile. When complete linkage has occurred, a single, composite vein is formed. These have irregular margins with remnant points of crack linkage marked by local displacement minima on d-x graphs. Bridges play an important role in accommodating crack dilation by maintaining displacement continuity across the array.

4

Vein thickness and spacing in layered rocks

4.1 INTRODUCTION

The objective of this study is to describe the frequency and spatial distribution of vein thickness (opening dispiacement discontinuity) and spacing in layered rocks, using measurements of veins from Millook Haven. Since the parameters which control these distributions can be inferred from the form of their distribution, some of the factors which control the geometric characteristics of vein patterns in layered sedimentary rocks can be determined. The mechanical control of layer thickness on vein development is examined, and the extension and strain represented by the veining analysed. Characterisation of these factors may also have useful implications for studies of fracture hydrology and models of rock fracture and fluid flow.

Data are presented for vein thickness measured along line traverses (1D) and by area sampling (2D). The field setting of the dataset is described and the frequency and spatial distributions of vein thickness and spacing are quantified statistically. From this analysis, the hypothesis that vein thickness variation takes the form of a power-law frequency distribution is evaluated. To achieve this, the cumulative frequency distribution of vein thickness and spacing is tested in terms of negative exponential, lognormal and power law models. Recent studies have suggested that the self-similarity and the self-affinity of rock fracture exists over many different scales of observation (Turcotte 1986,

1989; Main *et al.* 1990), with scale invariance also described for the spatial and temporal signatures of earthquake aftershock sequences (Aki 1981, Scholz 1990) and for the cumulative slip distributions of faults (Kakimi 1980, Childs *et al.* 1990, Walsh & Watterson 1992).

4.2 FIELD OBSERVATIONS

The area sampled includes sections from beach outcrops situated around Millook Haven, North Cornwall. Detailed observations and measurements of veins were made in the Crackington Formation (Namurian-Westphalian), an interbedded sequence of sandstones and shales of upper diagenetic-anchizone grade (Primmer 1985, Cornford *et al.* 1987). The outcrops sampled cover a range of local structural settings, which include normal and inverted fold limbs and various positions within individual folds. Although many vein sets exist in the area, these observations mainly concern the dominant pre- and syn-fold vein sets which are oriented NW-SE and NE-SW (Chapter 2, Beach 1977, Jackson 1991).

Most of the veins are orthogonal to bedding planes and are mainly confined to single sandstone units. They generally extend from the top to the bottom of individual layers and terminate near bed interfaces or lithological boundaries. Some veins do not extend entirely through each layer, and in some profiles these veins occur in en echelon arrays. Generally veins only penetrate more than one bed where stacked or amalgamated sandstone multilayers are separated by only thin shale or siltstone layers (<20mm). Between adjacent sandstone layers, veins of an individual set have consistent orientations, although they are only rarely connected across interbedded shales. These observations suggest the beds mainly fractured independently of each other. However there may have been some degree of mechanical coupling between veins in adjacent layers through the elastic interaction of the near-field fracture induced stresses.

Where veins extend entirely through a layer, a range of termination structures are developed. Some veins taper towards bed margins while others are truncated with blunt tips at the intersection with the bed boundary. Truncated veins appear as relatively planar fractures with blunt ends. Where veins

TRANSECT	POSITION	kn	LAYER THICKNESS (mm)	TRANSECT LENGTH (m)	$\sum_t$ (mm)	$\sum_t$ <10mm	$\sum_t$ >10mm	STRAIN (e) % EXTENSION	STRAIN (e) % EXTENSION ($\sum_t$ >10mm)	% TOTAL (e) $\sum_t$ >10mm
1	INVERTED	132	1030	30	464.8	165.0	299	0.016 (1.6)	0.016 (1.0)	62.5
2	NORMAL	35	330	2.6	312.5	70.5	242	0.137 (13.7)	0.10 (10.0)	72.9
3	INVERTED	42	600	6.5	-	-	-	-	-	-
4	NORMAL	180	300	-	-	-	-	-	-	-
5	INVERTED	122	380	20	461.7	172.7	289	0.024 (2.4)	0.015 (1.5)	62.5
6	INVERTED	84	350	10.5	433.3	153.3	280	0.043 (4.3)	0.027 (2.7)	62.7
7	INVERTED	31	680	5.0	432	55	377	0.095 (9.5)	0.082 (8.2)	86.3
8	INVERTED	72	190	6.0	321	169	152	0.057 (5.7)	0.026 (2.6)	45.6
9	INVERTED	21	1030	7.0	189	38	151	0.028 (2.8)	0.022 (2.2)	78.5
10	INVERTED	47	320	12.0	280	165	115	0.024 (2.4)	0.010 (1.1)	45.8
11	INVERTED	11	850	8.5	214	14	200	0.026 (2.6)	0.024 (2.4)	92.3
12	INVERTED	34	-	5.0	58	43	15	0.012 (1.2)	0.003 (0.3)	25.0
13	INVERTED	11	1100	2.5	121	32	89	0.051 (5.1)	0.037 (3.7)	52.9
14	INVERTED	19	280	7.0	261	34	227	0.039 (3.9)	0.034 (3.4)	87.2
15	NORMAL	21	300	4.5	319	15	304	0.078 (7.8)	0.072 (7.2)	92.3
16	NORMAL	45	190	4.0	266	102	164	0.073 (7.3)	0.043 (4.3)	58.9
17	NORMAL	18	130	1.8	219	20	199	0.139 (13.9)	0.124 (12.4)	89.2
18	INVERTED	15	220	6.0	154	25	129	0.026 (2.6)	0.022 (2.2)	84.6
19	INVERTED	26	310	15.0	325	60	265	0.022 (2.2)	0.018 (1.8)	81.8
20	INVERTED	33	300	2.6	231	96	135	0.098 (9.8)	0.055 (5.5)	56.1

TABLE 4.1

have propagated across layers they often have an out-of-plane arrangement at the interface and are slightly offset. At Millook Haven many of the bedding planes have also acted as interbed slip surfaces during part of the fold history: this mechanism may have had an important effect on vein formation.

4.3 DATA ACQUISITION

The thickness and spacing of veins were measured along line transects on bedding surfaces in the sandstone units using a measuring tape. A range of layer thicknesses (110-1100mm) were sampled (Table 4.1). Only veins which intersected the line transect were measured. All veins with thicknesses >0.2mm are recorded, although the varying condition (weathering, roughness) of some of the bedding surfaces may have lead to some undersampling of very thin veins (<1mm). Veins with smaller thicknesses were omitted as they were so small that they could not be measured accurately. The orientation and length of each transect were recorded together with the distance from the origin of each vein. The line transects were oriented perpendicular to the main vein set in normal fold limbs and sub-parallel to the E-W fold axes in inverted fold limbs due to the change of vein orientation. Several non-coplanar vein sets are developed in the inverted limbs. The individual datasets represent subhorizontal 1D transects, although where exposure was favourable area sampling (2D) was carried out. The database consists of 20 sets of line transect measurements (each with 10-180 veins) over lengths of 2.60-30m (Table 4.1).

4.4 DATA ON VEIN THICKNESS

4.4.1 Vein thickness distribution

At Millook Haven, vein thickness ranges from <0.2-230mm (Figs.4.1 and 4.2). The frequency distribution of vein thickness for the line transects are shown as a sequence of plots in Figures 4.1a, 4.1b and 4.1c. A prominent feature of these distributions is the decrease in frequency as thickness increases *ie.* veins >60mm thick occur only infrequently.

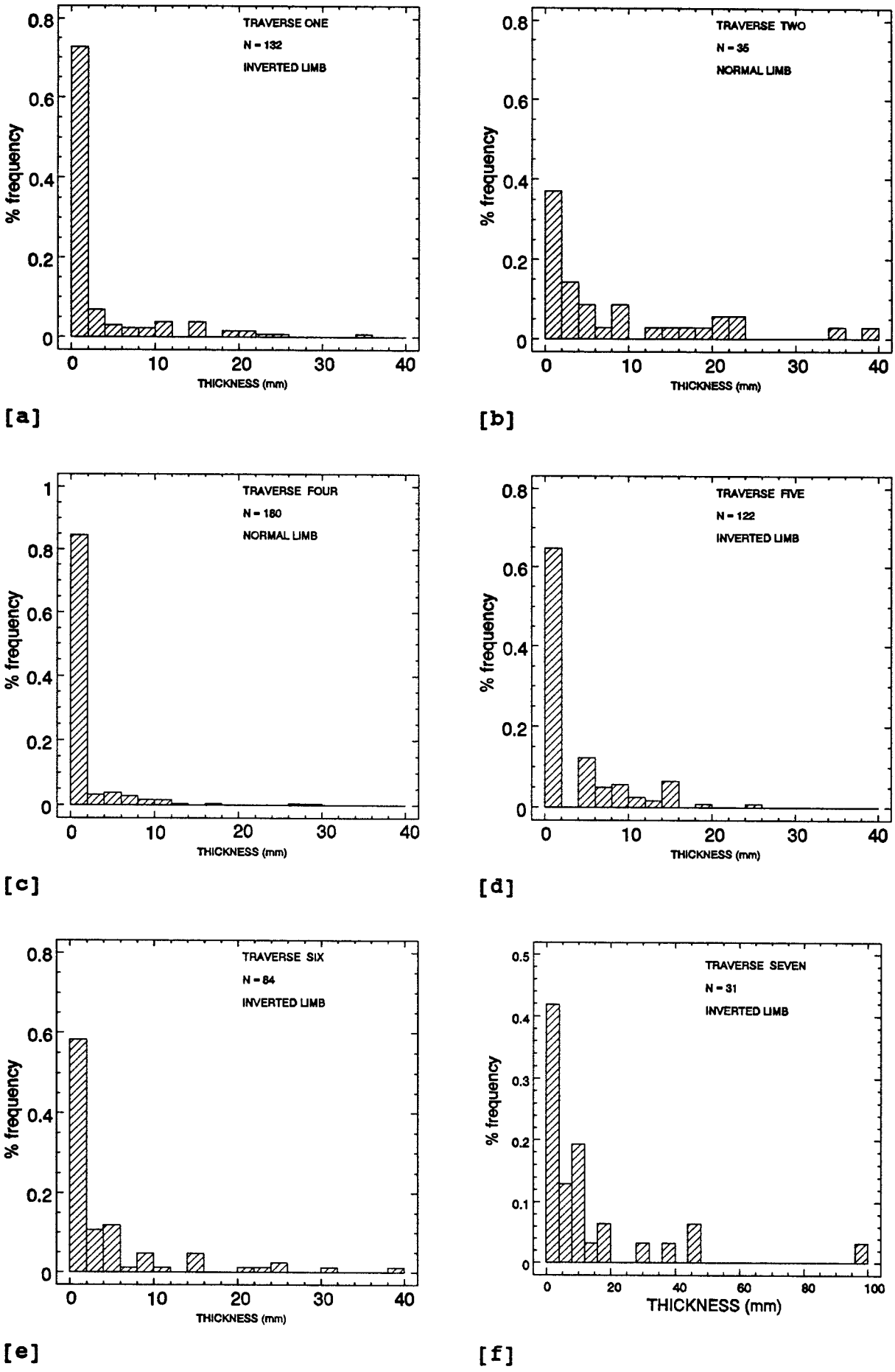

Figure 4.1a. Plots of the range and distribution of vein thickness for measurements from localities around Millook Haven.

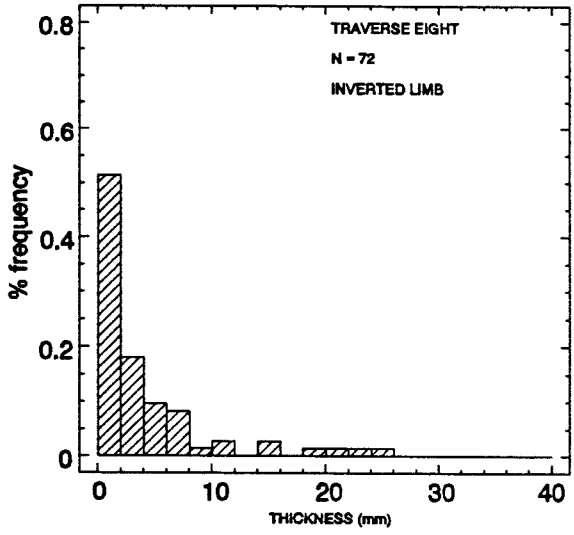

[a]

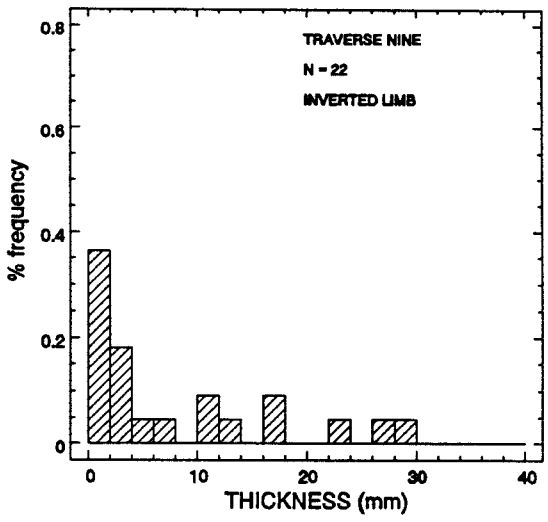

[b]

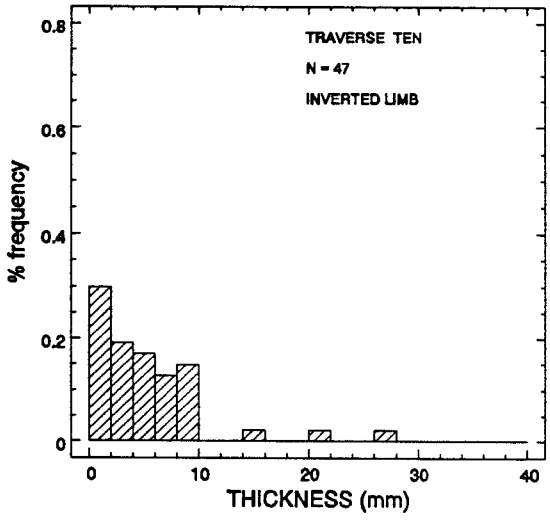

[c]

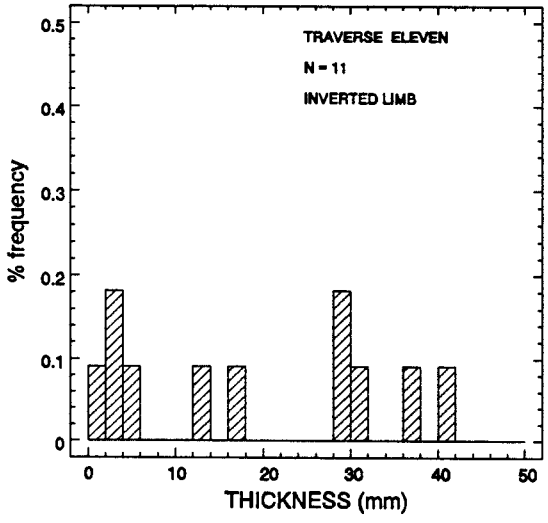

[d]

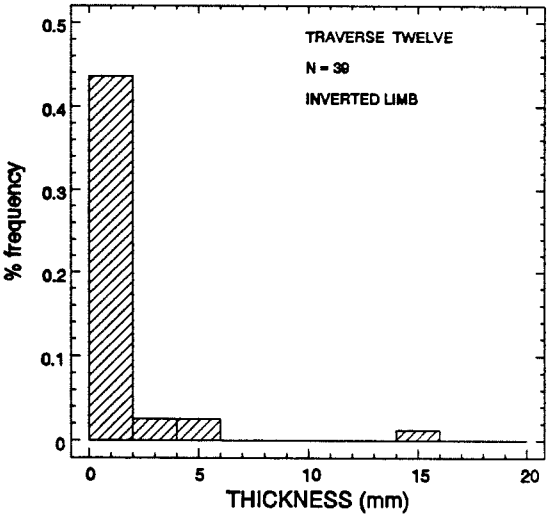

[e]

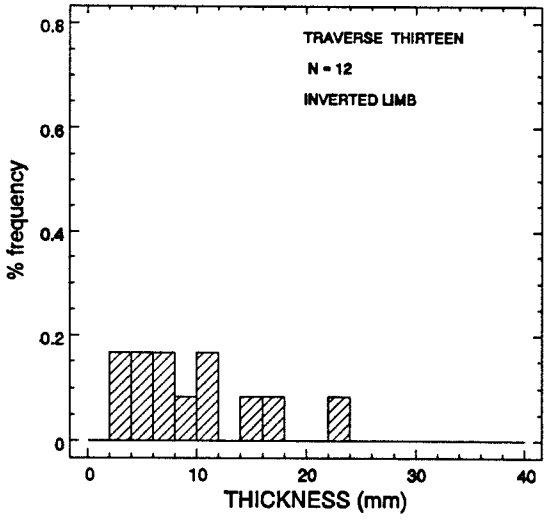

[f]

Figure 4.1b. Plots of the range and distribution of vein thickness for measurements from localities around Millook Haven.

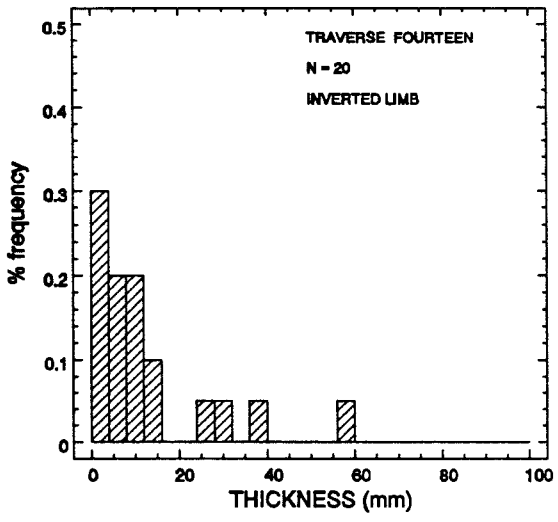

[a]

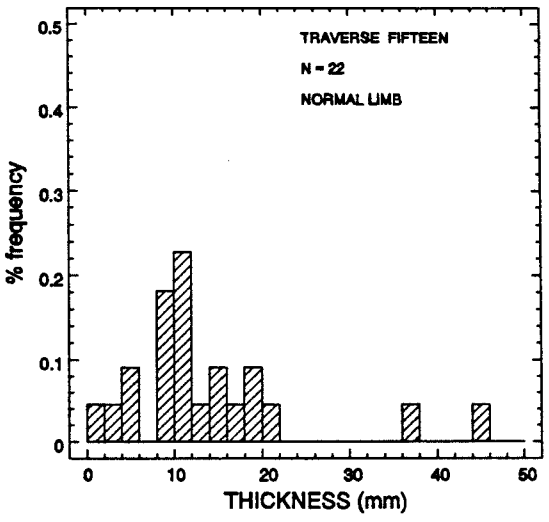

[b]

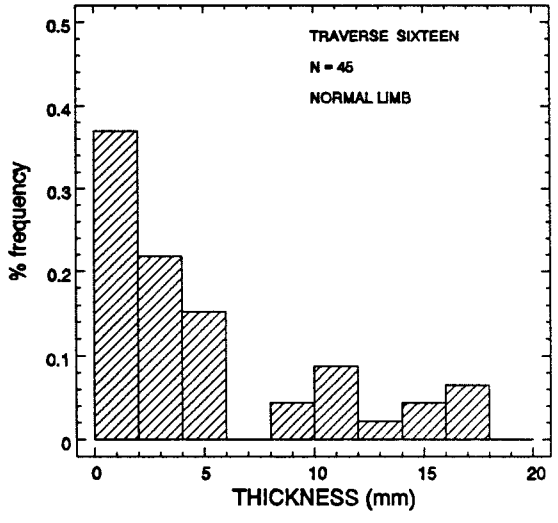

[c]

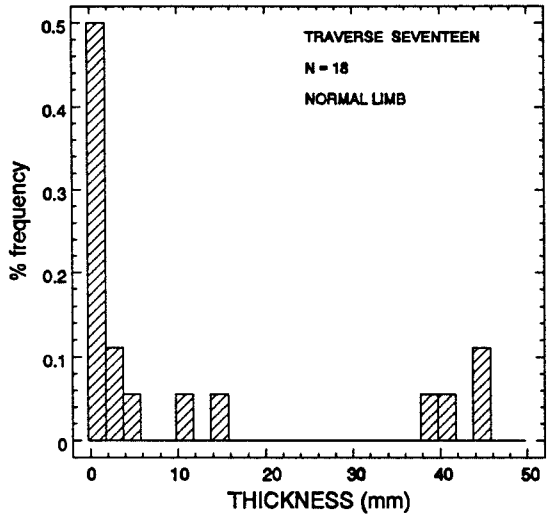

[d]

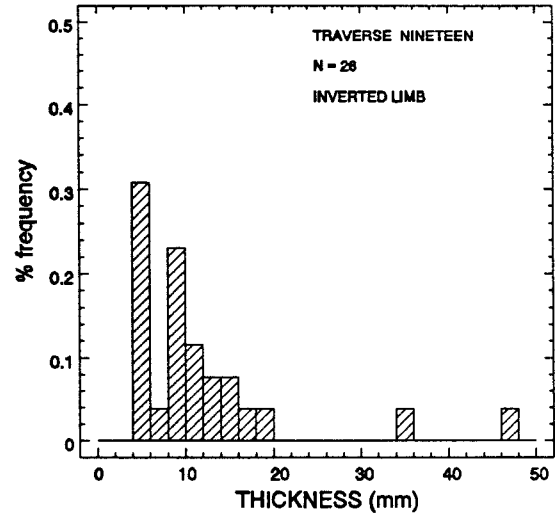

[e]

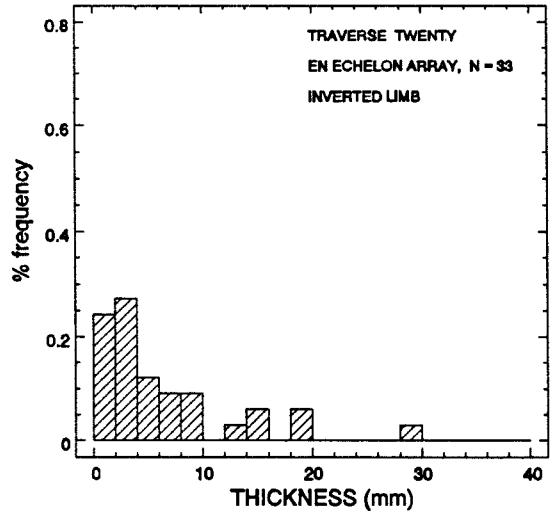

[f]

Figure 4.1c. Plots of the range and distribution of vein thickness for measurements from localities around Millook Haven.

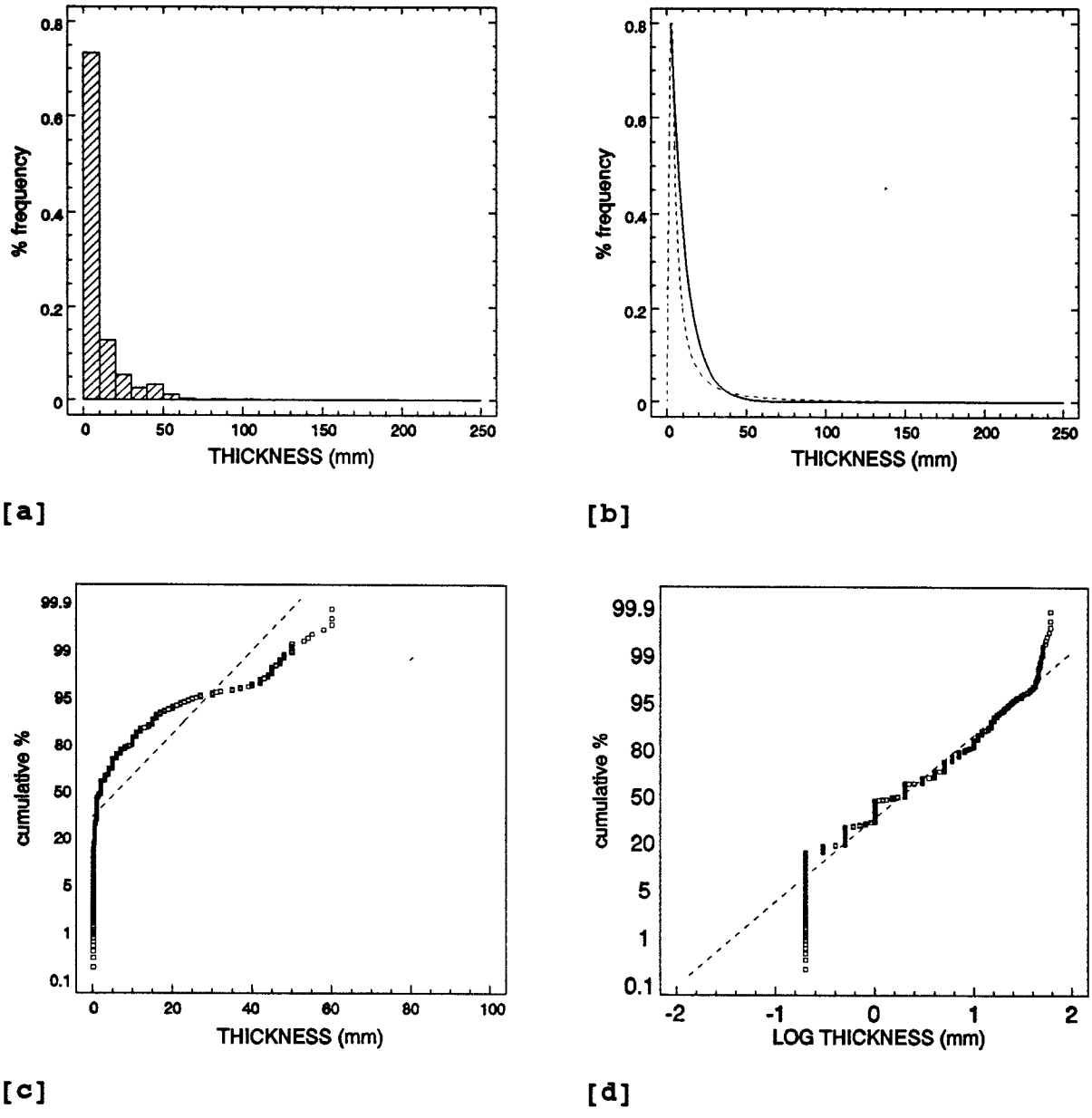

Figure 4.2. [a] Frequency histogram of all vein thickness measurements. [b] Frequency histogram showing fitted lines for negative exponential (solid) and lognormal (dashed) distribution functions. [c] Arithmetic (normal) probability plot of vein thickness, [d] arithmetic (normal) probability plot for log-transformed values (n = 967).

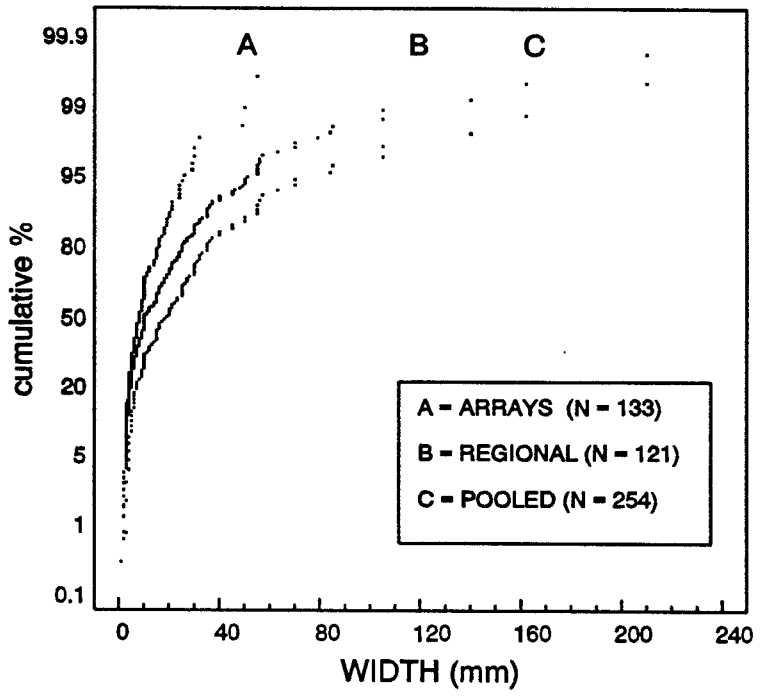

[a]

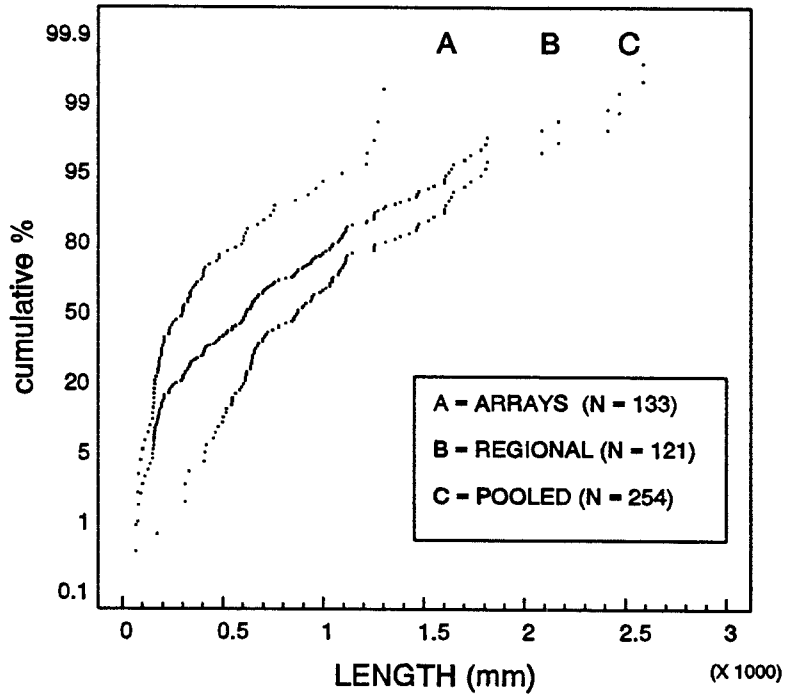

[b]

Figure 4.3. [a] Arithmetic (normal) probability plots of vein thickness for veins in en echelon arrays, regionally distributed and overlapping veins which are not in en echelon arrays, and the pooled measurements. [b] Arithmetic (normal) probability plots of vein length for veins in en echelon arrays, regionally distributed and overlapping veins which are not in en echelon arrays, and the pooled measurements.

Figure 4.2a shows the frequency distribution for all the measurements of vein thickness, and Fig.4.2b shows the dataset with lines fitted for negative exponential (solid) and lognormal (dashed) distribution functions. Although the negative exponential function provides an approximate description of the vein thickness frequency distribution, it underpredicts veins of thickness >60mm. Plotting the cumulative frequency of vein thickness on an arithmetic (normal) probability graph (Fig.4.2c) clearly indicates the non-gaussian nature of the distribution. Similar non-linear plots of log (thickness) (Fig.4.2d) also indicate that the distributions of vein thickness are not lognormal. These plots of the cumulative frequency distribution of vein thickness (Fig.4.2), indicate that negative exponential or power law distributions may be more appropriate to explain the variation of vein thickness.

From field observations of the vein characteristics, the veins can be subdivided into: [1] veins that occur in en echelon arrays and [2] regionally distributed, clustered and overlapping veins. Figure 4.3a shows arithmetic (normal) probability plots of vein thickness for these two geometries. It is clear that they do not follow normal distributions. The veins in en echelon arrays (Fig.4.3a and 3b) are more characterised by larger thickness values and lower lengths compared to the similarly oriented, regionally distributed and overlapping veins. A similar analysis of vein length (Fig.4.3b) also indicates a non-gaussian distribution. Since vein thickness is approximately proportional to vein length (see section 3.5) a similarity in the distribution between these parameters is to be expected. Vein length distributions are considered no further here, as the main emphasis of this chapter is on the analysis of the vein thickness distribution.

4.4.2 Vein thickness: A power-law (fractal) distribution ?

Vein thickness measurements, either line sampled (1*D*) or on a plane (2D) are shown as plots of log $N(t)$ against log (t), where t is measured vein thickness and $N(t)$ is the cumulative number of veins with thickness greater than t. The number of veins with thickness greater than t is given by $N(t) = Cu^{-D}$, *ie*. a power law. The slope of the straight line on a graph of $N(t)$ can then be used to define a fractal dimension D

$$D(t) = - \frac{d \log N(t)}{d \log t} \qquad (4.1)$$

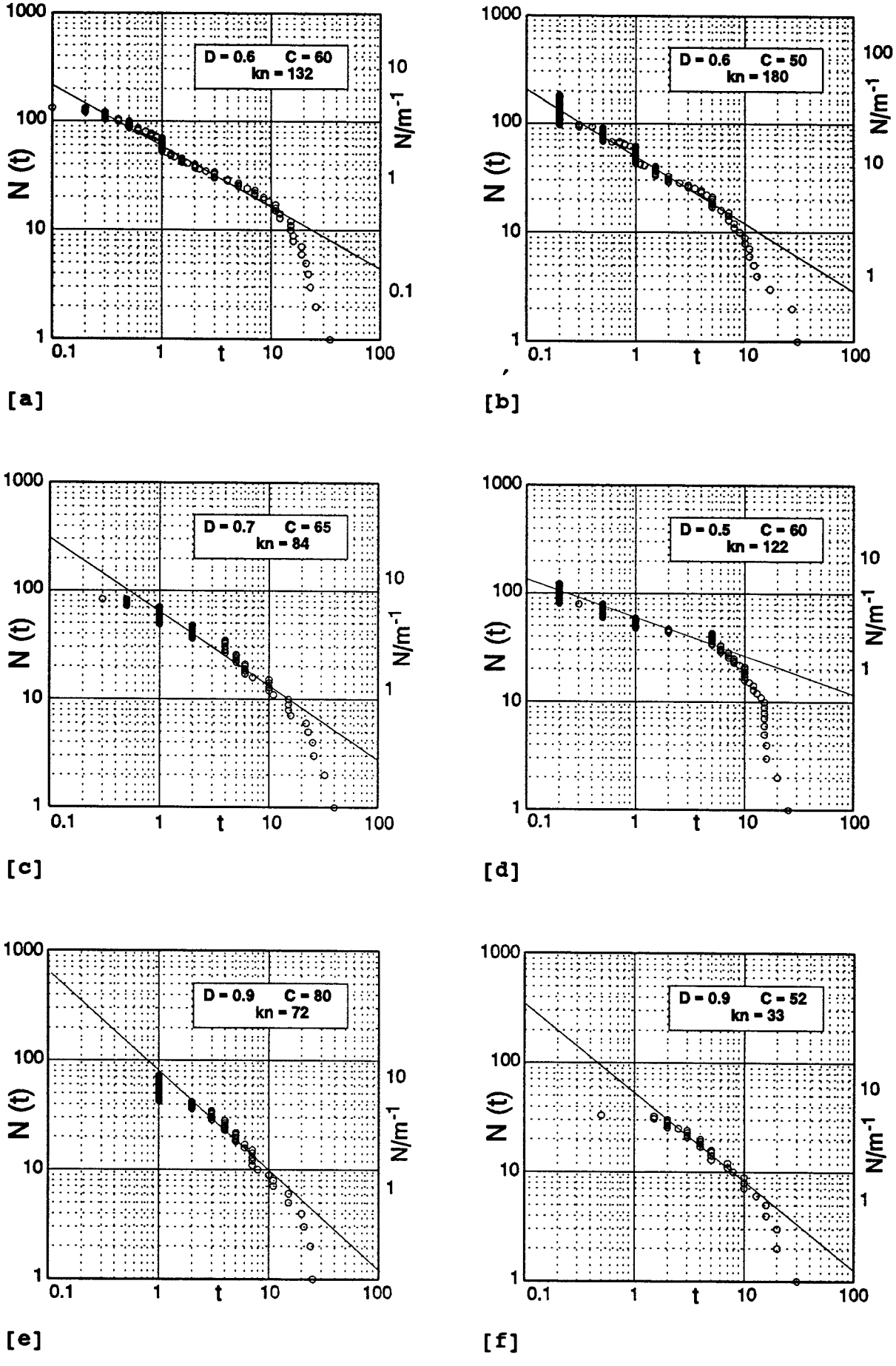

Figure 4.4. Log N(t) against log(t) for six layers at Miliook Haven (see Table 4.1).

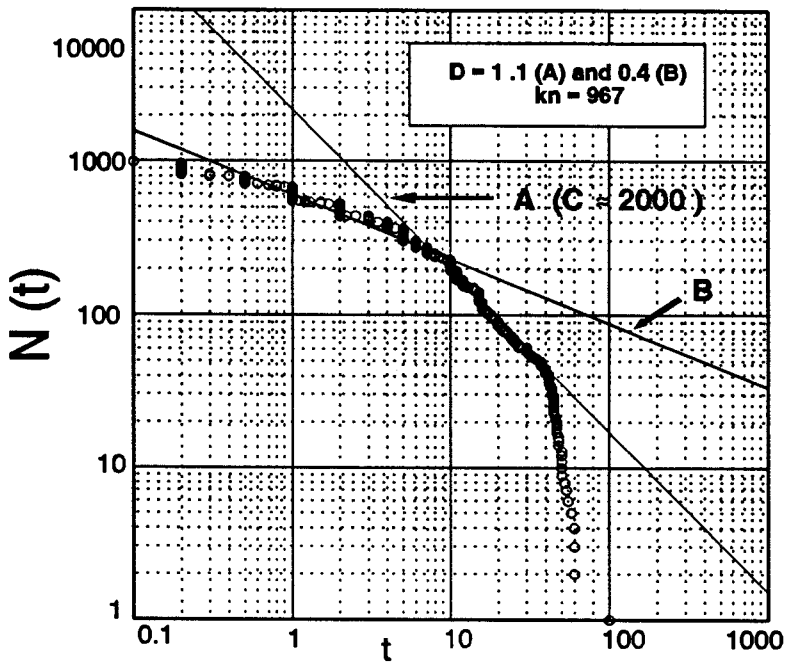

[a]

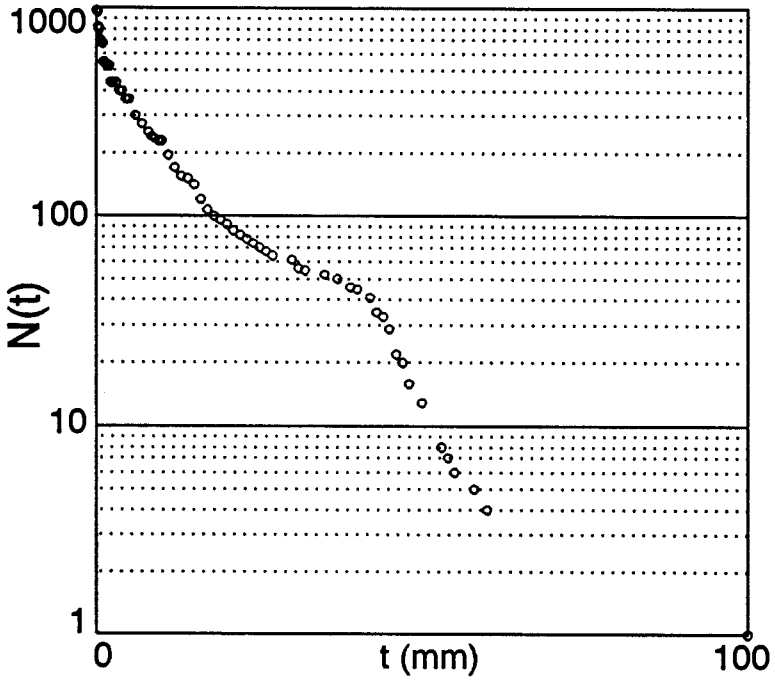

[b]

Figure 4.5. [a] Log N(t) against log(t) for all measurements from line transects at Millook Haven, and [b] Log N (t) against vein thickness (t) for all line transects at Millook Haven.

Fractal or power law distributions, theoretically extend for 0 to ∞, but in practice may be expected to be restricted to a scale between upper and lower limits. The lower limits may be expected to be imposed by particle size, as this controls the scale that the bulk material properties are retained. The upper limit is less easily defined be may be expected to be related to layer thickness in bedded sequences. Scholtz (1990) has related similar limits for faults and earthquakes to the thickness of the seismogenic zone.

Log$N$(t) against log$t$ graphs for vein thickness are shown for six datasets in Fig.4.4. These six datasets each contain >50 measurements, with the exception of Fig.4.4f which is included to illustrate en echelon vein arrays. All the plots have an overall upward convex profile, although they are characterised by several straight segments. The curves for each plot become flat at thicknesses below the effective limit of resolution (0.2mm), and they have steep right-hand segments that contain a central straight portion. In some studies of fault displacement and length these steep right-hand segments have been attributed to sampling effects (Childs *et al.* 1990, Heffer & Bevan 1990), although for Milliook Haven this upper limit on vein thickness is not regarded as a sampling artifact as there is an indication of a real decrease of veins of thicknesses >10mm. There are two main arguments in favour of this hypothesis: [1] The high t tails of the distributions generally involve more than 10% of the data (*eg.* Figs.4.4a, 4.4b, 4.4c and 4.4d), whereas the distributions for Figs.4.4e and 4.4f could be dismissed as sampling artifacts due to the censoring effect; and [2] the power law distribution predicts that veins of >1m thickness should occur at a frequency of about 10-12 per kilometre. Veins of this thickness (>1m) are not seen in the continuous coastal exposures around Milliook Haven.

The central segments of the curves of log$N(t)$ against log(t) (Fig.4.4) contain a straight line with D values that range between 0.4 and 1.1. For the best constrained line traverses (Fig.4.4a, 4b and 4c) the central, straight segments are characterised by low D values of 0.6 and 0.7 over thickness values which span nearly two orders of magnitude. Combining all the vein thickness measurements from the line transects produces a plot containing a curve with two straight portions with slopes of -0.4 and -1.1 (Fig.4.5a). A similar linear-log frequency plot (Fig.4.5b) for vein thickness for all the measurements, indicates that the negative exponential function is probably not the most appropriate distribution model.

FIGURE	TRANSECT	kn	D	C	N/m^{-1}
4.2a	1	132	0.6	60	2
4.2b	4	180	0.6	50	12.5
4.2c	6	84	0.7	65	6.2
4.2d	5	122	0.5	60	3
4.2e	8	72	0.9	80	13.3
4.2f	20	33	0.9	52	8.7

TABLE 4.2. D and C values for vein thickness from six line samples taken around Millook Haven.

The range of *D* values and estimates of *C* (the predicted number of veins with thicknesses ≥1mm) for the plots shown in Fig.4.4 are summarised in Table 4.2. For the line transects shown, estimates of *C* generally range between 2 and 15m^{-1}. The frequency of veins per metre (Nm^{-1}) for different sample lengths is also indicated for each transect shown in Fig.4.4. In contrast to the bulk of the datasets, Transect 4 (Fig.4.3b) and Transect 8 (Fig.4.3d) have relatively high *C* values of 12.5m^{-1} and 13.3m^{-1} respectively. These are thought to reflect the influence of local structural position on vein development, *le.* 4.3b was sampled adjacent to the hinge region of a fold, while 4.3d was sampled within an especially thin bed (Table 4.1).

Example of a non-power law fracture distribution

Figure 4.6 shows an example of a dataset which clearly does not conform, even approximately, to a power law distribution. These measurements are for a series of shale infilled fractures and faulted joints from a single bedding surface in an inverted fold limb (Transect 3, Table 4.1). A plot of log*N* against log*t* (Fig.4.5a) indicates that there is no straight central segment. and that it is dominated by fractures of relatively constant thickness of 5-10mm. The spatial extent of these measurements are insufficient to draw any definite conclusions, except that they do not follow a power law. Plotting the cumulative frequency of fracture thickness on an arithmetic (normal) probability graph (Fig.4.5b) indicates that the distribution is not normal. A similar plot of log (thickness) (Fig.4.5c) suggests that this thickness distribution is lognormal.

4.4.3 Discussion and summary of vein thickness distribution

Vein thickness for the interbedded sandstone-shale sequence at Millook Haven has lower and upper limits of 0.2 and 230mm. The lower limit of 0.2 is a set limitation of resolution, below which vein thickness could not be accurately measured; so this is an artificial limit. The upper limit of 230mm is less easily defined, although at ≈10mm thickness there appears to be a change in the characteristic of the vein thickness frequency distribution. Figure 4.7 shows a log*N*(t) against log(*t*) graph for vein thickness for Transect 1 (Fig4.4a, Table 4.1) where the dataset has been divided into thickness ranges of <5mm (A), <10mm (B) and (C) all measurements. This plot illustrates the change in the

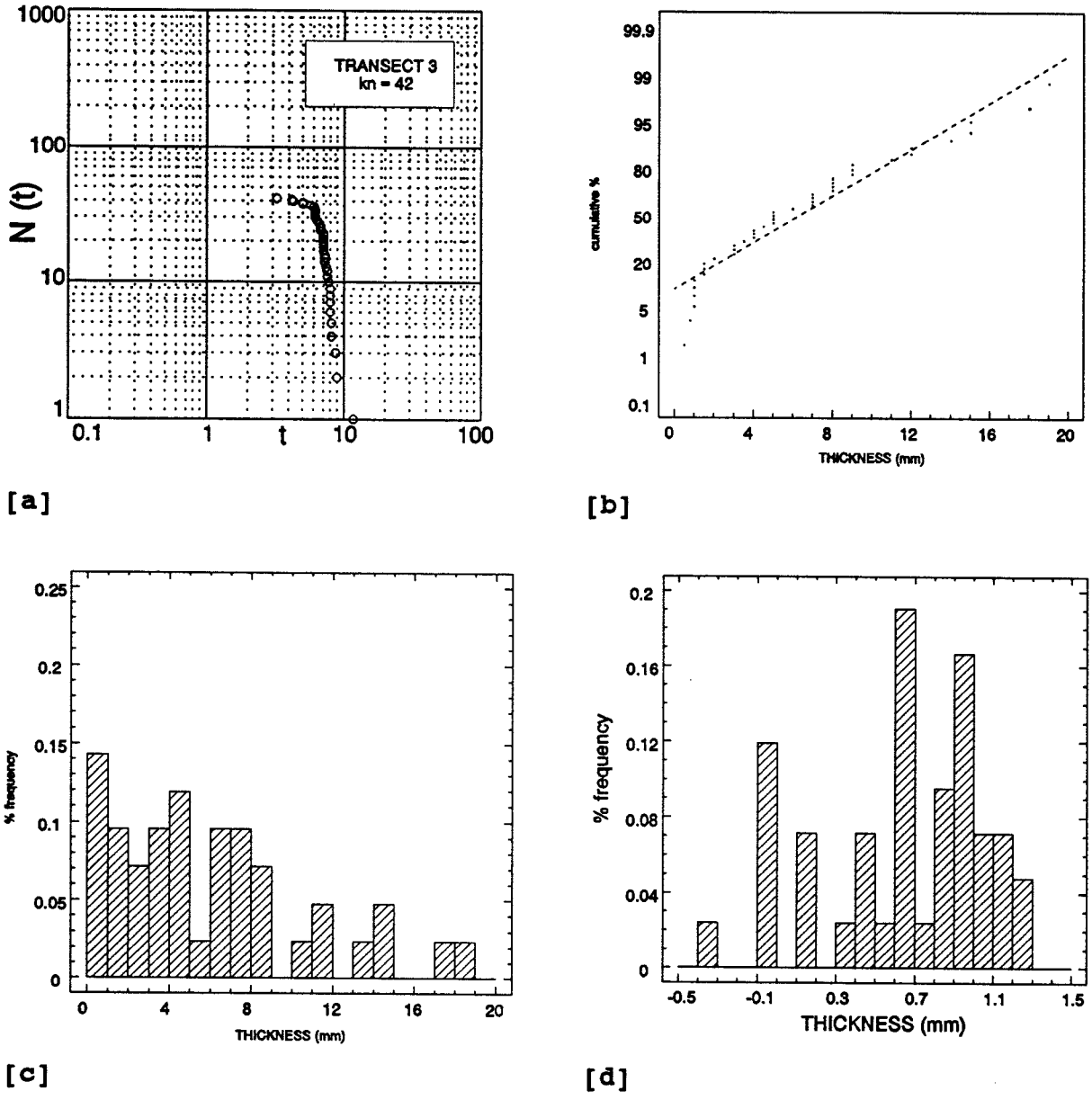

Figure 4.6. Data for shale infilled fractures and faulted joints from Millook Haven (Transect 3, see Table 4.1). [a] Log N(t) - log(t) plot of fracture thickness [b] arithmetic (normal) probability plot [c] frequency histogram of fracture thickness, and [d] arithmetic (normal) probability plot of log-transformed values.

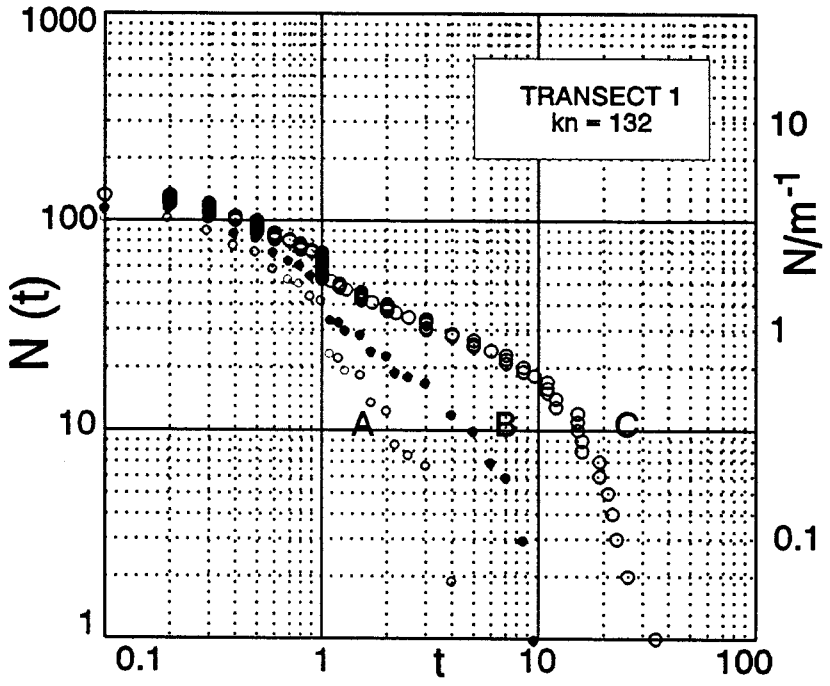

Figure 4.7. LogN(t) - log(t) graph for a single line sample (Transect 1), where the dataset has been plotted in subdivisions of thickness < 5mm (A), < 10mm (B) and (C) the complete dataset.

characteristic of the thickness frequency distribution at ≈10mm, and also the effect on the slope of the straight line segment and the *D* value when the thickest veins are not sampled. For the best constrained line samples, vein thickness Is characterised by *D* values of ≈0.6, over two orders of magnitude in the range 0.1 → 10mm. The vein thickness distributions are variable; many cannot be modelled in terms of a single power law. In almost all of the datasets there is a sharp break of slope on the log*N*(t)-log(*t*) plots. The position of this break is relatively constant, occurring at a vein thickness in the range of 10-15mm. Since the range of bed thickness at Millook Haven is in the range 100-1000mm, when the veins reach thicknesses of ≈10mm they penetrate the entire layer, so it is likely that they belong to a vein population where different scaling laws apply. This then raises questions about what the controls on maximum vein thickness are, and how layer thickness could effectively constrain the maximum vein thickness values. Factors which could constrain vein growth to single sandstone beds would be the shear capacity of the bed interfaces and the tensile strength of the adjacent beds, into which a vein could potentially propagate.

4.5 DATA ON VEIN SPACING

4.5.1 Scale of vein spacings in layered rock

Vein spacing at Millook Haven ranges from <0.008 to 3.2m within a range of layer thicknesses of 0.13-1.1m (Fig.4.8) in the Crackington Formation sandstone. Figure 4.9a shows the frequency distribution of vein spacing values from a line transect of 30m length (Transect 1) represented as: [a] a linear frequency histogram, [c] an arithmetic (normal) probability plot and [e] as an arithmetic (normal) probability plot of log-transformed spacing values. Similar plots are shown for a line traverse of 20m length (Transect 5) (Figs.4.9b, 9d and 9f). From these two examples it is apparent that either a negative exponential or power law could provide an adequate description of vein spacing distribution: the actual distribution may be some combination of both of these distributions.

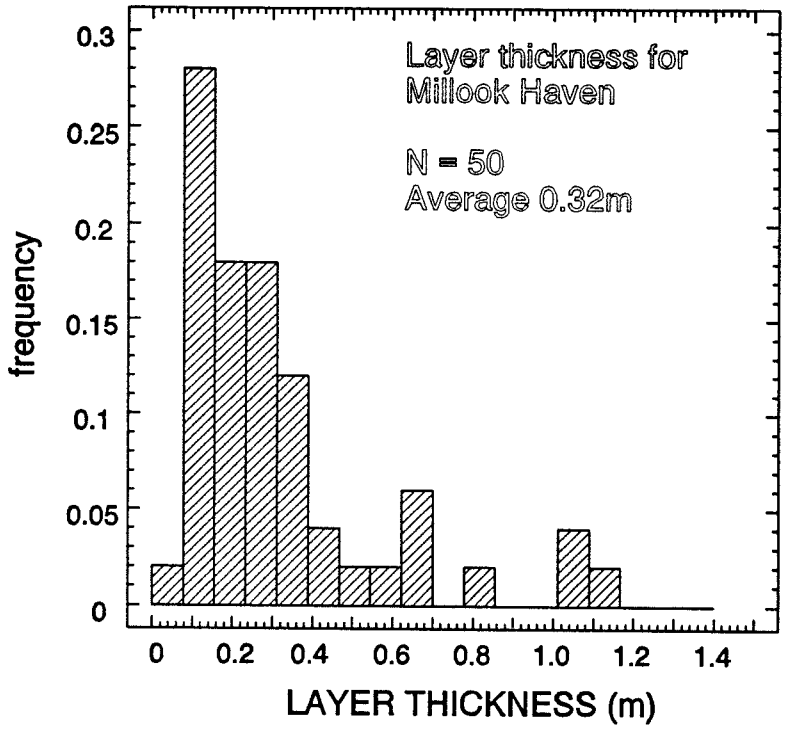

Figure 4.8. Frequency histogram of sandstone layer thickness in the Crackington Formation at Millook Haven.

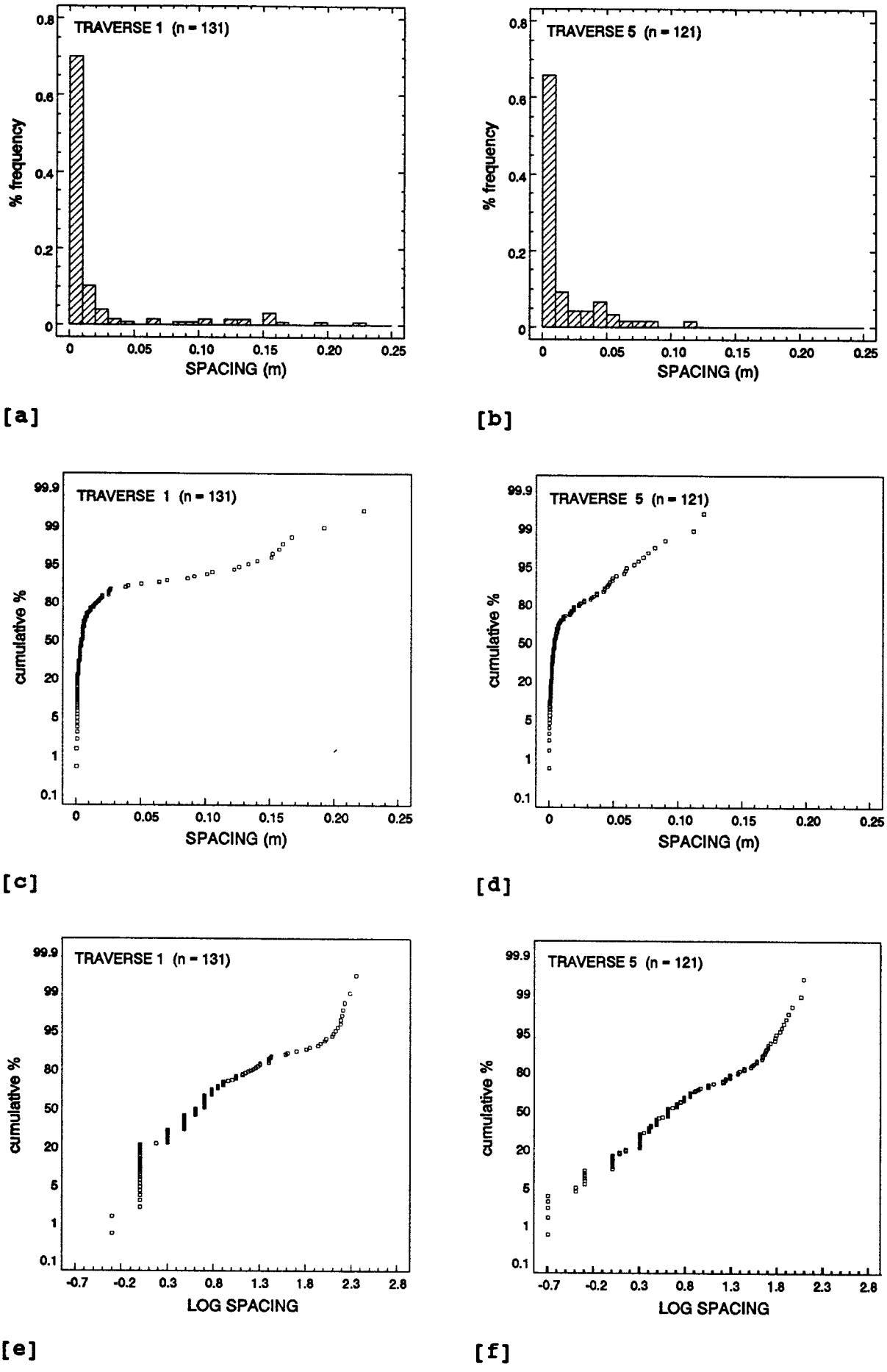

Figure 4.9. [a,b] Frequency histograms for vein spacing [c,d] Arithmetic (normal) probability plots of spacing and [e,f] Arithmetic (normal) probability plots of log-transformed spacing values.

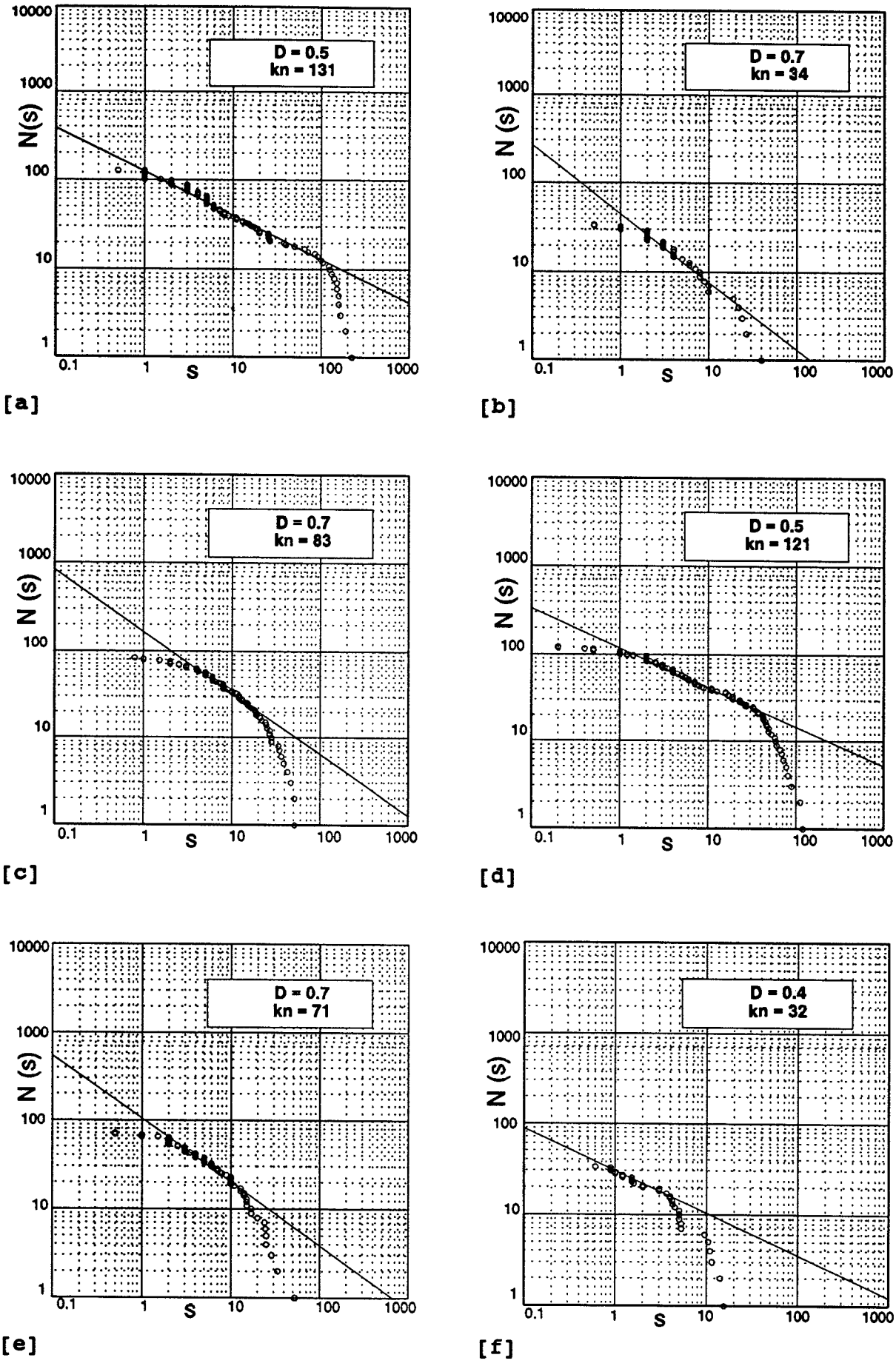

Figure 4.10. LogN(s) against log(s) (spacing) for six layers at Millook Haven.

Log$N$(s) against log(s) graphs of vein spacing (s) for six different line traverses are shown in Figure 4.10. These six datasets contain >50 measurements, and are the equivalent line transects used for the analysis of vein thickness distribution (Fig.4.4). The exception is Fig.4.10b (Transect 2, Table 4.1) which has been included because spacing was not measured for Transect 4 (Fig.4.4b). The data are characterised by upward convex profiles with straight, central segment portions with kinks of high gradient. The best constrained line traverses (Fig.4.10a, 4.10b, and 10d) contain straight segments with D values of ≈0.5-0.7.

A prominent break of slope occurs at 100-1000mm (based on Transects 1 and 5), *Ie.* in the range of bed thicknesses. For Transect 1 (Fig.4.10a) the break occurs at ≈1000mm (*cf.* bed thickness of 1030mm); and for transect 5 (Fig.4.10d) the break of slope occurs at ≈400mm (*cf.* bed thickness of 380mm). Similar trends are observed for the other datasets, where the break in slope for the straight section of the curve corresponds to layer thickness. This data suggests that the largest vein spacing values are approximately equal to bed thickness.

4.5.2 Vein spacing distribution and layer thickness

A number of hypotheses have been put forward to explain the spacing and distribution of fractures in sedimentary rock (Ladiera & Price 1981, Narr & Suppe 1991). However, few studies deal explicitly with vein propagation in layered sedimentary rock. Hypotheses to explain the relationships between crack spacing and layer thickness are generally based on theoretical mechanical models of the jointing process and engineering studies of composite layered materials. The main factors which are thought to influence fracture spacing in composite materials and layered rock include:

[1] The material properties, host rock stiffness and fracture toughness of the fractured layer and its bounding layers (Keer & Chen 1981, Theircelin *et al.* 1987).

[2] The frictional and tensile strength of interfaces between the layers (Cook & Erdogan 1972, Weertman 1980) and the effect of fracture-interface interaction.

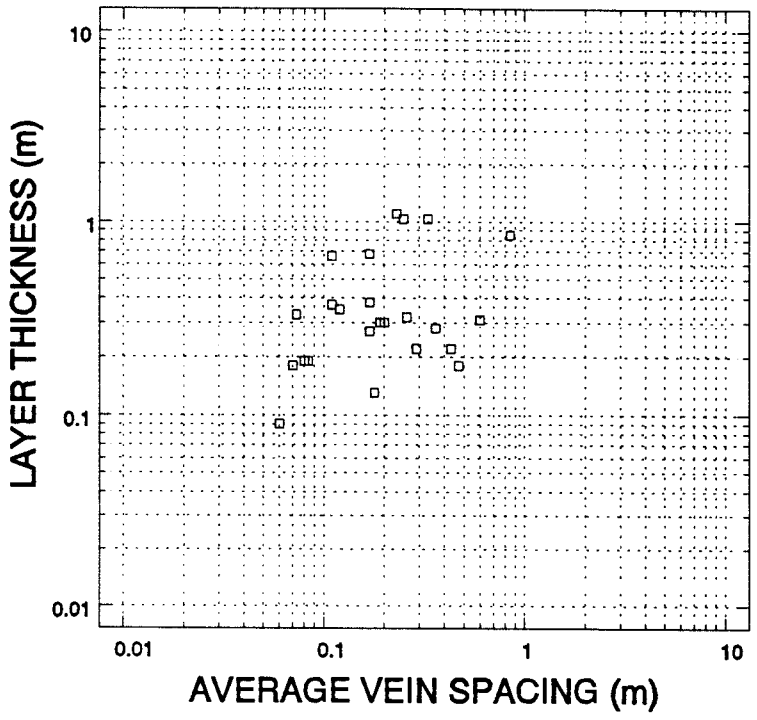

[a]

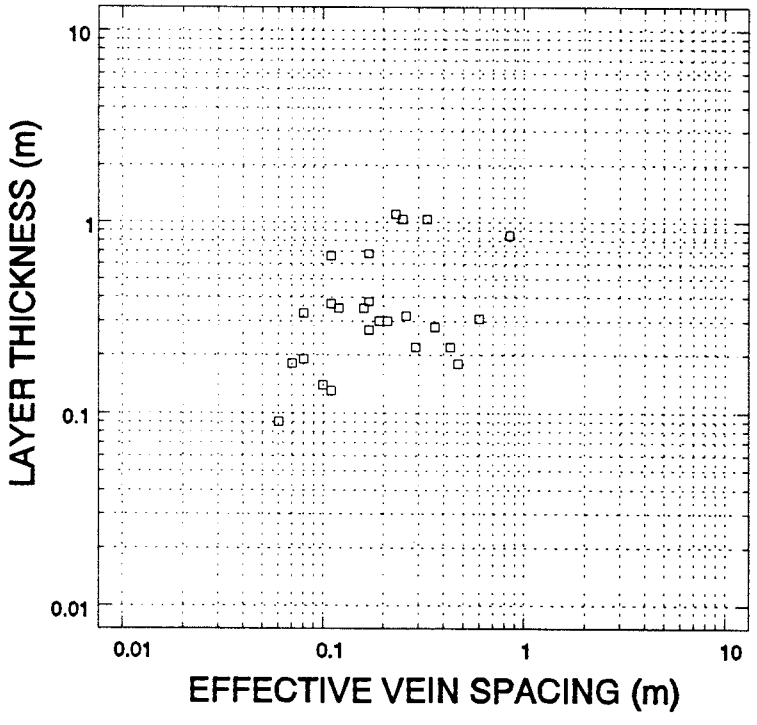

[b]

Figure 4.11. [a] Average vein spacing for individual line samples against layer thickness, and [b] calculated effective vein spacing for individual line samples against layer thickness.

[3] The near-field stresses produced by fractures within individual and adjacent layers (Pollard & Segall 1987, Olson 1991, Chapter 3) can enhance or inhibit crack propagation.

[4] The amount of tectonic strain due to layer extension or layer-normal shortening.

To describe vein spacing in layered rocks a simple effective vein spacing can be calculated by dividing the transect length by the number of veins intersected by the line sample. Vein spacings from Millook Haven calculated by this method correlate well with the average values of spacing measured over a single line traverse. These values are shown in Fig.4.11 as log-log plots of average vein spacing and effective spacing against layer thickness. The data have a large scatter and they do not have a good correlation to layer thickness. This suggests that there is not a simple linear relationship between spacing and layer thickness. Many spacing values are insensitive to bed thickness, and locally, veins have low spacing values (high densities) where they are clustered or in arrays.

4.6 EXTENSION REPRESENTED BY VEINS

The veins locally have high spatial densities, and at many outcrops the beds have been sequentially stretched during vein formation. By summation of vein thicknesses and fragmented bed lengths, minimum values of layer extension can be determined. To estimate the longitudinal strain (e), the vein thickness and spacing data from each line sample can be compared with initial bed lengths and the final veined (stretched) configuration by subtracting cumulative separations recorded by the veins. For this method we idealise each layer segment as a rigid-brittle inclusion and have to ignore changes of bed thickness. The simplest method to estimate longitudinal strain (e) and extension accommodated by the veins can be expressed by

$$e = \frac{\Delta l}{l_f - \Delta l} \qquad (4.2)$$

where l_f is the fragmented bed length and Δl is the extension represented by vein dilation. The results using this method (Equ.4.2) are shown in Table 4.1.

Since the estimates of D values for vein thickness are <1 (Fig.4.4, Table 4.2), this implies that most of the extension recorded by the veins will be accommodated in large veins. To examine how the extension has been accommodated and distributed amongst the veins, measurements for individual line samples were subdivided into groups of <10mm and >10mm vein thickness. Extension for each line transect was then calculated for veins of $\sum_i$ <10mm and $\sum_i$ >10mm. The results are shown in Table 4.1, indicating that veins of >10mm thickness generally represent 60-90% of the extension recorded by veins within an individual line sample. This suggests that veins of >10mm thickness have some special significance, *ie*. log$N(t)$-log(t) plots indicate that there is a prominent change in the frequency distribution at >10mm thickness, which may reflect the influence of layer thickness and layer properties on vein development. Several exceptions are apparent (cf. Transects 8, 10 and 12; Table 4.1), where veins of >10mm within line samples only take up 25-45% of the extension represented by veining, with the remainder of the extension accommodated by smaller veins of <10mm thickness. These transects generally have high vein densities (*cf.* Transect 8, C = 80; 13.3 N/m^{-1}, layer thickness 190mm) and low layer thicknesses.

4.7 DISCUSSION

Vein thickness and spacing distributions in layered sedimentary rocks are strongly influenced by the mechanical control exerted by layer thickness. Other factors which may affect the type of arrest mechanism constraining vein propagation to single layers, include contrasting material properties between different layers and the amount of traction at bed interfaces. Slip between beds during vein formation may be important, because of its effect on the stress intensity at the crack tip as it approaches a bedding plane. Weertman (1980) and Thiercelin *et al.* (1987) have shown how interbed slip and rock interfaces would affect the propagation of joints. Comparison of results from some of these theoretical treatments with field observations, may help to explain how different types of vein termination structure develop at some bed boundaries, *eg*. blunt and tapering veins. The mechanical

interaction which occurs between neighbouring veins, and amongst veins in adjacent layers is an additional factor that may influence vein thickness and spacing distributions.

4.8 CONCLUSIONS

From the analysis of vein thickness and spacing distributions in layered rocks, the following general conclusions are evident:

[1] Negative exponential and power-law distributions are the most appropriate models to explain the range of vein thickness and spacing values.

[2] Vein thickness at Miliook Haven has lower and upper values of <0.2 and 230mm. The lower limit of 0.2mm is the limit of resolution at which veins could accurately be measured, while the upper limit of 230mm represents the maximum vein thickness developed within a single layer. For the most well constrained line samples, vein thickness is characterised by low *D* values of ≈0.6, over nearly two orders of magnitude. At vein thicknesses of ≈10mm there is a change in the characteristic of the vein thickness frequency distribution with a departure from the power-law. Estimates of *C* values predict a range of vein frequencies of between 2-15m^{-1}.

[3] Vein spacing at Millook Haven ranges from <0.008 to 3.2m within a range of layer thicknesses of 0.13-1.1m. Negative exponential and power-law models provide the most appropriate descriptions of vein spacing frequency distributions. The best constrained line traverses yield *D* values of ≈0.5-0.7 over 1.5-2 orders of magnitude. Prominent breaks in slope for graphs of logN(s) against log(s) occur at 100-1000mm; these are in the range of bed thickness, suggesting that the largest spacing values are equivalent to bed thickness.

[4] Although some vein populations may be adequately described by single power-law distributions, many show distinct changes in graphs of logN(t) against log(t). These are not sampling artifacts, but

represent a real decrease in maximum vein thickness and spacing values, which can be attributed to the propagation of veins through the entire layer thickness.

[5] Estimates of extension accommodated by the veins indicate that most of the extension is taken up in large veins. Veins of >10mm thickness generally represent 60-90% of the total extension calculated for individual line samples.

[6] There is no simple linear relationship between vein spacing values and bed thickness. Vein growth behaviour and spacing within single and neighbouring beds, is also likely to be effected by fracture-induced stresses produced by mechanical interaction amongst overlapping and closely spaced veins.

5

Transtensional modelling of en echelon vein arrays

5.1 INTRODUCTION

En echelon vein arrays which are common features of brittle and semi-brittle rock deformation in low-grade metamorphic terranes have been the subject of much investigation. Largely on the basis of cross-sectional crack geometry, they have been widely applied to the analysis of strain state (Durney & Ramsay 1973, Ramsay & Huber 1983, Collins & De Paor 1986) and stress conditions (Pollard *et al.* 1982, Rickard & Rixon 1983, Du & Aydin 1991, Olson & Pollard 1991). Many explanations for the geometry of en echelon veins have been given. The most conventional interpretation involves vein formation in a zone of progressive simple shear, with extension fractures nucleating at 45° to the zone boundary and perpendicular to the maximum incremental extension (e_{max}) direction (Fig.5.1). Subsequent passive rotation during growth of the crack tip in the original direction, may produce sigmoidal vein profiles (Shainin 1950, Latjai 1969, Ramsay & Graham 1970).

Data collected from localities in the Culm Basin of SW England indicate that many natural arrays contain veins with very different orientations. Figure 5.2a shows that the angle, ω, between veins and arrays typically ranges from 0 to 60°, and has a mode of about 30°. This range of initial vein-array angles is confirmed by comparison with other data sets from North Cornwall (Fig.5.2b)(Hancock 1972) and from the Irish Midlands (Fig.5.2c)(Rothery 1988) which show ω values of 5-55°. The continuous variation of ω and $\omega \neq 45°$ cannot be explained in terms of simple shear deformation.

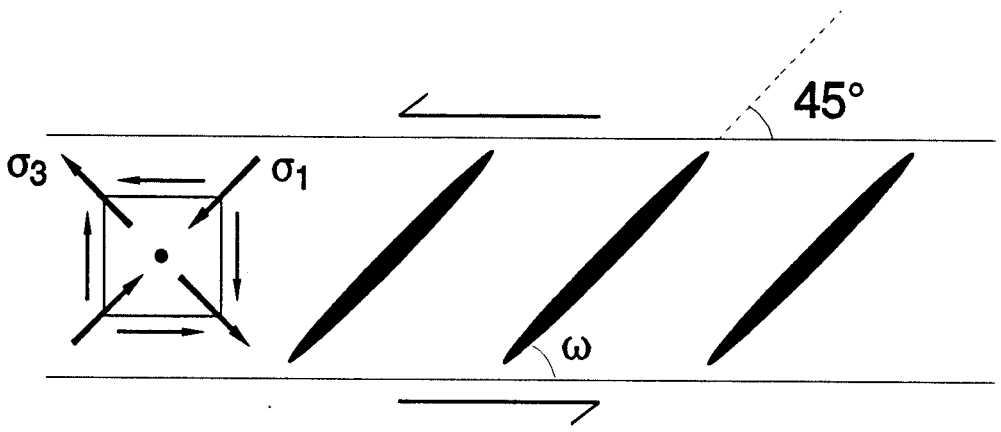

Figure 5.1. Schematic diagram illustrating the conventional interpretation of en echelon vein formation in terms of the growth of veins in a zone of simple shear. Initial vein growth is perpendicular to the direction of maximum incremental extension, ie. at 45° to the zone.

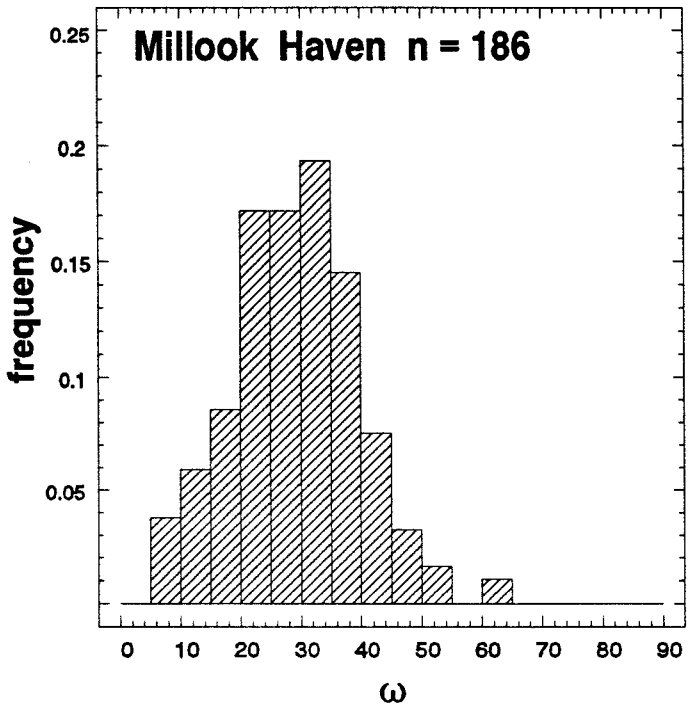

[a]

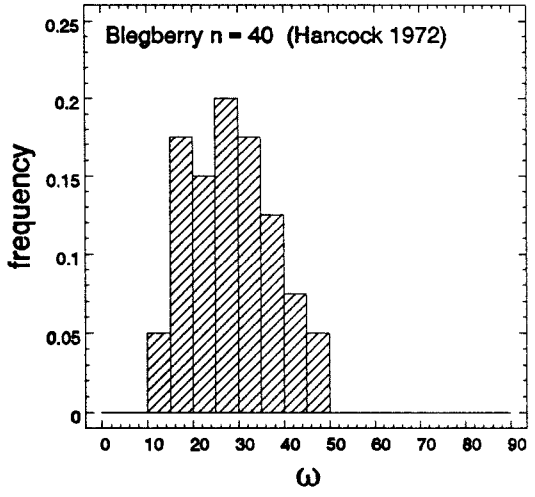

[b]

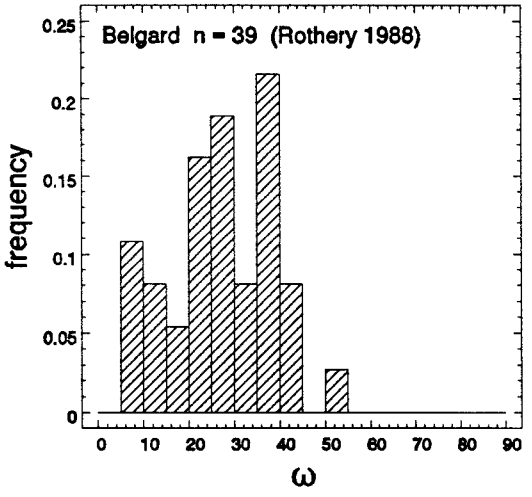

[c]

Figure 5.2. Frequency histogram of the angle, ω, between veins and arrays for: [a] vein sets exposed in profile on bedding planes in the Crackington Formation at Millook Haven, North Cornwall; [b] for vein sets in the Crackington Formation from Blegberry Beach, North Devon (Hancock 1972); and [c] for veins in Dinantian limestones from Belgard, Ireland (Rothery 1988).

The main objective of this chapter is to re-examine the geometry and kinematics of en echelon veins, in the context of transtensional-transpressional deformation (Sanderson & Marchini 1984, McCoss 1986) and the quasi-static models postulated by Pollard and co-authors (Pollard *et al.* 1982, Delaney *et al.* 1986, Pollard & Segall 1987). Analyses of a range of examples of en echelon veins and their zonal displacements are described, and the extent to which they reflect the underlying physical processes and stress conditions are examined.

5.2. OBSERVATIONS ON EN ECHELON VEINS

The vein sets described are from sandstone sequences of the Upper Carboniferous Crackington Formation in the Culm Basin, SW England. Each vein array is the product of a single, progressive deformation episode. Many of them are sub-parallel to contemporaneous isolated and distributed veins present in the same area. The vein sets are generally perpendicular to bedding with many of them terminating at bed margins. Some of the veins (ω <30°) can be traced below the bedding surface, into a single parent crack (Pollard *et al.* 1982). Serial sections of similar arrays of this vein set, described by Nicholson & Ejifor (1987) (Fig.5.3) indicate the veins are generally blade-like in three-dimensions, with a continuous transition from single, composite veins (ω = 0°) to en echelon veins (ω = 30°). The geometry and the field relations of these vein arrays were examined in Chapter 2 and are described by Beach (1977) and Jackson (1991).

A series of typical examples of en echelon vein arrays from Millook Haven are shown in Fig.5.4. Each array is described at length in the accompanying figure caption. These examples illustrate the spectrum of geometrical form, where measurable properties such as orientation, spacing and overlap, aspect ratio and zone width show systematic variation.

Figure 5.4a shows an example of an en echelon vein array interpreted to have formed in simple shear where the angle, ω, between the veins and the array is 45°. The vein length to thickness ratios are ≈5, the vein tips taper symmetrically and they have relatively large separations. The average crack-length overlap ratios are large (0.80) and they exceed the spacing between adjacent veins within the array.

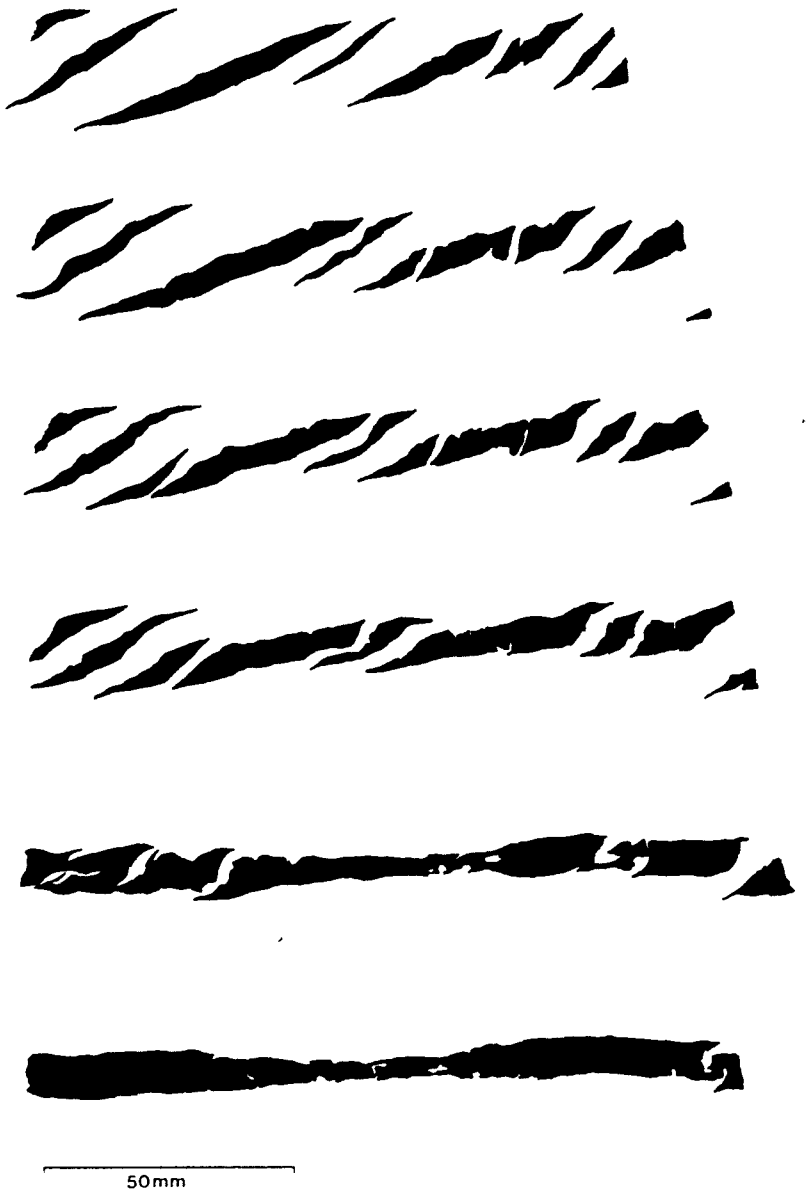

Figure 5.3. Serial section of a single, composite vein in the Crackington Formation, North Cornwall (Nicholson & Ejifor 1987, fig.4). The continuous transition from a single vein to en echelon veins suggests that there is a contribution of shear displacement parallel to the crack propagation front (ie. mixed mode I-III).

Figure 5.4

Fig.5.4a. An example of a simple shear type en echelon vein array. The angle between the veins and the array, ω is 45°. The vein length to thickness ratios are about 5, vein tips taper symmetrically and have relatively large separations. Crack-length overlap ratios are large (0.80) and exceed the spacing between adjacent veins within the array. The rock bridges, which separate the veins from its neighbours, have low aspect ratios (typically 1) and they show very little curvature of their margins. The vein fibres are normal to the margins at the vein tips, although they have an oblique angle towards the vein centre. The pressure-solution seams are at high angles to the vein margins, although they are rarely orthogonal to them. Deformation textures which might suggest that this was a zone of ductile shear strain are not visible.

Fig.5.4b. This example has a low angle between the vein and the array (ω = 5°), and a small ratio of length to thickness (aspect ratio = 20). The vein tips which are close together, have asymmetric, 'wedge' profiles with large apical angles (20-35°) and steep tip displacement gradients. The crack-length overlap ratio is low (0.10) and approximately equal to the steps between the veins. The bridges between adjacent vein tips have undergone significant rotation relative to the host-rock and the propagation direction, as they have bent to accommodate crack dilation. In this example there has been a change in sectional area, which may represent a fractional volume change. No pressure-solution structures (ie. seams) are visible at outcrop scale.

Fig.5.4c. In this example the vein-array angle, ω is 20° and the vein aspect ratio is 60. The veins taper asymmetrically, with low apical tip angles (<5°). The crack-length overlap ratio is moderate (0.70) and exceeds spacing between adjacent veins. The bridges are planar, suggesting they have undergone little significant rotation or bending strain during dilation. Vein fibres are orthogonal to the margins and at vein tips, although they become oblique towards the vein centre. There is little indication of pressure-solution deformation, although sectional area change is apparent, suggesting volume did not remain constant.

Fig.5.4d. In this example the vein-array, ω is 55° and the effects of solution transfer are very apparent. The veins are truncated against the solution seams, which indicates that during dilation the veins were being dissolved at their terminations. The zonal arrangement of these veins and solution-seams, suggest deformation was partitioned within the zone. The solution seams appear to have controlled vein development as pull-aparts, as it is apparent that displacement parallel to the solution-seams has occurred.

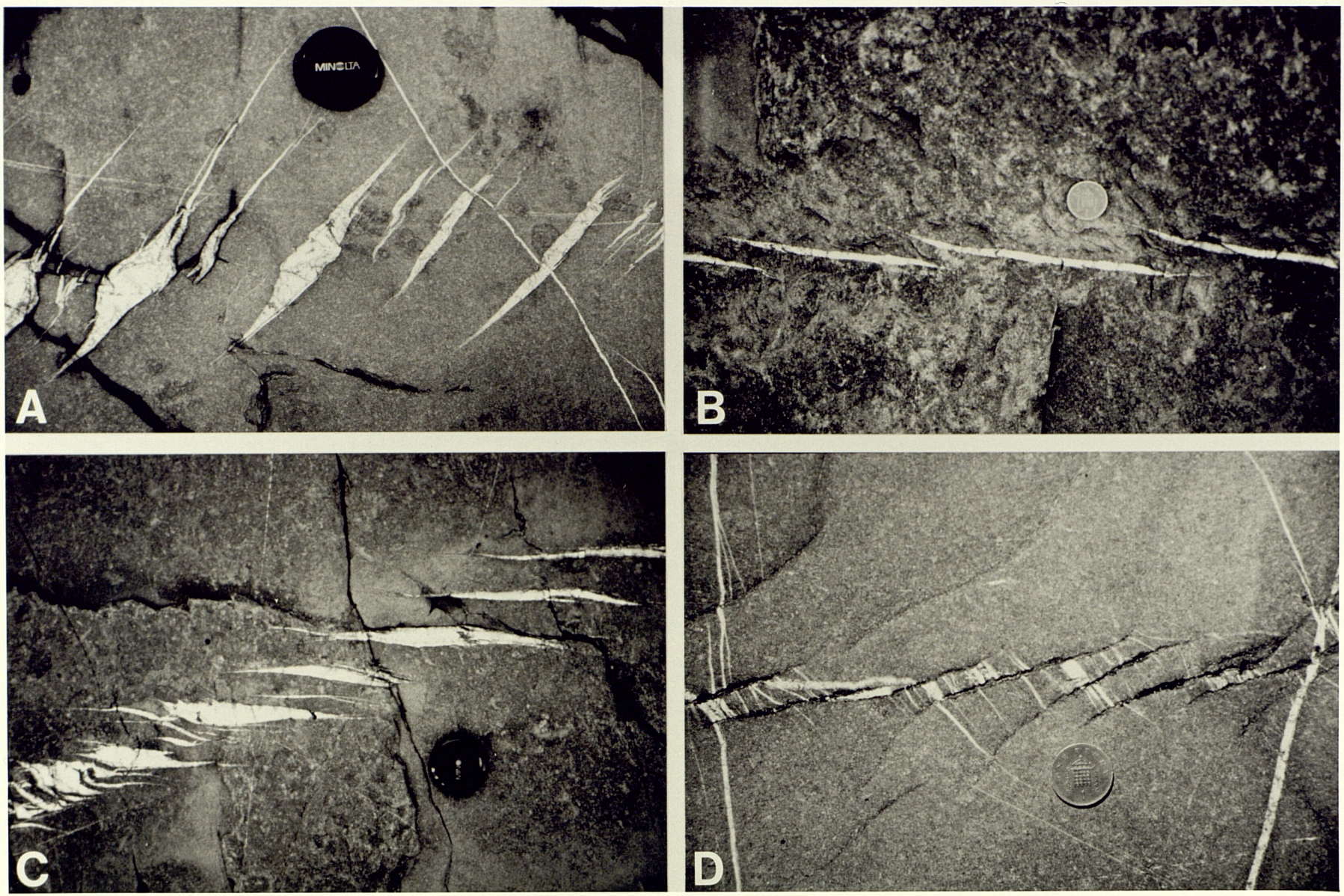
A
B
C
D

The rock bridges, which separate the veins from their neighbours have low aspect ratios (typically 1) and they show very little curvature of their margins. The vein fibres are normal to the margins at the vein tips, although they have a more oblique angle towards the vein centre. Pressure-solution seams form at high angles to the vein margins, although they are rarely orthogonal to them. Deformation textures which might suggest that this example was a zone of high shear strain are not visible.

Dilation of adjacent or closely spaced veins within an array tends to induce perturbations in near-field stress, which may inhibit or enhance further growth. This mechanical interaction of vein tips tends to become more pronounced at low ω values where the crack tip stress concentrations are closest together and overlapping (Pollard *et al.* 1982, Du & Aydin 1991). Features which may be diagnostic of this process of mutual crack interaction, are the asymmetry of vein tips and vein curvature. Figure 5.4b shows an example of a vein array with a low angle between the vein and the array ($\omega \approx 10°$); suggesting transtensional deformation with a large extensional component. The ratio of length to thickness (aspect ratio) is about 20, and the vein tips are close together with asymmetric, 'wedge' profiles with large apical angles (20-35°) and steep tip displacement gradients. The crack-length overlap ratio is low (0.10) and approximately equal to the steps between the veins. The bridges between adjacent vein tips have undergone significant rotation relative to the host-rock and the propagation direction, as they have bent to accommodate crack dilation. In this example a change in sectional area is inferred, which may represent a fractional volume change. No pressure-solution structures (ie. seams) are visible at the outcrop scale.

Figure 5.4c shows an array, where the effects of mechanical interaction are less pronounced, as the vein tips have a wider separation. The vein-array angle, ω is 25° and the vein length to thickness (aspect) ratio ≈25. The veins taper asymmetrically, with low apical tip angles (<5°). The crack-length overlap ratio is moderate (0.70) and exceeds the spacing between adjacent veins in the array. The bridges are planar, suggesting they have undergone little significant rotation or bending strain during dilation. Fibres are orthogonal to vein margins and vein tips, although they become oblique towards the vein centres. Both examples shown in Figs.5.4b and 5.4c have an absence of the deformation features and strains expected for simple shear (Ramsay & Graham 1970, Ramsay & Huber 1983)).

Figure 5.4d shows a special case from the spectrum of vein geometries. In this example the vein-array angle, ω, is 55°, indicating transpressive strain. The effects of solution transfer are very apparent as the veins are truncated against the solution seams, which suggests that during dilation the veins were being dissolved at their terminations. The zonal arrangement of the veins and solution-seams, also suggests deformation was partly partitioned within the zone. The solution seams appear to have controlled vein development as pull-aparts, as there are displacements parallel to the solution-seams.

5.3 ANALYSIS OF THE WALL-ROCK DISPLACEMENTS

In many zones of extensional deformation, the geometry and kinematics of fracture systems suggest bulk extension is oblique to the zone boundaries. This deformation is termed transtension, and involves a simultaneous combination of extensional and wrench strains (*ie.* simple shear combined with a simultaneous orthogonal pure shear). Transtension has been described from several different perspectives: geometry and kinematics (Harland 1971, Sanderson & Marchini 1984, McCoss 1987, McKenzie & Jackson 1989, Fossen & Tikoff 1991), small-scale analogue modelling (Withjack & Jamison 1986) and the analysis of natural vein arrays (Jackson & Sanderson 1991a,b).

5.3.1 Determination of zone displacements

In this analysis, the deformation zone is the extent of the en echelon vein array. The zone displacement vector *S* is determined using a geometrical method described by McCoss (1986). For this method the orientation of the maximum and minimum axes of sectional infinitesimal strain have to be known. In the case of vein arrays these can be determined from vein tips and solution seams, which for the purpose of this modelling are assumed to be parallel to the σ_1 and σ_3 directions within the zone. Reliance is placed on vein tips since they represent the final and least rotated strain increments. The McCoss construction is illustrated in Figure 5.5a and is constructed as follows:

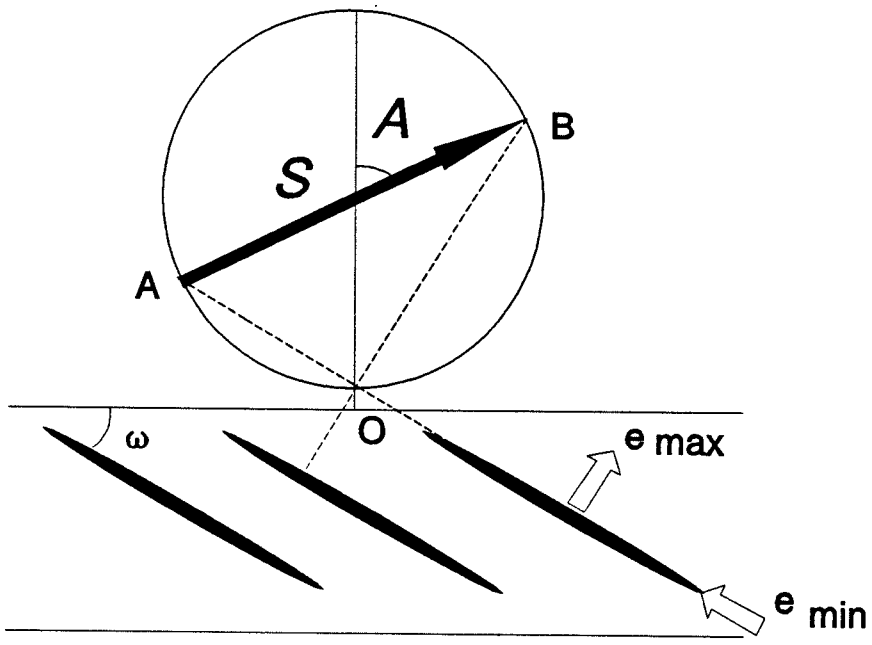

[a]

Figure 5.5. [a] Illustration of the analysis of the wall-rock displacements of en echelon veins using the McCoss (1986) construction. The orientation of minimum (OA) and maximum (OB) infinitesimal strain axes and the constructed zone displacement vector (S) are shown; e_{max} and e_{min} are the local (rotated) directions of maximum and minimum incremental strain.

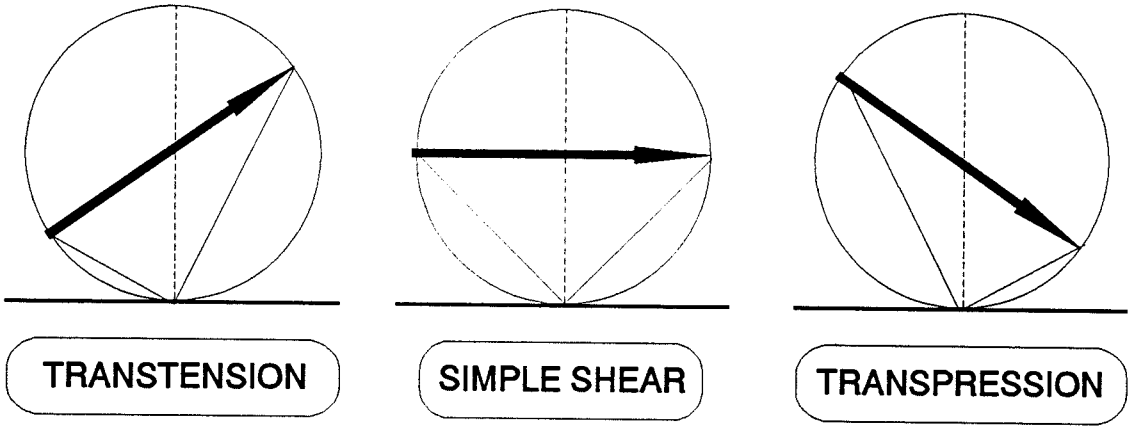

[b]

Figure 5.5. [b] Diagram showing how measurement of the angle, A, between S and the zone normal allows the definition of distinct tectonic regimes (bounded by precise values of A).

[i] Project a line normal to the zone boundary or azimuth of the vein array. Draw a circle of arbitrary radius centred on this line, tangential to the point (O) where the normal and the zone boundary intersect.

[ii] Draw lines through O, parallel (OA) and perpendicular (OB) to the vein until they intersect the circle at A and O respectively.

[iii] Draw the line (AB) through the centre of the circle; this line is parallel with the zone displacement vector, *S*. The vector sense is from the intersection with the minimum axis to the maximum axis.

Figure 5.5b shows how the McCoss construction illustrates, graphically the spectrum of tectonic deformations, ranging from extension through transtension to simple shear and transpression. The angle *A*, between the zone normal and the zone displacement vector, can be used to define regimes within this range of deformations.

5.4 OBSERVATIONS FROM ANALYSIS OF WALL-ROCK DISPLACEMENTS

En echelon vein arrays with ω values of: 10, 25, 45, and 55° which were described in section 5.2 are shown in Fig.5.6 together with the zone displacements determined by the McCoss construction. The vein arrays are treated as deformation zones, so statements about the deformation state refer to the zone rather than individual vein opening displacements.

ω = 45°

Figure 5.6a shows an en echelon vein array with a vein-array angle of 45°. According to the McCoss construction this vein array is in a simple shear configuration, as the zone displacement vector, *S*, is parallel with the array trend, and the angle *A* is 90° (Fig.5.5b).

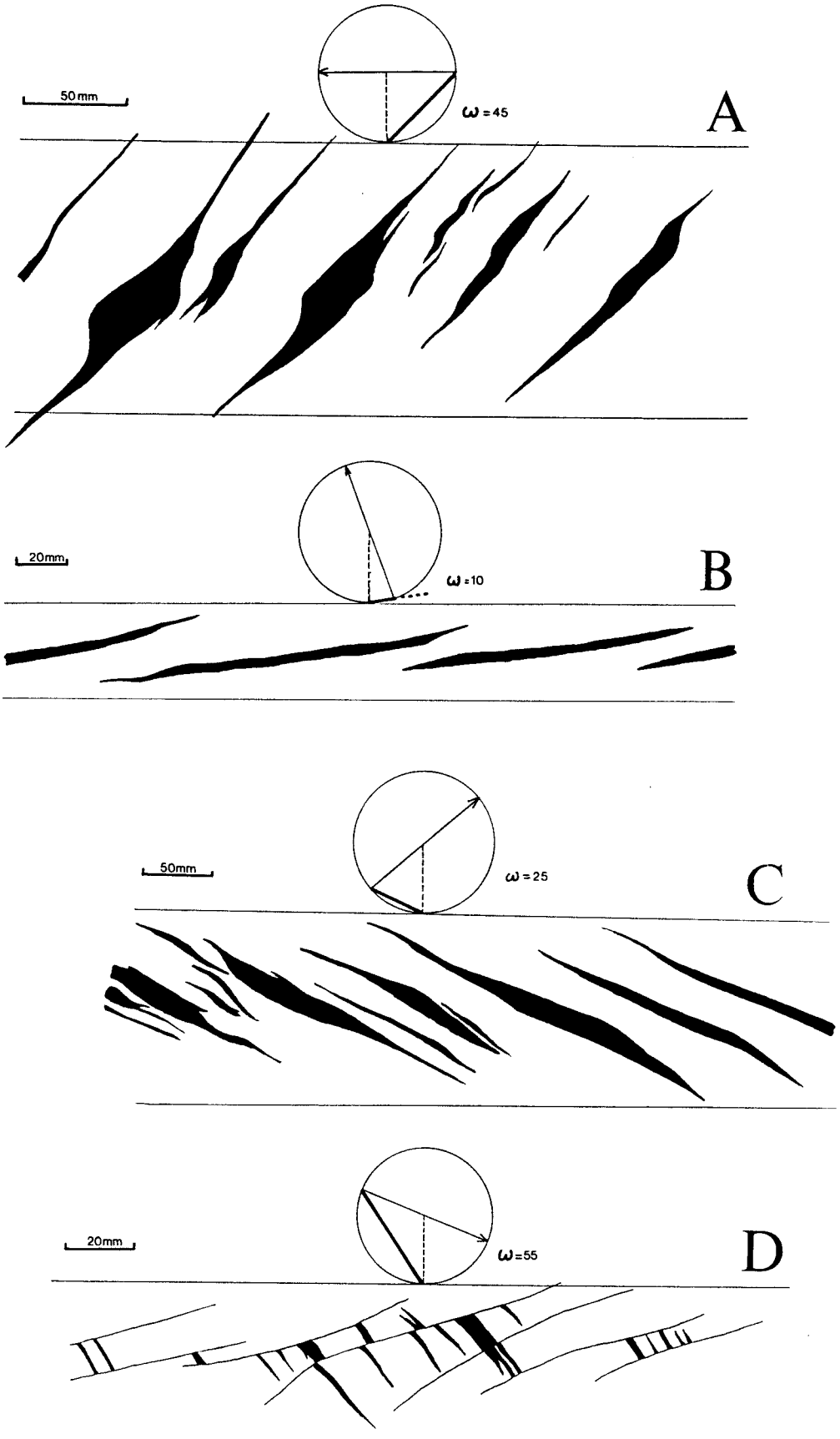

Figure 5.6. Type examples of en echelon vein arrays from Millook Haven, with their zone displacement vector, S, determined using the McCoss method, for: [a] ω = 45°, [b] ω = 10°, [c] ω = 25° and [d] ω = 55°.

ω = 10°

Figure 5.6b shows a vein array with an array-angle, ω, of 10°. The zone displacement vector, *S*, determined by the McCoss construction is almost perpendicular to the array trend. The angle *A* between *S* and the zone normal is 20°. The displacement, *S*, involves components of extension and shear, *ie* normal and parallel to the zone, and hence the zone is in transtension.

ω = 25°

Figure 5.6c shows a vein array with an ω value of 25°. The zone displacement vector, *S*, is divergent and oblique to the trend of the array, indicating that there are components of extension and shear, *ie*. the zone is in transtension.

ω = 55°

Figure 5.6b illustrates a vein array which is in transpression as the zone displacement vector, *S*, has a component directed towards the array. The small percentage of vein material and well developed solution seams support the transpressive nature of the deformation with sectional area change, and possible volume loss.

5.5 FIBRE KINEMATICS AND OBLIQUE OPENING VEINS

Vein fibres are used to track opening trajectories and the crack-wall displacements produced during vein dilation on the assumption that fibres grow in recognisable patterns (Durney & Ramsay 1973, Ramsay & Huber 1983), with long axes parallel to the displacement direction. Sigmoidal and curved vein fibres, either antitaxial or syntaxial, track crack opening and shearing displacements.

The displacement controlled mechanism is disputed in some recent studies (Cox 1987, Urai *et al.* 1991) which suggest that in certain cases, fibres do not track the full incremental opening trajectory. Crack-seal growth kinetics (Ramsay 1980) may depend on other factors such as crack-wall surface roughness or face-controlled growth (Cox 1987, Urai *et al.* 1991). Despite such criticism, many viable interpretations have been made with the fibre tracking hypothesis. In all the examples of vein arrays

studied, where the opening direction could be inferred independently, by the displacement of wall-rock markers (earlier veins, sedimentary structures), these features support measurements determined from vein fibre geometry.

To evaluate the viability of transtensional modelling of en echelon veins, the opening trajectories determined from fibres were compared with the zone displacement calculated from the vein array configuration alone. Figure 5.7a shows an example of a vein array where the vein opening direction indicated by fibre geometry can be compared with the zone displacement, *S*, determined by the McCoss method. This type of analysis could then allow inferences to be made about vein growth kinematics and the role of mechanical interaction (Olson & Pollard 1991) and crack linkage (Pollard *et al.* 1982, Nicholson & Pollard 1985) on wall-rock displacements produced by vein propagation and dilation.

In addition to fibres, vein opening directions and wall-rock displacements can also be determined from the paired projections and steps of some vein margins. These features, known as 'horns' or 'flanges' (Farmin 1941) are often present at the outer corners of rotated or failed bridges. They are interpreted as the remnant lateral tips of en echelon cracks (Pollard *et al.* 1982) which have fused by tip-to-plane breakthrough during vein dilation (Nicholson & Pollard 1985). These horns are dominantly opening (*ie.* mode I) cracks as the vein fibres are generally normal to their margins. Figure 5.7b shows an example of a continuous, composite vein with fibres at an angle to the fracture wall; the fibres tracking the opening of a mixed-mode crack. The vein comprises of a series of linked en echelon elements, with horns and cross-fractures (*cf.* Nicholson & Pollard 1985, fig.1c). At the margins, the fibres are normal although they become more oblique towards the vein centre. In the horns at the vein margin, fibres are straighter and are orthogonal at the tip. The vein opening vector, *S*, determined by the McCoss method, illustrates the tip geometry of these echelon cracks is consistent with the opening direction indicated by the fibres. This displacement configuration is also confirmed by the example shown in Fig.5.8 which illustrates a parent-vein with a series of en echelon veins extending from its tip. The parent vein has oblique fibres which are sub-parallel to the zone displacement, *S*, determined for the vein array using the McCoss method.

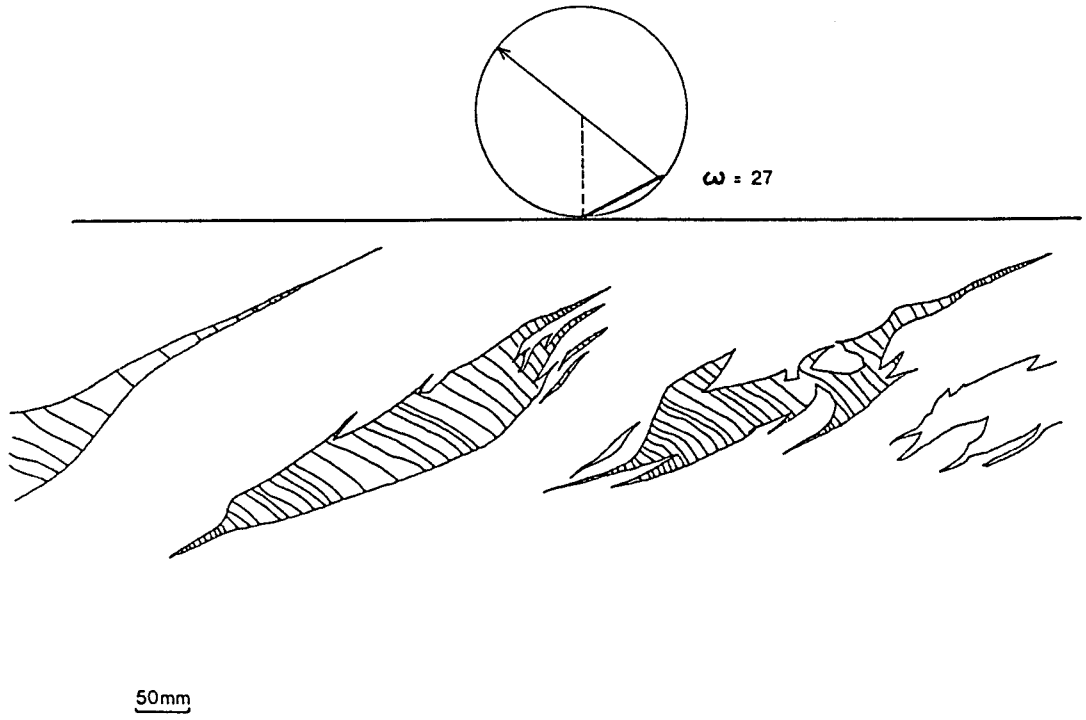

[a]

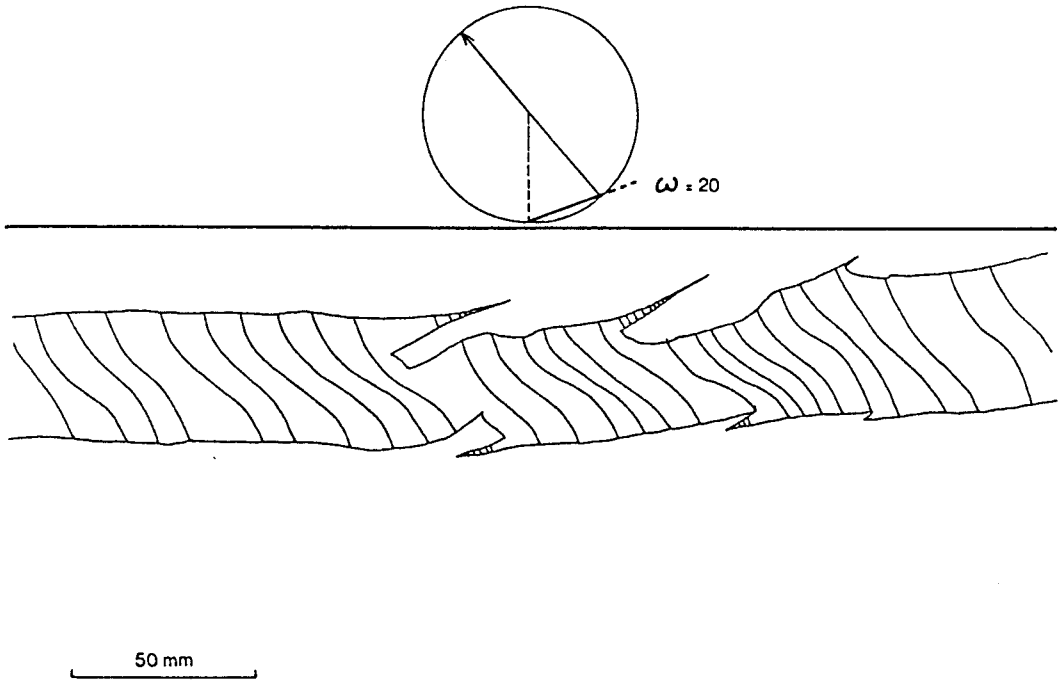

[b]

Figure 5.7. [a] A vein array with well developed fibres. The opening direction inferred from the average fibre orientation is subparallel to the zone displacement determined by the McCoss method. [b] An example of a vein with fibres oblique to the crack wall. The vein comprises of a series of linked en echelon elements, with horns and cross-fractures. The fibres are normal at the margin of the vein although they become more oblique towards the vein centre. In the horns at the vein margin, fibres are straighter and they are orthogonal at the tip. The vein opening vector determined by the McCoss method, using the tip geometry of these cracks is consistent with the opening direction indicated by the vein fibres.

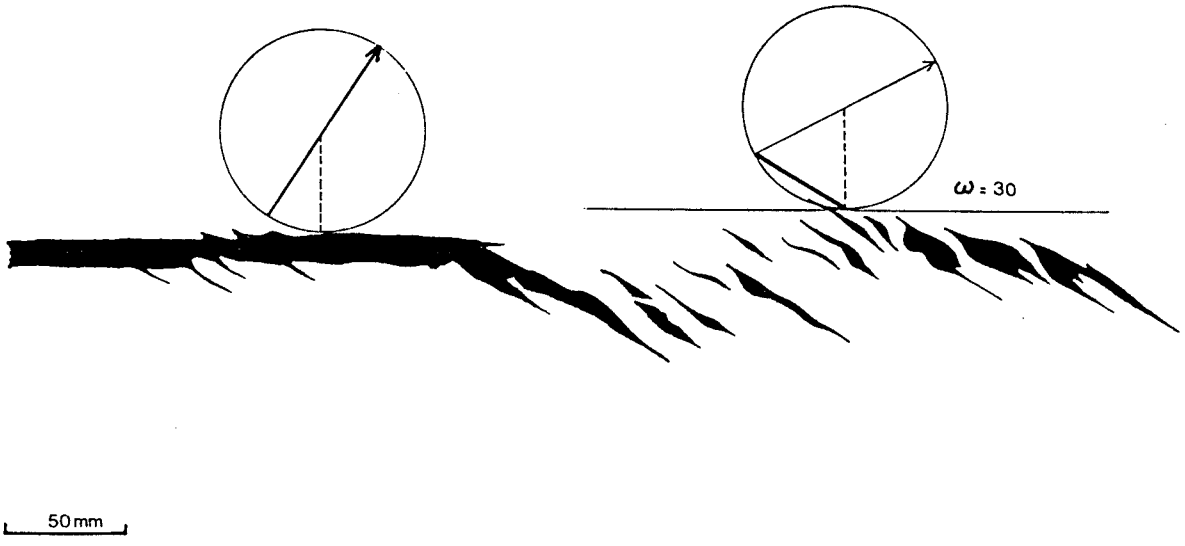

Figure 5.8. Line diagram of en echelon veins in front of the trace of a single vein from Millook Haven. Pinnate veins occur along the margin of the single vein and the fibres are oblique to the vein margins. This suggests that the vein was subject to a combination of predominantly mode I loading and sinistral shear. The en echelon veins near the termination of the single vein are oriented in a clockwise sense. According to the McCoss construction the zone displacement vector determined for the en echelon array is subparallel to the opening direction indicated by fibre orientation and pinnates from the single vein.

5.5.1 Summary of analysis of vein wall-rock displacements

The results of observations from these examples (Figs.5.6-8) suggest that transtensional modelling provides a viable explanation for en echelon vein array geometry and kinematics. The wall-rock displacement direction deduced from the vein-array angle (ω) is confirmed by vein fibre orientation and by matching wall-rock features. The mode I opening of most vein tips is also supported by fibres developed normal to the vein in this region.

The commonly observed transition to sigmoidal fibres, from orthogonal at the margin to oblique in the vein centre may represent the transition from crack tip opening displacements (preserved parallel to the margin), to the kinematic development of vein opening (*ie.* a change from crack propagation to dilation). This suggests that curved vein fibres need not represent changes in the far-field extension direction, but they are an integral record of crack development within a vein or vein array under fixed boundary conditions. This interpretation assumes syntaxial fibre growth; the opposite arrangement would be expected for antitaxial veins.

5.6 CONJUGATE EN ECHELON VEINS

There have been numerous attempts to relate the geometry of conjugate en echelon vein sets to their fracture mechanism and hence to their local (Beach 1975, Rickard & Rixon 1983, Du & Aydin 1991, Olson & Pollard 1991) and remote (Shianin 1950, Roering 1968, Beach 1975, Dietrich 1989) stress configuration. It is often assumed that the acute bisector between pairs of conjugate vein sets contains the σ_1 direction (Shianin 1950; Ramsay & Huber 1987, pages 624-629; Dietrich 1989). In this section the transtensional-transpressional modelling of en echelon vein array kinematics is extended to conjugate vein arrays, as the zone displacement vectors for pairs of vein arrays can be used to infer the relative block displacements of the rock between conjugate vein sets.

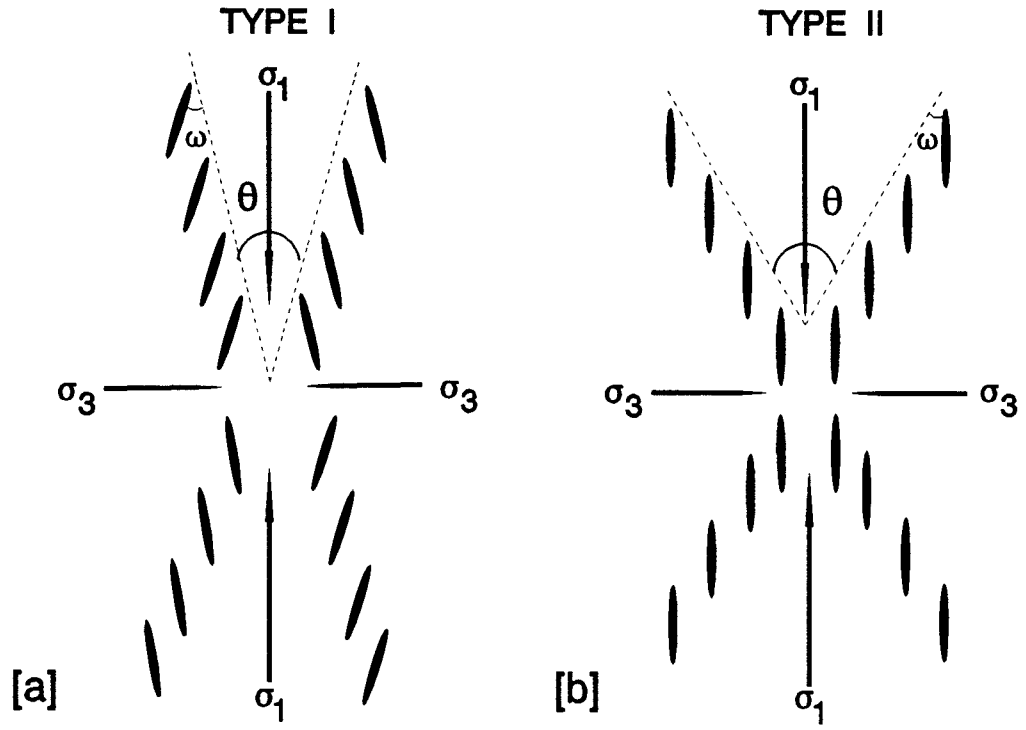

Figure 5.9. Two common patterns for conjugate sets of en echelon veins: [a] Type I ($\omega = 2\theta$) where the veins in one array parallel the trace of the complementary vein array and vice versa; and [b] Type II ($\omega = \theta$) where the veins in both arrays are initially parallel (after Beach 1975). A spectrum of conjugate en echelon vein array geometries occur between these two pattern types.

5.6.1 Observations on conjugate en echelon vein arrays

Two end members of a continuous spectrum of conjugate vein array configurations are shown in Fig.5.9. Beach (1975) proposed a classification scheme based on the angular relations between pairs of arrays: Type I conjugate arrays (Fig.5.9a) have veins in both of the arrays parallel to the conjugate zones ($\omega = 2\theta$), while Type II arrays (Fig.5.9b) have the veins in both arrays parallel to each other ($\omega = \theta$). In Beach's scheme veins in Type I arrays are attributed to be shear fractures, and those of Type II sets to extension fractures.

Ramsay & Huber (1987) and others have suggested that conjugate en echelon vein arrays can form with either acute or obtuse dihedral angles containing σ_1 (Ramsay & Huber 1987, page 629, fig.26.42). This assumption implies that for transtensional vein arrays the dihedral angle is acute, where for transpressional arrays it is obtuse. Data collected from localities in North Cornwall shown in Fig.5.10a, indicate that $2\theta < 90°$ and ranges between 15 and 60°. This suggests that the dihedral angle is acute for both transtensional and transpressional conjugate arrays, and it indicates that there is no real correlation of the dihedral angle with the vein-array angle, ω. Also shown in Fig.5.10a are two lines which outline the fields for the Type I ($\omega = 2\theta$) and Type II ($\omega = \theta$) conjugate vein array models of Beach (1975). Clearly there is no tendency for the data to conform to either of these models. The range of 2θ values for conjugate arrays is confirmed by comparison with vein sets from the Helvetic Alps described by Dietrich (1989) where 2θ ranges from about 5 to 90° (Fig.5.10b). These observations suggest the Type I and II scheme of Beach (1975) is unsatisfactory, and that they should now be viewed as special cases within a spectrum of conjugate vein array geometries.

5.6.2 Displacements across conjugate en echelon vein arrays

It is possible to apply the McCoss construction to each array in a conjugate set and compare the their wall-rock displacements.

[a] Symmetric zone displacement

The example shown in Fig.5.11a is of a conjugate array where the veins in each zone are sub-parallel

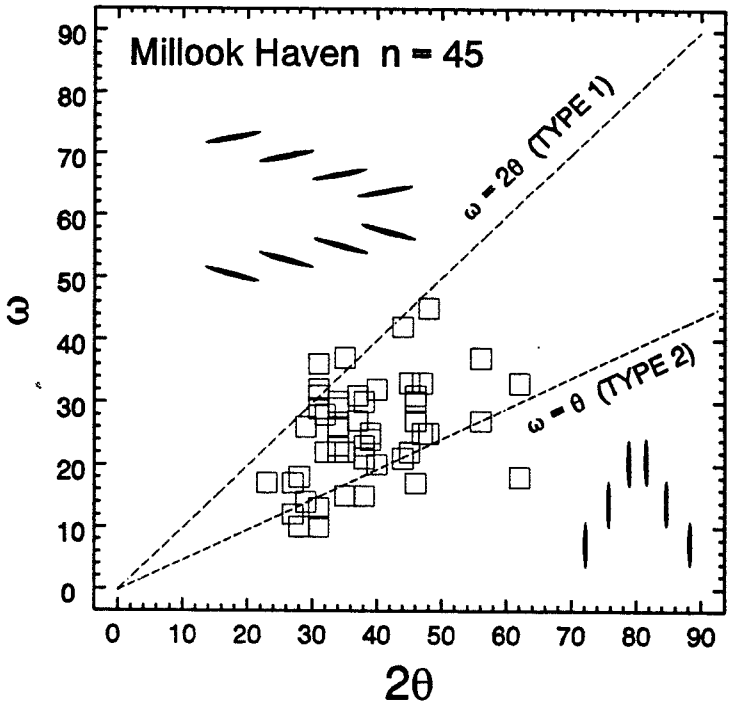

[a]

Figure 5.10a. Graph of ω against 2θ (the angle between two conjugate arrays) for conjugate en echelon veins from Millook Haven, North Cornwall.

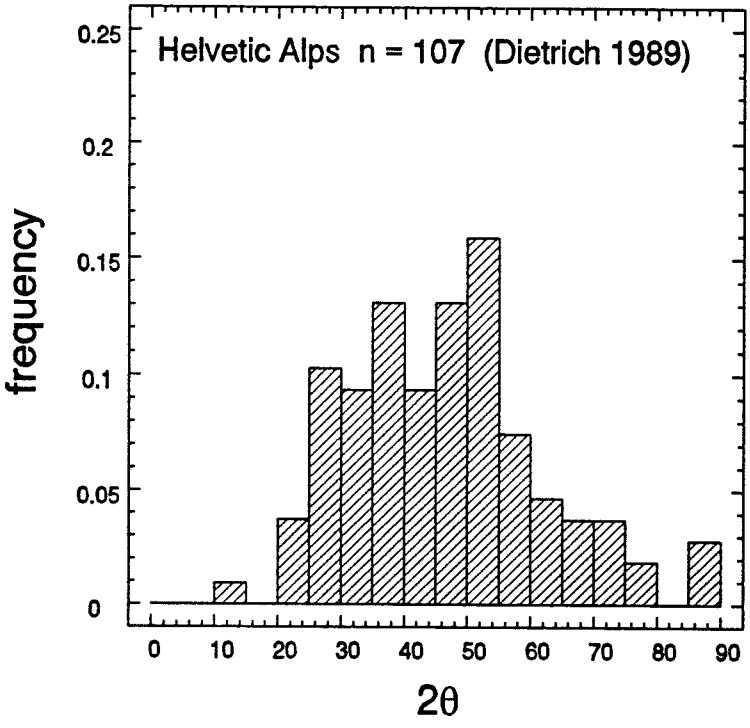

[b]

Figure 5.10b. Frequency histogram showing the 2θ angles for conjugate en echelon veins in Tertiary limestones of the Helvetic Alps, Switzerland (Dietrich 1989).

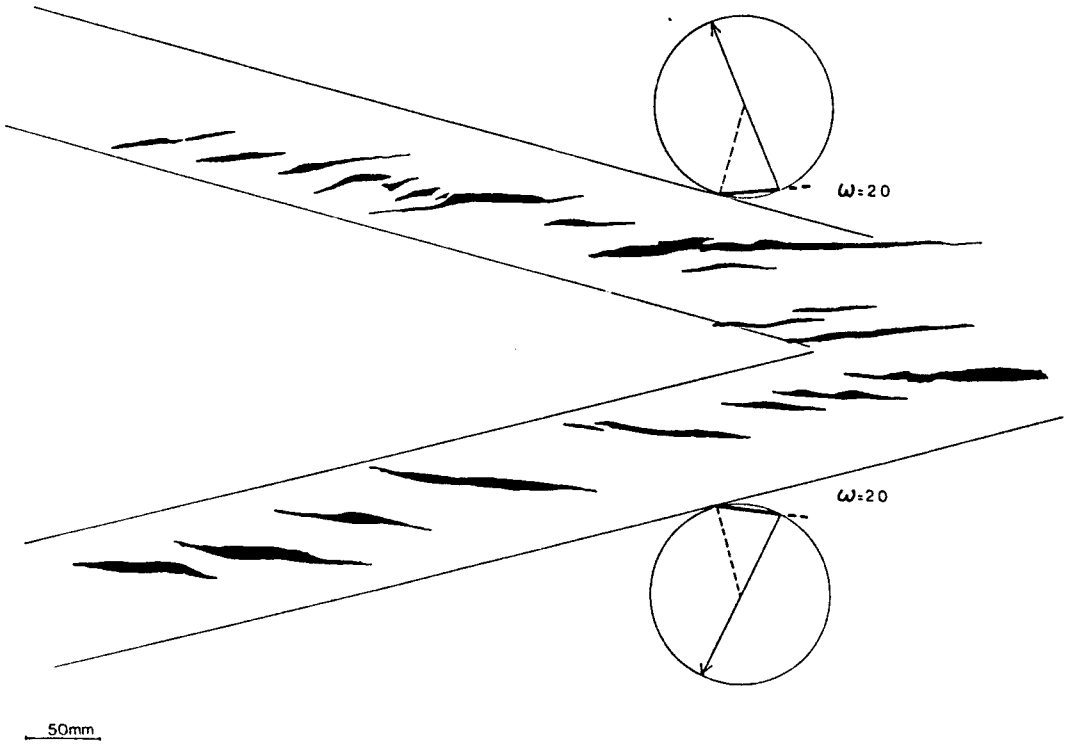

Fig.11a. Symmetric zone displacement.

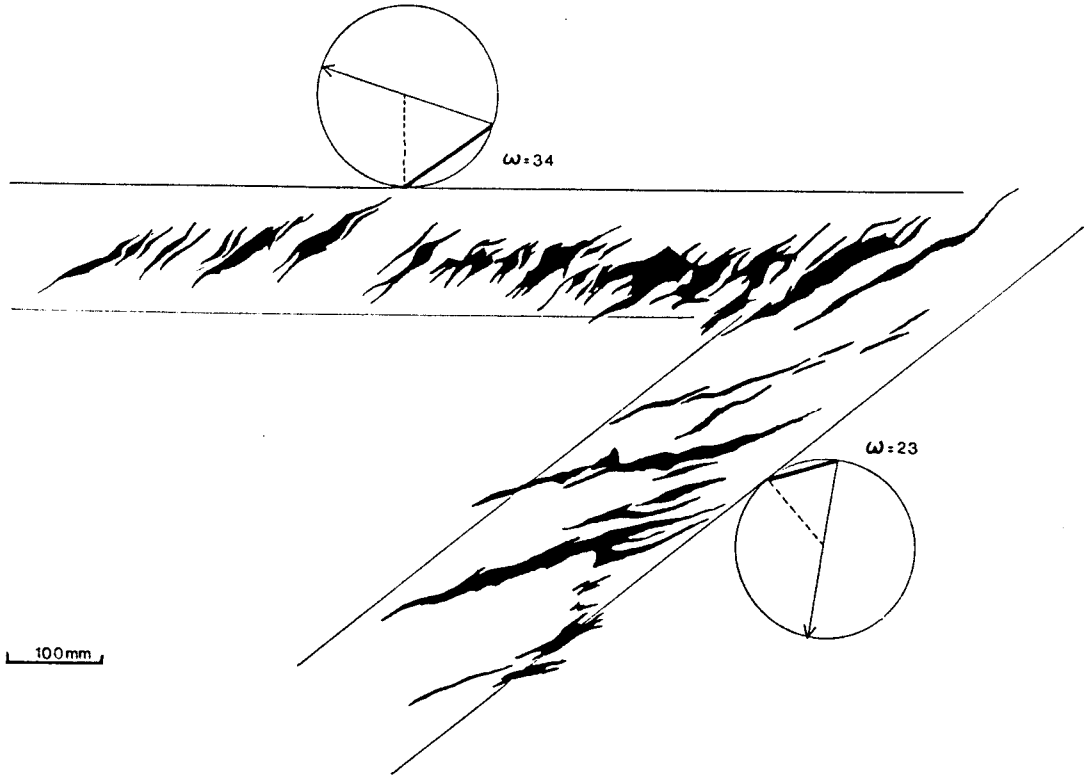

Fig.11b. Asymmetric zone displacement.

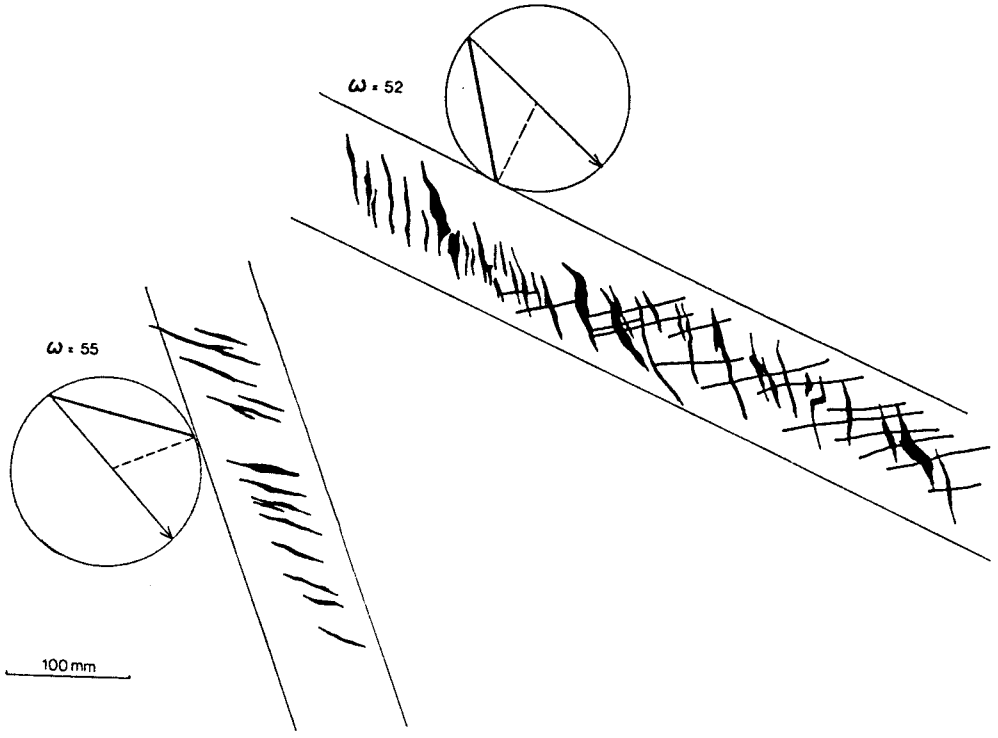

Fig.11c. Convergent zone displacement.

to each other, and where 2θ = 30°. The pairs of zone displacement vectors are symmetrically divergent, indicating a state of general transtension. There are solution-transfer effects within the array as some of the veins are truncated at solution-seams.

[b] Asymmetric zone displacement

Figure 5.11b shows an example where 2θ = 38° and the vein-array angle, ω, is different for each set. The zone displacements are divergent and strongly asymmetric to each other. The left-hand array (ω = 34°) is beginning to approach a wrench state, while the right-hand zone (ω = 24°) is transtensional.

[c] Convergent zone displacement

Figure 5.11c shows a conjugate en echelon array where the zone displacements indicate a strongly transpressional state as *S* shows convergence of the wall-rock. In this example which is from Ardmore, Co. Waterford, the veins of one of the arrays are sub-parallel to the complementary array and σ_1 is contained in the acute dihedral angle. This example is similar to examples described by Beach (1975, fig.13) and Burger (1977).

3.6.3 Summary of the main features of conjugate en echelon arrays

[1] Veins in en echelon arrays are generally mode I (extension) fractures, but they are oriented with respect to the local (rotated) stress in a zone of transtension. So conjugate sets contain veins which are oblique to one another and are often sub-parallel to the conjugate array (Type I of Beach (1975). The Type I and II sets of Beach (1975) are not genetically different, as both types are formed by extension (mode I) fractures in transtensional arrays. This means a spectrum of geometries between Beach's end members are found, indicating that the Type I and II classification is not satisfactory.

[2] The geometry and kinematics of conjugate en echelon vein arrays can be explained in terms of transtensional and transpressional deformation.

[3] Data collected from localities in North Cornwall indicate that the acute dihedral angles contain σ_1 in both transtensional and transpressional conjugate vein arrays; although comparatively few transpressional arrays were observed. Additionally, while σ_1 is contained in the acute dihedron it need not be parallel to the bisector of the conjugate array.

5.7. TRANSTENSIONAL-TRANSPRESSIONAL DEFORMATION

In the treatment of constant volume deformation in transpression-transtension by Sanderson & Marchini (1984) they point out that a strain discontinuity exists at the boundary of the deformation zone, because area (or volume) change is balanced by vertical or horizontal thinning. This discontinuity was not observed in the examples of vein arrays described here, except where some veins had linked and developed into compound pull-aparts and small-scale fault zones (Chapter 2).

If constant volume deformation is assumed, displacement, *S*, results in extension across the zone (α^{-1}) and an area change, with a compensating vertical or horizontal thinning (α) (Fig.5.12a). Transtensional and transpressional deformation can be factorised mathematically into components of pure shear and simple shear as follows (Sanderson & Marchini 1984)

$$D = \begin{bmatrix} 1 & \gamma \\ 0 & 1 \end{bmatrix} \begin{bmatrix} 1 & 0 \\ 0 & \alpha^{-1} \end{bmatrix} = \begin{bmatrix} 1 & \alpha^{-1}\gamma \\ 0 & \alpha^{-1} \end{bmatrix} \qquad \textbf{(5.1)}$$

where ψ is the angular shear strain and $\gamma = \tan \psi$ is the shear strain. From the relationships in Equation [5.1] the finite strain at various increments of stretching parallel to the zone displacement vector, *S*, can be calculated. The stretch across the zone (α^{-1}) can be expressed in terms of *S* by (Fig.5.12b)

$$\alpha^{-1} = [1 - S] \cos[\theta] \qquad \textbf{(5.2)}$$

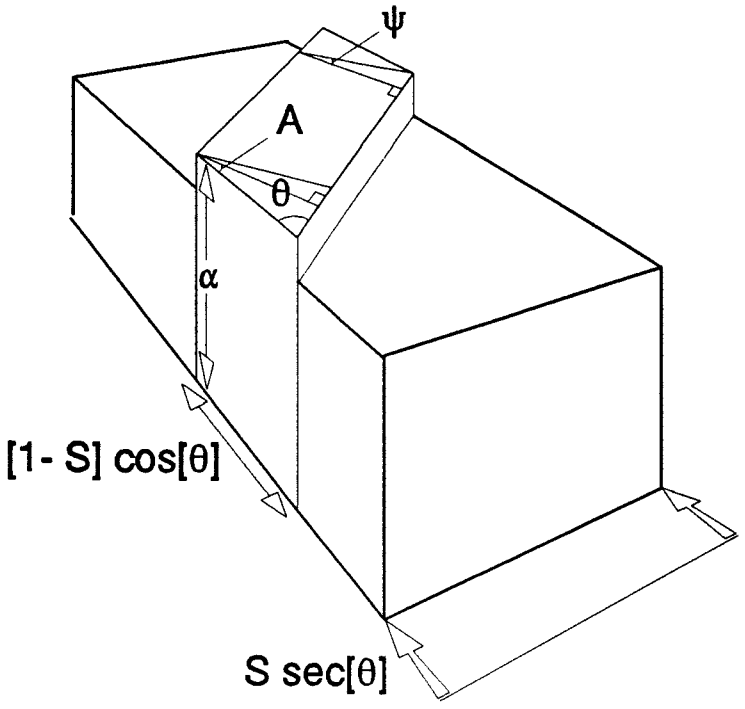

[a]

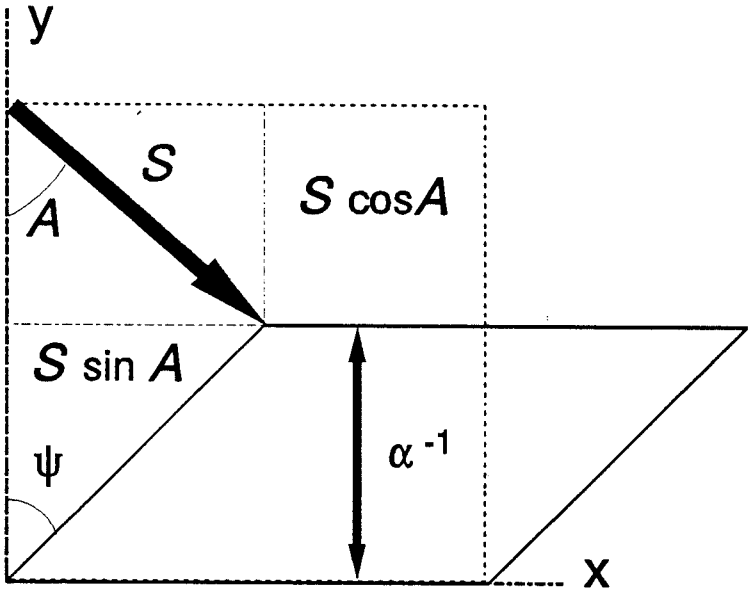

[b]

Figure 5.12. [a] Schematic diagram of transtensional deformation used to determine incremental strain as a function of the zone displacement vector, S, and zone orientation. Based on the diagram of Sanderson & Marchini (1984). [b] Block diagram of constant volume transtension to show how stretch can be resolved in terms of the zone displacement vector, S.

During transtension (α^{-1}) one of the principal strains is always vertical. This may be either Z or Y, so the XY-plane can be either vertical or horizontal.

Volume is not expected to remain constant during the formation and growth of en echelon veins. Some of the vein arrays from North Cornwall may involve some combination of transtensional-transpressional deformation with a differential volume or sectional area change. The presence of solution-seams implies that significant local dissolution and redistribution of material has occurred. The amount of volume change is difficult to quantify as there are a number of mechanisms which can contribute to this process. Those which have been observed for the vein arrays described here include: [1] A proportional increase in immobile mineral species through volume changes produced during pressure-solution deformation (Beach 1974, 1977); [2] possible volume changes through the introduction of exotic fluid and mineral phases (Beach 1974, Kerrich *et al.* 1978); [3] and host-rock extension through ductile flow (*ie.* incipient fracture-boudinage and bed thinning/flattening).

5.8 MECHANICS OF EN ECHELON VEINS

5.8.1 Vein arrays as pressurised zones

The previous sections of this chapter illustrate the variety of geometries for en echelon vein arrays. In this section the extent to which these structures reflect the underlying stress states and the role of the far-field stresses and internal fluid pressures are examined. In this analysis, en echelon vein arrays are treated by studying a single crack of infinite length, so they are visualised as being pressurised zones in a homogeneous isotropic elastic solid. A justification for this visualisation in the context of the field examples studied comes from the fact that there is a continuous transition from a single, composite oblique opening crack to en echelon veins (Nicholson & Pollard 1985, Nicholson & Ejifor 1987). In this way the opening condition for vein arrays can be expressed in terms of the principal stresses and their orientation (α). This means the initial opening conditions for en echelon veins can be expressed in terms of the stress ratio R as a function of α and ω (Fig.5.13) as follows

$$\frac{u_2}{u_1} = \frac{\tau}{\sigma_n + P_f} = \frac{\sin(2\alpha)}{R + \cos(2\alpha)} \qquad (5.3)$$

Equation 5.3 is equivalent to an expression used by Delaney *et al.* (1986) to analyse general crack problems concerning dyke emplacement. The notation used: u_1, u_2 are the zone dilational displacements, α is the angle between the normal to the array and the minimum horizontal stress S_h, σ_n is the crack normal stress and τ is the maximum shear stress (Fig.5.13).

Since $\tan A = u_1/u_2$ and $2\omega = A$

$$\tan 2\omega = \frac{\sin 2\alpha}{R + \cos 2\alpha} \qquad (5.4)$$

and hence,

$$R = \frac{\sin 2\alpha}{\tan 2\omega} - \cos 2\alpha \qquad (5.5)$$

These expressions link the geometry of the array (ω) to the orientation of the principal stresses (α) and the stress ratio R, where

$$R = \frac{2P_f - (\sigma_1 + \sigma_3)}{(\sigma_1 - \sigma_3)} = \frac{P_f - \sigma_m}{1/2\,(\sigma_1 - \sigma_3)} \qquad (5.6)$$

when σ_m is the mean stress and $1/2(\sigma_1 - \sigma_3) = \tau$ is the maximum shear stress. Equation 5.6 provides a link between the geometry and the mechanics of en echelon veins. By estimating R (Equation 5.5), which depends only on the geometry and orientation of the vein array, it is possible to determine the relative role of fluid pressure and mean stress in the mechanics of the vein array.

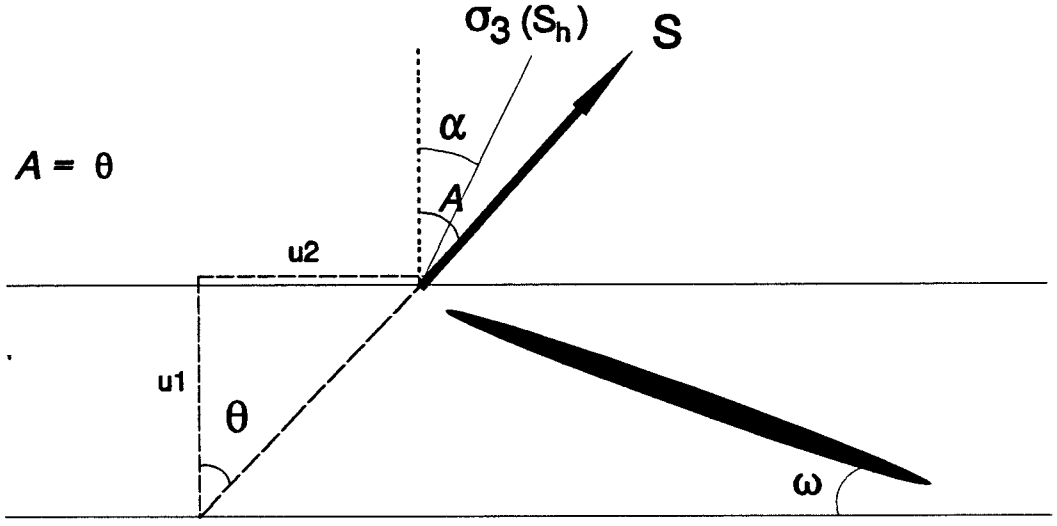

Figure 5.13. Diagram showing the visualisation of a vein array as a pressurised zone of infinite length, in a homogeneous and isotropic elastic solid.

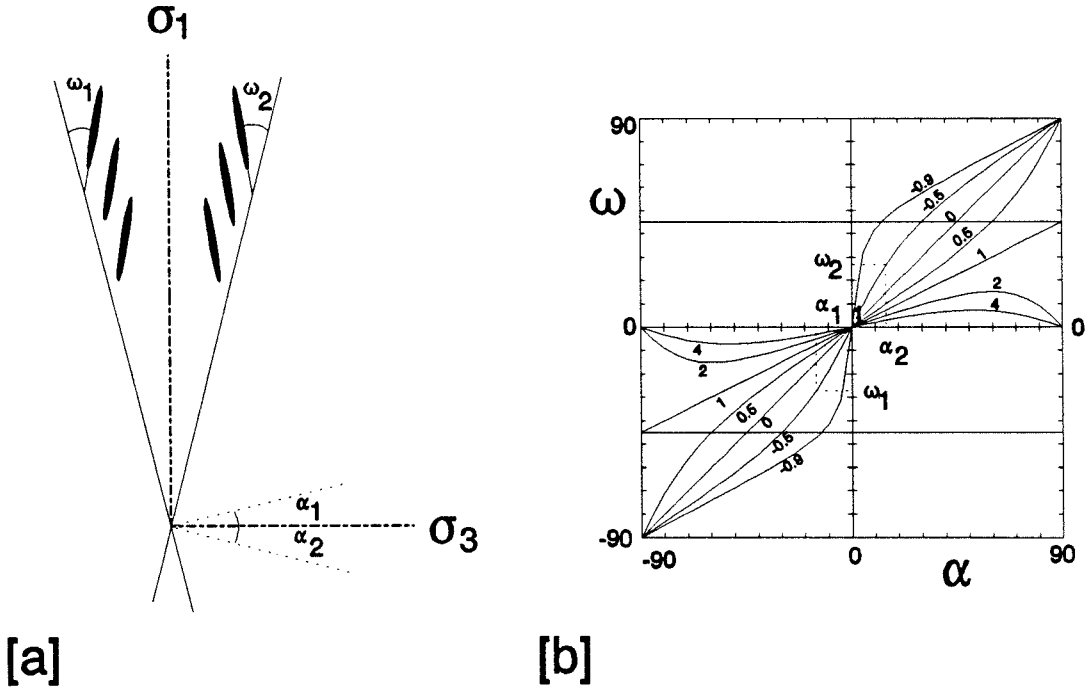

Figure 5.14. [a] Diagram to show how the geometry of en echelon arrays allows direct measurement ω_1, ω_2, α_1 and α_2; these parameters can be used to find a graphic solution for the stress ratio, R. [b] Graphical method for the determination of the stress ratio, R, on the graph of ω and α (see text for explanation).

5.8.2 Application of analysis to en echelon veins

In order to determine R (Equation 5.5) it is necessary to estimate the orientation (α) of the far-field stress. Since individual veins are considered to reflect the rotated (near-field) stress in the array, α must be determined from an independent argument. One approach is to consider conjugate en echelon arrays, formed under the same stress field (including P_f), and hence the same R value. Figure 5.14a shows how the geometry of en echelon arrays allows direct measurement of ω_1, ω_2, α_1 and α_2 (the angle between the arrays); parameters which can be used to determine the stress ratio, R, graphically. The sign of ω_1 and ω_2 are opposite since the shear sense is different. The graph of ω and α (Fig.5.14b) can then be used to locate $[\alpha_1, \omega_1]$ and $[\alpha_2, \omega_2]$ on a common curve for R. These points can be located by sliding the two plotted points along the α-axis; although in practise this procedure can be carried out for a set of ω and α values (where α_i is measured relative to an arbitrary reference direction) so that the best fit R curve can be determined.

An example of conjugate vein sets from Foxhole Point, North Cornwall (Fig.5.15a) indicates R values of between 0 and -0.5. The negative ratio of R suggests that $P_f < \sigma_m$ (Equation 5.6). Figures 5.15b and 5.15c show data for conjugate vein arrays at Millook Haven which belong to the same vein set as Fig.5.15a, and yield a similar range of R values (between 0 and -0.5). The data suggest that the vein sets at both localities developed in a stress field where the internal fluid pressure (P_f) did not exceed the remote mean stress (σ_m).

These initial attempts to determine the driving stress for en echelon veins are interesting in that they suggest that abnormal fluid pressures (*ie.* $P_f > \sigma_m$) are not required to form such arrays. Conversely, tectonic stresses must be involved in the generation of effective tensile stresses ($\sigma_n - P_f$) <0, implying large differential stresses. The stress ratio, R plays a significant role in effecting the geometry and mechanics of conjugate en echelon veins. Figure 5.16 shows how different R values can be correlated with some observed configurations for conjugate vein arrays. When $R = 0$ the veins are parallel to σ_1, *ie.* they have the same orientation (Fig.5.16a); when $R < 0$ the veins are convergent (Fig.5.16b); and where $R > 0$ the veins are divergent (Fig.5.16c).

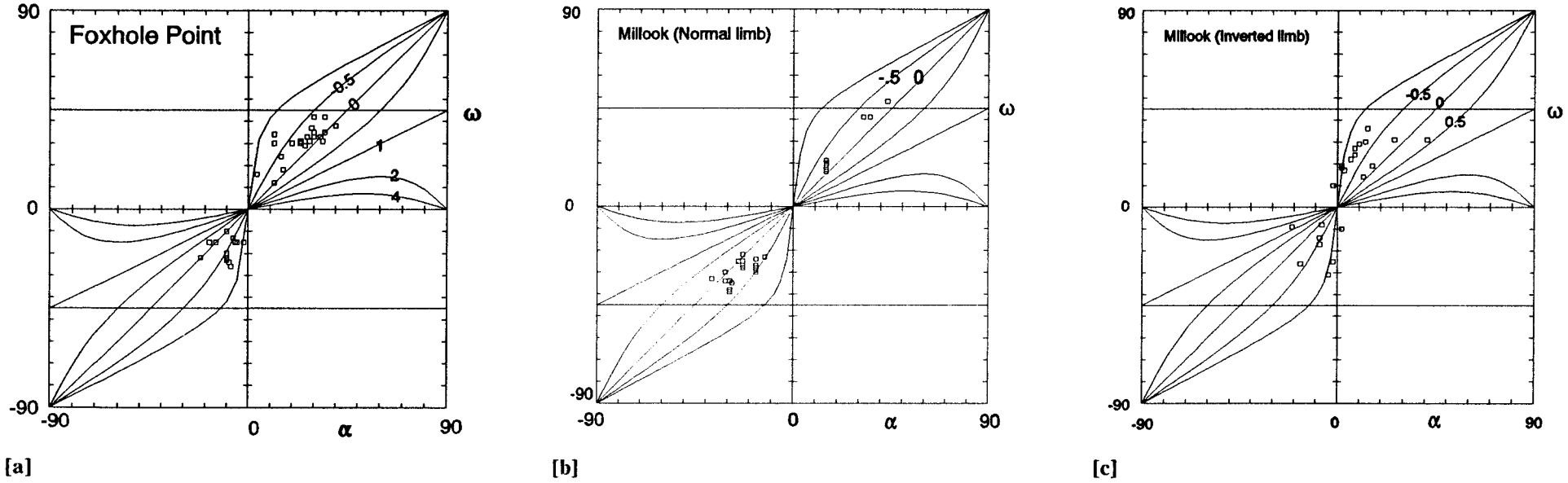

Figure 5.15. Graphs of α against ω for conjugate en echelon vein arrays in the Crackington Formation, North Cornwall: [a] Foxhole Point [b] normal fold limbs at Millook Haven and [c] inverted fold limbs at Millook Haven.

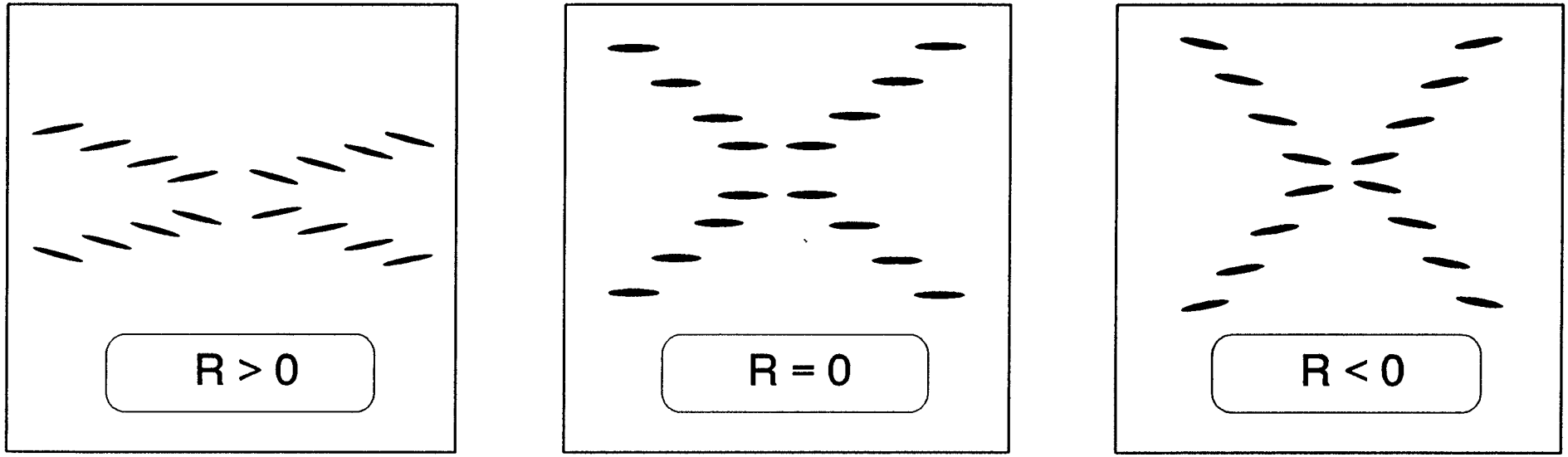

[a] [b] [c]

Figure 5.16. Schematic diagram to show the relationship between the geometric eonfigurations of eonjugate en echelon vein arrays and the magnitude of the stress ratio, R: [a] R >0 [b] R = 0 [c] R <0.

5.9 CONCLUSIONS

[1] En echelon vein arrays have a variety of geometries with veins that form at ω values of 5-55° to the array. This suggests that transtensional and transpressional deformation may be more important in their development than simple shear.

[2] Determination of relative wall-rock displacements across vein arrays, supported by bridge and mineral fibre geometry, suggests transtensional-transpressional deformation is more applicable In many cases. The models explains the full range of ω values, indicating that there is a spectrum of vein geometries which can be directly related to wall-rock displacement.

[3] Veins in en echelon arrays are generally mode I cracks; oriented with respect to the local (rotated) stress field in a zone of transtension or transpression. This suggests the propagation path of veins in en echelon arrays is consistent with minimising the effects of the stress intensity factor, K_{II}.

[4] Data collected for conjugate vein arrays indicate that acute dihedral angles contain σ_1 for both transtensional and transpressional conjugate sets. Additionally, while σ_1 is contained in the acute dihedron it need not be parallel to the bisector of the conjugate array. The Type I and II classes (Beach 1975) are not genetically different, as both types are formed by extension (mode I) fractures in transtensional arrays. This means a spectrum of geometries between Beach's end members are found, indicating that the Type I and II classifications are not appropriate.

[5] The stress ratio, R plays a significant role in effecting the geometry and mechanics of en echelon veins. For conjugate en echelon vein arrays when $R = 0$ this produces veins that are parallel to σ_1, *ie*. veins of the same orientation. For $R < 0$ the veins are convergent and when $R > 0$ veins are divergent.

[6] The argument that high internal fluid pressure ($P_f < \sigma_m$) are required (eg. Beach 1977, Reynolds & Lister 1987) for vein formation may not be justified.

6

Dyke intrusion and paleostress analysis

6.1 INTRODUCTION

Mafic dykes occur in oceanic and continental crust, in many different tectonic settings. Their widespread occurrence is evidence for their importance in igneous activity and in crustal extension. Field observations also suggest that fluid-driven fracture is an important mechanism for dyke propagation (Anderson 1951, Shaw 1980, Spence & Turcotte 1985) and for magma transport through the earth's crust (Aki *et al.* 1977, Ryan 1988, Lister & Kerr 1991).

In this study, the field relations of some mafic dykes are described for localities within the British Tertiary Volcanic Province around Easdale in Argyll, Scotland (Fig.6.1a). The dykes are of the order of a few centimetres or metres thick (Fig.6.2a), so they are sufficiently small to enable detailed observations of features which are often obscured in larger igneous intrusions. The distribution of flow lineations and the influence of dyke geometry on magma flow are described. Measurements of opening components normal and transverse to the dykes are analysed, and these are related to remote (far-field) stress and magma pressure. Analysis indicates that many of the dykes opened obliquely, and that this oblique opening was a function of their orientation. The study also provides opportunities to test and develop some of the ideas of Pollard and co-workers (Pollard 1973, Delaney & Pollard 1981, Delaney *et al.* 1986) on the stress control of dyke intrusion. Observations lead to the development of a simple mechanical model which provides a basis for assessment of some of the more important factors in dyke intrusion; principally the role of magma pressure and of remote differential stress.

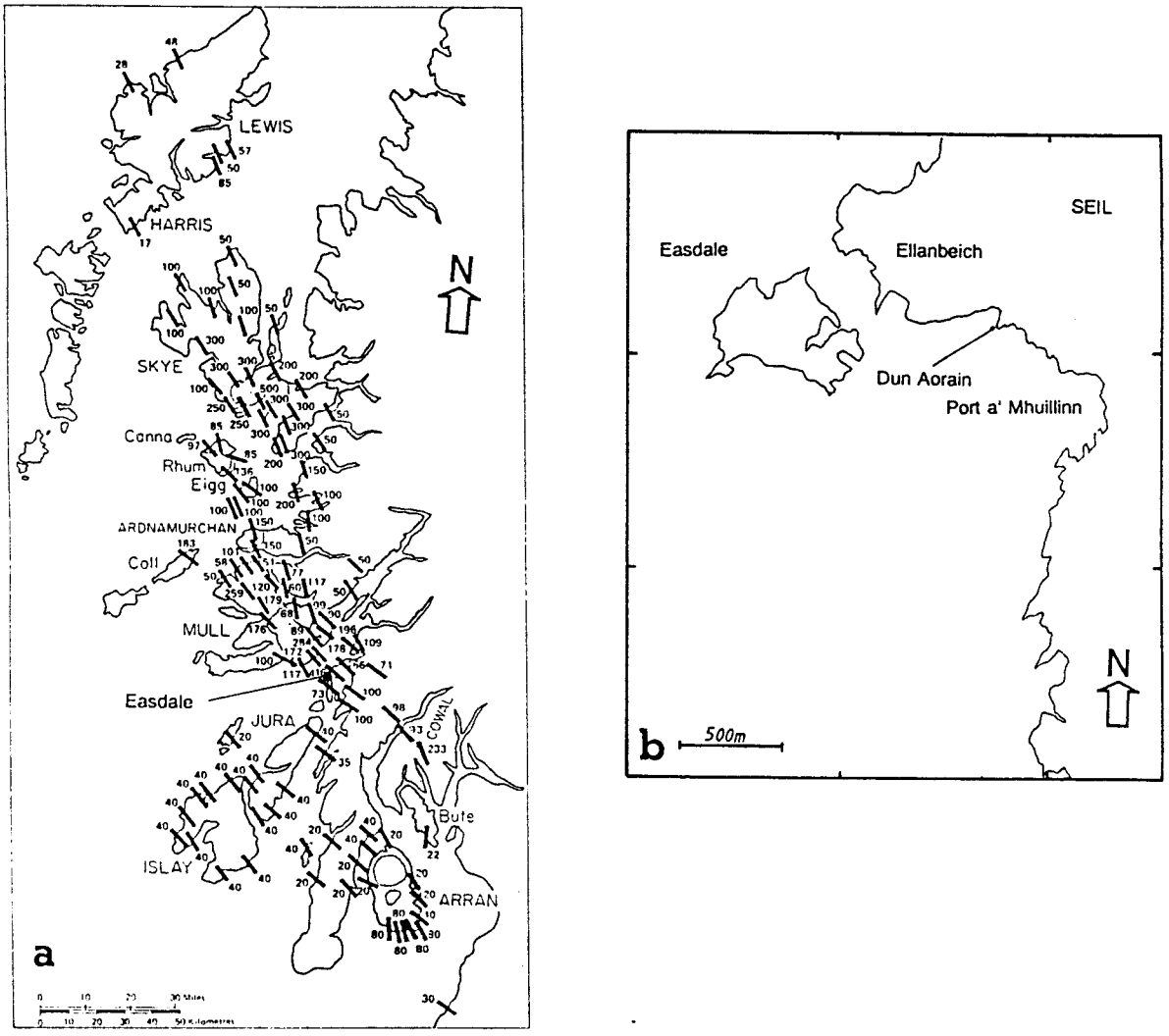

Figure 2.1. [a] Regional linear dyke swarms of north-western Scotland and the location of Easdale. The number of observations are printed beside each arithmetic average trend bar (from Speight et al. 1982, fig.33.1). [b] Map of localities around Easdale which are referred to in the text.

Of the many studies of dyke geometry most are regional, structural or petrological in orientation. Several generalisations of dyke characteristics are usually made: [1] dyke intrusion is within the plane normal to the direction of least compressive stress (Anderson 1951, Shaw 1980), and [2] dykes often occur in linear swarms which are characterised by little variation in thickness, orientation and spacing (Speight *et al.*1982, Gudmundsson 1990). However, dykes frequently display minor irregularities which cause them to deviate from simple geometric forms (Kaitaro 1952, Currie & Ferguson 1970, Delaney & Pollard 1981). Although paleostress directions are often determined from dyke orientation alone, based on the assumption that the minimum principal stress, σ_3, is normal to the dyke, there are cases when magma invades pre-existing fractures whose orientations are unrelated to the stress system at the time of injection. Criteria to determine emplacement mechanism and paleostress are discussed using the field examples.

6.2 GEOLOGICAL SETTING

The dykes described are from near Easdale in the British Tertiary Volcanic Province, north-western Scotland (Fig.6.1). These dykes form part of a regional linear NW-SE dyke swarm associated with the high-level plutonic centre situated on Mull (≈15 km NW of Easdale) (Speight *et al.* 1982). During emplacement of the centre at zeolite grade conditions meteoric fluids were active. Dates for the contemporaneous Mull lava series have ^{40}Ar-^{39}Ar ages of 59.4 to 61.1 Ma (Musset 1986). The field relations and the geometries for some of the dykes at Easdale are described by Roberts & Sanderson (1971).

The dykes outcrop on the coast SE of Easdale and Ellanbeich [NM 743173], between Dun Aorain [NM 747172] and Port a'Mhuilinn [NM 752166] (Fig.6.1b). The host-rocks are metasediments of the Easdale Group (Dalradian Supergroup), mainly comprising of dark slates with thin carbonate interbeds. The dykes are predominantly fine-grained and of basaltic composition. Many are zoned parallel to the dyke walls and have a chilled marginal zone with flow lineations.

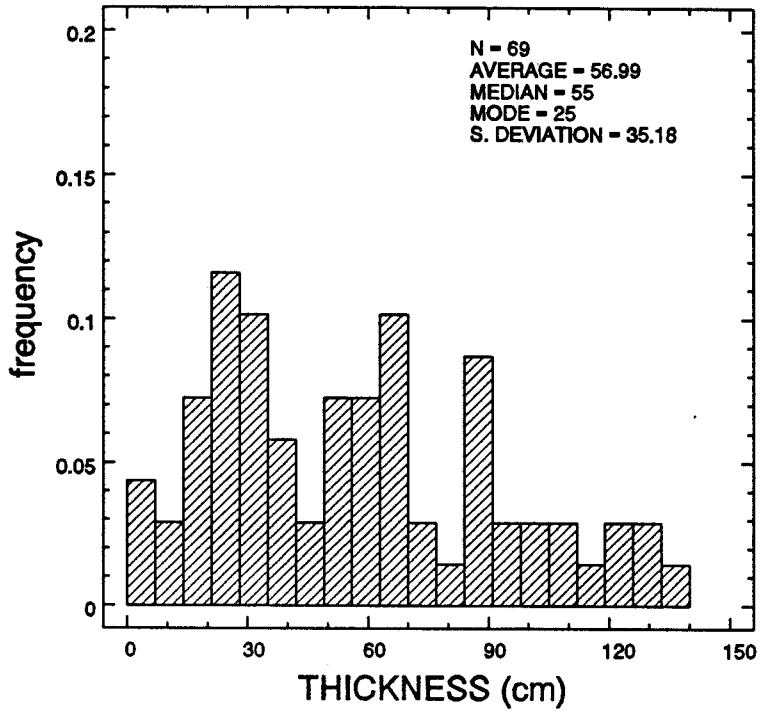

[a]

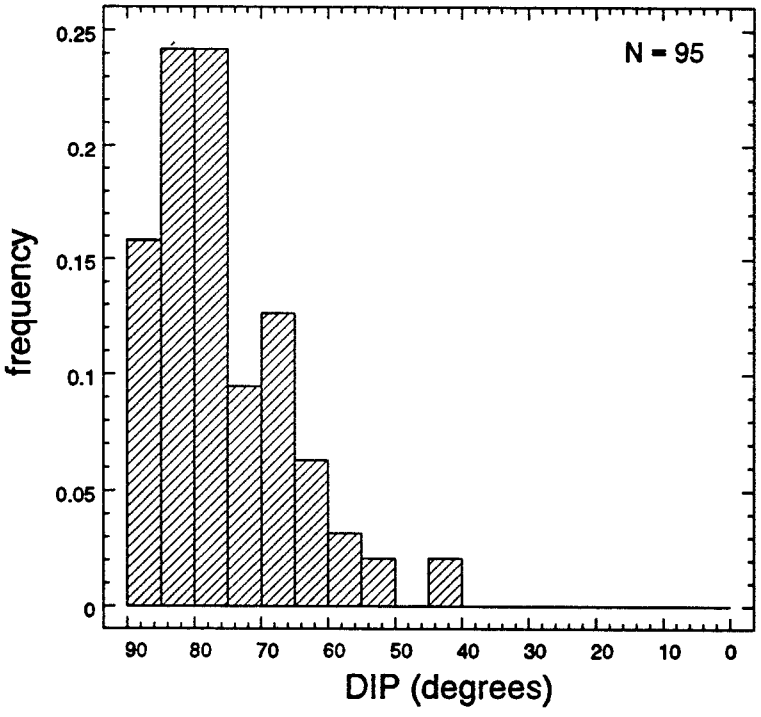

[b]

Figure 6.2. [a] Frequency histogram of thickness for the Easdale dykes. [b] Frequency histogram of dyke dip distribution at Easdale.

6.3 MAPPING METHODS

The dykes outcrop on the foreshore over nearly level ground, so conventional compass and tape traverse mapping was used to produce maps at of a scale of 1:50. A tape was aligned parallel to the dyke to produce a base line from which details were mapped directly, or from offsets normal to the tape or along a bearing of measured length. Outcrop and contact details were plotted directly onto squared graph paper. Additional measurements of structures in the host-rock (cleavage, joints and faults) and of flow lineations adjacent to dyke margins were also made.

6.4 FIELD OBSERVATIONS

6.4.1 Structures related to dyke propagation

The vertical and near vertical dykes have thicknesses in the range 0.1-1.5m (Fig.6.2a) with outcrop lengths of 0.5 to >50m; shallower dipping dykes tend to be thinner relative to the more steeply inclined dykes. Dyke margins are sharp and chilled with no evidence for host-rock brecciation. There are no obvious contact metamorphism effects within the host-rock adjacent to dyke margins. The dykes generally have gently undulating margins with minor trend changes and variations in dip around vertical and non-vertical axes. The dip distribution of the dykes shown in Figure 6.2b indicates that 60% of the data are within 15° of vertical. A diagram of poles to dyke contacts (Fig.6.3a) indicates that they lie in a partial girdle with a mean orientation of 88/053°. Four concentrations of poles to dykes can be recognised: [1] NW-SE trending dykes which may correlate with joints and small-scale faults (Fig.6.3c,d) that are at high angles to bedding and cleavage, and subparallel to the mean dyke orientations; [2] A more diffuse concentration dipping steeply SE which corresponds to dyke segments that are subparallel to cleavage (Fig.6.3e,f); [3] E-W trending dyke segments of variable dip; and [4] SW dipping dyke segments that are subparallel to cleavage. A rose diagram of dyke orientations (Fig.6.3b) indicates that they have a complex distribution, with a vector mean of 145.2°. The variations within this population reflects the sidestepping nature of the dykes.

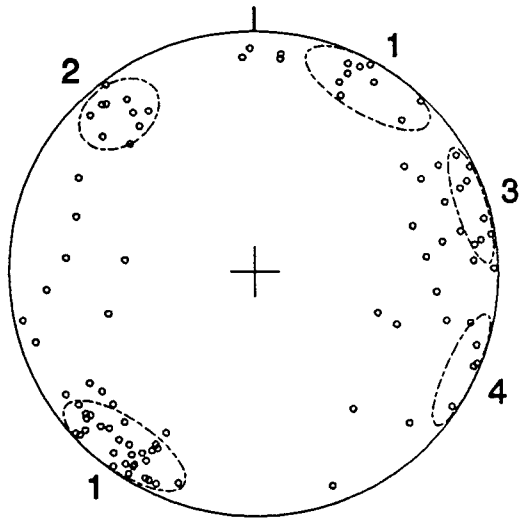

[a]

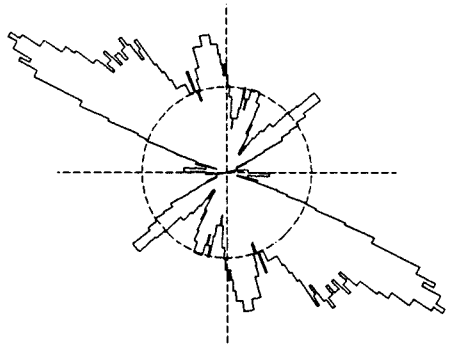

[b]

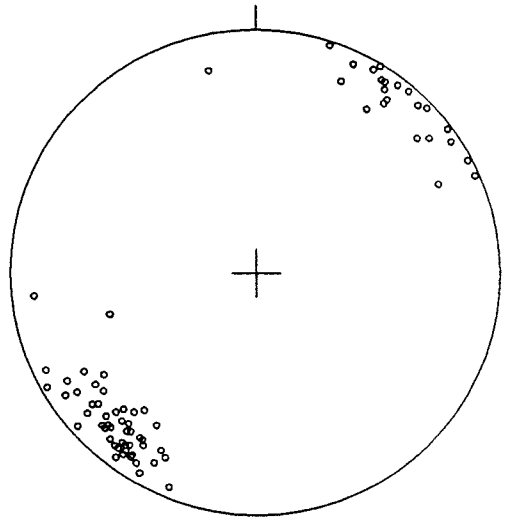

[c]

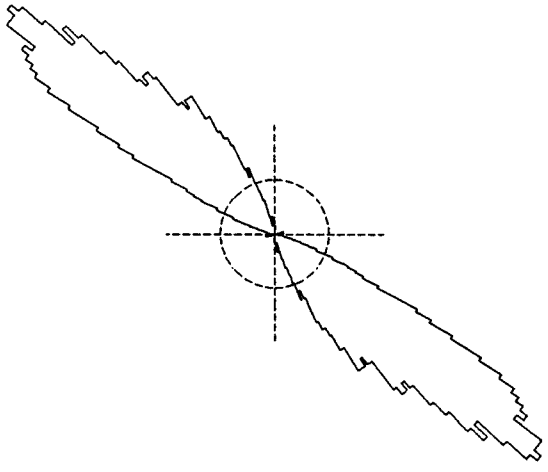

[d]

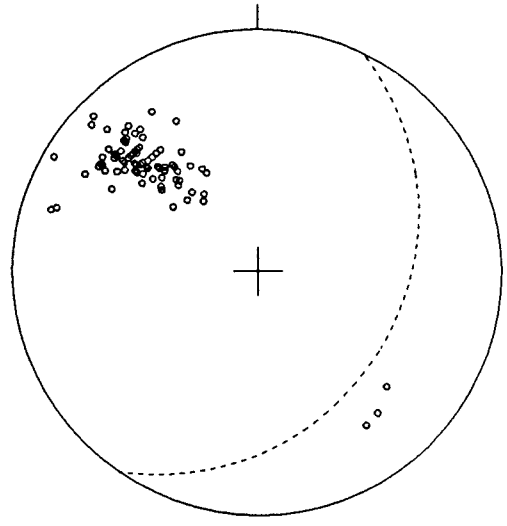

[e]

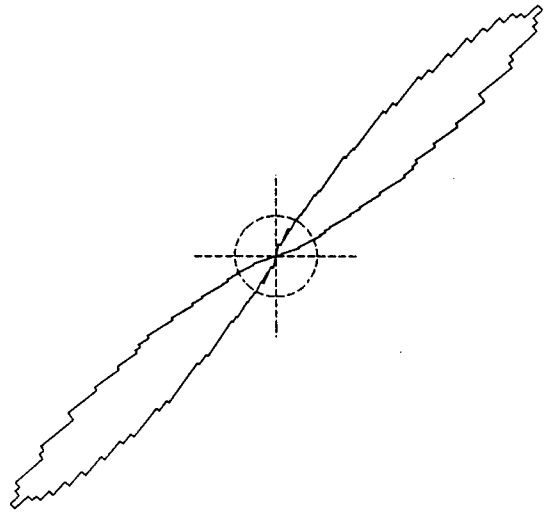

[f]

Fig.6.3. Orientation data: [a,b] poles and rose diagram of dykes (n = 95); [c,d] joints (n = 73); [e,f] cleavage (n = 81).

The non-planar geometry of the dykes at Easdale includes deviations (in horizontal sections) such as echelon-steps, dog-legs and splays. Figure 6.4 shows sketch maps of some examples of the geometries of these structures. Further examples, shown in Fig.6.5, are described in their accompanying caption. A sequence of six maps shown in Fig.6.6, indicates the range of dyke morphologies seen in the Easdale area.

The dykes commonly sidestep along cleavage and bedding planes. Figure 6.6a shows a typical example of a dyke sidestepping along cleavage; in this example, one segment of the dyke trails along cleavage with a marked reduction in its thickness. In more extreme cases these trails can produce transform fault geometries (Fig.6.4a). In this example (Fig.6.6a) and the dyke shown in Fig.6.6b, the displacements of the dyke margins, as they sidestep along cleavage are variable. The strip of rock which links these offsets are generally called connectors (*eg.*Bussell 1989), with step, the name more commonly given to the outer surface of a connector between two dyke segments (Fig.6.7).

Dyke terminations were seen in only a few cases (eg. Figs.6.4c, 6.6b and 6c). In these examples the dykes terminate with blunt and curved blunt tips; although for the dyke shown in Fig.6.6d its tip is offset along cleavage as a series of small segments. The curved terminations of the dykes in Figs.6.6b and 6c have probably been produced by mechanical interaction between the overlapping dyke segments. Other morphological features are apparent where dykes were exposed in vertical sections, as in the old quarries on Easdale (Fig.6.1b). Some of these dykes have irregular margins and composite geometries with horns (lateral extension fractures) and remnant bridge structures (Fig.6.4c & 6.5). These structures have been described for veins in previous chapters, and they are characteristic of the coalescence of en echelon cracks.

6.4.2 Joints and faulting

Jointing within the Easdale Slates is discontinuous and individual dykes do not invade a particular fracture plane for a great distance. The main joint set is vertical/subvertical with an average strike

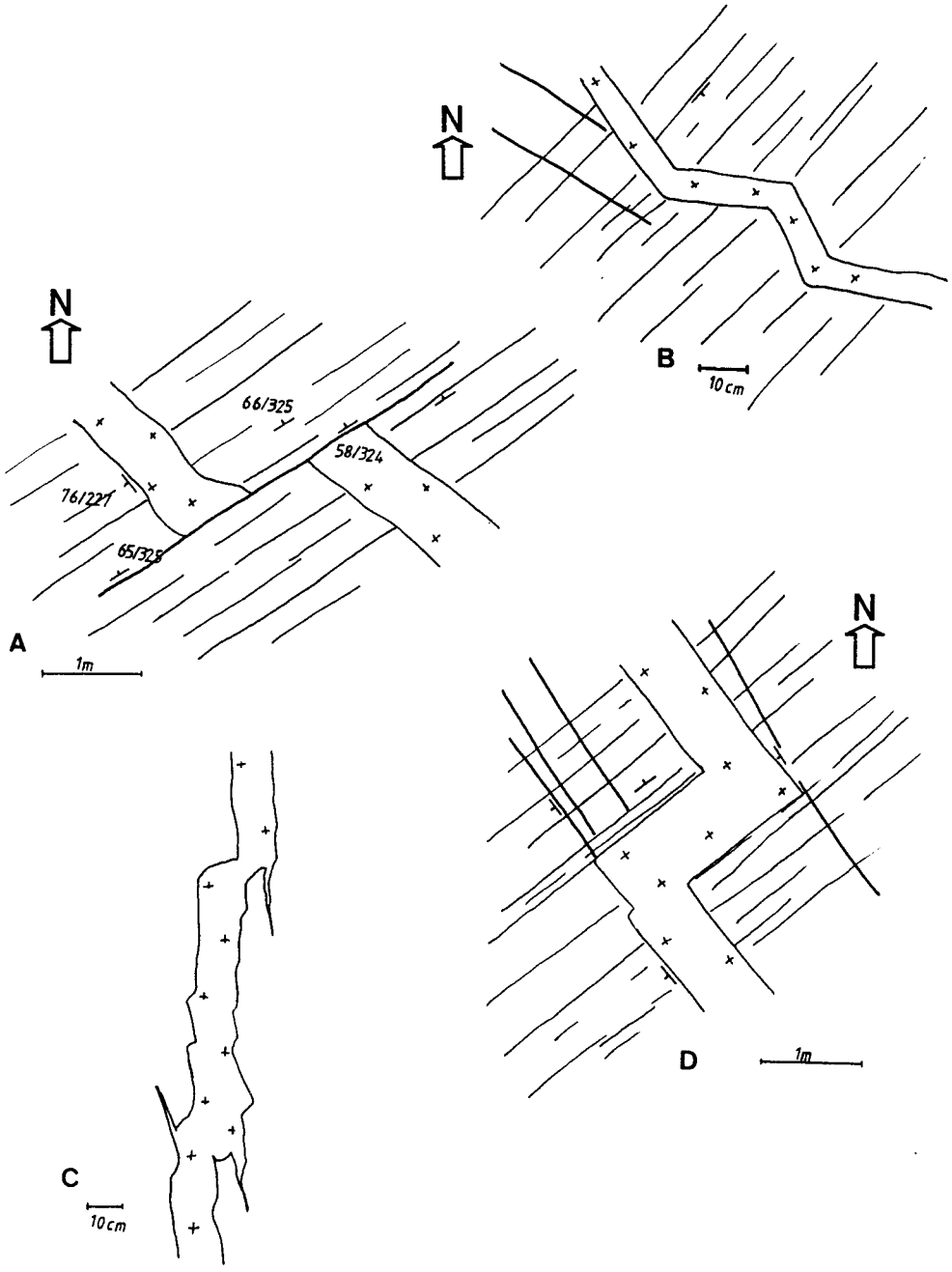

Figure 6.4. Sketch maps of examples of various dyke configurations at Easdale: [a] transform geometry [b] a dyke sidestepping between different fracture trends [c] dykes with horns and stubs and [d] a dyke offset along cleavage.

Figure 6.5

[a] A typical example of a sidestepping dyke from Easdale.

[b] Example of a dyke showing an irregular margin with lateral extension fractures and remnant bridge structures.

[c] Example of a dyke sidestepping between different fracture trends.

[d] Flow structures adjacent to a dyke margin (outlined in chalk), showing the change of orientation with dyke geometry.

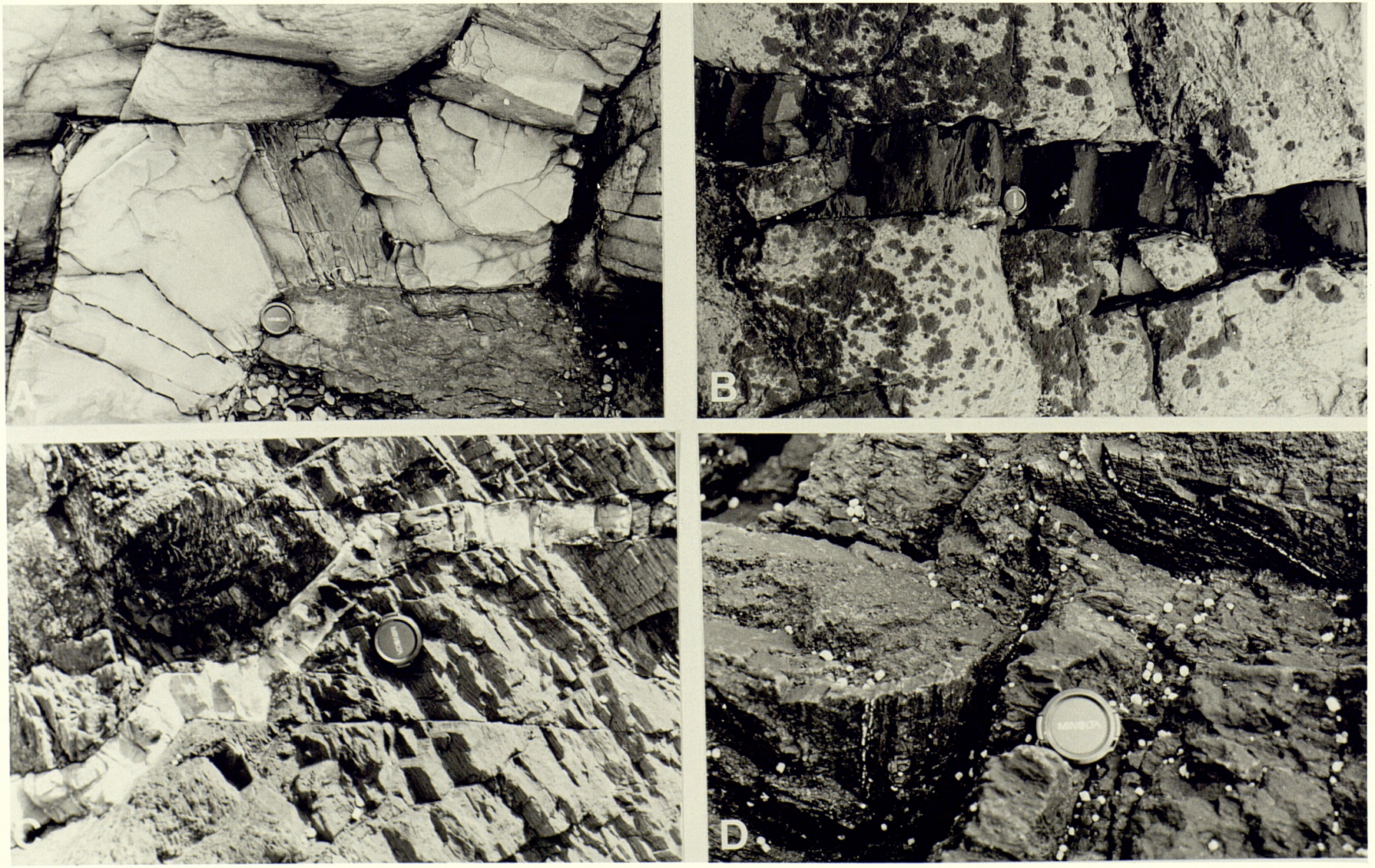
A
B
C
D

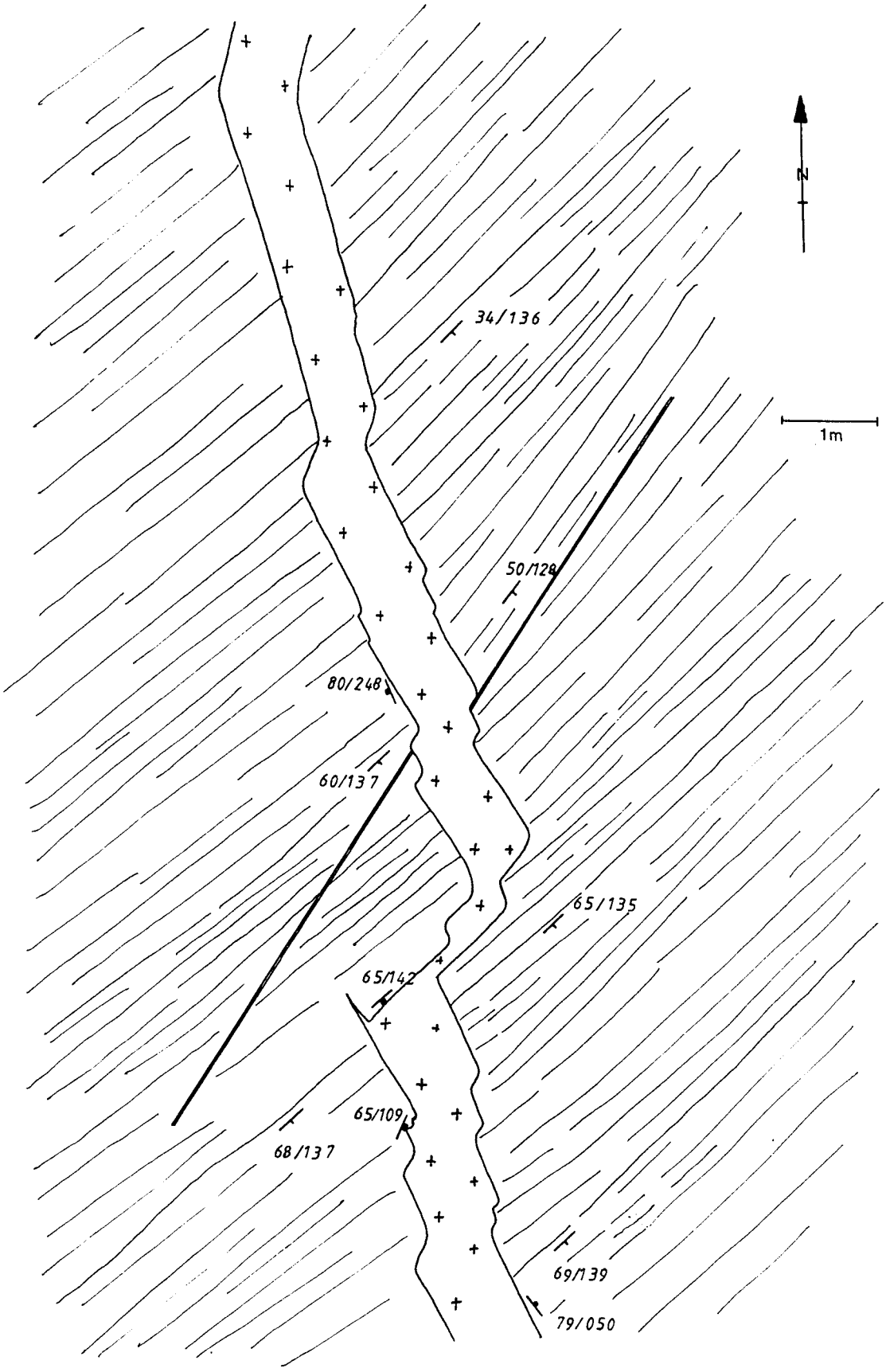
N
1m
34/136
50/128
80/248
60/137
65/135
65/142
65/109
68/137
69/139
79/050

Figure 6.6a.

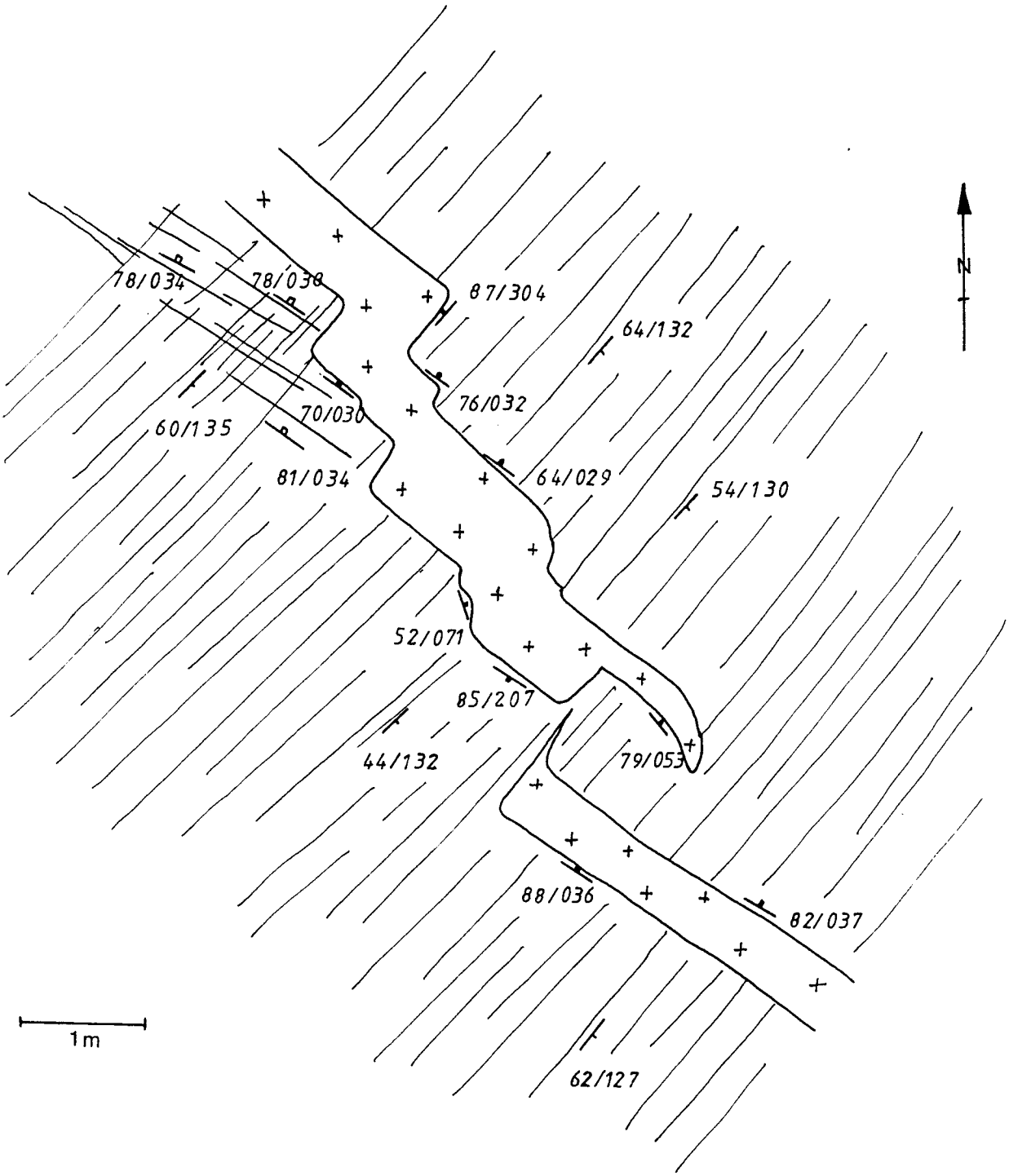
78/034
78/038
87/304
64/132
76/032
60/135
70/030
81/034
64/029
54/130
52/071
85/207
44/132
79/053
88/036
82/037
62/127
N
1m

Figure 6.6b.

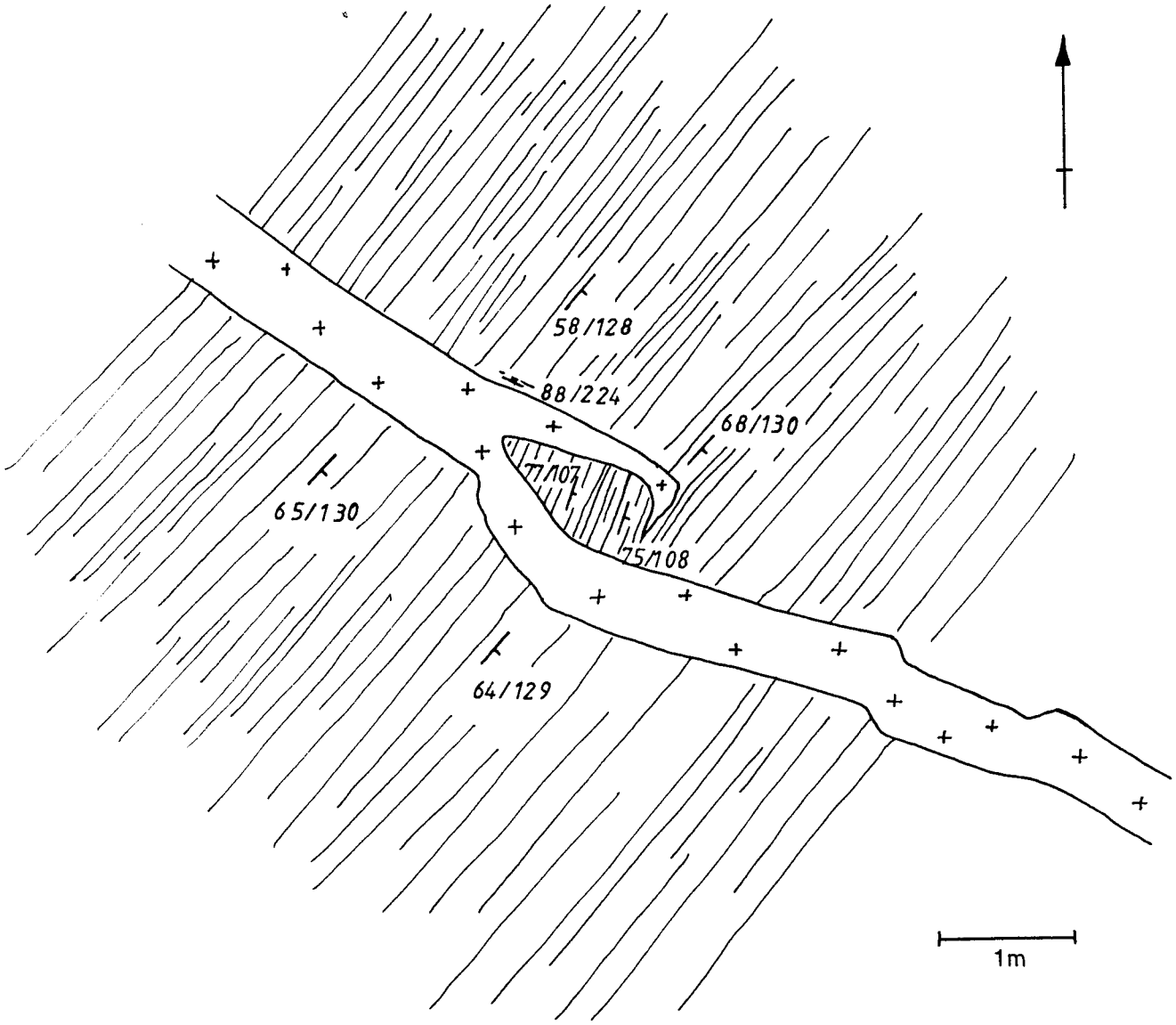

Figure 6.6c.

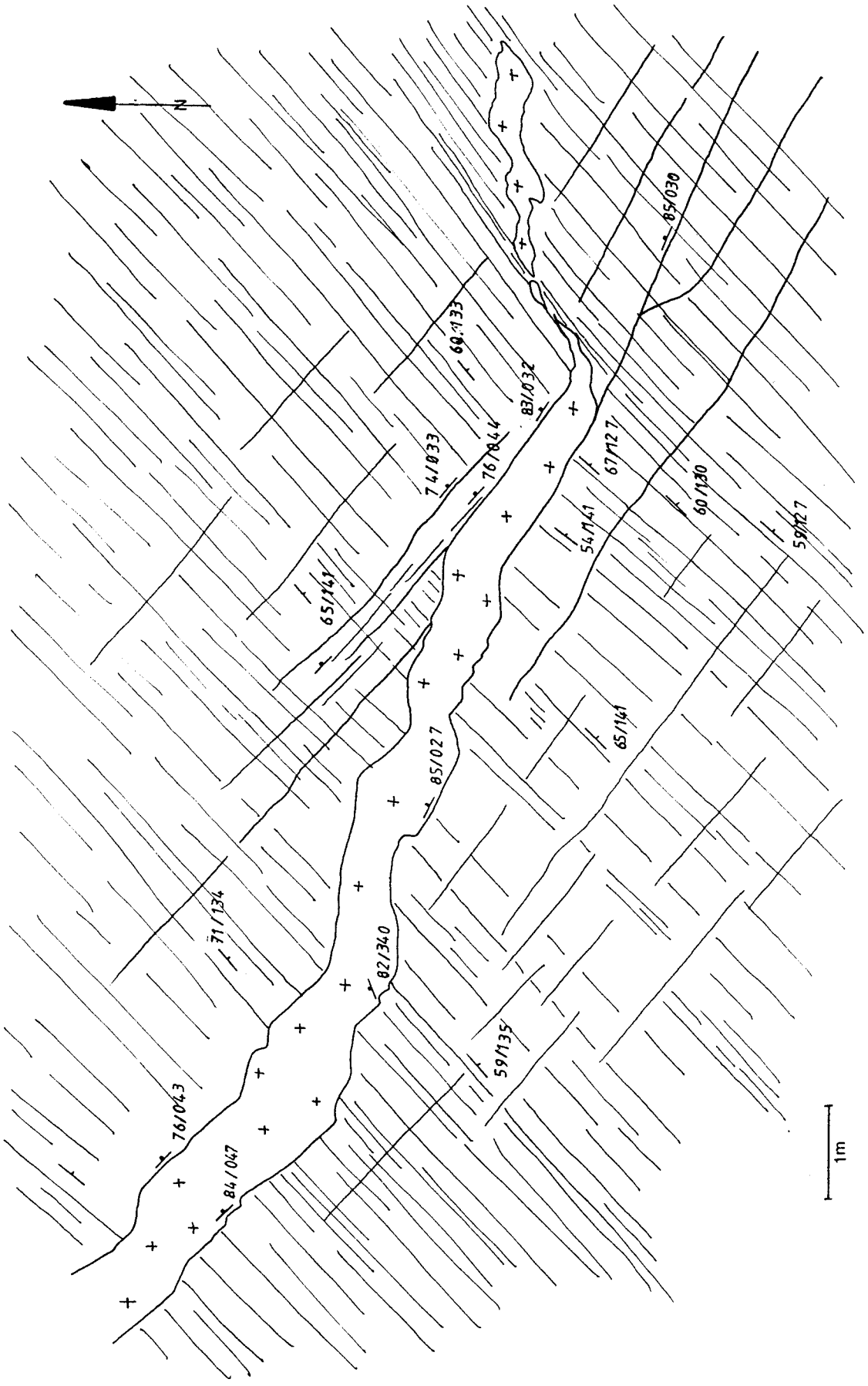
N
85/030
60/133
83/032
74/033
76/044
67/127
54/141
60/130
59/127
65/141
85/027
65/141
71/134
82/340
59/135
76/043
84/047
1m

Figure 6.6d.

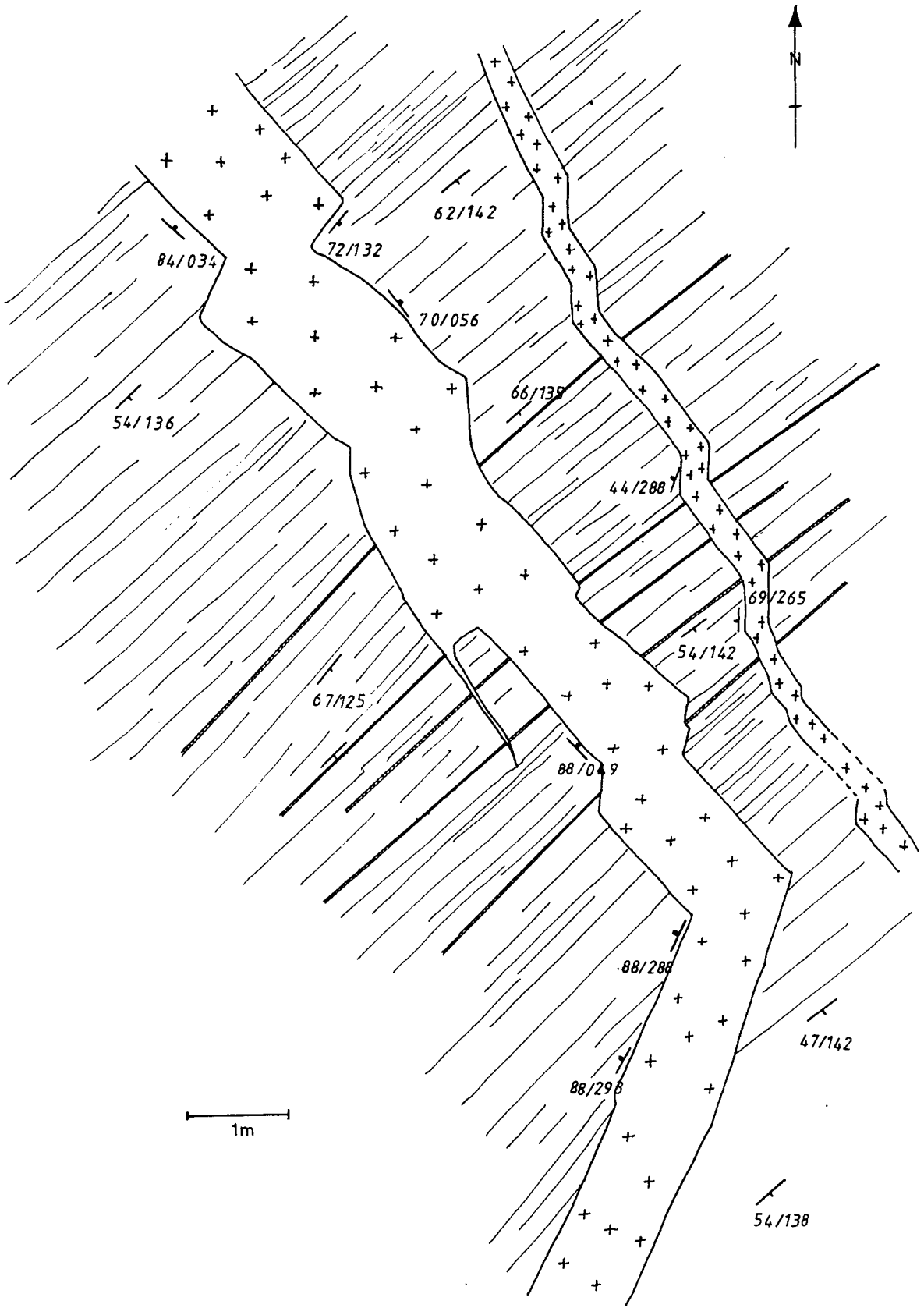
N
84/034
72/132
62/142
70/056
66/135
54/136
44/288
69/265
54/142
67/125
88/049
88/288
47/142
88/298
54/138
1m

Figure 6.6e.

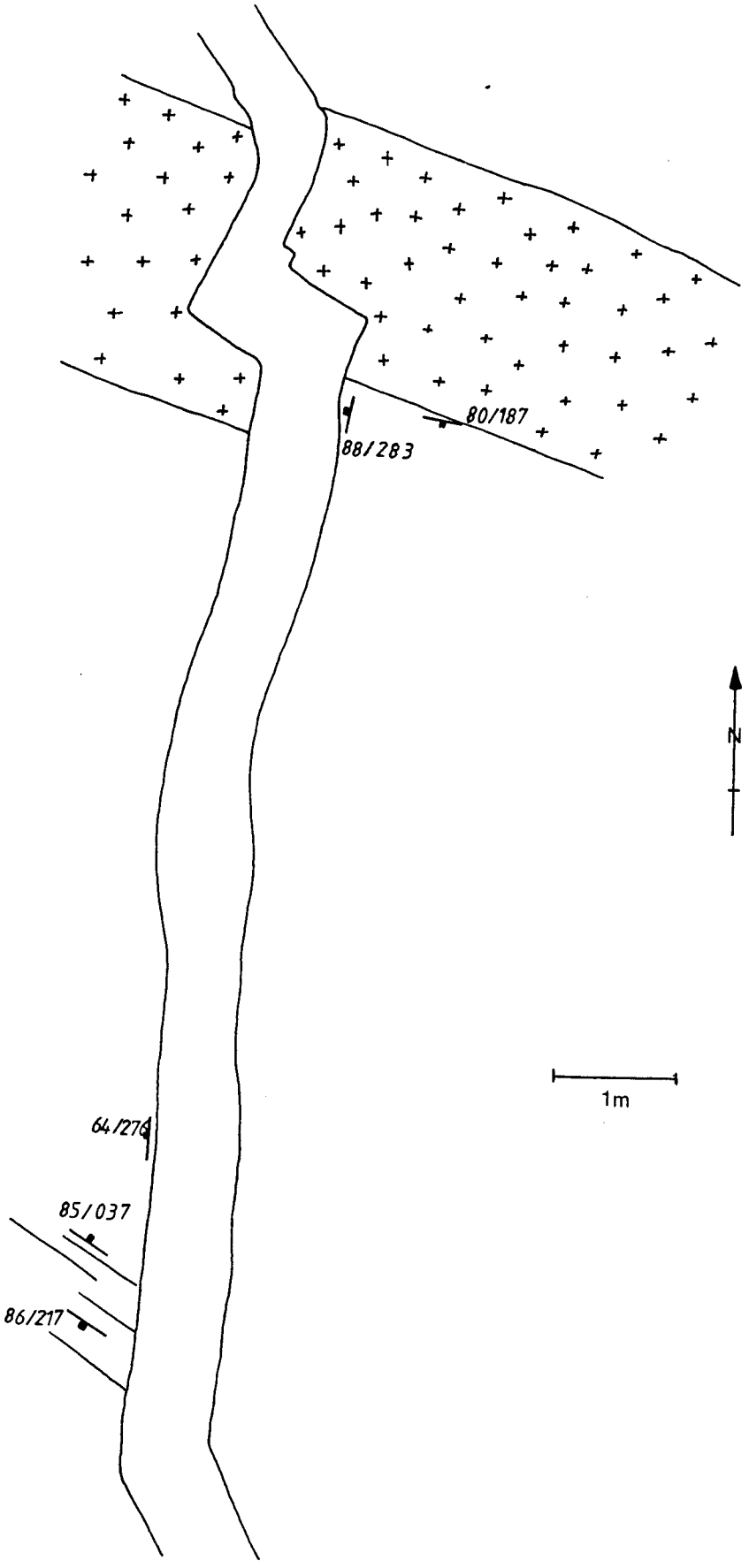

Figure 6.6f.

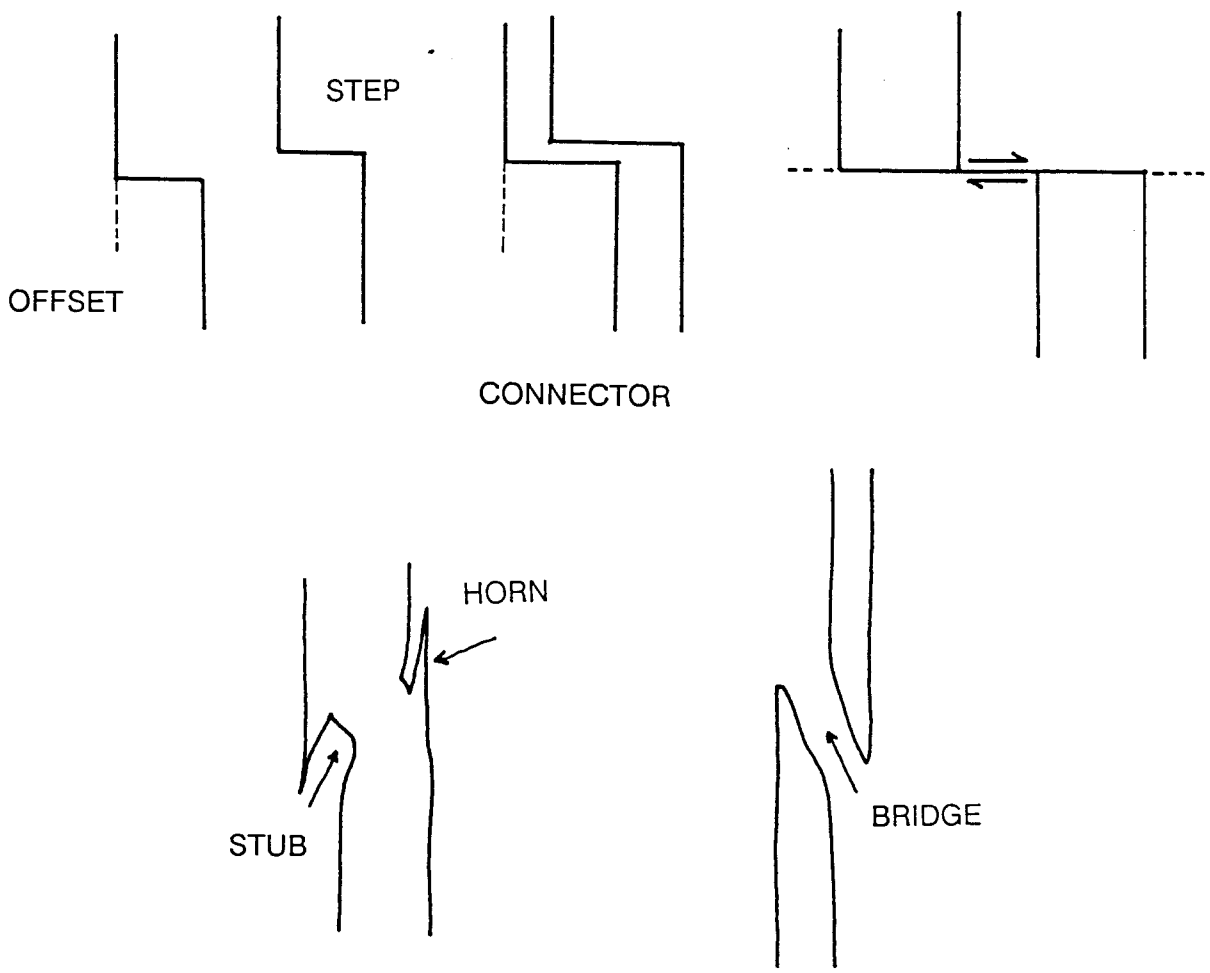

Figure 6.7. Schematic diagram of dyke morphology and the different types of dyke contact displacements.

of NW-SE (Fig.6.3c and 6.3d). Joints often occur in clusters that are strongly overlapping. Some of the joints terminate against, or are parallel to individual dykes. Figures 6.6b and 6d show situations where joints are subparallel to dyke margins and cases where joints terminate against dyke margins. The orientations of the dykes have a close correspondence with the jointing and the minor faults (Figs.6.3c and 3d). The mean dyke orientation is parallel to the major joint set (vector mean 132°). Slaty cleavage S_1 (Figs.6.3e and 3f) is generally at a high angle to the joints. Comparison of the dyke orientations with the joint and cleavage data show that the SW dyke maxima may correspond to jointing and the cluster in the NW sector with cleavage and bedding. Small scale N-S trending faults are present which predate dyke intrusion: two examples are included with the stereogram of poles to joints (Fig.6.3c).

6.5 MAGMA-FLOW AND FLOW INDICATORS

6.5.1 Flow lineations

Flow lineations are present at most of the dyke margins in association with a devitrified selvage and a chilled marginal zone which is usually fractured and platy with a range of thicknesses between 0.05-0.1m. The most common lineation comprises of aligned, elongated plagioclase phenocrysts which tend to be flattened within the dyke plane. Other flow structures include parallel, linear ridges and grooves (Fig.6.5d) which probably formed from the scour and erosion of more viscous magma near the chilled dyke contact by more fluid magma in the dyke interior. These flow lineations have a similar appearance to fault striations, and have orientations that are strongly influenced by the local dyke geometry. Roberts & Sanderson (1971) provide further description of the relationship between the flow lineation orientation and the dyke geometry.

The orientation of the flow lineation varies with the intrusive form of the dykes and its contact or association with local joint sets and the host-rock foliation. This is readily apparent from the example in Fig.6.5d which shows a dyke sidestepping along cleavage, the scour marks are subhorizontal in

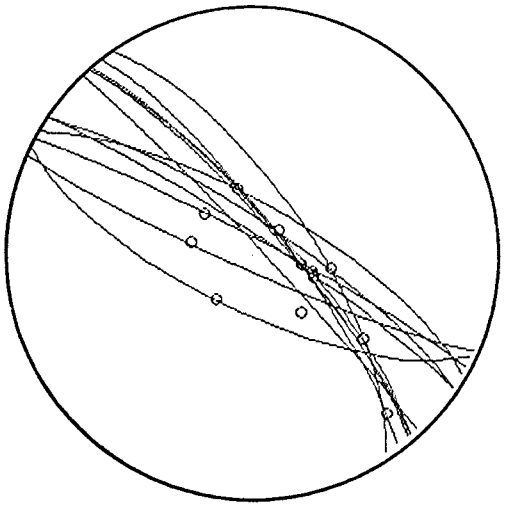

[a]

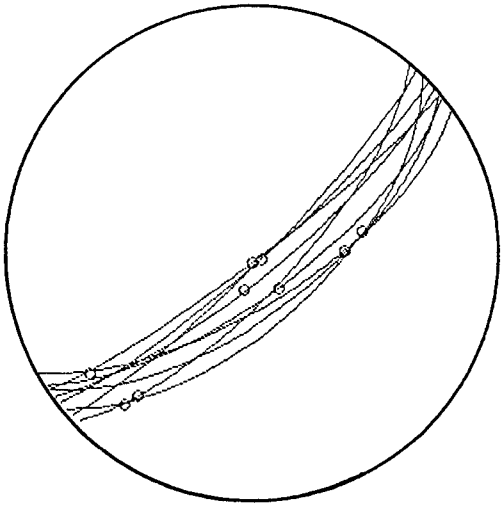

[b]

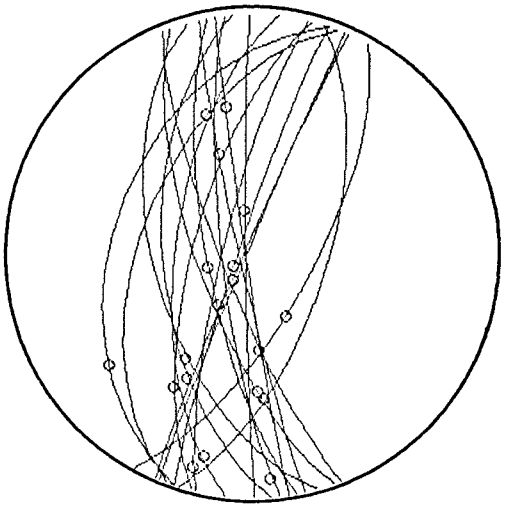

[c]

Figure 6.8. Flow lineations at dyke margins: [a] Set 1 (n = 9); [b] Set 2 (n = 12) and [c] Set 3 & 4 (n = 19).

the NE stepping segment and subvertical in the NW segment portion. Flow lineation data for the Easdale dykes are shown plotted in Fig.6.8 together with the great circle for each dyke contact.

The flow lineation data has been subdivided into groups to correspond with the subdivision of dyke margins shown in Fig.6.3a. The flow lineations for the first set (Fig.6.8a) are widely dispersed in a NW to SE plane and steeply inclined. In the second set (Fig.6.8b) the flow lineations are dispersed in a NE-SW plane. Many of the lineations in this group are shallowly inclined, with flow directed up to the NE. Figure 6.8c shows the flow lineations which correspond to Sets 3 and 4 for dyke orientation (Fig.6.3a). The flow lineations within this subgroup are widely dispersed in a N-S plane with variable plunges. Flow lineations from outcrops only a few metres apart, or from different portions of individual dykes show plunges of >90°. These observations imply that there were short range variations in magma flow directions, and that magma flow within dykes is irregular or undulating. Although, to determine the overall direction of magma flow for the Easdale dykes would require some prior knowledge of the magma source.

6.5.2 Magma solidification

Many of the Easdale dykes have a zoned structure with a systematic variation of phenocryst concentration across them. The wall-parallel zonation, which was described in some detail by Roberts & Sanderson (1971), comprises of a symmetrical alternation of accreted compositional bands or layers with a corresponding variation in grain size. For some dykes, these patterns of zonation are traceable along their exposed length. At irregularities and sidesteps in the margin of the dykes, the zonation generally parallels the wall-rock topography. In dyke sidesteps, the textural zonation curves and often displays gentle folds.

The interpretation of these types of dyke zonation can be attributed to two main processes: [1] wall accretion and [2] flow differentiation. Theoretical studies of magma flow and solidification (Delaney & Pollard 1982, Bruce & Huppert 1990) suggest that magma accretion on dyke walls can occur during both continuous and intermittent magma flow. The rate of accretion is dependent on several factors,

principally the dyke width and the magma flow rate. Textural zonation produced by magma flow differentiation, may be due to particles within a magma, migrating from the dyke margin as a result of hydrodynamic forces. Komar (1972) suggested that particle dispersive pressure (the Bagnold effect) could produce axial phenocryst concentrations within dykes. However, magma accretion at dyke margins while the dyke interiors are occupied by flowing magma suggests that many phenocryst distributions within dykes need not reflect hydrodynamic controlled flow differentiation processes.

For the Easdale dykes the compositional layering, and its continuity with irregularities and sidesteps, suggests that the central portions of the dykes were still fluid or plastic, when the marginal contact zones were solidified. The compositional variations in the dyke zonation patterns are successively dominated towards dyke centres by plagioclase and olivine. This feature is consistent with phase layering, and suggests there was a decrease in the degree of supercooling towards the dyke centres. There is some evidence for limited lateral flow of magma in the form of the subhorizontal oriented flow scour marks. It is unlikely that these dykes have resulted from regional lateral injection, since the dykes are relatively narrow and they would have been subject to rapid chilling and been incapable of extensive magma flow. Direct application of the model of Delaney & Pollard (1982) to the Easdale examples, implies that for dykes with chilled marginal zones of ≈0.1m thickness, and widths of <1m, magma flow would persist only for 3-18 hours before solidification.

6.5.3 Magma flow

Prior to solidification, dykes serve as conduits for the flow and transport of magma through the crust. If magma flow within a dyke is approximately laminar, the mean fluid velocity would be related to the magmatic pressure gradient and the driving stress (Emerman *et al.* 1986, Bruce & Huppert 1990). Following the model of Delaney & Pollard (1982), by idealising a dyke as a channel between rigid, parallel walls, solutions for laminar flow illustrate the dependence of volumetric flow rate, W, on dynamic viscosity μ, driving stress gradient $\Delta P/L$ and channel half-thickness $T/2$ where

$$W \propto \frac{\Delta P}{\mu L}(T/2)^3 \qquad (6.1)$$

This approximation is valid when the Reynolds number, *Re*, is $<10^3$, where

$$Re \propto V(\rho/\mu)(T/2) \qquad (6.2)$$

when V is the maximum flow velocity and ρ is the fluid viscosity. The Reynolds number, *Re*, is a ratio of the inertial viscous forces applied to the magma. For a constant pressure gradient *Re* and W vary with the cube of channel thickness, expressed by

$$Re \propto W \propto (T/2)^3 \qquad (6.3)$$

The Reynolds number can be estimated from field measurements of dyke thicknesses and by substitution of appropriate values for the other parameters into equation (6.2). Velocities of dyke propagation and hence estimates of magma flow velocity at depth, have been inferred from seismic and geodetic observations of rates of lateral dyke intrusion in active rift zones. For Kilauea, Hawaii and Krafla, Iceland these rates are in the range 0.1-1.0ms^{-1} with an average of 0.5ms^{-1} (Jackson *et al.* 1975, Delaney 1987). For a non-vesiculating basic magma (*ie.* no vapour phase) of average composition at temperatures of 1100-1200°C, a typical fluid density would be of the order of 2.6g/cm^3 (Bottinga & Weill 1970). A viscosity of 100 *Pa·s* is typical for a basic magma at 1100-1200°C (Spence & Turcotte 1985, Bruce & Huppert 1990). Using a dyke thickness of 0.5m for Easdale (Fig.6.2a) and substituting values of V = 0.5 ms^{-1}, and μ = 100 *Pa·s* into equation (6.2) yields a value of *Re* ≈3.25. Taking an average thickness of 1.5m for the whole Mull dyke swarm (Richey 1939) and using the previous values gives a Reynolds number of ≈ 9.75. Both of these values are well within the range for laminar flow, as the transition from laminar to turbulent flow for fluid flow in a channel between widely spaced parallel plane walls generally occurs at *Re* > ≈1000. For *Re* <1000 fluid flow is laminar. These values are for fluids of a wide range of viscosities (Massey 1975). An additional factor that may influence magma flow is the topography and roughness of the dyke wall surfaces. In some

situations slight roughness of the fracture walls may reduce frictional resistance, and suppress the transition to turbulent fluid flow. To produce turbulent flow within the Easdale dykes, the magma flow rates would have to be at least 2 orders of magnitude higher than the values used here. This condition is unlikely to be met, given that the maximum magma flow rates recorded for drainback during eruptions at Kilauea, Hawaii seldom exceeded $\approx 500 m^3/s$ (*eg.*Richter *et al.* 1970).

6.6 DYKE FORM AND DYKE OPENING DIRECTIONS

Detailed mapping was carried out to investigate the relationship of dyke opening directions and intrusive form to the remote least compressive stress. Field observations of dyke contacts show that matching pairs of angular offsets across opposed dyke contacts are common (Currie & Ferguson 1970, Pollard *et al.* 1975, Figs.6.6a-f). Currie & Ferguson (1970) have considered that lateral magma flow along dilatant en echelon cracks was responsible for the formation of pairs of offsets, and Nicholson & Pollard (1985) have described steps in dyke contacts that form through the linkage of en echelon cracks. These observations suggest that magma injection along fractures which are oblique to the main dyke trend, will result in the formation of an offset, and an offset plane (Busseli 1989). The intersection of this offset plane with the main dyke will produce two offset edges. Pairs of matching offset edges formed in this way, can be used to determine the dyke opening direction in plan view (Fig.6.9), and its three-dimensional orientation (Fig.6.10). Bussell (1989) and Kretz (1991) provide graphic and numerical solutions to the dyke dilation problem, using offset criteria and displaced wall-rock markers.

The presence of sidestepping dykes at Easdale allows analysis of the opening direction because opposing sectors can be matched across dyke contacts. This opening direction will only be valid where finite dilation has occurred in a horizontal plane. To verify this, the net dyke dilation direction was determined from offsets using Busseil's (1989) graphic solution. These opening directions were checked for consistency from piercing-point solutions for pre-existing veins within the host-rock.

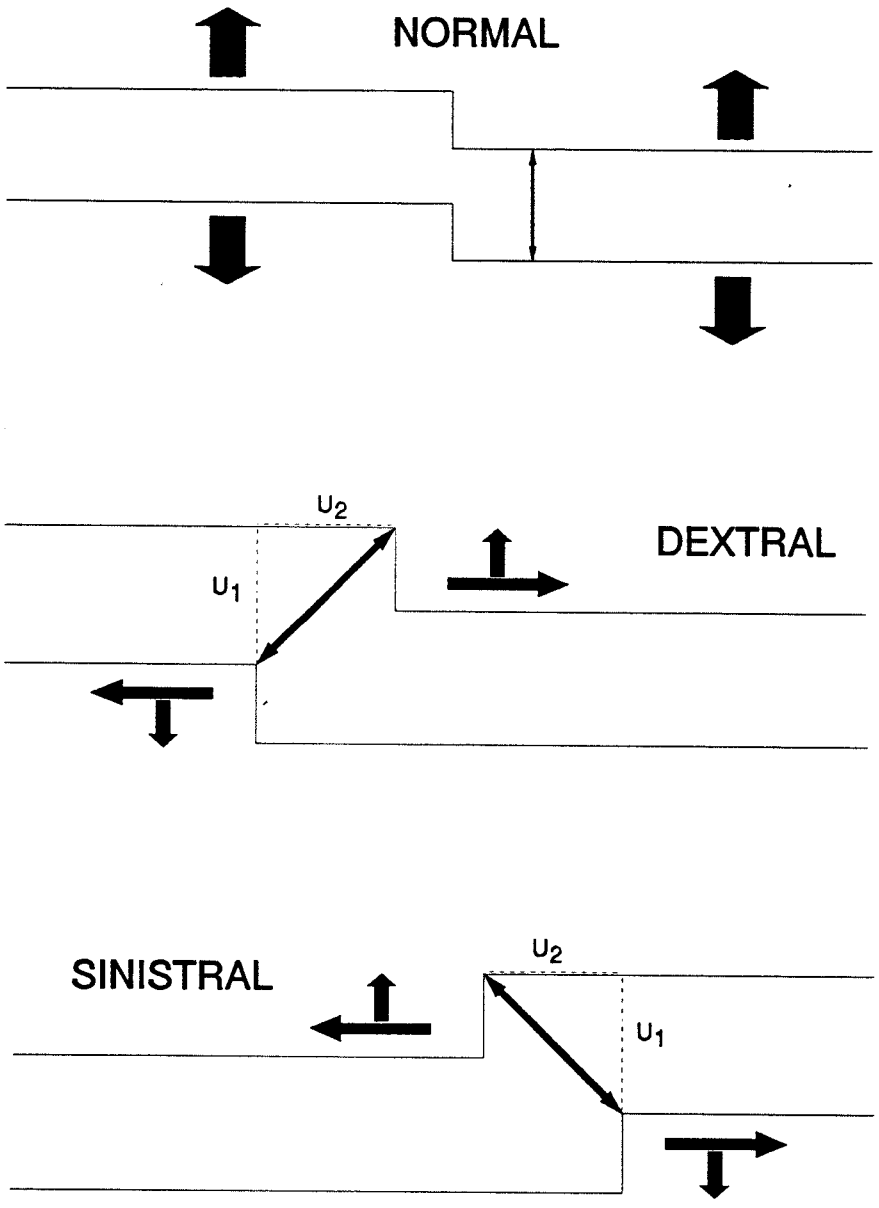

Figure 6.9. Measurement of the opening direction and opening angle from wall-rock markers for sidestepping dykes.

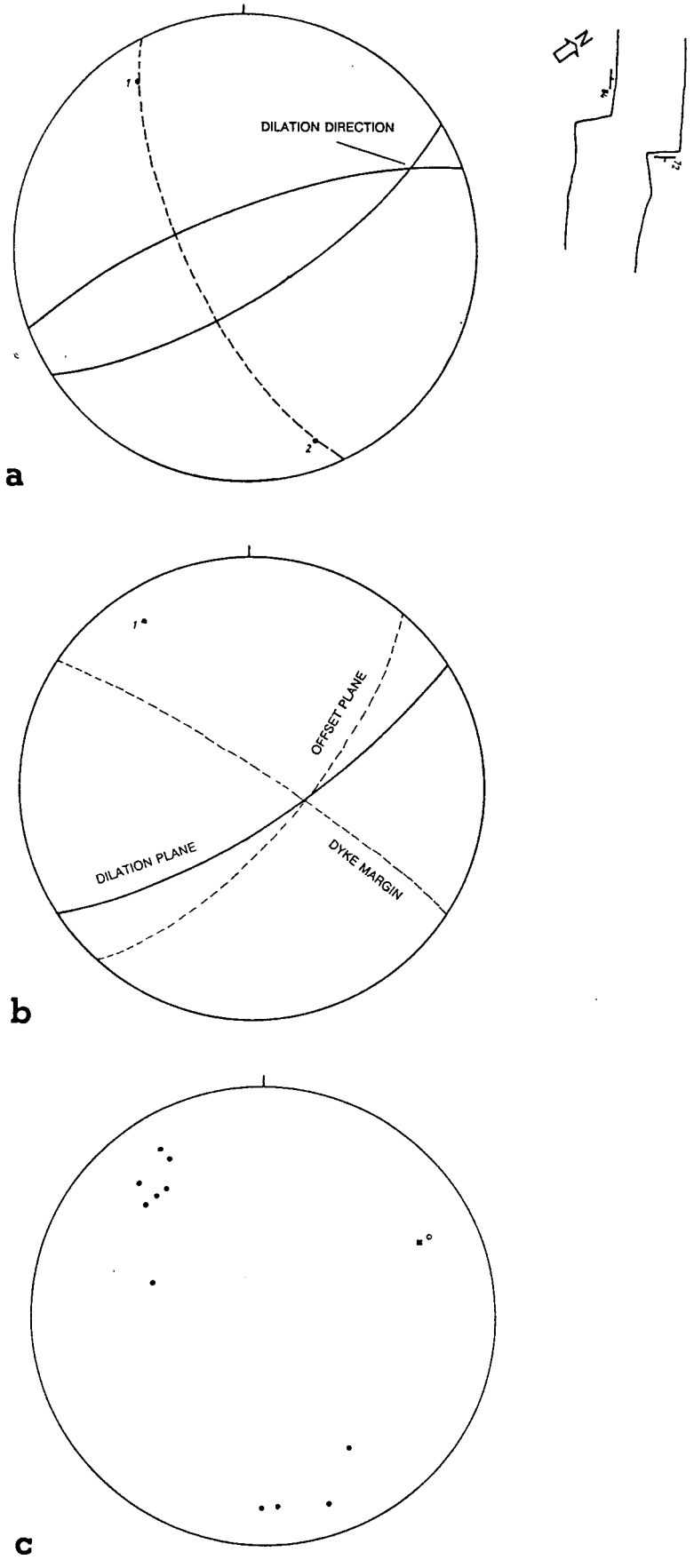

Figure 6.10. Determination of the net dilation direction using pairs of dyke offset edges and displacement of pre-existing wall-rock markers, based on the method of Bussell (1989)(See text for explanation). Note that the opening directions are subhorizontal and gently inclined.

Figure 6.10a shows an example of how the dilation plane has been determined, using a single pair of offsets from the dyke shown in Fig.6.6e. In Fig.6.10b a second offset edge and its dilation plane are shown. The dyke dilation direction is determined from the intersection of these two dilation planes, or from the pole to the great circle which most closely fits the distribution of poles to dilation planes (Fig.6.10b). In this example the dyke dilation direction plunges at a shallow angle towards 062°. An additional example of dyke dilation poles and directions determined using pairs of offsets and wall-rock markers is shown in Fig.6.10c. These examples indicate that at Easdale shallow-plunging opening directions predominate. These values are very similar to measurements of dyke opening direction made in horizontal sections.

Figure 6.11a shows the frequency distribution of dyke opening directions with a mean of 056.7°N; this can be compared with the range of dyke margin orientations shown in Fig.6.11b. The vector mean for dyke orientation (145.2°) is approximately 90° to the mean opening direction. However, the orientation of individual dykes is much more variable whereas dyke opening directions are more consistent. This can be observed by comparing the maps for two dykes (Fig.6.6a and 6d) that have different orientations. Although one dyke trends nearly NW-SE (Fig.6.6a) and the other nearly N-S (Fig.6.5d) their opening directions are essentially the same (045°). These 2D and 3D determinations of dyke dilation direction, for dykes of differing trend, indicate that they share a common opening direction.

Figure 6.12 shows scatter plots of dyke opening direction against segment azimuth (Fig.6.12a) and for average dyke orientation (Fig.6.12b). These plots show the spatial distribution of opening directions for dextral and sinistral sidestepping dykes and the consistency of opening direction for individual dykes. Roberts & Sanderson (1971) used the Fisher-Behrens test to compare the variances between these dextral and sinistral stepping dykes. Their results suggested that the dextral sidestepping dykes have more consistent opening directions than the sinistral sidestepping dykes.

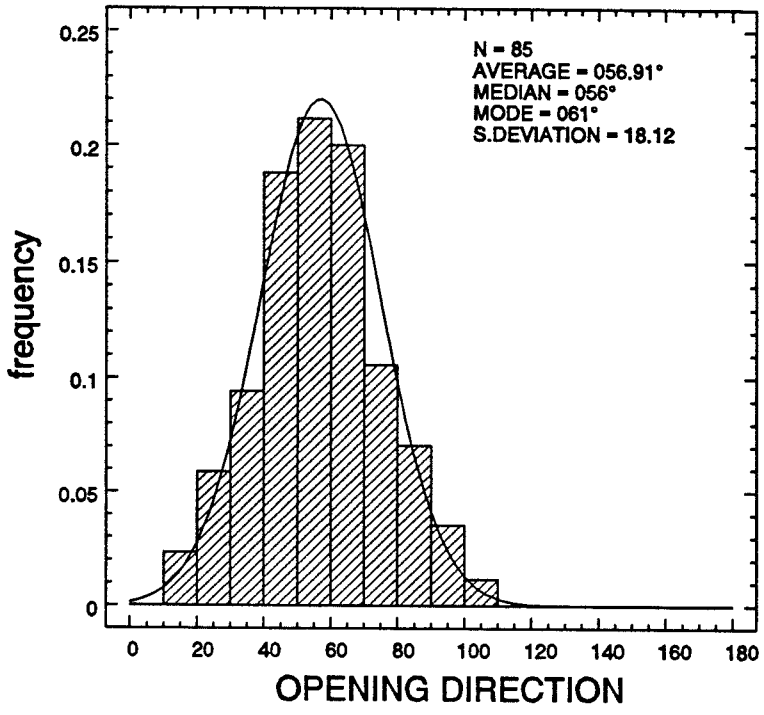

[a]

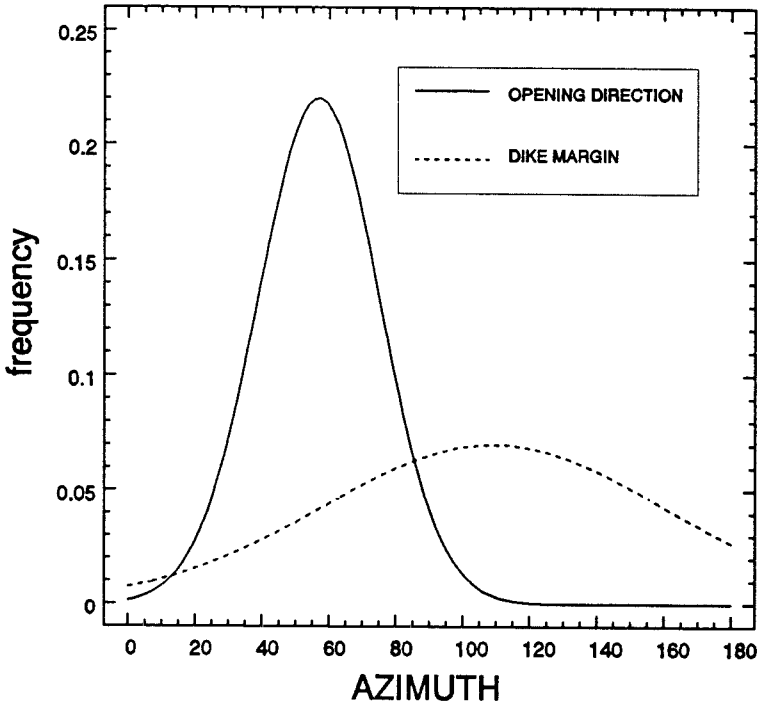

[b]

Figure 6.11. [a] Frequency histogram of opening directions of Easdale dykes, and [b] comparison of frequency distributions of opening directions and dyke margin orientations.

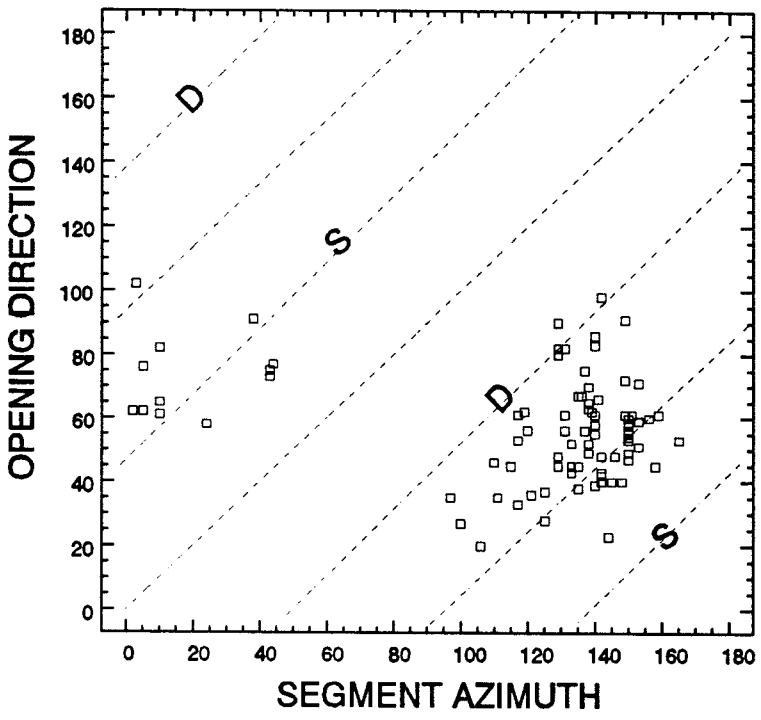

[a]

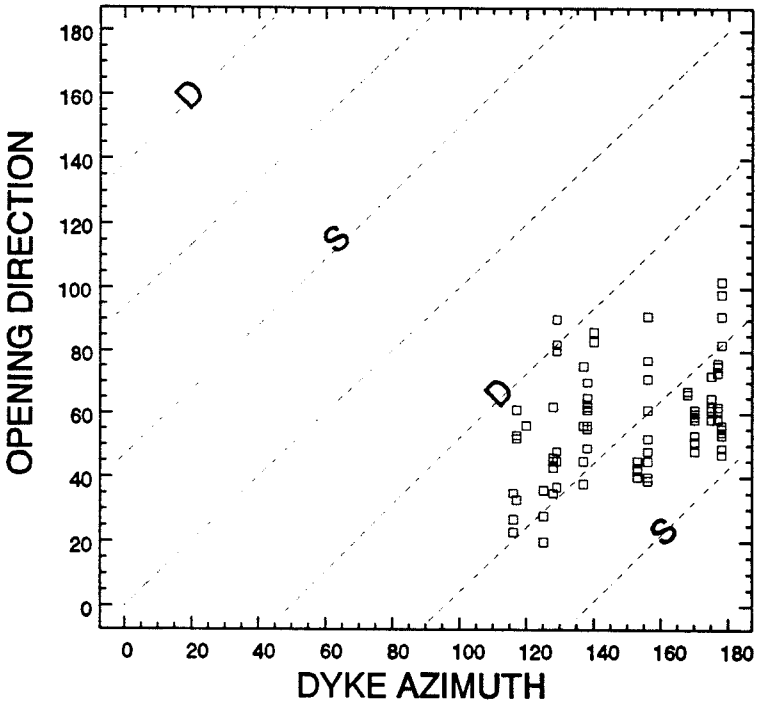

[b]

Figure 6.12. [a] Scatter plots of opening directions against segment orientation of dykes, and [b] scatter plots of opening directions against overall orientation of dykes.

6.7 DYKE DILATION

6.7.1 Magma pressure and tectonic stress

For magma-driven crack propagation, a dyke will propagate in a plane normal to the least compressive stress. For magma to invade pre-existing fractures, magma pressure must exceed the normal component of remote stress resolved on that fracture surface; although the principal stress need not be orthogonal to pre-existing fractures.

Timing relations between joints and dykes at Easdale

Despite the controversy as to what criteria are necessary to distinguish between dykes injected along pre-existing fractures (Delaney & Pollard 1981, Delaney *et al.* 1986) and magma-driven dyke propagation (Spence & Turcotte 1985, Turcotte *et al.* 1987, Lister & Kerr 1990,1991) a number of criteria can be established for the Easdale dykes. The dykes utilise cleavage as they sidestep between different fracture trends. The cleavage clearly predates dyke intrusion so the only unknown is the timing of the joints and fractures which are parallel to, or terminate against the dyke margins. Several observations indicate that joints immediately adjacent to the dykes predate dyke intrusion. At several locations the dykes have invaded along joint surfaces. Figure 6.6d shows an example of a dyke with an irregular and stepped margin, where at one of the steps the dyke follows the trace of a joint. This example indicates that at least some magma invaded joints, and dilated them to produce dykes. Dyke-parallel joints are associated with several dykes at Easdale (eg. Figs.6.4b and 6.4d), with the frequency of these joints decreasing with distance from the dyke margins. These observations suggest that some dykes may have propagated along pre-existing joints, while some of the joint clusters adjacent to the dyke margins were produced during dyke intrusion. The dyke splay and the series of offset segments near the termination of the dyke shown in Fig.6.6d, suggests that these fractures were not perpendicular to the least compressive stress at the time of dyke intrusion. In this particular example some of the joints terminate against the dyke margin; this provides further support for the assertion that joints of this set were formed prior to intrusion.

If pre-existing fractures are utilised during dyke emplacement, using stress analysis it is possible to derive the conditions necessary for the dilation of these pre-existing fractures. Delaney *et al.* (1986) provided a model for this type of analysis by considering the conditions necessary for dyke opening.

The initial conditions for dyke opening can be expressed in terms of the stress ratio R as a function of α and the ratio of the shear to dilational displacements at the dyke contact, u_2/u_1 (Figs.6.9 and 6.13a) when

$$\frac{u_2}{u_1} = \frac{\tau}{\sigma_n + P_m} = \frac{\sin 2\alpha}{R + \cos 2\alpha} \qquad (6.4)$$

Since $\tan A = u_2/u_1$

$$\tan A = \frac{\sin 2\alpha}{R + \cos 2\alpha} \qquad (6.5)$$

These expressions are similar to those used for the analysis of en echelon veins; they link the opening geometry of dykes (A) to the orientation of the principal stresses (α) and the stress ratio R.

Resolving the normal stress (σ_n) in terms of the principal stresses and the angle, α, (Delaney *et al.* 1986) yields

$$\frac{(P_m - S_H) + (P_m - S_h)}{S_H - S_h} = R > -\cos 2\alpha \qquad (6.6)$$

when S_H and S_h are the maximum and least compressive horizontal stresses respectively, and P_m is the magma pressure. Equation (6.6) then allows the definition of specific fields on a graph of the stress ratio R against angle α (Fig.6.13b):

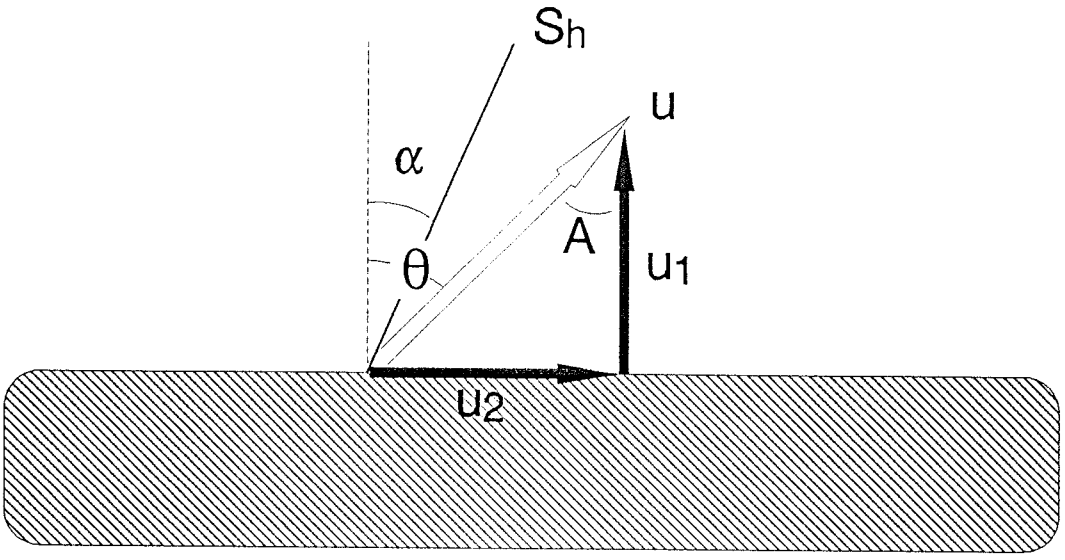

[a]

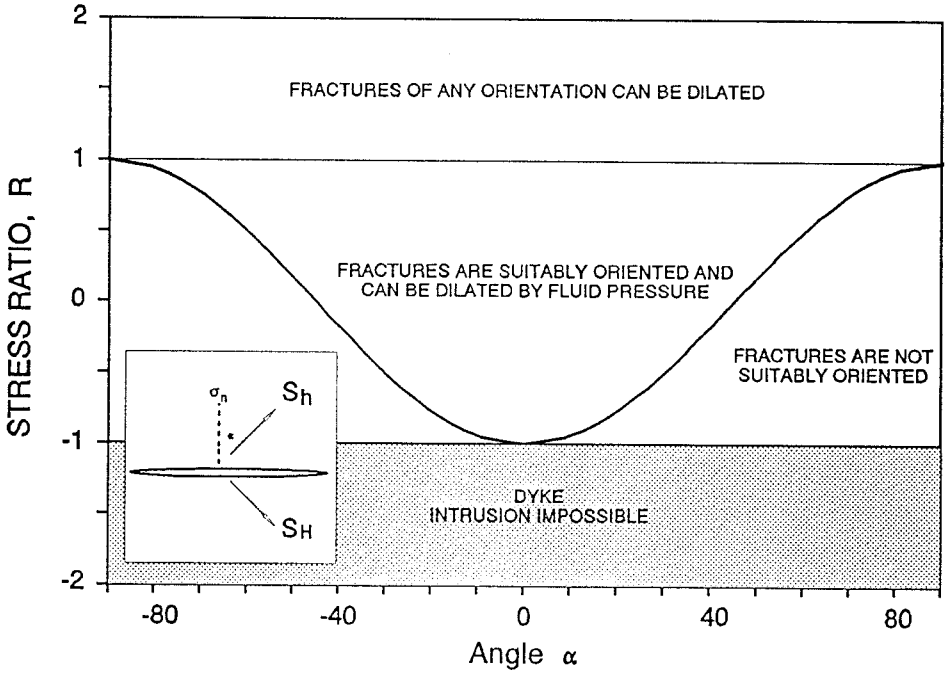

[b]

Figure 6.13. [a] Sketch defining stresses and contact displacements used at the dyke wall. [b] Stress ratio R as a function of the angle α and the direction of least principal stress (based on Delaney et al. 1986, fig.13).

[1] Where R is <-1, the magma pressure is lower than the least compressive remote stress (σ_2, S_h), so it is insufficient to open or dilate a fracture of any orientation.

[2] For R >1 magma pressure is higher than the maximum compressive remote stress (σ_1, S_H) and hence is able to open any vertical fracture.

[3] where -1 <R <1, there are two further fields [i] R >cos 2α where fluid pressure is able to open suitably oriented fracture and [ii] R <cos 2α where fluid pressure is insufficient to open the existing fracture.

6.7.2 Dyke dilation and the stress ratio *R*

The dyke which have been mapped around Easdale (Fig.6.6) and their relations with cleavage and jointing indicate that a range of fracture directions have been opened. For individual dykes the opening directions are relatively consistent. To test the idea that oblique opening is a function of dyke orientation, field measurements of dyke opening displacements (*A*) can be plotted on a graph of the stress ratio R as a function of α and A. Figure 6.14 shows an example of this analysis applied to a dyke with relatively constant opening directions (Fig.6.6a). This example indicates R values of between 1 and 0.5, suggesting that magma pressure was sufficiently high to dilate suitably oriented fractures.

6.8 CONCLUSIONS

Analysis of the field relations of these dykes and their opening directions with respect to remote tectonic stress and internal magma pressure indicates that useful insights into the fracture opening mechanisms and loading conditions at the time of dyke intrusion can be gained. The following general conclusions have been reached:

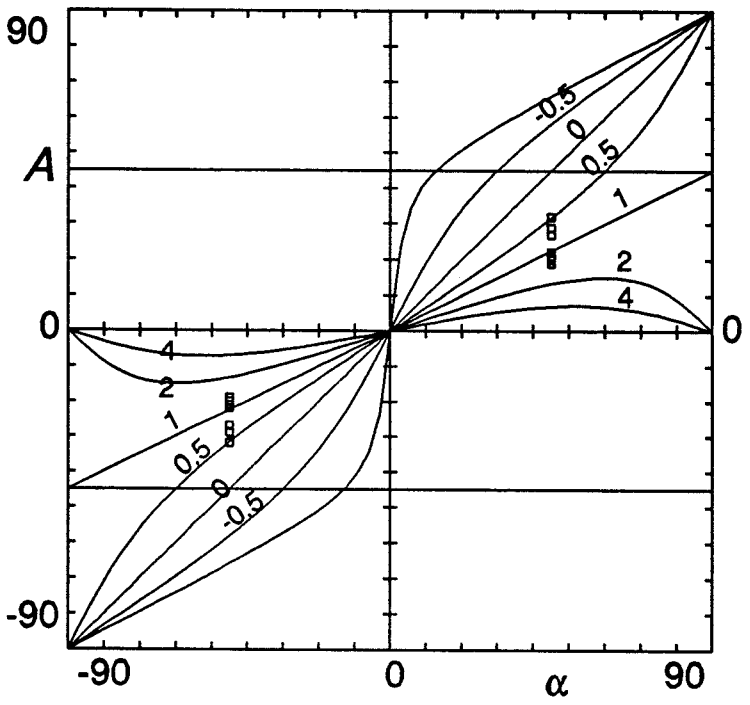

Figure 6.14. Dyke contact displacements (A) against α on a graph of the stress ratio, R.

[1] Dykes are rarely simple planar fractures, they often display small scale irregularities and structures such as sidesteps and horns. These structures can be used to determine dilation or opening directions, provided sufficient three-dimensional exposure exists.

[2] The flow history of dykes can be investigated by examination of internal structures and from the analysis of flow lineations adjacent to dyke walls. Field observations of the structure of the chilled margins, flow lineations, and the textural zonation, suggest that the magma solidified on the dyke walls as it continued to flow in the interior of the dyke, *ie.* inward growth of accreted material. The lack of obvious contact metamorphism effects in the host-rock suggests a short duration of heat transfer, and a small increase in wall-rock temperature, prior to magma solidification. Further observations of the features dependent on temperature distribution across dykes (*eg.* variation in chilled margin widths and contacts, phenocryst distribution) could allow more effective tests and comparison with theoretical models of heat transfer and magma flow during dyke intrusion.

[3] From measurements of dyke thicknesses, combined with estimates of magma flow rates, some inferences about magma flow conditions and factors that influence them can be made. Idealising the dykes as rigid, parallel-walled channels, yields estimates of Reynolds numbers (*Re)* in the range ≈3-10. These are well within the regime for laminar flow where the transition to turbulent flow is generally at $Re > 10^3$.

[4] Determination of 2D and 3D opening directions of dykes, suggest that sub-horizontal opening directions predominate. Comparing these opening directions with examples of dykes of differing trend indicates that the Easdale dykes share a common and consistent opening direction, trending N 057° E. Although the mean dyke trend is normal to their opening direction, individual dykes may be oblique to the mean, and these dykes open obliquely, *ie.* the opening direction is N 057° E.

[5] The stress ratio, *R*, for individual dykes at Easdale is ≈1 (ranges 0.5 to 1). This implies a constant opening direction and suggests that loading conditions were locally transtensional. Analysis of the Easdale dykes can be used to indicate the relative magnitudes of the remote principal stresses and

magma pressure. Some of the dykes were emplaced oblique to the regional extension direction, so magma pressure was only able to dilate fractures with suitable orientations.

[6] Previous methods of determining paleostress from dyke orientation alone are unreliable as they imply a simplistic view of the loading conditions at the time of intrusion.

CONCLUSIONS

Vein formation in the Culm Basin, SW England (Chapter 2)

[1] There are a number of recognisable geometric forms for the veins. These include: [a] single, overlapping and coplanar clusters of veins; [b] single, planar veins with kinked and curved terminations or single veins ornamented with pinnates and pressure solution structures; [c] veins with branched and forked terminations; and [d] veins in en echelon and conjugate en echelon arrays.

[2] At Millook Haven and for other localities in the Crackington Formation, there are a variety of vein geometries which have formed during essentially a single episode of progressive deformation. The type of geometry developed is partly dependent on the initial vein orientation with respect to the remote stress.

[3] The spatial distributions of veins and the type of geometry developed are mainly controlled by the bed thickness and the host-rock material properties. Other factors include local irregularities in the bedform geometry such as load casts and ripple marks.

[4] The infill textures and growth habits of veins are extremely variable. Many infills indicate composite growth histories, comprising of both fibrous morphologies and more equant habits; which involve both antitaxial and syntaxial crack-seal processes as well as growth in a free-fluid.

[5] The analysis of the geometry and kinematics of the veins, and their relations to fold development at Millook Haven and elsewhere in the Culm Basin show the following general features:

[a] Some veins initiated prior to folding, and were probably associated with episodes of layer-parallel shortening accompanying fold initiation and propagation. The veins are essentially compression-parallel structures.

[b] The principal stresses are oblique to the fold-axes because prior to folding the inferred maximum principal stress, σ_1 was directed NW-SE. This orientation was maintained through main fold amplification and during subsequent flattening.

[c] During folding, the early vein sets were modified due to a combination of mechanical crack interaction and the subsequent loading and opening effects as the fold limbs were rotated relative to the principal stresses. Complex cross-cutting and vein intersection relations were generated in the inverted fold limbs; although normal fold limbs have a simpler deformation history as they were subject to less stress re-orientation, by maintaining a relatively constant attitude in fold development. These phases of vein development can then in turn be related to a rotational deformation model.

[6] Structural relations between vein development and folding in the Culm Basin are consistent with an overall pre- and syn-fold E-W dextral transpression. This transpression may be generated by the oblique convergence and consequent inversion, produced by the interaction between regional Variscan thrust transport (NNW) and an approximately E-W trending basin margin.

Geometries and mechanics of veins (Chapter 3)

Detailed observations and measurements of vein profiles and their terminations yields important information about processes of vein formation. Examination of the displacements across veins and vein arrays provides useful observational links between theoretical and experimental investigations of vein initiation and growth. From these results we can verify hypotheses about the stress states and the host-rock response implied by some vein traces. General conclusions which emerge from this study are summarised:

[1] Veins initially propagate as essentially mode I elastic cracks. The geometry of their propagation path (*eg.* branches, tail-cracks) can be used to infer paleostress trajectories and to monitor changes in loading conditions.

[2] Vein initiation and growth kinematics can be described in terms of selective mechanical interaction. This can lead to the formation of en echelon and conjugate en echelon vein sets which have a wide range of vein-array angles and separation values.

[3] The variation of vein length and aspect ratio can be understood mechanically by considering the elastic interaction which occurs between closely spaced veins. Since the crack extension force varies linearly with crack length. and there is nearly an order of magnitude of variation for vein aspect ratio, this assumption implies a similar range of $(\sigma'_{11} - P_f)$ values.

[4] Displacement-distance (d-x) analysis plots for isolated veins (mode I fractures) display approximate conical displacement profiles. The scatter in the data is consistent with similar observations made for fault slip (modes II and III), suggesting that single event elastic crack models do not adequately describe vein shape and that cumulative slip models of the type discussed by Walsh & Watterson (1987) and Peacock & Sanderson (1991) for faults may be more appropriate.

[5] Different stages of vein initiation and growth during the interaction, coalescence and fusion of cracks can be identified from vein d-x profiles. Where crack overlap is low the graphs are characterised by data plotting above the conical profile. When complete linkage has occurred, a single, composite vein is formed. Bridges play an important role in accommodating crack dilation by maintaining displacement continuity across the array.

Vein thickness and spacing in layered rock (Chapter 4)

Vein thickness distributions and spacing in layered sedimentary rocks depend in part on the type of arrest mechanism that may constrain vein propagation to single layers (eg. layer thickness, contrasting material properties) and on the mechanical interaction that may occur between neighbouring veins, and veins in adjacent layers. The following conclusions are apparent from this study:

[1] Negative exponential and power-law distributions are the most appropriate models to explain the range of vein thickness and spacing values.

[2] Vein thickness at Millook Haven has lower and upper values of <0.2 and 230mm. For the most well constrained line samples, vein thickness is characterised by low *D* values of 0.6, over two orders of magnitude.

[3] Vein spacing at Millook Haven ranges from <0.008 to 3.2m within a range of layer thicknesses of 0.13-1.1m with the best constrained line traverses yielding *D* values of 0.5-0.7 over 1.5-2 orders of magnitude.

[4] Although some vein populations may be adequately described by power-law distributions, many show distinct changes in graphs of logN(t) against log(t). These are not sampling artifacts, but represent a real decrease in maximum vein thickness or spacing values, which can be attributed to propagation of veins through the entire layer thickness.

[5] Estimates of extension accommodated by the veins indicate that most of the extension is taken up in large veins. Veins of >10mm thickness generally represent 60-90% of the total extension calculated for individual line samples.

[6] There is no simple linear relationship between vein spacing values and bed thickness. Vein growth behaviour and spacing within individual and adjacent layers is likely to be effected by fracture-induced stresses produced by mechanical interaction amongst overlapping and closely spaced veins.

Transtensional modelling of en echelon vein arrays (Chapter 5)

[1] En echelon vein arrays have a variety of geometries with veins that form at ω values of 5-55° to the array. This suggests that transtensional and transpressional deformation may be more important in their development than simple shear.

[2] Determination of relative wall-rock displacements across vein arrays, supported by bridge and mineral fibre geometry, suggests transtensional-transpressional deformation is more applicable in many cases. The models explains the full range of ω values, indicating that there is a spectrum of vein geometries which can be directly related to wall-rock displacement.

[3] Veins in en echelon arrays are generally mode I cracks; oriented with respect to the local (rotated) stress field in a zone of transtension or transpression. This suggests the propagation path of veins in en echelon arrays is consistent with minimising the effects of the stress intensity factor, K_{II}.

[4] Data collected for conjugate vein arrays indicate that acute dihedral angles contain σ_1 for both transtensional and transpressional conjugate sets. Additionally, while σ_1 is contained in the acute dihedron it need not be parallel to the bisector of the conjugate array. The Type I and II classes (Beach 1975) are not genetically different, as both types are formed by extension (mode I) fractures in transtensional arrays, and, hence the classification is not appropriate.

[5] The stress ratio, R plays a significant role in effecting the geometry and mechanics of en echelon veins. For conjugate en echelon vein arrays when $R = 0$ this produces veins that are parallel to σ_1, *ie.* veins of the same orientation. For $R < 0$ the veins are convergent and when $R > 0$ veins are divergent.

[6] Attempts to determine R for conjugate vein arrays indicate the high internal fluid pressure ($P_f > \sigma_m$) normally suggested (*eg.* Beach 1977, Reynolds & Lister 1987) for vein formation may not be justified.

Dyke intrusion and paleostress analysis (Chapter 6)

Analysis of the field relations of the Easdale dykes and their opening directions with respect to remote tectonic stress and internal magma pressure indicates that useful insights into the fracture opening mechanisms and loading conditions at the time of dyke intrusion can be gained. The following general conclusions have been reached:

[1] Dykes, like veins, are rarely simple planar fractures, they often display small scale irregularities and structures such as sidesteps and horns. These structures can be used to determine dilation or opening directions, provided sufficient three-dimensional exposure exists.

[2] The flow history of dykes can be investigated by examination of internal structures and from the analysis of flow lineations adjacent to dyke walls.

[3] Field observations of the structure of the chilled margins, flow lineations, and the textural zonation, suggest that the magma solidified on the dyke walls as it continued to flow in the interior of the dyke, *ie*. inward growth of accreted material. The lack of obvious contact metamorphism effects in the host-rock suggests a short duration of heat transfer, and a small increase in wall-rock temperature, prior to magma solidification. Further observations of features dependent on temperature distribution across dykes (*eg*. variation in chilled margin widths and contacts, phenocryst distribution) could allow more effective tests and comparison with theoretical models of heat transfer and magma flow during dyke intrusion.

[4] From measurements of dyke thicknesses, combined with estimates of magma flow rates, some inferences about magma flow conditions and factors that influence them can be made. Reynolds numbers (*Re)* in the range ≈3-10 are estimated, which are well within the regime for laminar flow, where the transition to turbulent flow is generally at $Re > 10^3$.

[5] Determination of 2D and 3D opening directions of dykes, suggest that subhorizontal opening directions predominate. Comparison of these opening directions with examples of dykes of differing trend indicate that the Easdale dykes share a common and consistent opening direction, trending N 057° E. Although the mean dyke trend is normal to their opening direction, individual dykes may be oblique to the mean, and these dykes open obliquely, *ie*. with the opening direction at N 057° E.

[6] The stress ratio for individual dykes at Easdale is approximately $R = 1$. This implies a constant opening direction and transtensile loading conditions. Analysis of the Easdale dykes can be used to

indicate the relative magnitudes of the remote principal stresses and magma pressure. Some of the dykes were emplaced oblique to the regional extension direction, so magma pressure was only able to dilate fractures with suitable orientations.

[7] Previous methods of determining paleostress trajectories from dyke orientations alone are unreliable as they imply a simplistic view of the loading conditions at the time of intrusion.

REFERENCES

Aki, K. 1981. A probalisitic synthesis of precusory phenomena. In: Simpson, D. & Richards, P. G. (eds.), *Earthquake Prediction, an International Review*. American Geophysical Union, Washington, D. C., 566-574.

Aki, K., Fehler, M. & Das, S. 1977. Source mechanisms of volcanic tremor: Fluid-driven crack models and their application to the 1963 Kilauea eruption. *Journal of Volcanology and Geothermal Research*, **2**, 259-287.

Aki, K. & Richards, P. G. 1980. *Quantitative Seismology: Theory and Methods*. W. H. Freeman & Co., San Francisco.

Anderson, E. M. 1951. *The dynamics of faulting and dyke formation with applications to Britain*. Oliver & Boyd, London.

Anderson, O. L. & Grew, P. C. 1977. Stress corrosion theory of crack propagation with applications to geophysics. *Reviews of Geophysics and Space Physics*, **15**, 77-104.

Atkinson, B. K. 1984. Subcritical crack growth in geological materials. *Journal of Geophysical Research*, **89**, 4077-4114.

Atkinson, B. K. & Meredith, P. G. 1987. The theory of subcritical crack growth with applications to minerals and rocks. In: Atkinson, B. K. (ed.), *Fracture Mechanics of Rock*. Academic Press, London, 111-162.

Aydin, A. & Schultz, R. A. 1990. Effect of mechanical interaction on the development of strike-slip faults with echelon patterns. *Journal of Structural Geology*, **12**, 123-129.

Beach, A. 1974. A geochemical investigation of pressure solution and the formation of veins in a deformed greywacke. *Contributions to Mineralogy and Petrology*, **46**, 61-68.

Beach, A. 1975. The geometry of en echelon vein arrays. *Tectonophysics*, **28**, 245-263.

Beach, A. 1977. Vein arrays, hydraulic fractures and pressure solution structures in a deformed flysch sequence, SW. England. *Tectonophysics*, **40**, 201-225.

Bergkvist, H. & Guex, L. 1979. Curved crack propagation. *international Journal of Fracture*, **15**, 429-441.

Birch, F. 1966. Compressibilty, elastic constants. In: Clark, S. P. (ed.), Handbook of Physical Constants, *Geological Society of America Memoir*, **97**, 95-173.

Bottinga, Y. & Weill, D. F. 1970. Densities of liquid silicate systems calculated from partial volumes of oxide components. *American Journal of Science*, **269**, 169-182.

Brace, W. F. & Bombolakis, E. G. 1963. A note on brittle crack growth in compression. *Journal of Geophysical Research*, **68**, 3709-3713.

Bruce, P. M. & Huppert, H. E. 1990. Solidification and melting along dykes by the laminar flow of basaltic magma. In: Ryan, M. P. (ed.), *Magma Transport and Storage*, Wiley, New York, 87-101.

Burger, H. R. 1977. Solution cleavage in en echelon vein zones. In: Bayly, B. M., Borradaile, G. J. and Powell, McA. (eds.), *Atlas of Rock Cleavage*, University of Tasmania Press, Tasmania, Eu 34.

Bussell, M. A. 1989. A simple method for the determination of the dilation direction of intrusive sheets. *Journal of Structural Geology*, **11**, 679-687.

Casey, M. & Huggenberger, P. 1985. Numerical modelling of finite-amplitude similar folds developing under general deformation histories. *Journal of Structural Geology*, **7**, 103-114.

Childs, C., Walsh, J. & Watterson, J. 1990. A method for the determination of the density of fault displacements below the limits of seismic resolution in reservoir formations. In: *North Sea Oil and Gas Reservoirs II*, Norwegian Institute of Technology, Graham & Trotman, 309-318.

Collins, D. A. & De Paor, D. 1986. A determination of the bulk rotational deformation resulting from displacements in discrete shear zones in the Hercynian fold belt of South Ireland. *Journal of Structural Geology*, **8**, 101-109.

Cook, T. S. & Erdogan, F. 1972. Stresses in bonded materials with a crack perpendicular to the interface. *International Journal of Engineering Science*, **10**, 677-697.

Cornford, C., Yarnell, L. & Murchison, D. G. 1987. Initial vitrinite reflectance results from the Carboniferous of North Devon and Cornwall. *Proceedings of the Ussher Society*, **6**, 461-467.

Cotterell, B. & Rice, J. R. 1980. Slightly curved or kinked cracks. *International Journal of Fracture*, **16**, 155-169.

Cox, S. F. 1987. Antitaxial crack-seal vein microstructures and their relationship to displacement paths. *Journal of Structural Geology*, **9**, 779-787.

Cox, S. F. & Etheridge, M. A. 1983. Crack-seal fibre growth mechanisms and their significance in the developement of oriented layer silicate microstructures. *Tectonophysics*, **92**, 147-170.

Crouch, S. L. & Starfield, A. M. 1983. *Boundary element methods in solid mechanics*. Allen & Unwin, London.

Cruikshank, K. M., Zhao, G. & Johnson, A. M. 1991. Analysis of minor structures associated with joints and faulted joints. *Journal of Structural Geology*, **13**, 865-886.

Currie, K. L. & Ferguson, J. 1970. The mechanism of intrusion of lamprophyre dykes indicated by offsetting of dykes. *Tectonophysics*, **9**, 525-533.

Dearman, W. R. 1967a. Structural patterns in the Upper Carboniferous rocks at Welcombe Mouth, north Devon. *Rep. Trans. Devon Ass. Adv. Sci.*, **99**, 273-286.

Dearman, W. R. 1967b. On the significance of northward facing structures at Duckpool, near Bude in north Cornwall. *Proceedings of the Ussher Society*, **1**, 266-269.

Dearman, W. R. 1969. On the association of upright and recumbent folds on the southern margin of the Carboniferous synclinorium of Devonshire and north Cornwall. *Proceedings of the Ussher Society*, **2**, 115-121.

DeGraff, J. M. & Aydin, A. 1987. Surface morphology of columnar joints and its significance to mechanics and directions of joint growth. *Geological Society of America Bulletin*, **99**, 605-617.

Delaney, P. T. 1987. Heat transfer during emplacement and cooling of mafic dykes. In: Halls, H. C. and Fahrig, W. F. (eds.), Mafic Dyke Swarms, *Geological Association of Canada Special Paper*, **34**, 31-46.

Delaney, P. T. & Pollard, D. D. 1981. Deformation of host rocks and flow of magma during growth of minette dikes and breccia-bearing intrusions near Ship Rock, New Mexico. *United States Geological Survey Professional Paper* **1202**.

Delaney, P. T. & Pollard, D. D. 1982. Solidification of basaltic magma during flow in a dike. *American Journal of Science*, **282**, 856-885.

Delaney, P. T., Pollard, D. D., Ziony, J. I. & McKee, E. H. 1986. Field relations between dikes and joints: Emplacement processes and paleostress analysis. *Journal of Geophysical Research*, **91**, 4920-4938.

Dey, T. N. & Wang, C. Y. 1981. Some observations of microcrack growth and interaction in compressive rock failure. *International Journal of Rock Mechanics and Mining Science*, **18**, 199-209.

Dietrich, D. 1989. Fold-axis parallel extension in an arcuate fold-thrust belt: the case of the Helvetic nappes. *Tectonophysics*, **170**, 183-212.

Du, Y. & Aydin, A. 1991. Interaction of multiple cracks and formation of echelon crack arrays. *International Journal for Numerical and Analytical Methods In Geomechanics*, **15**, 205-218.

Durney, D. W. & Ramsay, J. G. 1973. Incremental strains measured from syntectonic crystal growths. In: de Jong, K. A. & Scholten, R. (eds.), *Gravity and Tectonics*, John Wiley, New York, 67-96.

Edmonds, E. A., Williams, B. J. & Taylor, R. T. 1979. Geology of Bideford and Lundy Island. *Memoir of the Geological Survey of Great Britain.*

Elliot, D. 1972. Deformation paths in structural geology. *Bulletin of the Geological Society of America*, **83**, 2621-2638.

Ellis, M. A. 1986. Determination of progressive deformation histories from antitaxial syntectonic fibres. *Journal of Structural Geology*, **8**, 701-709.

Emerman, S. H., Turcotte, D. L. & Spence, D. A. 1986. Transport of magma and hydrothermal solutions by laminar and turbulent fluid fracture. *Physics of the Earth and Planetary Interiors*, **41**, 249-259.

Engelder, T. & Geiser, P. 1980. On the use of regional joint sets as trajectories of paleostress fields during the development of the Appalachian Plateau, New York. *Journal of Geophysical Research*, **85**, 5319-6341.

Engelder, T. & Lacazette, A. 1990. Natural hydraulic fracturing. In: Barton, N. & Stephanson, O. (eds.), *Proceedings of the International Symposium on Rock Joints*, Balkema, Rotterdam, 35-43.

Erdogan, F. & Sih, G. C. 1963. On the crack extension in plates under plane loading and transverse shear. *Trans. Am. Soc. Mechn. Engng.*, **85**, 519-527.

Fossen, H. & Tikoff, B. 1991. Simultaneous pure and simple shear: the unified deformation matrix. *Mitt. aus den Geol. Inst. ETH Zürich, Neue Folge*, **239b**, 143-144.

Freshney, E. C., Mckeown, M. C., Williams, M. & Dearman, W. R. 1966. Structural observations in the Bude to Tintagel area of the coast of north Cornwall, England. *Geologie en Mijnbouw*, **45**, 41-47.

Freshney, E. C., Mckeown, M. C. & Williams, M. 1972. Geology of the coast between Tintagel and Bude. *Memoir of the Geological Survey of Great Britain.*

Griffith, A. A. 1920. The phenomena of rupture and flow in solids. *Philosophical Transactions of the Royal Society of London*, **A221**, 163-198.

Gudmundsson, A. 1990. Dyke emplacement at divergent plate boundaries. In: Parker, A. J., Rickwood, P. C. & Tucker, D. H. (eds.), *Mafic Dykes and Emplacement Mechanisms*, Balkema, Rotterdam, 46-62.

Hancock, P. L. 1972. The analysis of en echelon vein arrays. *Geological Magazine*, **109**, 269-276.

Hartley, A. J. & Warr, L. N. 1990. Upper Carboniferous foreland basin evolution in SW Britain. *Proceedings of the Ussher Society*, **7**, 212-216.

Heffer, K. & Bevan, T. 1990. Scaling relationships in natural fractures - data, theory and applications. *Proceedings of the European Petroleum Conference*, **2**, 367-376 (SPE Paper 20981).

Hubbert, M. K. & Rubey, W. W. 1959. Role of fluid pressure in mechanics of overthrust faulting. *Geological Society of America Bulletin*, **70**, 115-166.

Ingraffea, A. R. 1987. Theory of crack initiation and propagation in rock. In: Atkinson, B. K. (editor), *Fracture Mechanics of Rock*, Academic Press, London, 71-110.

Jackson, D. B., Swanson, D. A., Koyanagi, R. Y. & Wright, T. L. 1975. August and October 1968 east rift eruptions of Kilauea Volcano, Hawaii. *United States Geological Survey Professional Paper* **890**.

Jackson, R. R. 1991. Vein arrays and their relationship to transpression during fold development in the Culm Basin, central south-west England. *Proceedings of the Ussher Society*, **7**, 356-362.

Jackson, R. R. & Sanderson, D. J. 1991a. Transtensional modelling of en echelon vein arrays. *Geological Association of Canada Program with Abstracts*, **16**, A60.

Jackson, R. R. & Sanderson, D. J. 1991b. Transtensional modelling of en echelon vein arrays. *Mitt. aus den Geol. Inst. ETH Zürich, Neue Folge*, **239b**, 166-167.

Jackson, R. R. & Mapeo, R. B. M. 1992. Duplex and detachment structures in the Culm Basin: relations between regional shortening and fold development. Abstract, *Proceedings of the Ussher Society*, **8**, 80-81.

Jamison, J. 1987. Geometric analysis of fold development in overthrust terranes. *Journal of Structural Geology*, **9**, 207-219.

Kaitaro, S. 1952. On some offset structures in dilation dikes. *Bulletin de la Commission Geologique Finlande*, **157**, 67-74.

Kakimi, T. 1980. Magnitude-frequency relation for displacement of minor faults and its significance in crustal deformation. *Bulletin of the Geological Survey of Japan*, **31**, 467-487.

Keer, L. M. & Chen, S. H. 1981. The intersection of a pressurised crack with a joint. *Journal of Geophysical Research*, **86**, 1032-1038.

Kerrich, R., Beckinsale, R. D. & Shackleton, N. J. 1978. The physical and hydrothermal regime of tectonic vein systems: evidence from stable isotope and fluid inclusion studies. *Neues Jahrbuch Fur Mineralogie Abhandlungen*, **131**, 225-239.

Komar, P. D. 1972. Flow differentiation in igneous dikes and sills: profiles of velocity and phenocryst concentration. *Geological Society of America Bulletin*, **83**, 3443-3448.

Kranz, R. L. 1983. Microcracks in rock: a review. *Tectonophysics*, **100**, 449-480.

Kretz, R. 1991. The dilation direction of intrusive sheets. *Journal of Structural Geology*, **13**, 97-99.

Ladiera, F. L. & Price, N. J. 1981. Relationships between fracture spacing and bed thickness. *Journal of Structural Geology*, **3**, 179-183.

Latjai, E. Z. Mechanics of second order faults and tension gashes. *Geological Society of America Bulletin*, **80**, 2253-2272.

Lawn, B. R. & Wilshaw, T. R. 1975. *Fracture of Brittle Solids*. Cambridge University Press.

Lister, J. R. & Kerr, R. C. 1990. Fluid-mechanical models of dyke propagation and magma transport. *In:* Parker, A. J., Rickwood, P. C. & Tucker, D. H. (eds.), *Mafic Dykes and Emplacement Mechanisms*, Balkema, Rotterdam, 69-80.

Lister, J. R. & Kerr, R. C. 1991. Fluid-mechanical models of crack propagation and their application to magma transport in dykes. *Journal of Geophysical Research*, **96**, 10049-10077.

Lloyd, G. E. & Whalley, J. S. 1986. The modification of chevron folds by simple-shear: examples from North Cornwall. *Journal of the Geological Society, London*, **143**, 89-94.

Ma, J., Du, Y. & Liu, L. 1986. The instability of en echelon cracks and its precursors. *Journal Phys. Earth*, **34**, Supplement, S141-S157.

Mackintosh, D. M. 1967. Quartz-carbonate veining and deformation in Namurian turbidite sandstones of the Crackington Measures, North Cornwall. *Geological Magazine*, **104**, 75-85.

Main, I. G., Meredith, P. G., Sammonds, P. R. & Jones, C. 1990. Influence of fractal flaw distributions on rock deformation in the brittle field. In: Knipe, R. J. & Rutter, E. H. (eds.), *Deformation Mechanisms, Rheology and Tectonics*, Special Publication of the Geological Society of London, **54**, 81-96.

Mapeo, R. B. & Andrews, J. R. 1991. Pre-folding tectonic contraction and extension of the Bude Formation, North Cornwall. *Proceedings of the Ussher Society*, **7**, 350-355.

Massey, B. S. 1975. *Mechanics of fluids*. Van Nostrand Reinhold & Co.

McCoss, A. M. 1986. Simple constructions for deformation in transpression/transtension zones. *Journal of Structural Geology*, **8**, 715-718.

McCoss, A. M. 1987. Geometry and kinematics of transpression and transtension. *Doctural thesis*, Queens University, Northern Ireland.

McKenzie, D. & Jackson, J. 1989. Kinematics and dynamics of distributed deformation. In: Kissel, C. and Laj. C (eds.), *Paleomagnetic Rotations and Continental Deformation*, Kluwer Academic Publishers, The Hague, 17-31.

Melin, S. 1983. Why do cracks avoid each other? *International Journal of Fracture*, **23**, 37-45.

Melin, S. 1987. Fracture from a straight crack subjected to mixed-mode loading. *International Journal of Fracture*, **32**, 257-263.

Mitra, S. & Namson, J. 1989. Equal-area balancing. *American Journal of Science*, **289**, 563-599.

Muroaka, H. & Kamata, H. 1983. Displacement distribution along minor fault traces. *Journal of Structural Geology*, **5**, 483-495.

Musset, A. E. 1986. ^{40}Ar-^{39}Ar step-heating ages of Tertiary igneous rocks of Mull, Scotland. *Journal of the Geological Society, London*, **143**, 887-896.

Narr, W. & Suppe, J. 1991. Joint spacing in sedimentary rocks. *Journal of Structural Geology*, **13**, 1037-1048.

Nemat-Nasser, S. & Horii, H. 1982. Compression induced nonplanr crack extension with application to splitting, exfoliation and rockburst. *Journal of Geophysical Research*, **87**, 6805-6821.

Nicholls, J. 1990. The mathematics of fluid flow and a simple application to problems of magma transport. In: Nicholls, J. & Russell, J. K. (eds.), *Mineralogical Society of America, Reviews in Mineralogy*, **24**, 107-123.

Nicholson, R. 1991. Vein morphology, host rock deformation and the origin of the fabrics of echelon veins. *Journal of Structural Geology*, **13**, 635-641.

Nicholson, R. & Ejifor, I. B. 1987. The three-dimensional morphology of arrays of echelon and sigmoidal, mineral-filled fractures: data from North Cornwall. *Journal of the Geological Society, London,* **144**, 79-83.

Nicholson, R. & Pollard, D. D. 1985. Dilation and linkage of echelon cracks. *Journal of Structural Geology*, **7**, 583-590.

Olson, J. E. 1991. Fracture mechanics analysis of joints and veins. Doctural thesis, Stanford University, USA.

Olson, J. E. & Pollard, D. D. 1988. Inferring stress states from detailed joint geometry. In: Cundall, P. A., Sterling, R. L. & Starfield, A. M. (eds.), *Key Questions in Rock Mechanics* (Proceedings 29th. U.S Symposium on Rock Mechanics): Balkema, Rotterdam, 159-167.

Olson, J. E. & Pollard, D. D. 1989. Inferring paleostresses from natural fracture patterns: a new method. *Geology*, **17**, 345-348.

Olson, J. E. & Pollard, D. D. 1991. The initiation and growth of en echelon veins. *Journal of Structural Geology*, **13**, 595-608.

Paterson, M. S. 1978. *Experimental Rock Deformation - The Brittle Field*. Springer-Verlag.

Peacock, D. C. P. 1991. A comparison between the displacement geometries of veins and normal faults at Kilve, Somerset. *Proceedings of the Ussher Society*, **7**, 363-367.

Peacock, D. C. P. & Sanderson, D. J. 1991. Displacements, segment linkage and relay ramps in normal fault zones. *Journal of Structural Geology*, **13**, 721-733.

Pollard, D. D. 1973. Derivation and evaluation of a mechanical model for sheet intrusions. *Tectonophysics*, **19**, 233-269.

Pollard, D. D. & Aydin, A. 1984. Propagation and linkage of oceanic ridge segments. *Journal of Geophysical Research*, **89**, 10017-10028.

Pollard, D. D. & Muller, O. H. 1976. The effect of gradients of regional stress and magma pressure on the form of sheet intrusions in cross section. *Journal of Geophysical Research*, **81**, 975-984.

Pollard, D. D. & Segall, P. T. 1987. Theoretical displacements and stresses near fractures in rock: with applications to faults, joints, veins, dikes and solution surfaces. In: Atkinson, B. K. (editor), *Fracture Mechanics of Rock*, Academic Press, London, 277-349.

Pollard, D. D., Segall, P. & Delaney, P. 1982. Formation and interpretation of dilatant echelon cracks. *Bulletin of the Geological Society of America*, **93**, 1291-1303.

Pollard, D. D., Zeller, S., Haiqing, W. & Thomas, A. 1990. Origins of joint spacing distributions in sedimentary rocks: new results from numerical and physical model studies. *Geological Society of America, Abstracts with Programs*, **22**, A142.

Price, N. J. 1966. *Fault and joint development in brittle and semi-brittle rock*. Pergamon Press, Oxford.

Primmer, T. J. 1985. A transition from diagenesis to greenschist facies within a major Variscan fold-thrust complex in south-west England. *Mineralogical Magazine*, **49**, 365-374.

Ramsay, J. G. 1974. Development of chevron folds. *Bulletin of the Geological Society of America*, **85**, 1741-1754.

Ramsay, J. G. 1980. The crack-seal mechanism of rock deformation. *Nature,* **284**, 135-139.

Ramsay, J. G. 1990. Transpression during fold development in the Culm of SW England. *21st Tectonic Studies Group Meeting, Abstracts.*

Ramsay, J. G. & Graham, R. H. 1970. Strain variation in shear belts. *Canadian Journal of Earth Sciences*, **7**, 786-813.

Ramsay, J. G. & Huber, M. I. 1983. *The Techniques of Modern Structural Geology, Volume One: Strain Analysis*. Academic Press, London.

Ramsay, J. G. & Huber, M. I. 1987. *The Techniques of Modern Structural Geology, Volume Two: Folds and Fractures*, Academic Press, London.

Rattey, P. R. & Sanderson, D. J. 1982. Patterns of folding within nappes and thrust sheets: Examples from the Variscan of southwest England. *Tectonophysics*, **88**, 247-267.

Reynolds, S. J. & Lister, G. S. 1987. Structural aspects of fluid-rock interactions in detachment zones. *Geology*, **15**, 362-366.

Richey, J. E. 1939. The dykes of Scotland. *Edinburgh Geological Society Transactions*, **13**, 393-435.

Richter, D. H., Eaton, J. P, Murata, K. J., Ault, W. U., & Krivoy, H. L. 1970. Chronological narative of the 1959-1960 eruption of Kilauea Volcano, Hawaii. *United States Geological Survey Professional Paper,* **474-D**.

Rickard, M. J. & Rixon, L. K. 1983. Stress configurations in conjugate quartz-vein arrays. *Journal of Structural Geology*, **5**, 573-578.

Ridley, J. & Casey, M. 1989. Numerical modelling of folding in rotational strain histories: Strain regimes expected in thrust belts and shear zones. *Geology*, **17**, 875-878.

Riedal, W. 1929. Zur mechanik geologischer Brucherscheinungen (Ein Beitrag zum problem der feiderspatten). *Zentbl. Miner. Geol. Palaeont, Abh.*, **354B**, 107-123.

Rispoli, R. 1981. Stress fields about strike-slip faults inferred from stylolites and tension gashes. *Tectonophysics*, **75**, T29-T36.

Roberts, J. L. & Sanderson, D. J. 1971. The intrusive form of some basaltic dykes showing flow lineation. *Geological Magazine*, **108**, 489-499.

Roering, C. 1968. The geometrical significance of natural en echelon crack arrays. *Tectonophysics*, **5**, 107-123.

Rothery, E. 1988. En echelon vein array development in extension and shear. *Journal of Structural Geology*, **10**, 63-71.

Rubin, A. M. & Pollard, D. D. 1987. Origins of blade-like dikes in volcanic rift zones. *United States Geological Survey Professional Paper,* **1350**.

Ryan, M. P. 1988. The mechanics and three-dimensional internal structure of active magmatic systems: Kilauea, Hawaii. *Journal of Geophysical Research*, **93**, 4213-4248.

Sanderson, D. J. 1974. Chevron folding in the Upper Carboniferous rocks of north Cornwall. *Proceedings of the Ussher Society*, **3**, 96-103.

Sanderson, D. J. 1979. The transition from upright to recumbent folding in the Variscan foid belt of south-west England: a model based on the kinematics of simple shear. *Journal of Structural Geology*, **1**, 171-180.

Sanderson, D. J. & Marchini, W. R. D. 1984. Transpression. *Journal of Structural Geology*, **6**, 449-458.

Scholz, C. H. 1990. *Mechanics of earthquakes and faulting*. Cambridge University Press, Cambridge.

Schultz, R. A. 1988. Stress intensity factors for curved cracks obtained with the displacement discontinuity method. *International Journal of Fracture*, **37**, R31-R34.

Seago, R. D. & Chapman, T. J. 1988. The confrontation of structural styles and the evolution of a foreland basin in central southwest England. *Journal of the Geological Society, London*, **145**, 789-800.

Secor, D. T. 1965. Role of fluid pressure in jointing. *American Journal of Science*, **263**, 633-646.

Secor, D. T. 1969. Mechanics of natural extension fracturing at depth in the earth's crust. In: *Research in tectonics, Geological Survey of Canada Paper*, **68-52**, 3-47.

Segall, P. 1984. Formation and growth of extensional fracture sets. *Bulletin of the Geological Society of America*, **95**, 454-462.

Segall, P. & Pollard, D. D. 1983. Joint formation in granitic rock of the Sierra Nevada. *Bulletin of the Geological Society of America*, **94**, 563-575.

Selwood, E. B. 1990. A review of basin development in central south-west England. *Proceedings of the Ussher Society*, **7**, 199-205.

Shackleton, R. M., Ries, A. C. & Coward, M. P. 1982. An interpretation of the Variscan structures in southwest England. *Journal of the Geological Society, London*, **139**, 533-541.

Shaw, H. 1980. The fracture mechanisms of magma transport from the mantle to the surface. *In:* Hargraves, R. B. (ed.), *Physics of Magmatic Processes*, Princeton University Press, New Jersey, 201-264.

Shianin, V. E. 1950. Conjugate sets of en echelon tension fractures in the Athens limestone at Riverton, Virginia. *Bulletin of the Geological Society of America*, **61**, 509-517.

Speight, J. M., Skelhorn, R. R., Sloan, T. & Knaap, R. J. 1982. The dyke swarms of Scotland. *In:* Sutherland, D. S. (ed.), *Igneous rocks of the British Isles*, Wiley, New York, 449-459.

Spence, D. A. & Turcotte, D. L. 1985. Magma-driven propagation of cracks. *Journal of Geophysical Research*, **90**, B1, 575-580.

Sumi, Y., Nemat-Nasser, S. & Keer, L. M. 1985. On crack path stability in a finite body. *Engineering Fracture Mechanics*, **22**, 759-771.

Swain, M. V. & Hagan, J. T. 1978. Some observations of overlapping interacting cracks. *Engng. Fract. Mechn.*, **10**, 299-304.

Tanner, P. W. G. 1989. The flexural-slip mechanism. *Journal of Structural Geology*, **11**, 635-656.

Tanner, P. W. G. 1992. The duplex model: implications from a study of flexural-slip duplexes. In: McClay, K. R. (ed.) *Thrust Tectonics*, Chapman & Hall, London, 201-208.

Tapponnier, P. & Brace, W. F. 1976. Development of stress induced microcracks in Westerly granite. *International Journal of Rock Mechanics and Mining Science*, **13**, 103-112.

Thiercelin, M., Roegiers, J. C., Boone, T. J. & Ingraffea, A. R. 1987. An investigation of the material parameters that govern the behaviour of fractures approaching rock interfaces. In: Shaffer, R. J. (ed.), *Proceedings of the 6th International Conference on Rock Mechanics*, Montreal. Volume One, 263-269.

Turcotte, D. L. 1986. Fractals and fragmentation. *Journal of Geophysical Research*, **91**, 1921-1926.

Turcotte, D. L. 1989. Fractals in geology and geophysics. *Pure & Applied Geophysics*, **131**, 171-196.

Turcotte, D. L., Emerman, S. H. and Spence, D. A. 1987. Mechanics of dyke injection. In: Halls, H. C. & Fahrig, W. F. (eds.), Mafic Dyke Swarms, *Geological Association of Canada Special Paper*, **34**, 25-29.

Ural, J. L., Williams, P. F. & Van Roermund, H. L. M. 1991. Kinematics of crystal growth in syntectonic fibrous veins. *Journal of Structural Geology*, **13**, 823-836.

Walsh, J. & Watterson, J. 1987. Distributions of cumulative displacement and seismic slip on a normal fault surface. *Journal of Structural Geology*, **9**, 1039-1046.

Walsh, J. & Watterson, J. 1988. Analysis of the relationship between displacements and dimensions of faults. *Journal of Structural Geology*, **10**, 239-247.

Walsh, J. & Watterson, J. 1992. Populations of faults and fault displacements and their effects on estimates of fault-related extension. *Journal of Structural Geology*, **14**, 701-712.

Weertman, J. 1980. The stopping of a rising, liquid-filled crack in the Earth's crust by a freely slipping horizontal joint. *Journal of Geophysical Research*, **85**, 967-976.

Whalley, J. S. & Lloyd, G. E. 1986. Tectonics of the Bude Formation, North Cornwall - the recognition of northerly directed decollement. *Journal of the Geological Society, London*, **143**, 83-89.

Whalley, J. S. & Lloyd, G. E. 1991. Facing directions in shear-modified folds within thrust sheets. *Mitt. aus den Geol. Inst. ETH Zürich, Neue Folge*, **239b**, 81-82.

Wickham, J. S. 1973. An estimate of strain increments in a naturally deformed carbonate rock. *American Journal of Science*, **273**, 23-47.

Williams, G. D. & Chapman, T. 1983. Strains developed in the hangingwalls of thrusts due to their slip/propagation rate: a dislocation model. *Journal of Structural Geology*, **5**, 563-571.

Withjack, O. M. & Jamison, W. R. 1986. Deformation produced by oblique rifting. *Tectonophysics*, **126**, 99-124.

Wu, H. & Pollard, D. D. 1992. Propagation of a set of opening-mode fractures in layered brittle materials under uniaxial strain cycling. *Journal of Geophysical Research*, **97**, 3381-3396.

Zwart, H. J. 1964. The development of successive structures in the Devonian and Carboniferous of Devon and Cornwall. *Geologie en Mijnbouw*, **43**, 516-526.

COMPOUND VEIN PULL-APART

SALTSTONE STRAND
NORTH CORNWALL

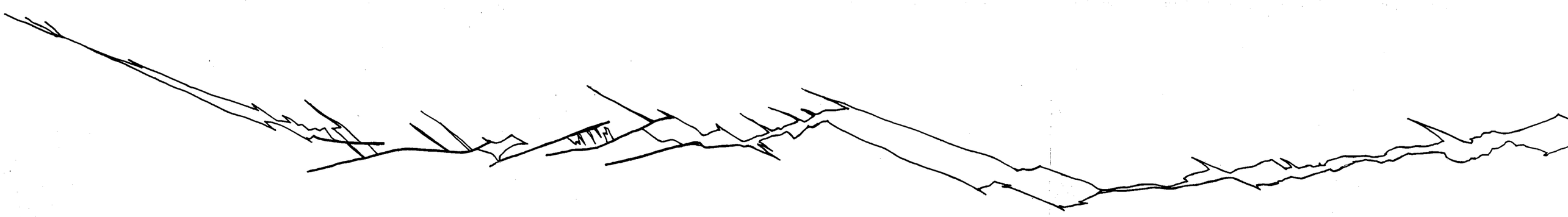

10cm

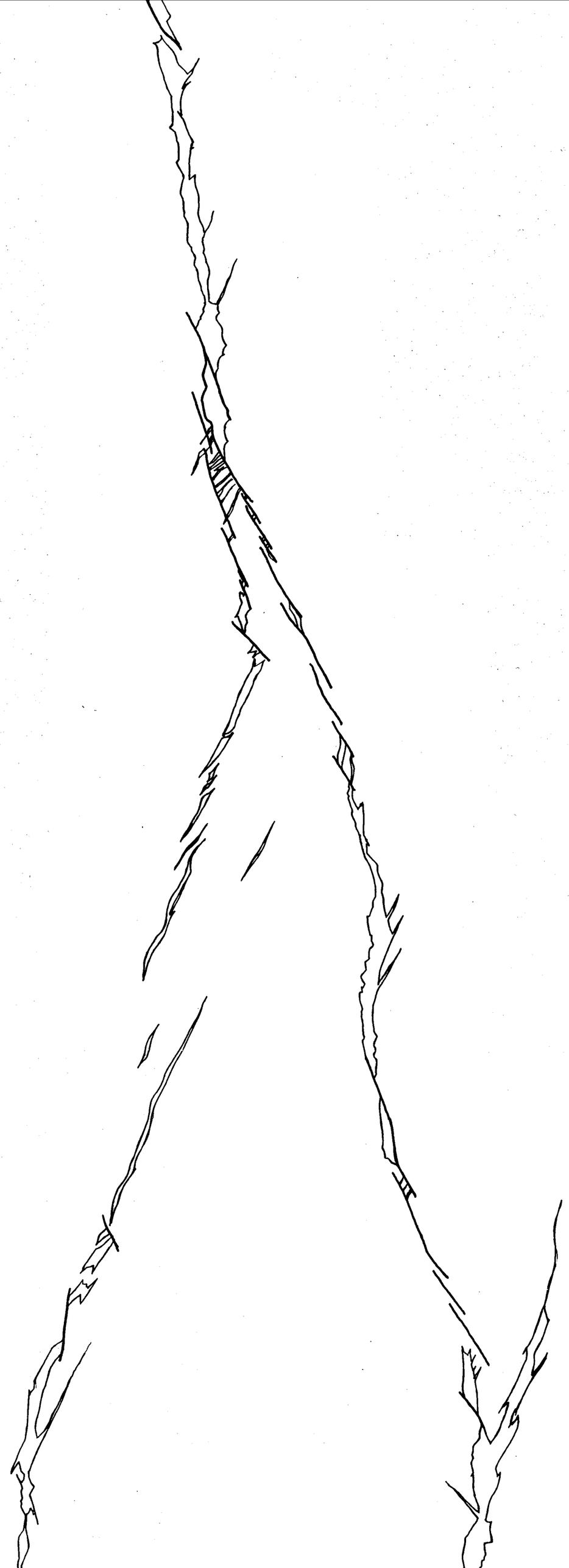

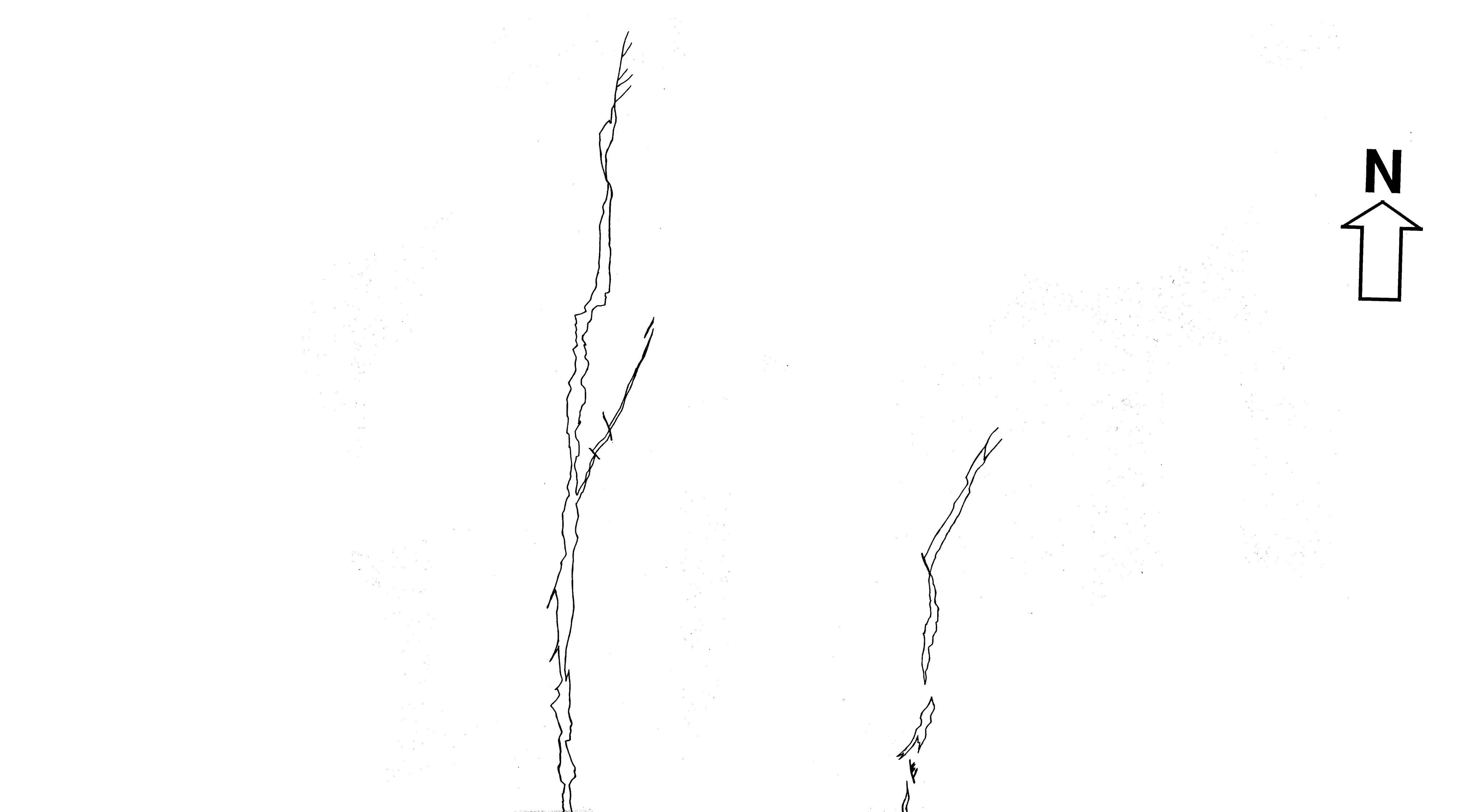
N